



---

**PROGRAMA DE PÓS-GRADUAÇÃO EM ECOLOGIA E BIODIVERSIDADE**

---

**FENOLOGIA REMOTA E OS PADRÕES DE TROCAS FOLIARES AO LONGO DE UM  
GRADIENTE DE SAZONALIDADE**

**BRUNA DE COSTA ALBERTON**

Tese apresentada ao Instituto de Biociências do Campus de Rio Claro, Universidade Estadual Paulista, como parte dos requisitos para obtenção do título de Doutor em Ecologia e Biodiversidade.

**Agosto – 2018**

BRUNA DE COSTA ALBERTON

FENOLOGIA REMOTA E OS PADRÕES DE TROCAS FOLIARES AO LONGO DE UM  
GRADIENTE DE SAZONALIDADE

Tese de Doutorado apresentada ao  
Instituto de Biociências da  
Universidade Estadual Paulista  
“Júlio de Mesquita Filho”, Campus  
de Rio Claro, para obtenção do título  
de Doutora em Ecologia e  
Biodiversidade.

Orientadora: Profa. Dra. LEONOR PATRICIA CERDEIRA MORELLATO

Co-orientador: Prof. Dr. RICARDO DA SILVA TORRES

Rio Claro – SP

2018

581.5  
A334f      Alberton, Bruna de Costa  
Fenologia remota e os padrões de trocas foliares ao longo de um  
gradiente de sazonalidade / Bruna de Costa Alberton. - Rio Claro, 2018  
252 f. : il., figs., gráfs.

Tese (doutorado) - Universidade Estadual Paulista, Instituto de  
Biociências de Rio Claro

Orientadora: Leonor Patricia Cerdeira Morellato

Coorientador: Ricardo da Silva Torres

Agência de fomento e n. de processo: FAPESP: 2014/00215-0,  
FAPESP: 2016/01413-5, FAPESP: 2013/50155-0

1. Ecologia vegetal. 2. Fenocâmeras. 3. Sazonalidade. 4. Fenologia  
vegetativa. 5. Produtividade do ecossistema. 6. Imagens digitais. I. Título.

**CERTIFICADO DE APROVAÇÃO**

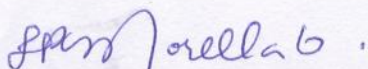
**TÍTULO DA TESE:** Fenologia remota e os padrões de trocas foliares ao longo de um gradiente de sazonalidade

**AUTORA:** BRUNA DE COSTA ALBERTON

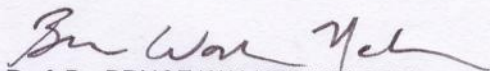
**ORIENTADORA:** LEONOR PATRICIA CERDEIRA MORELLATO

**COORIENTADOR:** RICARDO DA SILVA TORRES

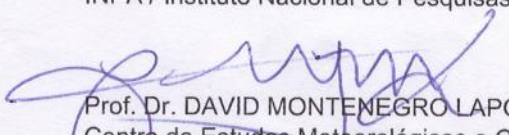
Aprovada como parte das exigências para obtenção do Título de Doutora em ECOLOGIA E BIODIVERSIDADE, área: BIODIVERSIDADE pela Comissão Examinadora:



Prof. Dra. LEONOR PATRICIA CERDEIRA MORELLATO  
Departamento de Botânica / UNESP - Instituto de Biociências de Rio Claro - SP




Prof. Dr. BRUCE WALKER NELSON  
INPA / Instituto Nacional de Pesquisas da Amazônia - AM



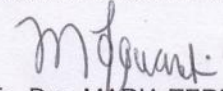
Prof. Dr. DAVID MONTENEGRO LAPOLA

Centro de Estudos Meteorológicos e Climáticos Aplicados à Agricultura (CEPAGRI) / Universidade de Campinas - SP



Prof. Dra. SIMONE APARECIDA VIEIRA

Núcleo de Estudos e Pesquisas Ambientais - NEPAM / Universidade Estadual de Campinas - SP



Prof. Dra. MARIA TEREZA GROMBONE-GUARATINI

Núcleo de pesquisa em Ecologia / INSTITUTO DE BOTÂNICA - SÃO PAULO

Rio Claro, 03 de agosto de 2018



À minha família, Pai, Mãe e Lucas

## AGRADECIMENTOS

À minha família, que é o meu alicerce e o meu refúgio, onde sei que sempre poderei voltar e ser bem acolhida. Meu pai Antônio, minha mãe Janete e meu irmão Lucas, agradeço ao suporte de cada um e por tudo que representam em minha vida. Ao meu companheiro de vida, amigo, namorado, colega de profissão, Renan, que nunca mediu esforços em me ajudar e me apoiar, sobretudo nos últimos meses de finalização desta tese. É um prazer dividir a vida contigo. Eu amo vocês. Obrigada por tudo.

Agradeço aos meus orientadores, Patrícia e Ricardo, aos quais sou eternamente em débito, por todo o aprendizado, conselhos, lições e network que me foi passado ao longo destes anos de mestrado e doutorado. Gratidão.

Patrícia tem papel fundamental na construção de minha carreira científica ao longo da pós-graduação. Foi ela quem me apresentou as fenocâmeras e me incentivou a desenvolver meus estudos sobre a fenologia remota próxima. Graças à sua visão de carreira, pude aproveitar grandes oportunidades, interagir com excelentes pesquisadores e entrar no universo multidisciplinar da pesquisa acadêmica, que muito me inspira. São inúmeros os motivos para lhe agradecer, não somente como orientadora, mas como uma grande amiga que tive nestes últimos anos. Em especial neste final de tese, minha gratidão pelo esforço em me ajudar nos tópicos de maior dificuldade e pela paciência com todas as correções.

Meu co-orientador, Ricardo Torres, com quem tive a oportunidade de aprender muito e poder contar sempre com sua disposição em me ajudar. Foram muitas reuniões, presenciais ou por Skype, com orientações muito bem direcionadas, esclarecedoras e sempre incentivadoras.

Um agradecimento mais do que especial aos meus amigos. Àqueles de longa data e que ainda permanecem próximos, mesmo que distantes (fisicamente), e àqueles que se tornaram minha família ao longo dos lugares onde vivi e passei nestes últimos anos. Por sorte, tenho muitos, especialmente nesta cidade (Rio Claro), a qual tem sido minha casa na maior parte destes últimos sete anos. A minha amizade inabalável do sul do país, minha amiga e irmã da vida Mainara Cascaes, e minhas amigas “bioloukas”: Thereza Garbelotto, Patricia Correa, Gabriela Thomaz e Beatriz Wessler. Aos meus colegas de laboratório que se tornaram grandes amigos e por muito tempo minha família rio-clarense:

Gabriela Camargo, Vanessa Staggemeier, Nathália Miranda, Daniel Carstensen, Irene Mendoza e Natália Costa, com quem não somente dividi o mesmo laboratório, mas também foi minha grande companheira ao dividirmos o mesmo teto por quase cinco anos. A todos os meus queridos amigos que o forró me trouxe, em especial a Thais Helena Condez e sua família, pela amizade sincera, leve e tão cheia de amor. Um agradecimento especial aos amigos incríveis que fiz durante minha vivência em Boston, os quais foram essenciais para tornar minha vida norte-americana mais leve, mais divertida e um pouco menos fria, em especial à Laura Zoffoli, por sua amizade e companheirismo.

Agradeço ao Laboratório de Fenologia, a todos os membros que já passaram por ele e aos atuais, por sempre proporcionarem um ambiente leve e inspirador para o trabalho, pelas trocas de conhecimentos e colaborações ao longo de todos os encontros e workshops realizados. É realmente um prazer fazer parte deste grupo e um orgulho tê-lo dentro de minha carreira profissional. Agradeço especialmente aos meus queridos amigos e colegas, Bruno Defane e Leonardo Cancian, por todo o suporte técnico ao longo dos trabalhos de campo, processamento das imagens digitais e auxílio em SIG. Agradeço também aos alunos de graduação, os quais tive a oportunidade de auxiliar na orientação de seus trabalhos, e que se interessaram pela fenologia remota próxima me auxiliando no processamento das imagens: Marina Muller, Carolina Crivelin e Rodrigo Lacerda.

Agradeço aos colaboradores na pesquisa desta tese. Ao Professor Dr. Andrew Richardson, por aceitar ser meu supervisor e me receber em seu laboratório durante os 12 meses de estágio na Universidade de Harvard, entre maio de 2016 e maio de 2017. Foi sob a supervisão de Andrew, que aprendi a manipular e processar os dados de alta frequência de fluxo de carbono, bem como associá-los aos dados da fenologia remota próxima das câmeras digitais e estabelecer as primeiras questões ecológicas dentro do trabalho que viria a se tornar o capítulo 3 desta tese. Agradeço ao Professor Dr. Humberto Rocha, da Universidade de São Paulo (USP), por colaborar disponibilizando os dados das estações meteorológicas e os dados de fluxo de carbono das áreas do cerrado Pé-de-Gigante e de Santa Virgínia, bem como pela disponibilidade presencial e remota com a qual vem auxiliando no desenvolvimento desta tese, através de sua experiência nas trocas de fluxos de energia em ecossistemas tropicais. Também agradeço à sua equipe, Emília Brasilio pela compilação e pré-processamento dos dados meteorológicos e de fluxo de carbono, e ao Eduardo Gomes Lopes e Helber

Freitas pelo suporte técnico indispensável nos trabalhos realizados de instalação e manutenção das câmeras digitais nas torres de fluxo. Agradeço por toda colaboração da EMPRABA Semi-árido, em especial à Magna Soelma Bezerra de Moura, por todo o suporte técnico na instalação, manutenção e coleta dos dados da câmera digital na torre de fluxo da área de caatinga, por disponibilizar os dados meteorológicos e de fluxo de carbono, e por colaborar no desenvolvimento dos trabalhos desta tese, contando com sua experiência em ecossistemas áridos.

Agradeço aos pesquisadores que participaram e aos que ainda participam do projeto e-Phenology, com os quais tive a oportunidade de trabalhar, aprender e colaborar. Um agradecimento especial aos professores Jurandy Almeida, Jefersson dos Santos, Fabio Faria, João Comba e Lucas Schnorr, e aos colegas que também desenvolveram suas teses e dissertações dentro do projeto: Greice Mariano, Roger Leite e Alexandre Almeida.

Agradeço ao Departamento de Botânica e a todos os técnicos que auxiliaram nos trabalhos de campo ao longo do doutorado, em especial ao Rafael Consolmagno, que participou ativamente das instalações, manutenções e reparos das câmeras digitais, pelos muitos quilômetros rodados por todas as áreas monitoradas e pela parceria leve e pró ativa sempre presente.

Agradeço ao Instituto Florestal (IF) do Estado de São Paulo, bem como aos dirigentes das unidades, pela liberação concedida de desenvolver as pesquisas desta tese nas áreas da Estação Ecológica de Itirapina, do Parque Estadual do Vassununga (área do cerrado Pé-de-gigante), e no Parque Estadual da Serra do Mar Núcleo Santa Virgínia (área da Mata Atlântica). Também agradeço aos donos da Fazenda São José e do Instituto Arruda Botelho (IAB) por permitir o trabalho de campo realizado em sua fazenda (área de cerrado) em Itirapina.

Agradeço à Seção de Pós-Graduação do Instituto de Biociências da UNESP, pelo suporte ao longo de todos os anos de doutorado, e ao conselho do Programa de Pós-Graduação em Ecologia e Biodiversidade, pelo suporte, boa relação e abertura estabelecida aos alunos matriculados, no intuito de sempre melhorar as normativas do curso.

Agradeço à Fundação de Amparo à Pesquisa do Estado de São Paulo (FAPESP) pelas bolsas de doutorado e de estágio de pesquisa no exterior concedidas (#2014/00215-0, #2016/01413-5); pelo financiamento dos projetos e-Phenology (#2010/52113-5, #2013/50155-0, FAPESP-Microsoft

Research Virtual Institute); e pelo financiamento de projetos paralelos que contribuíram nesta tese (#2007/59779-6, e FAPESP-VALE-FAPEMIG # #2010/51307-0). Ao CNPq pelo apoio dado por meio das bolsas de produtividade de meus orientadores (#306243/2010-5 #306587/2009-2). Ao Programa de Apoio à Pós-Graduação (PROAP) pelo auxílio concedido para participação em eventos científicos durante o período de doutorado.



A maior riqueza  
do homem  
é sua incompletude.  
Nesse ponto  
sou abastado.  
Palavras que me aceitam  
como sou  
— eu não aceito.  
Não aguento ser apenas  
um sujeito que abre  
portas, que puxa  
válvulas, que olha o  
relógio, que compra pão  
às 6 da tarde, que vai  
lá fora, que aponta lápis,  
que vê a uva etc. etc.  
Perdoai. Mas eu  
preciso ser Outros.  
Eu penso  
renovar o homem  
usando borboletas.

(Manuel de Barros)

## RESUMO

O estudo da fenologia vegetal busca monitorar, compreender e prever os ciclos de vida recorrentes das plantas, principalmente influenciados pelo clima. O monitoramento das fenofases vegetativas de brotamento e senescência foliar são essências para a compreensão de processos ecossistêmicos importantes como, a produtividade primária, as trocas de energia entre atmosfera e superfície terrestre, o fluxo de carbono, e a ciclagem de nutrientes. Logo, entender a resposta das plantas ao clima e ser capaz de prever alterações em sua fenologia, é essencial para o entendimento das dinâmicas de comunidades vegetais e da funcionalidade dos ecossistemas em frente a cenários de mudanças climáticas. Nos últimos anos, a busca por novas tecnologias dentro de estudos científicos vem crescendo com o intuito de tornar mais viável e amplo o monitoramento fenológico. Neste trabalho, buscamos incorporar novas tecnologias de observações fenológicas com o uso de câmeras digitais (fenocâmeras) instaladas em campo para o monitoramento de dados fenológicos de brotamento e senescência foliar em ambientes tropicais. Os objetivos gerais deste trabalho de tese, dividida em quatro seções, foram de : (i) compilar informações sobre conceitos e propriedades da técnica de fotografias repetidas (*repeated photograph technic*), criando um protocolo para o uso de câmeras digitais nos trópicos e levantar suas principais contribuições no âmbito na biologia da conservação; (ii) monitorar e descrever os padrões da fenologia vegetativa em diferentes comunidades vegetais sazonais, através dos dados obtidos de imagens digitais e investigar os principais gatilhos ambientais atuando nas diferentes vegetações; (iii) associar dados de fenologia foliar juntamente com dados de produtividade primária bruta dentro de ecossistemas sob diferentes pressões de sazonalidade para um melhor entendimento das respostas entre vegetação-atmosfera mediadas pela fenologia foliar; e (iv) apresentar resultados das principais iniciativas em análises de imagens digitais para o monitoramento da fenologia foliar desenvolvidas dentro da rede de fenocâmeras do projeto *e-phenology*, no âmbito da colaboração *e-science*. As vegetações estudadas neste trabalho estão distribuídas ao longo de um gradiente de sazonalidade de distribuição de chuvas e incluem: uma vegetação de caatinga; três diferentes fisionomias de cerrado que correspondem a um cerrado campo sujo, um cerrado *sensu stricto*, e um cerrado denso; e uma vegetação de Mata Atlântica. Séries temporais relacionadas às fenofases vegetativas foram extraídas do conjunto de imagens digitais coletadas em cada uma das áreas e analisadas dentro do contexto de cada um dos objetivos deste trabalho. Demonstramos que o estabelecimento de uma rede de fenocâmeras é uma poderosa ferramenta para a biologia da conservação, através da capacidade de obtermos dados de alta frequência temporal associados a uma ampla gama de dados ambientais monitorados. Através da aplicação de fenocâmeras pode-se obter novas informações sobre prática de manejo e restauração de ambientes, além de sua potencial contribuição nas esferas de educação ambiental e ciência cidadã. Observamos que a disponibilidade de água e luz no ambiente são os fatores mais importantes para o desenvolvimento foliar ao longo de diferentes comunidades sazonais. Relações hídricas em plantas

foram mais importantes para vegetações mais áridas, como a caatinga, enquanto que a disponibilidade de luz, quantificada através da sazonalidade do comprimento do dia, teve maior influência no gatilho do desenvolvimento foliar nas comunidades de cerrado. No âmbito dos ecossistemas, demonstrou-se uma nova abordagem ao se relacionar a fenologia foliar derivada de câmeras com a produtividade de ecossistemas tropicais. A dinâmica fenológica analisada através da variabilidade de sinais fenológicos encontrados dentro das diferentes vegetações, foram importantes para explicar os padrões temporais de produtividade dos ecossistemas. A compilação de trabalhos realizados através da colaboração *e-science*, apresentados na seção 4, foram de grande importância para o desenvolvimento dos métodos e análises, bem como para o alcance dos resultados obtidos dentro desta tese. Este trabalho oferece uma nova ferramenta para o monitoramento fenológico em vegetações tropicais, e sugere novos desafios a serem desenvolvidos bem como incentiva uma maior abrangência no uso de fenocâmeras a fim de cobrir um maior número de áreas e diferentes tipos de vegetação, além de associar estes estudos com abordagens desenvolvidas em diferentes escalas como as observações diretas, a aplicação de imagens de drones, bem como com as imagens de satélite. A comparação de diferentes escalas espaciais e temporais irá nos ajudar a entender melhor a própria escala de informações provenientes das fenocâmeras em termos de abrangência e detalhamento dos ecossistemas.

**Palavras-chave: fenocâmeras, sazonalidade, fenologia vegetativa, produtividade do ecossistema, imagens digitais**

## ABSTRACT

Plant phenology is a traditional science focused on monitoring, understanding, and predicting recurrent life cycles events, which are mainly related to climate. Leaf development stages are essential plant phenophases for the better understanding of ecosystems processes such as carbon and water fluxes, regulation of productivity, and nutrient cycling. Through the investigation of plant responses to climate and phenological shifts prediction, we can better forecast climatic change effects on vegetation dynamics and prevent loss of ecosystems functionalities. Aiming to become the phenological collection wider and more feasible worldwide, the seek for new technologies has stimulated several research centers of plant phenology monitoring. Here, we incorporated a new technology of field phenological observations using digital cameras for the monitoring of leaf exchanges in tropical vegetations. On this work, divided into four sections, we aimed to: (i) compile information about concepts and properties of the repeated photograph technic, create guidelines for the phenocams setup in tropical vegetation sites, and to provide key contributions of daily imagery monitoring on biological conservation; (ii) to establish a monitoring of different seasonal vegetations, describing the phenological trends, and identify the environmental cues which are triggering the leaf flushing and senescence for each vegetation type; (iii) analyze the canopy greenness obtained from digital cameras in relation to gross primary productivity measurements, to better understand the role of leaf phenology controlling ecosystem productivity in the tropics; and (iv) present some results of phenocam image analysis research initiatives and tools devised in the context of *e*-Science collaborations and built in the framework of the e-phenology project and the e-phenology network of phenocams. The selected study sites belong to different seasonal biomes, which comprehends areas from caatinga, savanna grasslands, savanna woodlands and Atlantic rainforest. Temporal series representing foliar phenology were extracted from the data imagery of each vegetation site and were analyzed into the context of each section of this work. We demonstrated that the establishment of phenocam networking is a powerful tool for biological conservation through its capability of fine temporal resolution data associated with wide spatial monitoring coverage. Besides, phenocams applications can bring new information for management and restoration practices at several sites and environments and contribute for the education for conservation and citizen science initiatives. We observed that water and light were the most important predictors for the leaf phenological patterns across seasonal vegetation communities. Water-plant relationships were more important for the caatinga community, and light, through day-length seasonality, had more influence in the leafing patterns of the cerrado communities. Regarding the ecosystem, we demonstrated a novel approach to relate leaf phenology to seasonality of tropical ecosystems productivity. The phenological dynamics regarding the variability of species phenological signals, and how they are built in into each contrasting vegetation communities explains drivers of leaf phenology and productivity. A compilation of articles developed through the e-science collaboration, presented in Section 4, were of

great importance for the generation of methods and analytical work, as well as for the results achievements in this thesis. This work will offer a new tool for the phenological monitoring in the tropics, and suggests next challenges to be addressed and the continuity of the e-phenology network and the spread of new cameras covering new vegetation types; the development of bottom-up studies, integrating on-the-ground observations, cameras, drones, and satellites, inter-comparing them and placing camera-derived phenology in its own scale, by understanding how much and what kind of information can be retrieved from ecosystems.

**Key words: phenocameras, seasonality, leaf phenology, ecosystem productivity, digital images**



## SUMÁRIO

INTRODUCTION.....	12
SECTION 1: Introducing digital cameras to monitor plant phenology in the tropics: applications for conservation.....	17
SECTION 2: Leafing patterns and drivers across seasonally dry tropical communities.....	50
SECTION 3: Leaf phenology correlates to gross primary productivity: an inter-comparison across tropical biomes.....	94
SECTION 4: <i>e</i> -Science and the multidisciplinary research built on the integrations of big data ecological research and computational science.....	142
CONCLUSIONS.....	146
REFERENCES.....	148
APPENDIX A: Leafing patterns and leaf exchange strategies of a cerrado woody community.....	150
APPENDIX B: Phenological visual rhythms: Compact representations for fine-grained plant species identification.....	189
APPENDIX C: Time series-based classifier fusion for fine-grained plant species recognition.....	201
APPENDIX D: Fusion of Time Series Representations for Plant Recognition in Phenology Studies.....	211
APPENDIX E: PhenoVis – Visual Phenological Analysis of Forest Ecosystems.....	222
APPENDIX F: Unsupervised distance learning for plant species identification.....	238

## 1 INTRODUCTION

Plant phenology is a traditional science focused on monitoring, understanding, and predicting recurrent life cycles events, which are mainly related to climate (Morellato et al., 2016). Leaf development stages are plant phenophases responsible for indicating the growth season and for controlling crucial ecosystems processes such as carbon and water fluxes, regulation of productivity, and nutrient cycling (Reich, 1995; Baldocchi et al., 2005). Tropical ecosystems have significant importance in the global carbon budget (Field et al., 1998; Ometto et al., 2005). By understanding phenological patterns of tropical vegetations and what drives leaf production seasonality within tropical communities, we can better forecast climatic change effects on vegetation dynamics and prevent loss of ecosystems functionalities (Polgar and Primack, 2011).

Phenological studies in the tropics preclude the observation of many species across several sites with intense human labor and costs (Alberton et al., 2014; Morellato et al., 2016). The scarcity of long-term monitoring in tropical regions, necessary to understand the effects of global warming on organisms (Abernethy et al., 2018) has stimulated several research centers to seek for new tools of plant phenology monitoring. The near-surface remote phenology consists in the application of sensors in the ground for the monitoring of plant to ecosystem-scale vegetation changes. The use of digital cameras to track leaf exchanges came to fill the gap between the traditional on-the-ground monitoring by human direct observation and remote sensing derived land surface phenology (Richardson et al., 2007; Morisette et al., 2009; Morellato et al., 2016).

The technique of repeated photographs using digital cameras for phenology monitoring, or phenocams, has increased in the last 10 years due its advantages of low cost investment, reduction in size, easy set-up installation, the reduced human labor, increased temporal resolution, and the opportunity of simultaneously monitoring several sites improving the spatial resolution of ground-based phenology monitoring and offering the possibility of handling high resolution data (Crimmins and Crimmins, 2008, Morisette et al., 2009; Graham et al., 2010; Alberton et al., 2017), leading phenocams to a widely range of ecological applications worldwide.

The ongoing addition of new devices, high-resolution data survey, and sensor networks has been improving the quality of data collected in biological studies, but at the same time increasing the

magnitude of scientific data collected. Near-surface monitoring systems in the tropics, for instance, are necessarily complex since the environmental conditions are harsh and the diversity of species is usually high. This leads to a next generation of scientific problems, which will require the establishment of multidisciplinary teams (Hey and Hey 2006). To the process of data retrieval, management, and analysis it will be required the collaboration between ecologists and computer scientists. *e-Science* is about the collaboration of key areas of science, not considered a discipline, but a network of research initiative focused on the specification and implementation of a set of tools and technologies capable of supporting, improving, and speeding up data analysis, knowledge discovery, and decision making (Hey and Hey 2006).

In Brazil, we have the e-phenology Network (<http://www.recod.ic.unicamp.br/ephenology> - As of June 2018), introduced in this thesis, that comprehends the application of digital cameras as tools to detect leaf flushing and senescence across different vegetation types from drylands, grasslands, and cerrado savannas to rainforests. This project is innovative and puts Brazil in the state of the art of near-remote phenology monitoring, already established in areas of temperate forests in northern hemisphere. The e-phenology project also integrates the development of computational tools for the methodological applications of algorithms for data mining and time series analysis (e.g., Almeida et al., 2014; Almeida et al., 2016).

In this context, the present thesis is divided into four sections that all together, aim to present the development of phenocams tools in tropical systems, their application in ecological studies and the integration of e-science insights on peripheral approaches that contributed for this work. Sections are described below.

## **Section 1 - Introducing digital cameras to monitor plant phenology in the tropics: applications for conservation**

Digital-camera-based monitoring phenology is growing in the tropics (e.g., Alberton et al., 2014; Nagai et al., 2016; Moore et al., 2017; Lopes et al., 2017), but it is still sparse when compared with temperate regions (Brown et al., 2017). Protocols and methodological approaches developed for camera systems were launched from networks researchers of these regions. We aimed to spread our

experience of using digital cameras to monitor tropical vegetations across multiple sites to encourage, among the scientific community of Brazil and tropics worldwide, their potential usability in a broader ecological context.

This section brings a published article with compiled information about concepts and properties of the technic, guidelines for the phenocams setup in tropical vegetation sites, and to provide key contributions of daily imagery monitoring on biological conservation (Alberton et al., 2017).

## **Section 2 - Leafing patterns and drivers across seasonally dry tropical communities**

Investigating the main drivers of plant phenology is of paramount importance for a better understanding of plant shifts in response to a changing climate and for effective biodiversity conservation from species to ecosystems (Polgar and Primack, 2011; Morellato et al., 2016). As already mentioned, plant phenology remains poorly understood for the tropics, and so the triggers of phenological transitions (Morellato et al., 2013; Chambers et al., 2013; Abernethy et al., 2018).

The traditional phenology monitoring, made by direct observations, provides confident data from individuals species to vegetation communities that contribute with pattern validation for remote-monitoring methods such as phenocameras and satellite images. Despite the coarse time-scale of observations (monthly), long-term on-the-ground phenology may be used for the investigation of leaf development drivers and further analysis of climatic changes impacts. A study using a 7-year on-the-ground phenological time series, compiled with leaf flushing and senescence monthly data, aimed to investigate the main environmental drivers of a cerrado *sensu stricto* community and their leaf exchange strategies species. This work, which I co-authored, was conducted in one of the sites, where an e-phenology camera was installed and was carried out in parallel along this thesis development (Appendix A).

By tracking daily images combined with environmental measurements, we can fine-tune plant color changes to leafing exchange patterns and unravel the influence of climatic variables. A wide range of questions might be investigated. In this section, we conducted, for the first time, a phenological research across multiple-sites monitoring leafing exchange patterns using phenocams. We aimed to

describe the leaf phenological patterns across seasonally dry tropical communities monitored by digital cameras, investigating the main environmental factors influencing the timing and length of growing seasons, and intercompare vegetations under distinct severity of dry season and across key life forms (grassy – woody), regarding their phenological dynamics and drivers of leaf phenology.

### **Section 3 - Leaf phenology correlates to gross primary productivity: an inter-comparison across tropical Biomes.**

Tropical leaf phenology is regarded as a first order mechanism regulating seasonality of carbon assimilation in tropical evergreen forests (Restrepo-Coupe et al., 2013; Restrepo-Coupe et al., 2017; Wu et al., 2016; Wu et al., 2017). Studies in temperate ecosystems have demonstrated that the camera-derived  $G_{cc}$  index, a measure of vegetation greenness, is well related to the gross primary productivity (GPP) curves (Richardson et al., 2010; Migliavacca et al., 2011; Keenan et al., 2014; Toomey et al., 2015). Phenocams have played an important role in those ecosystem-scale studies, contributing to link ground observed changes to ecosystem scale assessments derived from flux towers and remote sense indices (Ahrends et al., 2009; Migliavacca et al., 2011; Tomey et al., 2016). Leaf phenology should also be considered on Dynamic Global Vegetation Models (DGVMs). These models are based on coupled information between plant biogeography and biogeochemical processes to simulate ecosystem fluxes and climate shifts in a climatic change scenario (Foley et al., 1998; Restrepo-Coupe et al., 2017). In this context, understanding vegetative phenological transitions is essential to better estimate measurements of gross primary productivity (GPP), because there is still a gap of knowledge about the drivers of productivity in the tropics (Restrepo-Coupe et al., 2017). In this context, camera-derived phenological time series might provide key information to understand the photosynthetic seasonality of tropical forests and atmospheric-vegetation feedbacks to a changing climate (Richardson et al., 2013; Restrepo-Coupe et al., 2017).

In this section, we propose to analyze the relationship between the leaf phenology extracted from phenocameras and the ecosystem photosynthetic activity from GPP measurements of eddy-covariance towers across three distinct Neotropical biomes: Caatinga, Cerrado, and Rainforest. We



aim to inter-compare the phenology-GPP dynamics across sites belonging to each vegetation domain and contrasting seasonality.

#### **Section 4 – *e*-Science and the multidisciplinary research built on the integrations of big data ecological research and computational science**

Throughout this section, we present some results of phenocam image analysis research initiatives and tools devised in the context of *e*-Science collaborations and built in the framework of the e-phenology project and the e-phenology network of phenocams. The published papers are presented in Section 4 and all are directly connected to the development of this thesis and opened up the possibility to explore the results presented in Sections 1 to 3.

### Section 1

Article published in the Journal of Perspectives in Ecology and Conservation:

ALBERTON, B.C. et al. Introducing digital cameras to monitor plant phenology in the tropics: Applications for conservation. **Perspectives in Ecology and Conservation**, v. 15, p. 82-90, 2017.

**Introducing digital cameras to monitor plant phenology in the tropics: applications for conservation**

Authors: Bruna Alberton<sup>1\*</sup>, Ricardo da S. Torres<sup>2</sup>, Leonardo F. Cancian<sup>1</sup>, Bruno D. Borges<sup>1</sup>, Jurandy Almeida<sup>3</sup>, Greice Mariano<sup>2</sup>, Jefersson dos Santos<sup>4</sup>, Leonor Patricia C. Morellato<sup>1</sup>

<sup>1</sup> UNESP Universidade Estadual Paulista, Instituto de Biociências, Departamento de Botânica, Laboratório de Fenologia, Rio Claro, São Paulo, Brazil.

\*Corresponding author

Email address: brualberton@gmail.com

<sup>2</sup> RECOD Lab, Institute of Computing, University of Campinas – UNICAMP  
13083-852, Campinas, SP – Brazil

<sup>3</sup> Institute of Science and Technology, Federal University of São Paulo – UNIFESP, 12247-014, São José dos Campos, SP, Brazil

<sup>4</sup> Department of Computer Science, Universidade Federal de Minas Gerais – UFMG, 31270-010, Belo Horizonte, MG, Brazil

Short title: **Introducing phenocams and their applications on conservation biology.**

**Keywords:** leaf phenology; repeated photography; RGB color channels; conservation biology; *e-science*

## **Abstract**

The application of digital cameras to monitor the environment is becoming global and changing the way of phenological data collection. The technique of repeated digital photographs to monitor plant phenology (phenocams) has increased due to its low-cost investment, reduced size, easy set up installation, and the possibility of handling high-resolution near-remote data. Considering the widespread use of phenocams worldwide, our main goals here are: (i) to provide a step-by-step guide for phenocam set up in the tropics, reinforce its appliance as an efficient tool for monitoring tropical phenology and foster networking, (ii) to discuss phenocam applications for biological conservation, management, and ecological restoration. We provide the concepts and properties for image analysis which allow representing the phenological status of the vegetation. The association of a long-term imagery data with local sensors (e.g., meteorological stations and surface-atmosphere flux towers) allows a wide range of studies, especially linking phenological patterns to climatic drivers; and the impact of climate changes on plant responses. We show phenocams applications for conservation as to document disturbances and changes on vegetation structure, such as deforestation, fire events, and flooding and the vegetation recovery. Networks of phenocams are growing globally and represent an important tool for conservation and restoration, as it provides hourly to daily information of monitored systems spread over several sites, ecosystems, and climatic zones. Moreover, websites enriched by vegetation dynamic imagery data can promote science knowledge by engaging citizen science participation.

## 1 INTRODUCTION

The use of digital cameras to document plant changes is not novel. Photographs have been used to monitor landscape since 1965 by Hastings and Turner to verify changes in the ecosystem dynamics and structure of the arid southwest region of the US. Thompson et al. (2002) used photographic registers for the long-term study of glacial retreat in the Antarctic ice sheet. Repeated digital images have been used to document changes in cultural landscapes (Peñuelas & Boada 2003, Webb et al. 2007); to measure vegetation growth and biomass (Crimmins & Crimmins 2008, Graham et al. 2009); to detect plant stress and nitrogen status (Wang et al. 2004) and to monitor crops (Slaughter et al. 2008). More recently, the application for monitoring leaf exchanges patterns or leafing phenology (Richardson et al. 2007, 2009, Nagai et al. 2011) has brought the technique to the agenda of global change research and conservation (Richardson et al. 2013, Morellato et al. 2016).

Phenology is an integrative environmental science focused on monitoring, understanding, and predicting recurrent life cycles events of organisms, which are mainly related to climate (Morellato et al. 2016). Leafing is the plant phenological event that defines the growth season and controls crucial ecosystems processes such as, nutrient cycling, water storage, regulates productivity in terrestrial ecosystems, and the dynamics of carbon sequestration (Reich 1995, Baldocchi et al. 2005).

Phenological studies have been efficiently applied to track effects of environmental changes on plants and animals in temperate regions, answering questions about the current scenario of global climate change and stimulating the search for innovative tools of plant monitoring (Polgar & Primack 2011). Detect plant responses to environmental changes across tropical systems, especially in the Southern Hemisphere, is an important question on the global agenda since few studies have addressed trends related to global warming (Rosenzweig et al. 2008, Morellato et al. 2013, 2016, Chambers et al. 2013). However, the tropical high diversity of species precludes the observation of many species across several sites due to the intense human labor and costs (Alberton et al. 2014, Morellato et al. 2016).



The technique of repeated photographs to monitor plant phenology may overcome those difficulties. The application has increased due to its low-cost, reduced size, easy set up, and the possibility of handling high-resolution data, making digital cameras reliable tools for a wide range of ecological applications (Crimmins & Crimmins 2008, Morisette et al. 2009, Graham et al. 2010, Nasahara et al. 2015, Brown et al. 2016). Digital cameras for plant phenology observation, also called phenocams, have allowed the detection of leaf phenological events through the analysis of color changes along time. By quantifying the red, green, and blue (RGB) color channels, it is possible to estimate, for instance, leaf flushing and senescence, using the green and red channels, respectively (Ahrends et al. 2009, Morisette et al. 2009, Richardson et al. 2009).

The term “Near-surface remote phenology” consists in the use of sensors installed on the ground, as the phenocams, with the objective of monitoring ecosystem-scale vegetation changes. Digital cameras monitoring canopy vegetation has an important role by filling the “gap of observations” between satellite monitoring and the traditional on-the-ground phenology (Alberton et al. 2014, Brown et al. 2016, Morellato et al. 2016, Morisette et al. 2009). The use of imagery data over the traditional phenological observations allows simultaneous multi-sites monitoring, long-term monitoring collecting high-frequency data (daily, hourly), and reduced human labor fieldwork for data acquisition. Phenocams networks are already covering a wide range of ecosystems in the world (Richardson et al. 2013, Brown et al. 2016). The main networks websites are the Phenocam Network in the United States (<http://phenocam.sr.unh.edu> - as of Jan. 2017), the EuroPhen in Europe (<http://european-webcam-network.net> - as of Jan. 2017) and the Phenological Eyes Network (PEN) in Japan (<http://pen.agbi.tsukuba.ac.jp> - as of Jan. 2017). Together these initiatives combine more than 250 outdoor cameras (Brown et al. 2016, Nasahara & Nagai et al. 2015). For the tropics, we have the Tropidry project as a successful example of ecological project with intense multidisciplinary data collection, including the use of phenology towers with phenocams, covering dry tropical sites (<http://tropi-dry.eas.ualberta.ca/> - as of May 2017). In Brazil, the *e*-phenology Network (<http://www.recod.ic.unicamp.br/ephenology> - as of Jan. 2017) introduced in this paper, target the challenge of monitoring different vegetation types from dry forest, grasslands, and cerrado savannas to rainforests.

Therefore, considering the worldwide applications of phenocams in ecological studies, our main goals here are: (i) to provide a step-by-step guide for phenocam set up in the tropics, reinforce its appliance as an efficient tool for monitoring tropical phenology, (ii) to show how phenocams can provide key contributions to biological conservation, and (iii) to encourage this promising research field in Brazil and tropical areas based on the *e*-phenology project experience, and foster networking and e-science collaborative research.

## 2 PHENOCAMS AS TOOLS FOR THE MONITORING OF PLANT PHENOLOGY

Digital images are typically based on the RGB color model (red, green, and blue color channels). These channels encode the brightness values of the scene and can be combined in more than 16 million of colors, representing basically all the colors perceived by humans (Cheng 2001). Through the quantification of the RGB color channels, it is possible to calculate vegetation indices, which are related to leaf color changes representing the phenological status of the vegetation (Richardson et al. 2007, Sonnentag et al. 2012) (Fig. 1).

By capturing daily digital images of a given site, we derivate time series encoding RGB color changes over time. Thus, the leaf patterns can be described based, for instance, on the proportion of the green fraction in the images (Richardson et al. 2007). The association of digital imagery data with local sensors (e.g., meteorological stations and surface-atmosphere fluxes) uncovers a wide range of research opportunities, especially linking phenological patterns to climatic drivers, and analyzing long-term data to detect phenological shifts due to the impact of anthropogenic changes (Polgar & Primack 2011, Brown et al. 2016, Morellato et al. 2016).

The collection of daily vegetation color changes has been motivated also by the need to understand ecosystem-scale energy fluxes (Baldocchi et al. 2005, Richardson et al. 2007). Studies from temperate vegetation have found the start of the vegetation greenness controls the gross primary productivity (GPP) curves (Richardson et al. 2010, Migliavacca et al. 2011, Keenan et al. 2014). Therefore, temporal changes in the vegetation drive carbon exchange processes via influencing the photosynthesis process, respiration, and litter production (Peichl et al. 2014).

Most of the studies using phenocams have been developed in the Northern hemisphere, covering mainly deciduous forests (Richardson et al. 2007, 2009, Nagai et al. 2011). However, the application of repeated digital photographs is also efficient for the phenology monitoring of temperate grasslands (Inoue et al. 2015, Julitta et al. 2014), peatland (Peich et al. 2015), and evergreen forest (Toomey et al. 2015). Its reliability for tropical vegetation was recently validated for woody cerrado savanna (Alberton et al. 2014) and applied for tropical forest (Nagai et al. 2016, Lopes et al. 2016). The use of camera-derived vegetation indices in association with leaf demography-ontogeny models has been recently applied in the Amazon forest to investigate ecosystem-scale photosynthetic seasonality (Wu et al. 2016). However, there is still little focus on the species level analysis and on grasslands, mountains and other tropical vegetation.

### **3 PROCEDURES FOR PHENOLOGICAL MONITORING USING DIGITAL CAMERAS**

Digital cameras are reliable tools for the monitoring of vegetation because they have low price and easy setup, while providing high frequency and resolution data. Here, we introduce the main steps for phenology camera set up and basic information about image processing for data analysis (Fig. 1). A detailed protocol is available in the Supplementary Material.

#### *3.1 Camera set up and image settings*

In general, the camera is placed in a tower built in the middle of vegetation (Fig. 2a and b). The choice of the site and the field of view must maximize the vegetation to be monitored. Hemispherical lens cameras are reliable for capturing images of the canopy, reducing crown cover among individual species (Fig. 2c). Cameras should be positioned facing North - Northeast to maximize the light over the canopy and to minimize lens flare. Cameras can be set up on small towers, close to the ground, to capture landscape images (Fig. 2d and e) when the focus are shrublands, grasslands, or other vegetations with short canopies and across heterogeneous landscapes as rupestrian grasslands (Fig. 2f).

Different digital cameras have been used in repeated photography monitoring (see Sonnentag et al. 2012, Steenweg et al. 2017). Internet protocol (IP) cameras are ideal because they can be connected to a network and the image download performed remotely. For instance,

Stardot IP cameras record landscape images, have been successfully applied in temperate ecosystem monitoring, and were chosen as the standard camera for two of the major networks in North Hemisphere (Brown et al. 2016). Hemispherical lens (also called fish-eye) have been chosen for monitoring tropical vegetation sites (Alberton et al. 2014, Nagai et al. 2016) and by PEN (Nasahara & Nagai et al. 2015). The fish-eyes lens (360°) improve the selection of crowns with more precision and less covered areas (see Alberton et al. 2014).

We recommend capturing a high frequency of images (a set of 3-5 images per hour, from 6 a.m. to 6 p.m.), which provides fine-tuned information about phenology, a confident quality data collection, and also a high volume of data for light calibration, smoothing and the development of computational tools (Alberton et al. 2014, Almeida et al. 2014, 2015, 2016). When it is not possible due to storage constraints, we recommend taking at least one image per hour during the midday hours (10 a.m. to 2 p.m., for more details see the SM). A complete meteorological station or at least some minimum set of sensors (rain gauge, thermometers, and Photosynthetically Active Radiation (PAR) sensors) is an important additional component to phenology towers. If not possible, it is important to search for the closest meteorological station to the study site.

### *3.2 Color information analysis*

The image analysis usually depends on the definition of regions of interest (ROI). The ROI is a region within the input images defined for analysis (Fig. S1 and see Alberton et al. (2014). After defining a ROI, we can remove irrelevant areas, such as those lacking vegetation or depicting the tower structure. Therefore, we define the sample size as ROIs from crowns of several species, a population, a portion of the canopy, a community profile, or a habitat or vegetation type in a heterogeneous landscape (Fig. S1).

Several indexes have been applied to detect leaf color changes in time series of digital images exploring the RGB color channels (Richardson et al. 2007, Nagai et al. 2011, Sonnentag et al. 2012, Zhao et al. 2012, Zhou et al. 2013). Woebbecke (1995) was one of the first to calculate several indexes using RGB channels of digital images to evaluate which are better to detect weeds considering different types of soil, residue, and light conditions. A normalized index called RGB

chromatic coordinates (RGB<sub>cc</sub>) was developed by Giles et al. (1987) and it is considered up to now the most efficient to detect the color of plants in relation to their background (Sonnentag et al. 2012).

The RGB chromatic coordinates (R<sub>cc</sub>, G<sub>cc</sub>, and B<sub>cc</sub>) is a normalized index, defined by dividing each component (R, G, or B) by the sum of all components (R + G + B):

(1)

$$R_{cc} = \frac{R}{R + G + B}$$

$$G_{cc} = \frac{G}{R + G + B}$$

$$B_{cc} = \frac{B}{R + G + B}$$

The Excess Green (ExG) index is also applied in color time series analysis (Sonnentag et al. 2012). This metric has proved to be a consistent color index, able to distinguish between green plants and their background (soil, residue), as well as to minimize variations in illumination, enhancing the green signal of the plants (Woebbecke 1995).

(2)

$$ExG = 2G - (R + B)$$

After performing the RGB color extraction and the vegetation index computation, it is necessary a data filtering to minimize noise in the time-series information (RGB<sub>cc</sub>) caused by illumination effects of seasonal changes and time of day (Sonnentag et al. 2012). To that end, the 90th percentile value is calculated from all daily values in a 3-day window (Sonnentag et al. 2012).

#### 4. PHENOCAMS CONTRIBUTIONS FOR BIOLOGICAL CONSERVATION

The importance of phenology for biodiversity conservation and ecological restoration has been recently explored by Morellato et al. (2016) and Buisson et al. (2017) respectively, with a special focus on conservation of tropical systems (Morellato et al. 2016). Phenology is recognized as an essential biodiversity variable required for study, report, and manage biodiversity (Pereira et al., 2013), pointing out the potential of remote sensing phenology and phenocam networks.

Therefore, near-surface phenology with cameras can play a key role for biodiversity conservation at several scales. On the other hand, phenology has not yet been included in the formal guidelines or recommendations for ecological restoration by SER (Society for Ecological Restoration), but Buisson et al. (2017) bring a fresh perspective on why and how phenology should be incorporated to ecological restoration guidelines. Systematic, long-term phenological monitoring programs are needed at local to large spatial scales to ensure conservation and effective management and for the success of ecological restoration programs.

### **Plant responses to climate**

The search for the main factors triggering plant phenology is of paramount importance for better understanding plant responses facing climate changes and the conservation of species to ecosystems (Polgar & Primack 2011, Morellato et al. 2016). Plant phenology triggers remain poorly understood across the tropics. Therefore, systematic and long-term phenological observations are needed at large spatial scales for tropical ecosystems (Morellato et al. 2013, Chambers et al. 2013). However, high diversity of species precludes the observation of many species across several sites, due to the intense human labor and high costs (Alberton et al. 2014, Morellato et al. 2016).

The *e*-phenology network was built based first on a core cerrado area where we tested and validated all protocols considering the local long-term cerrado phenology project (Alberton et al. 2014). We expanded the network, integrating flux measurements towers and larger research projects, choosing sites across a seasonality gradient. We are reaching out several key tropical vegetations from Amazon forest, Atlantic rainforest, Cerrado, to Caatinga, tracking changes and investigating drivers for phenology. Also, within the Amazon-FACE project, we will be able to monitor vegetation phenological responses to CO<sub>2</sub> enrichment on Amazon forest. Elevated CO<sub>2</sub> (eCO<sub>2</sub>) would affect photosynthesis biochemistry leading to an increase of productivity for tropical ecosystems. (Norby et al. 2016)

Through daily color changes information in association with daily measurements of climatic variables (Fig. 3a and b), a wide range of questions might be investigated. For instance,

modeling leaf phenology patterns of multi sites and time series to investigate drivers of leaf development and senescence. Another important approach is in the ecosystem scale studies. Vegetative phenology has a significant role in the Dynamic Global Vegetation Models (DGVM). These models are based on a coupled information between plant biogeography and biogeochemical process to simulate ecosystem fluxes and climate shifts in a climatic change scenario (Noormets, 2010). In the tropics, understand leaf phenological stages is essential to better estimate measurements of gross primary productivity (GPP), because there is a gap of knowledge about drivers of carbon fluxes (Restrepo-Coupe 2017). Camera derived color time series might provide high frequency and quality information to understand photosynthetic seasonality as the vegetation responses and feedbacks to a changing climate (Richardson et al 2013, Restrepo-Coupe et al 2017).

### **Beyond phenology: repeated photography monitoring for conservation, management and restoration**

Phenocams can monitor one to several tropical vegetation types and species with a reduced manpower and high temporal scale (daily basis). Near remote monitoring systems using digital repeated photograph can be also one of the most powerful tools to observe and detect shifts on vegetation structure to land-use changes, disturbances, climate warming and pre- and post-restoration of natural and agroecosystem. Changes detected by cameras such as events of deforestation, fire, flooding, vegetation recovery after disturbances, and species invasion, likely help to take fast and appropriated conservation and management measures.

For example, digital cameras from *e*-phenology project have been integrated into the Brazilian long-term ecological program (PELD) conducted in the fire-prone vegetation mosaic of *campo rupestre* of Serra do Cipó, Minas Gerais, Southeastern Brazil (PELD CRSC, Fernandes 2016, [http://labs.icb.ufmg.br/leeb/index\\_peld.html](http://labs.icb.ufmg.br/leeb/index_peld.html)). The resulting time series are the first description of the leafing patterns across four *campo rupestre* vegetations (Borges *in prep.*). The phenocam monitoring system has also allowed detecting the time of fire occurrence and vegetation recovery after fire in real time at Serra do Cipó (Fig. 4) (Alberton et al. *in prep.*).

Through a set of daily photographs, it is possible to visualize the process of post fire vegetation recovery showing the regrowth response of this wet grassland vegetation (Fig. 5, see legend for more details), also tracked by the camera derived vegetation index (Fig. 5 a and b). Anthropogenic fire may threaten even the *campo rupestre* fire-prone vegetation, since the time, intensity, and frequency of human-induced fires impose additional stress on plants (Alvarado et al. 2017). The time lapse cameras are therefore accessible tools to monitor, manage and prevent fire.

Phenological information has a key role in restoration process, such as timing improvement for restoration implementation, provides suitable indicator to assess restoration success, and allows schedule restoration actions through continuum monitoring (Buisson et al. 2017). Phenocams can improve restoration by matching key steps raised by Buisson et al. (2017) for restoration projects, such as: identifying and monitoring fire regime; using phenological metrics as indicators of restoration success, optimizing fire management; and improving restoration monitoring with continuum vegetation record that might be used to evaluate predefined goals and future practices of the restoration process. Successful restoration ideally requires previous knowledge of the vegetation structure and species' phenology, a critical information to define restoration practices, assess the post-restoration success, plan management actions and improve new restoration procedures (e.g., Carter and Blair 2012).

### **Biological conservation in a digital world**

Phenocams networks built in interactive websites enriched with dynamic vegetation imagery may engage volunteer participation of population to generate science knowledge, playing an important role in education for conservation and citizen science programs. One example is the project called Season Spotter (Kosmala et al. 2016). Through volunteer participation involving tasks as detection of flowers and new leaves in an image database, the project has gained useful science knowledge. The main results were related to: detection of reproductive phenophases; selection of tree individuals by the users, facilitating the scaling from organisms to ecosystems; and the validation of phenological observations by the images, which improves the development of new algorithms for automatic detection. Besides, these initiatives go beyond scientific knowledge valuing citizen participation and boosting population interest for nature conservation.



The growth of cameras sensors technology has the potential to build global networks able to monitor not only plants, but also all biodiversity. A worldwide system with standardized metadata, field protocols, and databases developed by scientific community and integrated with citizen science participation, is one of the actions needed to achieve the objectives of the Convention on Biological Diversity's 2011-2020 plans. Current applications to collect ecological data using remote cameras have been used by eMammal and TEAM projects (Steenweg et al. 2017). Examples of focal species included were: grizzly bear (*Ursus arctos*), tragopan (*Tragopan blythii*), wolverine (*Gulo gulo*), mule deer (*Odocoileus hemionus*), coyote (*Canis latrans*), African bush elephant (*Loxodonta Africana*), and others. The studies involved not only biodiversity measurements, but also the underlying causes of biodiversity changes (e.g., impacts of climate change and trophic interactions in a cervid in Brodie et al. 2014; evaluating landscape connectivity in Barrueto et al. 2014; camera surveys including large carnivores and herbivores communities, and the effects in food webs respectively in Ripple et al. 2014, Hooper et al. 2012; and evaluate reproductive success in female grizzly bears in Fisher et al 2014).

The ongoing addition of new devices, high-resolution data survey, and sensor networks has improving the quality of data collected in biological studies, but at the same time increasing the magnitude of scientific data collected. Big data is one important challenge for biodiversity conservation. This leads to the next generation of scientific problems, which will require the establishment of multidisciplinary teams (Hey & Hey 2006). *e-Science* is about the collaboration of key areas of science, as a network of research initiative focused on the specification and implementation of a set of tools and technologies capable of supporting, improving, and speeding up data analysis, knowledge discovery, and decision making (Hey & Hey 2006). The e-phenology was designed as an e-Science project, and we present some examples of our research on digital camera image analysis and the tools devised in the context of e-Science collaboration. We use machine learning algorithms to plant species identification concerning the identification of each tree crown of the vegetation in the image (Almeida et al. 2014). The tool helps important steps from plant identification in the field to the definition of new ROIs for the image analysis speeding up the process and allowing grouping similar species in an image even with no previous

identification, a useful tool for conservation remote monitoring systems. Through the years, several approaches have been proposed to support the identification of individuals of particular species (Almeida et al. 2015, Almeida et al. 2016, Faria et al. 2016a, Faria et al. 2016b). We developed a tool to map the greenness in the image time series, the chronological percent map by PhenoVis (Leite et al. 2016). A database specific for phenological data was also developed in the framework of *e-phenology* project to deal big-data issues and improve access to information (Mariano et al, 2016).

## 5 Conclusions

We have presented a first-step protocol with the main information about repeated photography method and set up (Supplementary Material), to increase the potential of a new tropical phenology research program in this promising area, fostering network and collaboration (Box 1).

Phenology has its well-defined role in conservation biology (Morellato *et al.* 2016) and, in this context, we demonstrate that near-surface remote phenology and phenocam networks are powerful tools for conservation. Besides the capability of a fine temporal resolution associated with wide spatial monitoring coverage, phenocams can bring new information for management and restoration practices at several sites and environments, and can also be applied in education for conservation and citizen science through websites with phenological databases enriched by imagery data. The creation of phenology networks, still lacking for tropical countries, will broaden and fine-tune research on phenological drivers and long-term monitoring to investigate and model the impacts of climate changes in the tropics. The pioneer *e-phenology* is the venue to reach those goals in Brazil. Lastly, phenocams could be easily integrated as a monitoring tool at any conservation unit, aggregating invaluable information of wide use for researchers and managers, from phenology to ecosystem dynamics and changes over space and time.

## 6 Acknowledgements

Our research is supported by the São Paulo Research Foundation (FAPESP), the FAPESP - Microsoft Research Virtual Institute (grants #2010/52113-5, #2011/51523-8 and #2013/50155-0). LPCM and RST receive a Research Productivity Fellowship from CNPq (grants #306243/2010-5 and #306587/2009-2). FAPESP also provided fellowships to BA (grants #2014/00215-0 PhD and #2016/01413-5 BEPE), LFC (grant #2014/13354-8), BDB (grant #2014/07700) and GM (grant #2011/51523-8). GM receives a PhD fellowship from CNPq (grant #162312/2015-6). We have also been benefited from funds of CNPq, CAPES, and FAPESP (grants #2007/52015-0, #2007/59779-6, #2009/18438-7, #2010/51307-0, and #2016/06441-7). We thank the members of the Phenology Laboratory from UNESP, and RECOD Laboratory from UNICAMP and all our collaborators, especially: Dr Magna Soelma from Embrapa Petrolina and leader of the Caatinga Flux Project, Dr. Humberto Rocha and his technical-team from the IAG (USP), Dr GW Fernandes, Reserva Vellozia and the PELD-SC and research team supported by CNPq, the Cedro Company, the Parque Nacional da Serra do Cipó, private land owners, and the *Instituto Florestal de São Paulo* for allowing the research in the ecological stations, reserves and sites.

## 7 REFERENCES

- Ahrends, H., Etzold, S., Kutsch, W., Stoeckli, R., Bruegger, R., Jeanneret, F., Wanner, H., Buchmann, N., Eugster, W., 2009. Tree phenology and carbon dioxide fluxes: use of digital photography at for process-based interpretation the ecosystem scale. *Clim. Res.* 39, 261–274.
- Alberton, B., Almeida, J., Helm, R., da Torres, S.R., Menzel, A., Morellato, L.P.C., 2014. Using phenological cameras to track the green up in a cerrado savanna and its on-the-ground validation. *Ecol. Inform.* 19, 62–70.

Almeida, J., dos Santos, J.A., Alberton, B., da S. Torres, R., Morellato, L.P.C., 2014.

Applying machine learning based on multiscale classifiers to detect remote phenology patterns in cerrado savanna trees. *Ecol. Inform.* 23, 49–61.

Almeida, J., Santos, J. A., Alberton, B., Morellato, L. P. C., Torres, R. S. 2015.

Deriving Vegetation Indices for Phenology Analysis using Genetic Programming. *Ecol. Inform.*, 26:61–69.

Almeida, J., Santos, J. A., Alberton, B., Morellato, L. P. C., Torres, R. S. 2015.

Phenological visual rhythms: Compact representations for fine-grained plant species identification, *Pattern Recognit. Lett.*, vol. 81, pp. 90–100.

Almeida J, Pedronette, D.C.G., Alberton, B., Morellato, L. P. C., Torres, R. S. 2016b.

Unsupervised Distance Learning for Plant Species Identification. *IEEE J. Sel. Top. Appl. EARTH Obs. Remote Sens.*, 9:1–14.

Alvarado, S. T., Fornazari, T., Cóstola, A., Morellato, L. P. C., & Silva, T. S. F. 2017.

Drivers of fire occurrence in a mountainous Brazilian cerrado savanna: Tracking long-term fire regimes using remote sensing. *Ecological Indicators*, 78, 270-281.

Baldocchi, D.D., Black, T.A., Curtis, P.S., Falge, E., Fuentes, J.D., Granier, A., Gu, L.,

Knohl, A., Pilegaard, K., Schmid, H.P., Valentini, R., Wilson, K., Wofsy, S., Xu, L.,

Yamamoto, S., 2005. Predicting the onset of net carbon uptake by deciduous forests

with soil temperature and climate data: A synthesis of FLUXNET data. *Int. J.*

*Biometeorol.* 49, 377–387.

Barrueto M, Ford AT, and Clevenger AP. 2014. Anthropogenic effects on activity patterns of wildlife at crossing structures. *Ecosphere* 5: art27.

Brodie J, Post E, Berger J, and Watson F. 2014. Trophic interactions and dynamic herbivore responses to snowpack. *Clim Change Response* 1: 4.

Brown, T.B., Hultine, K.R., Steltzer, H., Denny, E.G., Denslow, M.W., Granados, J., Henderson, S., Moore, D., Nagai, S., Sanclements, M., Sánchez-Azofeifa, A., Sonnentag, O., Tazik, D., Richardson, A.D., 2016. Using phenocams to monitor our changing earth: Toward a global phenocam network. *Front. Ecol. Environ.* 14, 84–93.

Buisson, E., Alvarado, S.T., Le Stradic, S., Morellato, L.P.C., 2016. Plant phenological research enhances ecological restoration. *Restor. Ecol.* 1–8.

Chambers, L.E., Altwegg, R.E.S., Barbraud, C., Barnard, P., Beaumont, L.J., Crawford, R.J.M., Durant, J.M., Hughes, L., Keatley, R.M., Low, M., Morellato, P.C., Poloczanska, E.S., Ruoppolo, V., Vanstreels, R.E.T., Woehler, E.J., Wolfaardt, A.C. 2013. Phenological Changes in the Southern Hemisphere. *Plos One*, 8: 1-12

Cheng, H. D., Jiang, X. H., Sun, Y., & Wang, J. 2001. Color image segmentation: advances and prospects. *Pattern recognition*, 34(12), 2259-2281.

Crimmins, M.A., Crimmins, T.M., 2008. Monitoring plant phenology using digital repeat photography. *Environ. Manage.*, 41:949–958.

Fernandes, G.W., 2016. Ecology and conservation of mountaintop grasslands in Brazil. Springer, Switzerland. DOI 10.1007/978-3-319-29808-5

Faria, F.A., Almeida, J., Santos, J. A., Alberton, B., Morellato, L. P. C., Torres, R.S. 2016a. Fusion of time series representations for plant recognition in phenology studies. *Pattern Recognit. Lett.*, 0:1–10.

Faria, F.A., Almeida, J., Santos, J. A., Alberton, B., Morellato, L. P. C., Torres, R.S. 2016b. Time series-based classifier fusion for fine-grained plant species recognition. *Pattern Recognit. Lett.*, 81:101–109.

Fisher, J.T., Wheatley, M., Mackenzie, D. 2014. Spatial patterns of breeding success of grizzly bears derived from hierarchical multistate models. *Conserv Biol* 28: 1249–59.

Gillespie AR, Kahle AB & Walker RE, 1987. Color enhancement of highly correlated images. II. Channel ratio and “chromaticity” transformation techniques. *Remote Sens. Environ.*, 22:343–365.

Graham, E.A., Riordan, E.C., Yuen, E.M., Estrin, D., Rundel, P.W., 2010. Public Internet-connected cameras used as a cross-continental ground-based plant phenology monitoring system. *Glob. Chang. Biol.* 16, 3014–3023.

Graham, E.A., Yuen, E.M., Robertson, G.F., Kaiser, W.J., Hamilton, M.P., Rundel, P.W., 2009. Budburst and leaf area expansion measured with a novel mobile camera system and simple color thresholding. *Environ. Exp. Bot.* 65, 238–244.

Hastings, J.R., Turner, R.M. 1965. The changing mile. An ecological study of vegetation change with time in the lower mile of an arid and semiarid region. Tucson, Arizona: Univ. Arizona Press.

Hey, T., Hey, J., 2006. e-Science and its implications for the library community. *Libr. Hi Tech*, 24:515–528.

Hooper, D.U., Adair, E.C., Cardinale, B.J., 2012. A global synthesis reveals biodiversity loss as a major driver of ecosystem change. *Nature* 486: 105–08.

Inoue, T., Nagai, S., Kobayashi, H., Koizumi, H., 2015. Utilization of ground-based digital photography for the evaluation of seasonal changes in the aboveground green biomass and foliage phenology in a grassland ecosystem. *Ecol. Inform.* 25, 1–9.

Julitta, T., Cremonese, E., Migliavacca, M., Colombo, R., Galvagno, M., Siniscalco, C., Rossini, M., Fava, F., Cogliati, S., Morra di Cella, U., Menzel, A., 2014. Using digital camera images to analyse snowmelt and phenology of a subalpine grassland. *Agric. For. Meteorol.* 198–199, 116–125

Keenan, T.F., Darby, B., Felts, E., Sonnentag, O., Friedl, M.A., Hufkens, K., O’Keefe, J., Klosterman, S., Munger, J.W., Toomey, M., Richardson, A.D., 2014. Tracking forest

phenology and seasonal physiology using digital repeat photography: A critical assessment. *Ecol. Appl.* 24, 1478–1489.

Kosmala, M., Crall, A., Cheng, R., Hufkens, K., Henderson, S., Richardson, A., 2016. Season Spotter: Using Citizen Science to Validate and Scale Plant Phenology from Near-Surface Remote Sensing. *Remote Sens.* 8, 726

Leite, R.A., Schnorr, L., Almeida Jr, Torres, R.S., Alberton, B., Morellato, LPC, & Comba, J. 2016. PhenoVis: A tool for visual phenological analysis of digital camera images using chronological percentage maps. *Inf. Sci. (Ny)*, 372:181-195.

Lopes, A.P., Nelson, B.W., Wu, J., Graça, P.M.L. de A., Tavares, J.V., Prohaska, N., Martins, G.A., Saleska, S.R., 2016. Leaf flush drives dry season green-up of the Central Amazon. *Remote Sens. Environ.* 182, 90–98.

Mariano, G., Morellato, LPC, Almeida J. Alberton, B, Camargo, MGG & Torres, RS. 2016. Modeling plant phenology database: Blending near-surface remote phenology with on-the-ground observations. *Ecol. Eng.*, 91:396–408.

Migliavacca, M., Galvano, M., Cremonese, E., Rossini, M., Meroni, M., Sonnentag, O., Cogliati, S., Manca, G., Diotri, F., Busetto, L., Cescatti, A., Colombo, R., Fava, F., Mora Di Cella, U., Pari, E., Siniscalco, C., Richardson, A.D. 2011. Using digital repeat digital photography and eddy covariance data to model grassland phenology and photosynthetic CO<sub>2</sub> uptake. *Agric. Forest Meteorol.* 151:1325-1337



Morellato, L.P.C., Camargo, M.G.G., Gressler, E., 2013. A review of plant phenology in South and Central America, in: Schwartz MD (ed.). *Phenology: An Integrative Environmental Science*. Springer Netherlands. p. 91–113.

Morellato L.P.C., Alberton B., Alvarado S.T., Borges B.D., Buisson E., Camargo M.G.G., Cancian L.F., Carstensen D.W., Escobar D.F.E., Leite P.T.P., Mendoza I., Rocha N.M.W.B., Silva T.S.F., Soares N.C., Staggemeier V.G., Streher A.S., Vargas B.C., Peres C.A. 2016. Linking plant phenology to conservation biology. *Biol. Conserv.*, 195:60-72.

Morisette, J.T., Richardson, A.D., Knapp, A.K., Fisher, J.I., Graham, E.A., Abatzoglou, J., Wilson, B.E., Breshears, D.D., Henebry, G.M., Hanes, J.M., Liang, L. 2009. Tracking the rhythm of the seasons in the face of global change: phenological research in the 21st century. *Front. Ecol. Environ.* 7: 253-260

Nagai, S., Maeda, T., Gamo, M., Muraoka, H., Suzuki, R., Nasahara, K.N., 2011. Using digital camera images to detect canopy condition of deciduous broad-leaved trees. *Plant Ecol. Divers.* 4, 79–89.

Nagai, S., Ichie, T., Yoneyama, A., Kobayashi, H., Inoue, T., Ishii, R., Suzuki, R., Itioka, T., 2016. Usability of time-lapse digital camera images to detect characteristics of tree phenology in a tropical rainforest. *Ecol. Inform.* 32, 91–106.

Nasahara, K.N., Nagai, S., 2015. Review: Development of an in situ observation network for terrestrial ecological remote sensing: the Phenological Eyes Network (PEN). *Ecol. Res.*, 30:211–223.

Peichl, M., Sonnentag, O., Nilsson, M.B., 2014. Bringing Color into the Picture: Using Digital Repeat Photography to Investigate Phenology Controls of the Carbon Dioxide Exchange in a Boreal Mire. *Ecosystems*, 18:115–131.

Peñuelas, J., Boada, M., 2003. A global change-induced biome shift in the Montseny mountains (NE Spain). *Glob. Chang. Biol.*, 9:131–140.

Pereira, H.M., Ferrier, S., Walters, M., Geller, G.N., Jongman, R.H.G., Scholes, R.J., Bruford, M.W., Brummitt, N., Butchart, S.H.M., Cardoso, A.C., Coops, N.C., Dulloo, E., Faith, D.P., Freyhof, J., Gregory, R.D., Heip, C., Höft, R., Hurtt, G., Jetz, W., Karp, D.S., McGeoch, M.A., Obura, D., Onoda, Y., Pettoirelli, N., Reyers, B., Sayre, R., Scharlemann, J.P.W., Stuart, S.N., Turak, E., Walpole, M., Wegmann, M., 2013. Essential biodiversity variables. *Science* 339, 277–278.

Polgar, C.A. & Primack, R.B., 2011. Leaf-out phenology of temperate woody plants: From trees to ecosystems. *New Phytol.*, 191:926–941.

Reich, P.B., 1995. Phenology of tropical forests: patterns, causes, and consequences. *Can. J. Bol.*, 73:164-174.

Restrepo-Coupe, N., Levine, N. M., Christoffersen, B. O., Albert, L. P., Wu, J., Costa, M. H., Galbraith D., Imbuzeiro H., Martins, G., Araujo, A. C., Malhi, Y. S. Zeng, X., Moorcroft, P., Saleska, S. R. 2017. Do dynamic global vegetation models capture the seasonality of carbon fluxes in the Amazon basin? A data-model intercomparison. *Global change biology*, 23(1), 191-208.

Richardson, A.D., Jenkins, J.P., Braswell, B.H., Hollinger, D.Y., Ollinger, S.V., Smith, M.L. 2007. Use of digital webcam images to track spring green-up in a deciduous broadleaf forest. *Oecologia* 152: 323–334

Richardson, A.D., Braswell, B.H., Hollinger, D.Y., Jenkins, J.P., Ollinger, S.V. 2009. Near-surface remote sensing of spatial and temporal variation in canopy phenology. *Ecol. Appl.* 19: 1417–1428

Richardson, A.D., Black, T.A., Ciais, P., Delbart, N., Friedl, M.A., Gobron, N., Hollinger, D.Y., Kutsch, W.L., Longdoz, B.B., Luyssaert, S., Migliavacca, M., Montagnani, L., Munger, J.W., Moors, E., Piao, S., Rebmann, C., Reichstein, M., Saigusa, N., Tomelleri, E., Vargas, R., Varlagin, A., 2010. Influence of spring and autumn phenological transitions on forest ecosystem productivity. *Philos. Trans. R. Soc. B Biol. Sci.* 365, 3227–3246.

Richardson, A.D., Keenan, T.F., Migliavacca, M., Ryua, Y., Sonnentag, O., Toomey, M. 2013. Climate change, phenology, and phenological control of vegetation feedbacks to the climate system. *Agric. Forest Meteorol.* 169: 156– 173

Ripple, W. J., Estes, J. A., Beschta, R. L., Wilmers, C. C., Ritchie, E. G., Hebblewhite, M., Schmitz, O. J. 2014. Status and ecological effects of the world's largest carnivores. *Science*, 343: 1241-1244.

Rosenzweig, C., Karoly, D., Vicarelli, M., Neofotis, P., Wu, Q., Casassa, G., Menzel, A., Root, T.L., Estrella, N., Seguin, B., Tryjanowski, P., Liu, C., Rawlins, S., Imeson, A. 2008. Attributing physical and biological impacts to anthropogenic climate change. *Nature* 453: 353-357

Slaughter, D.C., Giles, D.K., Downey, D., 2008. Autonomous robotic weed control systems: A review. *Comput. Electron. Agric.*, 61:63–78.

Sonnentag, O., Hufkens, K., Teshera-Sterne, C., Young, A.M., Friedl, M., Braswell, B.H. 2012 Digital repeat photography for phenological research in forest ecosystems. *Agric. Forest Meteorol.*, 22: 152

Thompson, L.G., Mosley-thompson, E., Davis, M.E., Henderson, K.A., Brecher, H.H., Zagorodnov, V.S., Mashiotta, T.A., Lin, P., Mikhalenko, V.N., Hardy, D.R., 2015. Kilimanjaro Ice Core Records : Evidence of Holocene Climate Change in Tropical Africa. *Science* (80-. ). 298, 589–593.

Toomey, M., Friedl, M.A., Frohling, S., Hufkens, K., Klosterman, S., Sonnentag, O., Baldocchi, D.D., Bernacchi, C.J., Biraud, S.C., Bohrer, G., Brzostek, E., Burns, S.P.,

Coursolle, C., Hollinger, D.Y., Margolis, H.A., McCaughey, H., Monson, R.K., Munger, J.W., Pallardy, S., Phillips, R.P., Torn, M.S., Wharton, S., Zeri, M., Richardson, A.D., 2015. Greenness indices from digital cameras predict the timing and seasonal dynamics of canopy-scale photosynthesis. *Ecol. Appl.* 25, 99–115.

Webb, R.H., Leake, S.A., Turner, R.M., 2007. The ribbon of green: change in riparian vegetation in the southwestern United States. University of Arizona Press.

Woebbecke, D.M., Meyer, G.E., Vonbargen, K., Mortensen, D.A. 1995. Color indexes for weed identification under various soil, residue, and lighting conditions. *Trans. ASAE* 38: 259–269

Wu, J., Albert, L.P., Lopes, A.P., Restrepo-Coupe, N., Hayek, M., Wiedemann, K.T., Guan, K., Stark, S.C., Christoffersen, B., Prohaska, N., Tavares, J. V., Marostica, S., Kobayashi, H., Ferreira, M.L., Campos, K.S., Silva, R. da, Brando, P.M., Dye, D.G., Huxman, T.E., Huete, A.R., Nelson, B.W., Saleska, S.R., 2016. Leaf development and demography explain photosynthetic seasonality in Amazon evergreen forests. *Science* (80-. ). 351, 972–976.

Zhao, J., Zhang, Y., Tan, Z., Song, Q., Liang, N., Yu, L., Zhao, J., 2012. Using digital cameras for comparative phenological monitoring in an evergreen broad-leaved forest and a seasonal rain forest. *Ecol. Inform.* 10, 65–72.

Zhou, L., He, H.L., Sun, X.M., Zhang, L., Yu, G.R., Ren, X.L., Wang, J.Y., Zhao, F.H.,  
2013. Modeling winter wheat phenology and carbon dioxide fluxes at the ecosystem  
scale based on digital photography and eddy covariance data. *Ecol. Inform.* 18, 69–78.

**8 BOX****Recommended Procedures**

- install phenocams in a wide variety of landscapes and ecosystems, taking advantage of low-cost cameras when necessary
- use electricity in the towers whenever it is possible, when setting up powerful cameras
- choose sensors with good seal capability, adopt careful procedures in the installation process considering problems as excess of humidity, sun exposition, and invasion by bugs
- standardize images formats and settings for multi-site monitoring
- integrate your phenocams to a network, facilitating wide-scale collaborative research, enabling combine information across biomes and climatic zones, and widening the applicability for biodiversity conservation
- set up new cameras in association with sites where long-term studies are being developed, such as the Brazilian Long-term Ecological Research PELD (*Projetos Ecológicos de Longa Duração*) and flux towers
- explore tools or even create your own software and scripts for images processing, to support and facilitate data analysis
- establish a e-Science collaborative research with computer scientists, improving visual and image analysis techniques, big-data management, investing in a new generation of “hybrid” scientists with a multidisciplinary profile and larger spectrum of actuation.

## 9 FIGURES LEGENDS

**Figure 1** Workflow showing the steps of a protocol for implementation of a repeated photograph monitoring system.

**Figure 2** Brazilian sites from e-phenology network and their different phenology monitoring setups for woody and open vegetation: (a) sketch of the hemispherical lens camera mounting design for forest canopy; (b) camera set up in the field; (c) sample image captured by the hemispherical lens digital camera in the cerrado *sensu stricto* vegetation (Itirapina, SP); (d) sketch of the camera mounting design for a landscape perspective; (e) camera set up in the field, (f) sample image of the heterogeneous landscape in the Serra do Cipó mountain range (Santana do Riacho, Minas Gerais State, Brazil).

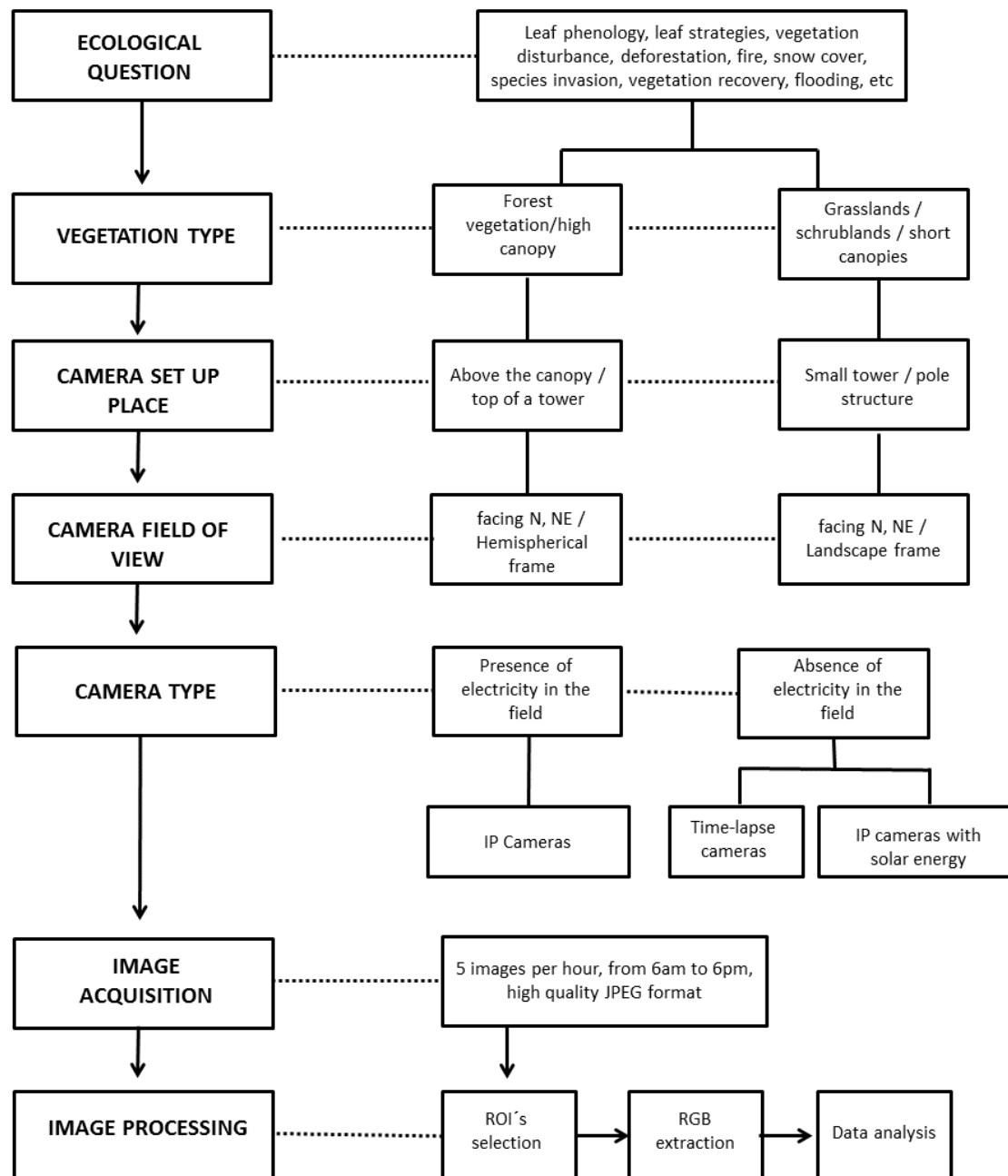
**Figure 3** Vegetation canopy greenness, as quantified by green chromatic coordinate (Gcc; green dots) using phenocam imagery, in relation to local seasonal patterns of daily precipitation (blue bars) and air temperature (black line). In both graphics, Gcc values represent a 3-day window filter time-series of the growing season length (from day of the year DOY 152 to 214, 2013-2014) of two cerrado physiognomies, a grassland savanna vegetation (a) and a woody savanna (b), both in the same location in Itirapina city, São Paulo State, Brazil.

**Figure 4** Sequence of photographs showing timing of burn and the post-fire vegetation recovery process in a heterogeneous landscape, Serra do Cipó, Minas Gerais, Southeastern Brazil.

**Figure 5** Visual analysis showing post-fire vegetation recovery scheme of a wet grassland habitat (red dots selection) in Serra do Cipó, southern part of the Espinhaço Mountain Range, Minas Gerais State, Brazil. The graphic represents a camera derived vegetation index (Excess Green) from a set of photographs showing the green curve after a fire event. (a) first day after fire event; (b) vegetation recovered after 34 days; Green dots represent Green daily value of the 90th percentile of the Excess green index (90th ExcG) from digital images taken every hour (6:00 h to 18 h)



Fig. 1



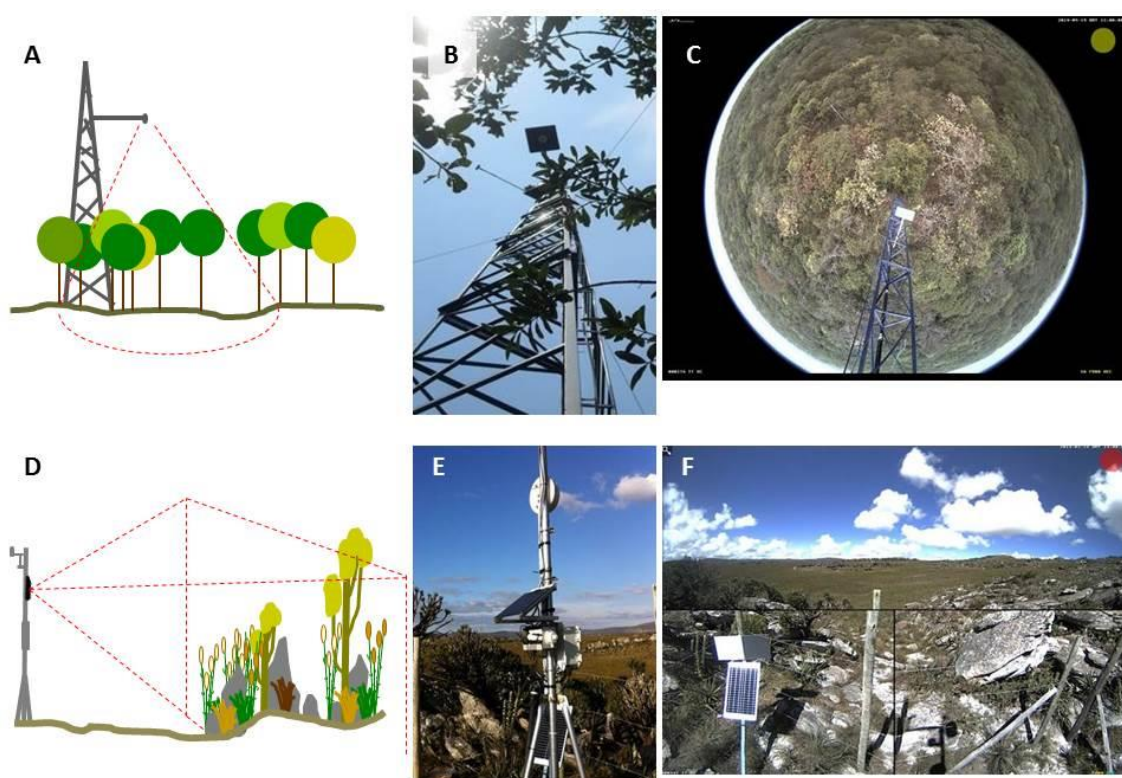
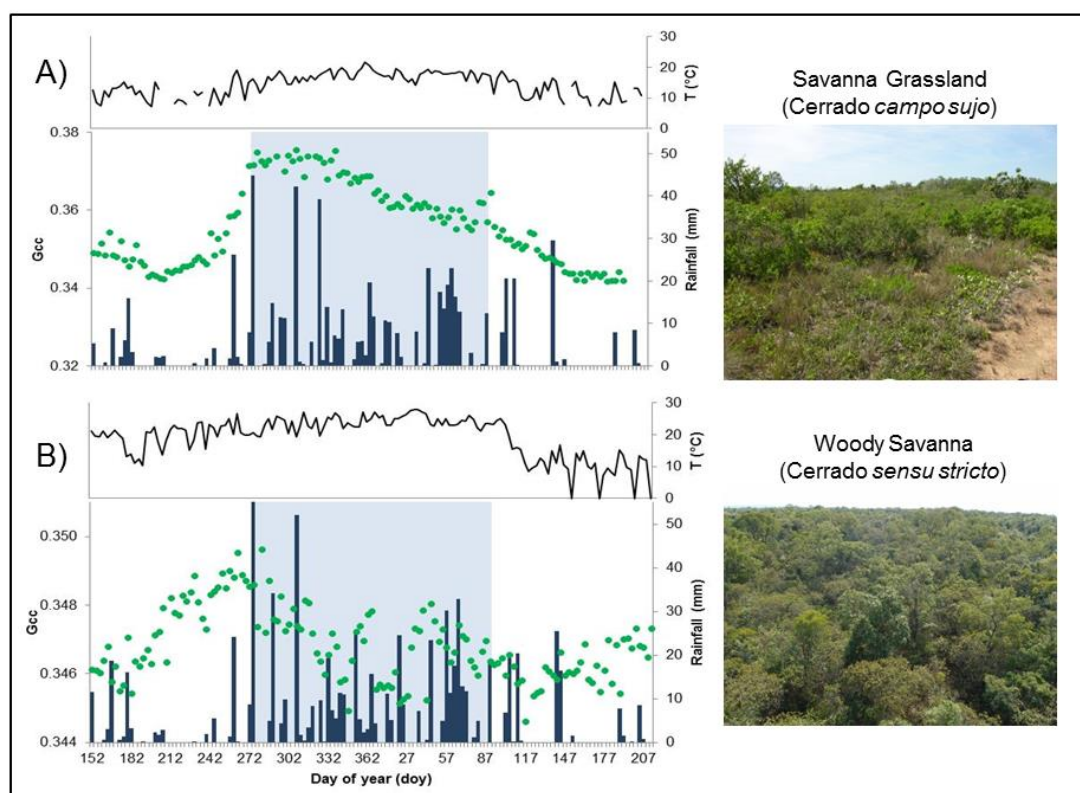
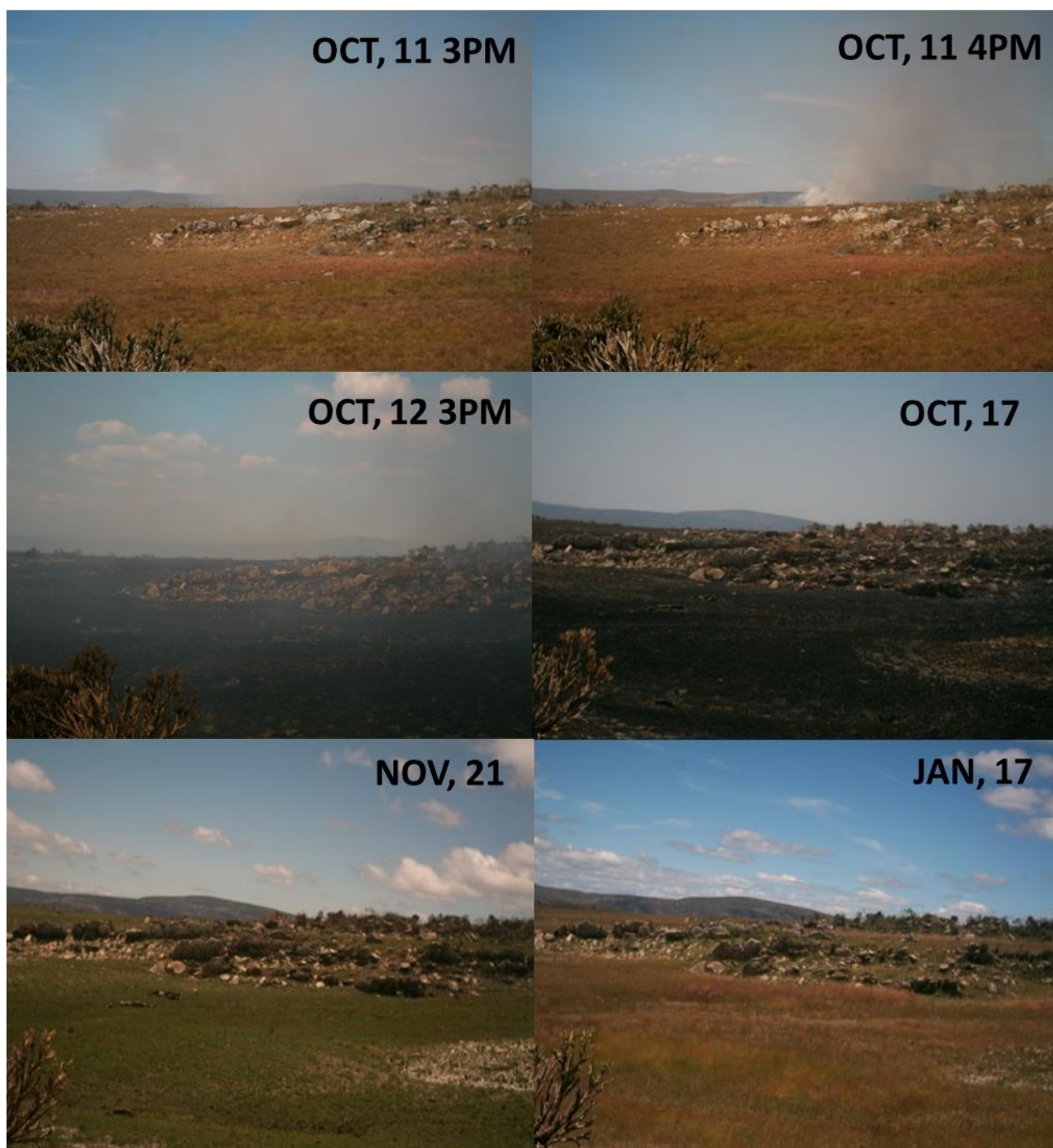
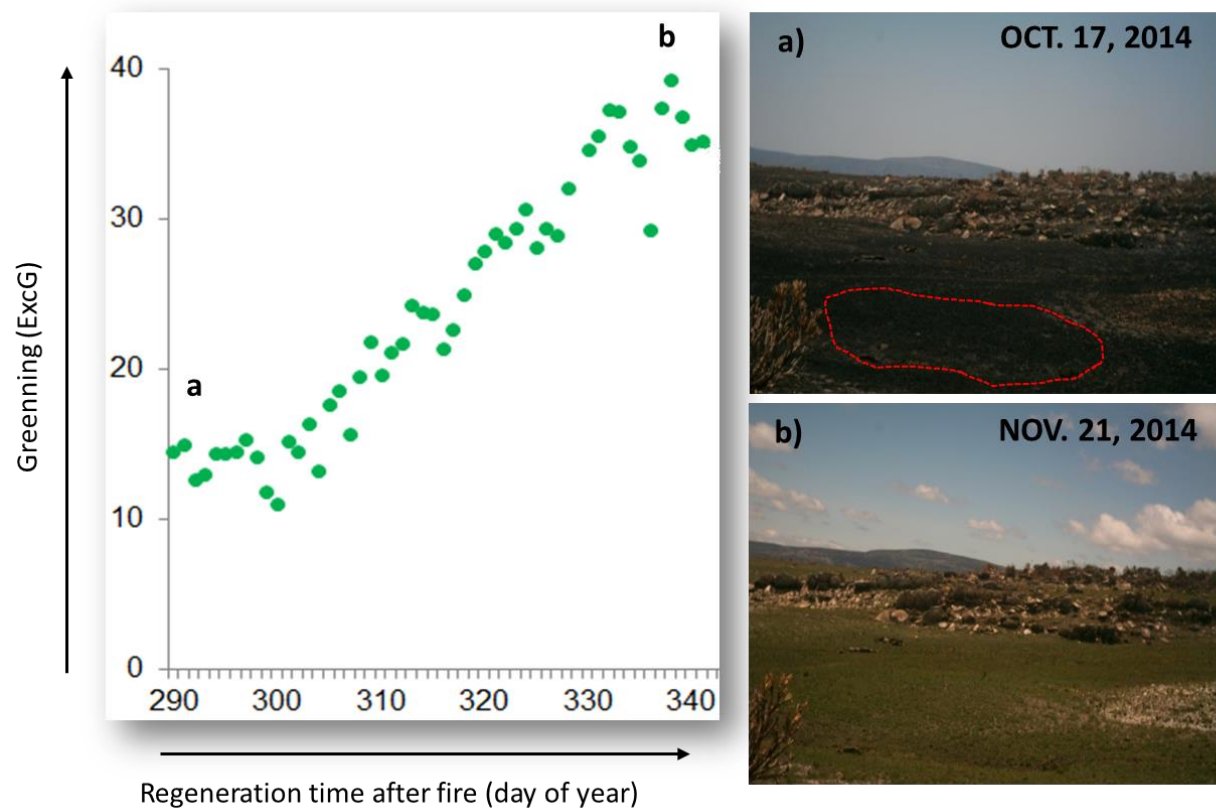
**Fig. 2**

Fig. 3



**Fig. 4**

**Fig. 5**

## Section 2

## LEAFING PATTERNS AND DRIVERS ACROSS SEASONALLY DRY TROPICAL COMMUNITIES

Bruna Alberton<sup>1</sup>, L., Ricardo da S. Torres<sup>2</sup>, Thiago S. F. Silva<sup>3</sup>, Humberto Rocha<sup>4</sup>, Magna Soelma<sup>5</sup>,  
Patricia C. Morellato<sup>1</sup>

<sup>1</sup> Laboratório de Fenologia, Universidade Estadual Paulista (Unesp), Instituto de Biociências, Rio Claro, São Paulo, Brazil

<sup>2</sup> Institute of Computing, University of Campinas, Brazil

<sup>3</sup> Ecosystem Dynamics Observatory, Universidade Estadual Paulista (Unesp), Instituto de Geociências e Ciências Exatas, Rio Claro, São Paulo, Brazil;

<sup>4</sup> Instituto de Astronomia, Geofísica e Ciências Atmosféricas, USP, São Paulo (Brasil)

<sup>5</sup> EMBRAPA Empresa Brasileira de Pesquisas Agropecuárias, Semi Árido, Petrolina, Pernambuco (Brasil)

### 1 ABSTRACT

The study of phenology is a key component to track vegetation transitions that respond to climate changes, since plants are mainly constrained by the environment. Water and light availability are considered the main abiotic limitations for leaf production in the tropics. The search for answering questions about the environmental triggers of tropical phenology has stimulated the application of new tools for plant monitoring. Digital cameras have been applied for the monitoring of leaf temporal changes in seasonal tropical environments. We conducted, for the first time, a multi-site phenological monitoring across tropical vegetations using leaf phenology derived by digital cameras. An analytical procedure was used to unravel the main drivers influencing leaf phenology time series across seasonally dry vegetations using digital cameras to describe the leafing patterns of seasonally dry tropical vegetation communities. Our main questions are: (i) Can community growing seasons be detected by near-surface remote cameras in tropical vegetation sites? (ii) Do the growing seasons vary across different seasonality conditions? (iii) Do the environmental factors driving leaf phenology differ and how they vary across sites? Growing seasons from each vegetation type were delineated using derivatives. From our results, we demonstrated that water and light were the most important predictors



for the leaf phenological patterns across the sites. Water-plant relationships were more important for the Caatinga community, and light, through day-length seasonality, had more influence in the leafing patterns of the cerrado communities. An interesting outcome was the increasing variability of phenological signals (leafing behaviors) and predictor-response relationships (distinct smooth functions) across sites where seasonality was less pronounced and/or distinct species life-form were capable of overcoming drought-effects, such as deep root systems trees from woodland cerrado compared to grassy cerrado.

## 2 INTRODUCTION

The patterns of temporal leaf replacement or vegetative phenology is of major importance to understand ecosystem processes, such as carbon, water, and energy exchanges controlling seasonal cycles of photosynthetic activity (REICH, 1995; RÖTZER et al., 2004; RICHARDSON et al., 2013). Leafing patterns of plant species define the growing season of a vegetation community, and are mainly constrained by environmental cues, from temperature in temperate regions to water in the tropical realm (REICH, 1995). Therefore, the study of leaf phenology is a key component to track vegetation transitions that respond to climate changes (POLGAR and PRIMACK, 2011; MORELLATO et al., 2016). There is high heterogeneity among leafing patterns across tropical forests, mostly related to the intensity and length of the dry season (REICH, 1995, CAMARGO et al., 2018). A wide range of studies are necessary to identify the main factors regulating leaf phenology across the tropics and, therefore, understand vegetation dynamics, and efficiently forecast climate change impacts (POLGAR and PRIMACK, 2011; CHAMBERS et al., 2013). The majority of phenology studies have accessed reproductive and leafing patterns through the direct observation of individual trees (MORELLATO et al., 2013, 2016; ABERNETHY et al., 2018), and try to access the cues for leaf fall and leaf flushing.

Water and light availability have been considered the main abiotic cues regulating the time and periodicity of leaf production in the tropics (VAN SCHAIK; TERBORGH; WRIGHT, 1993; WRIGHT and VAN SCHAIK, 1994; MORELLATO et al., 2000; RIVERA et al., 2002; BORCHERT et al., 2015; CAMARGO et al., 2018). A major factor regulating the length of growing season and species synchronicity is the seasonal availability of water. Seasonal tropical forests, with increasing dry season



severity, present a marked annual periodicity of the community leaf flushing and senescence, and as a consequence, a greater proportion of deciduous species (MURPHY and LUGO, 1986; REICH, 1995, WILLIAMS et al., 2008). In fact, in the seasonally-dry tropical forests or dry forests, nearly the entire assemblage of individuals of their species lose all leaves in a synchronic deciduous behavior during the dry season (REICH and BORCHERT, 1984; REICH, 1995; QUESADA et al., 2009; SINGH and SINGH, 1992). Under a reduced rainfall seasonality and less pronounced dry season, species and individuals may display different degrees of deciduity, forming communities with a widely range of leafing behaviors, that may change in proportion according to conditions of soil moisture, topography (BORCHERT 1994; RIVERA et al., 2002), and intensity of dry season (CAMARGO et al., 2018 and references therein). Regarding light, the consistent signal of day length seasonality in the tropics would have a major importance towards higher latitudes, triggering the input of new leaves (WRIGHT and VAN SCHAIK 1994; RIVERA et al., 2002). Day length seasonality has also been reported as a trigger for the onset of the community early leaf flushing in the dry season, anticipating the rains, in seasonal tropical vegetations, as semideciduous forests and savannas (RIVERA ET AL., 2002; MORELLATO ET AL., 1989, SINGH and KUSHWAHA, 2005, HIGGINGS et al., 2011; CAMARGO et al., 2018). Conversely, in tropical rain or moist forests, where moisture is not a constrain, elevated irradiance due reduced cloud cover during the dry season can promote a species synchronicity of leaf production (VAN SCHAIK; TERBORGH; WRIGHT, 1993; WRIGHT and VAN SCHAIK, 1994, RIVERA et al., 2002).

Plant life forms have direct implications on water and light species adaptation and thereby on leafing phenology (ARCHIBALD and SCHOLES, 2007, HIGGINGS et al., 2011, WHITECROSS et al., 2017). The temporal niche separation hypothesis proposed by Scholes and Walker (1993) indicates that trees would deploy leaves earlier than grasses, even before the start of the growing season, given trees a competitive advantage over grasses. Trees can input new leaves still in the dry season due to stored carbon reserves and their better capacity to access and accumulate groundwater sources (rooting depths), allowing plant growth when radiation is maximum (ELLIOTT ET AL., 2006; EAMUS, 1999; ARCHIBALD and SCHOLES, 2007). On the contrary, grasses are much more dependent on the rainfall seasonality given their shallow root system, and can present multiple peaks of leaf production along the

growing season as a fast response to rainfall events in seasonally dry environments (BATALHA and MANTOVANI, 2000; ARCHIBALD and SCHOLE, 2007).

A comprehensive survey of phenology data and trends over the Southern Hemisphere (SH) highlights the gaps in the phenology knowledge of tropical species and ecosystems (CHAMBERS et al., 2013). The search for answering questions about the environmental triggers of tropical phenology and the potential changes in the current scenario of climatic changes has stimulated the application of new tools of plant monitoring. Imagery based on satellite and digital cameras imagery has been considered alternative methods for successfully monitoring plant greening continuously across the landscape (RICHARDSON et al., 2007; MORISETTE et al., 2009). In particular, repeated photographs taken by digital cameras (phenocams) have been applied for the monitoring of leafing temporal changes in seasonal tropical environments (ALBERTON et al., 2014; ALBERTON et al., 2017; MOORE et al., 2017). The application of phenocams to monitor leaf phenology reduces human labor, increases accuracy by eliminating possible discrepancies related to observer subjectivity, improves temporal resolution to hourly/daily basis and the spatial resolution, allowing simultaneous monitoring of different vegetations and sites (CRIMMINS and CRIMMINS, 2008, RICHARDSON et al., 2007; BROWN et al., 2016; ALBERTON et al., 2017).

We conducted, for the first time, a phenological multi-site monitoring across Neotropical seasonal vegetations using digital cameras or phenocams to describe the leafing patterns of four seasonally dry tropical vegetation communities: three cerrado savanna vegetations and one xeric shrubland, the Brazilian Caatinga. We combined the camera-derived phenology with local environmental variables to evaluate the constraints imposed by temperature, water, and light on the patterns of leaf flushing and senescence across different seasonality condition and vegetation structure. Our main questions are: (i) Can we detect distinct community growing seasons across the four tropical vegetations? We expect leafing season at caatinga responding to immediate rainfall while cerrado may present a more variable response due to mild and shorter dry season; wood cerrado would have reserves or access to underground water and may be able to start leafing earlier in the dry season, before the first rains; (ii) Do the growing seasons vary according to the vegetation structure (woody-grassy) and degree of seasonality? We expect a cerrado vegetation response differs between woody and grassy dominated

vegetations in accordance with the temporal niche separation hypothesis (SCHOLLES and WALKER, 1993), while Caatinga response is restricted to the first rains starting the wet season; and (iii) Do the main environmental drivers of start and length of growing season differ according to environmental seasonality and vegetations? We expect light and accumulated rainfall to be the main drivers for cerrado and immediate rainfall the cue for the start of caatinga growing season. The proportion of woody species and individuals at each leaf exchange strategy (deciduous, semideciduous, or evergreen) may also vary among the vegetations studied and influence the plant responses to environmental cues and were considered in our analyses (EAMUS, 1999; WILLIAMS et al., 2008, CAMARGO et al., 2018).

### 3 METHODS

#### 3.1 Sites description

Sites are geographically distributed across two main vegetational domains (VELOSO et al., 1991) or biomes (OLSON et al., 2001), the Caatinga or desert and xeric shrubland and, the Cerrado or grasslands, savannas and shrublands, respectively (see map in Fig. 1). We collected near-surface leaf phenology of four sites, one from Caatinga and three belonging to different vegetation types of Cerrado. Table 1 summarizes the study sites characteristics and phenocam monitoring period analyzed here. The four study sites are part of the e-phenology network (<http://www.recod.ic.unicamp.br/ephenology/client/index.html#/home> - As of June 2018).

Caatinga - The first site is the exclusive Brazilian vegetation, the **caatinga**, a xeric, sclerophyllous vegetation located in the Semi-Arid region distributed mostly in Northeastern Brazil, denominated the xeric shrubland Biome according to Olsen et al., (2001). The area of phenocam monitoring has approximately 600 ha, 342 m a.s.l, and belongs to the *Reserva Legal da Embrapa Semiárido* (9°05'S; 40°19' W), Petrolina municipality, Pernambuco State, Northeastern Brazil. (KILL, 2017). The climate is classified as semiarid (KÖPPEN, 1931) and, according to the normal climate from 1970 to 2014 (source: Experimental station of Bebedouro, 10km from the site), the total annual mean precipitation is 510 mm distributed mainly from January to April, and the mean annual temperature is 26.2°C. During our three-years of study, annual mean precipitation was around 260mm, and annual mean temperature 27.05°C (Fig. 2A), characterizing a period even drier than usual. Local vegetation is

composed of xerophilous trees and shrubs and a continuous herbaceous layer of species adapted to the xeric and harsh conditions. The plant species belong mostly to the Fabaceae, Euphorbiaceae, Poaceae, and Cactaceae families, and the discontinuous canopy reaches proximally 5 m high (KILL, 2017).

Cerrado - The other three sites encompass different vegetation physiognomies of Cerrado, a neotropical savanna, from a wooded grassland or scrubland to a dense woodland, all part of the Cerrado domain or Cerrado *sensu lato* classification (OLIVEIRA-FILHO and RATTER, 2002) and included in the grasslands, savannas, and shrublands Biome according to Olsen et al., (2001) (Fig. 1). All three sites are in the São Paulo state, Southeastern Brazil: the second and third at Itirapina municipality and the last one at Santa Rita do Passa Quatro (Fig. 1). Climate classification is humid subtropical (KÖPPEN, 1931), with a cool dry winter (mean monthly temperature of 18°C) and a hot wet summer (mean monthly temperature of 32°C), and a total annual precipitation of 1524 mm. A cluster analysis using 30 years of climatic data (1982-2012) showed four seasons: a rainy season (November to March), a transitional rainy-to-dry season (April), a dry season (May to August), and a transitional dry-to-rainy season (September to October) (ESCOBAR et al., 2018). Historic climatic information was made available by the Centro de Recursos Hídricos e Estudos Ambientais (CRHEA-EESC/USP), about 15 km distant from the study sites. Local environmental variables at each site were daily collected from meteorological stations (Hobo U30 USB Weather Station Data Logger) set up in the phenological towers at each vegetation site. Sensors were connected to a central data logger constantly sending data information to a web platform ([www.hobolink.com](http://www.hobolink.com)) via GSM. Although cerrado scrubland and cerrado woodland sites belong to the same original vegetation patch (see below) and are just about 10km distance, a meteorological station was placed within each physiognomy. Gap filling for second and third sites were obtained from a nearby meteorological station (CRHEA-EESC/USP).

Our second monitoring site, the **cerrado campo sujo** (“dirty grassland”), is a wooded savanna or shrubland vegetation physiognomy dominated by an herbaceous layer with scattering shrubs and small trees (OLIVEIRA-FILHO and RATTER, 2002, BATALHA and MANTOVANI, 2001). The study site is part of the Itirapina Ecological Station (22°13'23"S;47°53'02.67"W), encompassing 2,300 ha, 700 m a.s.l. A local vegetation survey found a proportion of 79% of species from the herbaceous-shrubland layer, dominated by Asteraceae, Fabaceae, Poaceae, and Cyperaceae families, and 21% of

small trees species most from families, Fabaceae, Myrtaceae, and Melastomataceae (TANNUS et al., 2006). During the three years of monitoring, local climatic time series show a mean annual total precipitation of 1,272 mm and mean annual temperature of 23.5°C (Fig. 2B).

The third study site is located in a nearby private area of 260 hectares and 700 m a.s.l. (22°10'52" S, 47°52'25" W), belonging to the same original “patch” of cerrado that once covered all that region. The associated vegetation is a **cerrado sensu stricto**, a woody cerrado savanna dominated by trees and shrubs from 3 to 8 m tall, sometimes reaching up to 12 m, with crowns arranged in a discontinuous canopy, and a presence of a fair amount of herbaceous vegetation (REYS et al., 2013). From the local 5-year meteorological data (2011 - 2015), mean annual total precipitation was 1,478 mm and mean annual temperature 22.9 °C (Fig. 2C). Plant species composition is distributed mostly in the Myrtaceae, Fabaceae, and Malpighiaceae families (REYS et al., 2013), and vegetation was classified as a semideciduous, according to the species long-term leaf exchange strategies (CAMARGO et al., 2018).

The last site it is also a woody cerrado formation that belongs to the Reserva Ecológica Pé-de-Gigante (PEG), located within the Parque Estadual do Vassununga, at Santa Rita do Passa Quatro county. The PEG reserve comprehends a contiguous area of 1,060 ha and 649 m a.s.l. (47° 34' – 47° 41' W; 21° 36' – 21° 44' S), covered by a heterogeneous landscape of savanna vegetations, from open grasslands to woody dense cerrado. The seasonal humid subtropical climate (KÖPPEN, 1931) presents a dry season from May to September and the wet season from October to April, a total annual rainfall of 1,499 mm and mean temperature 21.5°C (BATALHA and MANTOVANI, 2000). Our local climatic data from 2013 to 2015 shows a total annual average precipitation of 1,150 mm and mean air temperature of 22.5°C (Fig. 2D). The study site, where the camera system is located, is a transition from woody cerrado to a cerradão (OLIVEIRA-FILHO and RATTER, 2002), that we classified as a **dense cerrado**, characterized by a discontinuous canopy, nearly without an herbaceous layer and high density of shrubs and trees (RIBEIRO and WALTER, 1998). The site has a predominant woody layer reaching 10m to 15m high, composed mainly of the species *Ptedoron pubecens*, *Copaifera langsdorfii*, and *Anadenanthera peregrina* var. *falcata* from the Fabaceae family. The closed canopy results in a shading and cooler understory covered by a scattered herbaceous component (PIVELLO et al., 1998).

The vegetation communities studied here differ in their seasonality, from a very constrained climate in the Caatinga domain with an 8-month dry season to less restricted conditions of the Cerrado domain physiognomies with a 6-month dry season length. Sites also differ in the structure of vegetation, from a dominant to equivalent herbaceous component (cerrado *campo sujo* and caatinga) to woody formations of cerrado *sensu stricto* (woody cerrado and dense cerrado). To facilitate the identification of the four studied sites and vegetation, hereafter we will name site one to four according to the vegetation monitored, respectively, as follows: caatinga, cerrado shrubland, woody cerrado, and dense cerrado. We can order our study sites into a sequence that corresponds to their degree of seasonality and woody cover, from caatinga and cerrado shrubland, to woody cerrado and dense cerrado.

### 3.2 Camera set up and near-surface phenology monitoring

For each one of the study sites, a digital hemispherical lens camera Mobotix Q 24 (Mobotix AG — Germany) was placed at the top of a phenological tower attached to an extension arm facing northeast at a mean vertical distance of 10 m from the tree canopy, except for the cerrado shrubland, where the camera system is based 3 meters distance from the vegetation in a landscape standing point (see ALBERTON et al., 2017). Energy supply is a 12V battery charged by a solar panel. Cameras are configured to automatically take a daily sequence of five JPEG images (at  $1280 \times 960$  pixels of resolution) in the first 10 min of each hour, from 6:00 to 18:00 h (UC-3; Universal Time Coordinated) as described in Alberton et al., (2014). The camera system installation occurred at different times among sites (see Table1). For data analysis, we used time series spanning from 2013 to 2015 for all sites, with the exception of the woody cerrado, where time-series started at 2011. Due to a sequence of energy supply issues along the years in the woody cerrado site, we gap filled sequences of more than 7 days with no images recorded using an algorithm that we created (see Supplementary material for more details) in R language (R CORE TEAM, 2017).

Raw images were firstly processed with a visual filter to remove interferences, disturbing the canopy viewing. Image analysis was conducted as described by Richardson et al., (2009), Ahrends et al., (2009) and Alberton et al., (2014). We carried out field trips for plant identification to compile a list of the main species captured by the field of view of the cameras (see Supplementary material).

Then, we matched the plant identification information with the crowns identified within the images. This information, associated with imagery visual inspections, was essential for the classification of individual crowns into plant functional groups based on plant leaf exchange strategies.

Regions of interest (ROIs) were defined for each site considering that time series from the whole image can encompass phenological signals from many species with different leafing exchange strategies (deciduous, semideciduous, and evergreen) and dominant life forms (woody vs grassy). Thus, the ROIs defined for the community took into account the woody and grassy-dominated vegetation, and individuals' crowns of woody species were grouped by leaf exchange strategy following Camargo et al., (2018) into deciduous, semideciduous, and evergreen. Since Camargo et al., (2018) did not consider in their functional classification the time of leaf flushing, we add that information and refine their proposed strategy splitting the deciduous and semideciduous strategies into two categories. All ROIs' names, description, and their coverage (% of pixels) in relation to the vegetation community ROI, are follow: community = region representing the community or the complete image area, excluding tower and the exposed ground; deciduous = ROIs from crowns that represent individuals of deciduous species (caatinga = 19.80% / cerrado shrubland = 16.16% / woody cerrado = 5.44% / dense cerrado = 21.5%), fast deciduous = ROIs representing individuals of deciduous fast-responsive species (caatinga = 7.20%); semideciduous wet = ROIs representing individuals of semideciduous species and start of wet season leaf flushing (woody cerrado = 5.77% / dense cerrado = 2.50%); semideciduous dry = ROIs from crowns that represent individuals of semideciduous species, and a dry season leaf flushing (woody cerrado = 3.90%); evergreen = ROIs from crowns that represent individuals of evergreen species (woody cerrado = 1.15% / dense cerrado = 6.17%); and grass = ROIs representing the herbaceous layer of the cerrado scrubland (23.70%).

We analyzed the ROIs of each image in terms of the contribution of the relative brightness of the green, red, and blue color channels (RGB chromatic coordinates in WOEBBECKE et al., (1995)) in relation to the primary colors (red, green, and blue). The normalized RGB chromatic coordinate ( $RGB_{cc}$ ) index is referred to as the most suitable index to detect leaf color changes, and the most efficient to suppress light variation (GILLESPIE et al., 1987; WOEBBECKE et al., 1995). The Green chromatic coordinate ( $G_{cc}$ ) index has been applied to relate changes on the vegetation greenness,

tracking phenological transitions of leaf development as well as ecosystem photosynthetic dynamics and the search for environmental cues (RICHARDSON et al., 2009; AHRENDTS et al., 2009; MIGLIAVACCA et al., 2011; ALBERTON et al., 2014; MOORE et al., 2017; RICHARDSON et al., 2018). We calculated the normalized index of the green color channel ( $G_{cc}$ ), as:

$$Total_{avg} = Red_{avg} + Green_{avg} + Blue_{avg}$$

$$G_{cc} = \frac{Green_{avg}}{Total_{avg}}$$

The  $G_{cc}$  index was calculated for all images taken by the camera at each day. One single measurement was extracted by taking the 90<sup>th</sup> percentile of the values every three days, a procedure that has been shown to minimize noise in the color channels series ( $RGB_{cc}$ ) related to the illumination effects of seasonal changes and time of the day (SONNENTAG et al., 2012).

### 3.3 Defining the growing season

We extracted some phenological metrics for the definition of the growing seasons. There are several methods for modelling phenological time series (e.g., thresholds, derivatives, smoothing algorithms, model fitting) allowing the detection of phenological transitions (DE BEURS and HENEERY, 2010). A critical issue raised for most of the methods is the lack of a statistical error structure that promotes an analysis of the significance or robustness of the model (DE BEURS and HENEERY, 2010). Tropical vegetation time series are often more difficult to deal with, because they are mostly rain-green systems, where vegetation green-up responses are coupled with precipitation events, resulting in noisier observations (DE BEURS and HENEERY, 2010). In the attempt to overcome these problems, we propose an approach for the calculus of derivatives with significant chances of occurrence along the time. The first step was the fitting of Generalized Additive models (GAM) over the  $G_{cc}$  community time series. Time (sequence of days) was used as a smoother independent variable. Assuming that errors are not independent, an inherent condition of time series structure, we nested an auto-regressive moving average (ARMA) of order 1, as a correlation structure, into our fitting models. Then, we build confidence intervals (95%) for the rate changes along the curve applying montecarlo simulations to perform the curve fitting and calculate the time derivatives (MOULIN, 1996) that significantly differed from zero, making sure that changes were happening in



these particular regions. From the derivatives calculations, we were able to extract phenological metrics corresponding to vegetation transitions along the curves. Based on previous classification of land surface phenology time series (ZHANG et al., 2003; JONSSON and EKLUNDH, 2004) and to conform to the classical nomenclature of direct observation phenological variables (MORELLATO et al., 2000), we define the phenological metrics as:

Start of growing season (SOS) – represents the beginning of the growing season. It is measured as the first day detected by the significant derivative from the total seasonal amplitude on the left side of the curve.

End of growing season (EOS) - represents the termination of the growing season. It represents the last day detected by the significant derivative from the total seasonal amplitude on the right side of the curve.

Length of growing season (LOS) – represents the duration of growing season and it is calculated as the difference SOS and EOS.

Peak of the growing season (POS) – represents the highest percentage greenness or species flushing new leaves. It is measured as the highest value of the seasonal curve.

### **3.4 Environmental cues of leafing phenology**

Photoperiod, temperature, water availability, and a water-energy interaction were chosen as the potential environmental factors to characterize the leafing phenological patterns across sites. The set of explanatory variables was selected based on a priori assumptions and published literature on tropical plant leaf phenological responses to seasonal environmental conditions summarized in the introduction. Day-length, the number of sunlight hours, was chosen as the variable to represent the seasonality of photoperiod and was calculated using the latitude of each location (*geosphere* package for R). The variables of daily maximum and minimum temperature were used to calculate the variation of temperature amplitude along the year, as:

$$T_{max} - T_{min} = T_{amp}$$

All other local climatic variables were derived from the weather station at each particular site. Rainfall effects were tested using the variables of cumulative precipitation (mm) from the last 30 days

(*Rainfall\_cum30*), and lagged rainfall events from the last seven (*Rainfall\_Lag7*) and 30 (*Rainfall\_Lag30*) days.

The water and energy interactions were calculated to evaluate the effects of the dry season intensity through the Cumulative Water Deficit (CWD) calculation, as:

$$CWD_n = CWD_{(n-1)} + P_n - ET_n$$

The  $CWD_n$  is the computed cumulative water deficit for a given time  $n$ , where  $P_n$  is the precipitation of the day (mm) and  $ET_n$  is the evapotranspiration of the day ( $\text{mm day}^{-1}$ ). When a positive value of  $(P-ET)$  is identified, zero is used to set a starting point. Every time  $CWD_n \geq 0$ , then  $CWD_n$  is set to zero again (more details in STEPHENSON, 1998; MURRAY-TORTAROLO et al., 2016; JAMES et al., 2013). The interactions between the vegetation evapotranspiration demand induced by the energy in the system (able to heat and/or stress the plant) and the water availability reaching the soil are explained by the climatic water balance (see STEPHENSON, 1990 and STEPHENSON, 1998). When the evaporative demand does not meet the available water, a deficit situation occurs, which explains the CWD, a measure of absolute drought (STEPHENSON, 1998; MURRAY-TORTAROLO et al., 2016; JAMES et al., 2013).

Environmental variables were aggregated in a three-day 90<sup>th</sup> percentile window approach (SONNENTAG et al., 2012), the same applied for the  $G_{cc}$  time series.

### 3.5 Data Analysis

Phenological metrics extracted from  $G_{cc}$  community time series were identified and compared in terms of the growing season dynamics among the different vegetations. To investigate the relationship between leafing phenology and environmental cues, we fitted Generalized Additive Mixed Models (GAMMs) using the  $G_{cc}$  time series (community, leaf exchange strategy, and dominant life-form) separately as dependent variables (Y) and the abiotic variables as the explanatory terms (X). The main reason for the additive models application in this study is related to its potential of dealing with nonlinear functions among multiple covariates and its reliability of handling time-series structural data in ecological studies and vegetation modelling analysis (FRESCINO et al., 2001; WOOD, 2011; YANG et al., 2012).

The general formula of a GAM is:

$$g(\mu) = \alpha + \sum_{j=1}^P f_j x_j$$

where  $g$  is a specified link function and  $(\mu)$  the expected mean response,  $\alpha$  is the linear model components, and  $f_j$  are smooth functions of the covariates  $x_j$  (Yang et al. 2012). Basically, generalized additive models aim to maximize the quality of prediction of Y, from various exponential families, by estimating non-parametric functions of the predictor variables (X), through a connection with the dependent variable established by a link function (WOOD, 2011, MARRA and WOOD, 2011). The degree of smoothing of an additive model is expressed by the effective degrees of freedom (edf), which mean that the higher the edf, the lower is the linearity of the curve interaction.

Initially, scatterplots among covariates were verified for the identification of linear and non-linear relationships. After running a multicollinearity inspection, we entered all the chosen explanatory variables in a full model for each dependent variable. The variable selection, which means a smooth component selection when dealing with the additive models, was carried out using a shrinkage approach. Shrinkage procedures are considered continuous processes where variable selection is running in one single step, opposed to other used algorithms as the subset selection and stepwise approaches (MARRA and WOOD, 2011). The method here applied, named double penalty, relies on the fact that the space of the smoother (a spline basis) can be decomposed into the components of a range space and a null space. The method penalizes both components shrinking them to zero. By introducing a penalty in the null space, the model smoothing parameter estimator is able to select the most significant terms from the model (for more details about the method, see MARRA and WOOD, 2011). By analyzing the approximate smooth estimators from the models, we can verify the terms that are not influential, with no significance achieved at  $P < 0.001$ . Finally, to understand how each term is related with the response variable, we plot the partial fits of each smoother parameter and evaluate the edf and F-test from the model's outcomes.

## 4 RESULTS

### 4.1 Growing seasons detection across sites

The  $G_{cc}$  index calculated for the community time series tracked the seasonality of leafing patterns among all sites (Fig. 3). The timing of vegetation phenological transitions was found for all the cycles, using the derivatives (Table 2). In general, growing seasons differed among vegetations in relation to initial and end of growing season dates, length of growing season and the shape of the growing season curves related to the leafing response of the species community. According to the expectations, there was a constraint of leaf production to the wet period for extreme seasonal vegetation (caatinga), as well as the grassy dominated vegetation (cerrado shrubland).

The start of the growing season (SOS) occurred earlier among the cerrado physiognomies, ranging from day 147 to day 239. The woody cerrado was the vegetation with the earliest SOS (mean day 163), mid of June, in the dry season. The dense cerrado and the cerrado shrubland were more similar, with a SOS mean date on day 221 and day 233, respectively, but the first with a more marked seasonality. The start of the season in the Caatinga occurred by the end of October (mean day 296), only after the first rainfall events. Vegetation biomes reached the peak of season (POS), in the average, 78 days after the SOS. Caatinga and dense cerrado were the first to reach the highest values of the growing season (69 and 67 days, respectively), while for the cerrado shrubland and the woody cerrado the average mean was of 80 to 96 days for the POS, respectively. For the two woodland cerrado vegetations, POS occurred earlier in the transition from the dry to the wet periods. Conversely, for the caatinga and cerrado shrubland, POS dates were within the wet season.

The end of season (EOS) was faster and earlier in the caatinga vegetation, with just about a month of difference (31 days) between the first and the second cycles (2013/2014 = 183, 2014/2015 = 214). The length of the season (LOS) was also the shortest in caatinga, with a mean LOS of 274 days. The green-down was more abrupt in the xeric caatinga, with the EOS right after the end of the wet season. The cerrado physiognomies showed a lower transition and extended green-down curve, reaching their lowest values from the mid to the end of the dry season (Fig. 3). Woody cerrado presented a different EOS among the years, ranging from mid-May (day 134) to mid-June (day 170), and a LOS from 314 to 342 days. There was one LOS registered for the grassland and the dense cerrado sites, because there was only one complete year cycle. They presented the longest LOS, with 345 days.

## 4.2 Model predictions

Predictor variables entered as smooth terms in most of the models produced. Two of the explanatory variables (*Rainfall\_lag7* and *Tamp*) showed a linear relationship when modelling ROIs data from the caatinga and the woody cerrado, respectively. In general, GAM procedure produced models with medium to high explanation ( $R^2$  values ranging from 0.29 to 0.88). The variables day-length and the cumulative water deficit (*CWD*) were the most recurrent predictors with the highest significance achieved among models across all vegetations (Table 3). All the plots from figures 5 and 6 show the significant variables resulted from the GAM models explaining leaf phenology time-series. The most important relationships are described with more details below.

The *CWD* and rainfall (*lag7* and *cum\_30*) showed the main relationships with the caatinga community pattern of greening (Fig. 5A). The partial fits between predictors and  $G_{cc}$  demonstrated a vegetation sensitive to low values of precipitation rates and increases of  $G_{cc}$  values in a threshold between -10 and -5 of *CWD* values. The day-length, also included in the model as a significant variable (edf = 7.83, F-test = 12.324,  $P < 0.001$ ), demonstrated to affect the community  $G_{cc}$  after reaching 12.5 hours of sunlight.

Day-length was the variable that best interacted with the community  $G_{cc}$  time series from the cerrado physiognomies (Table 3). The same values, ranging from 11.5 and 12.0 hours, were observed as a sensitive threshold for  $G_{cc}$  transitions across all vegetations (Fig. 5 B, C and D). *CWD* presented different smooth functions of interaction among the cerrado sites, where we can notice a sensitive point of change around values between -150 and -100 more strength for the cerrado shrubland and the dense cerrado (Fig. 5B and D) and less for the woody cerrado (Fig. 3C).

The cumulative rainfall (*Rainfall\_Cum\_30*) was significant for the cerrado shrubland and the dense cerrado (6.678, 13.189,  $P < 0.001$ ; 7.94, 8.317,  $P < 0.001$ , respectively). Both demonstrated sensitive to changes in  $G_{cc}$  after accumulated precipitation rates of 25 to 30 mm (Fig. 5 B and D). The  $G_{cc}$  time-series from the woody cerrado community was the only one to relate with the temperature amplitude (*Tamp* – 3.558, 17.05,  $P < 0.001$ ). The relationship between the covariates was positive and linear with  $G_{cc}$  values rising as *Tamp* increases (Fig. 5 C).

In general, the ROIs separated according to leaf exchange strategies interacted with different variables across vegetations and among groups. The deciduous and fast deciduous species from caatinga

demonstrated high similarity to the community pattern, with *CWD* and the lagged seven days of accumulated rainfall (*Rainfall\_lag7*) variables being more important for both ROIs and presenting similar thresholds in points of transition (Fig. 5 A and Fig. 6 A). The fast deciduous presented a high significant relation to *rainfall\_lag7* (1.00, 30.309,  $P<0.001$ ), and demonstrated an oscillated relation with the day-length variable (Fig. 6 A).

The *CWD* was the most significant smooth term to interact with the leaf phenology of the deciduous ROIs (dec = 8.302, 23.169,  $P<0.001$ ) from caatinga; evergreen (ever = 4.569, 21.991,  $P<0.001$ ) and wet flushing semideciduous (semi = 7.881, 40.59,  $P<0.001$ ) from the woody cerrado, and semideciduous (semi = 8.717, 29.203,  $P<0.001$ ) and deciduous (dec = 8.264, 28.548,  $P<0.001$ ) from the dense cerrado (Fig. 6 A, C, and D).

Day-length was more significant for the evergreen (ever = 7.288, 38.316,  $P<0.001$ ) and dry flushing semideciduous (semi dry = 2.693, 32.952,  $P<0.001$ ) ROIs from the woodland sites of dense and woody cerrado, respectively. In the first, curve inflection was sensitive to daylight hours from 12.0 to 12.5 (Fig. 6 D). In the latter, an inverse relationship was found, with decreasing of  $G_{cc}$  as daylight increases, starting from 11.5 hours (Fig. 6 C). Photoperiod also presented positive relationship (5.948, 41.807,  $P<0.001$ ) with the deciduous ROI (dec), composed mostly of shrubs, from the cerrado shrubland (Fig. 6 B).

The dominant grassy component (grass) from the cerrado shrubland and deciduous (dec) ROIs from the woody cerrado, were significant related to the *Tamp* (1.00, 19.53,  $P<0.001$ ; 3.663, 25.49,  $P<0.001$ , respectively). Grass ROI showed an inverse sigmoid relationship with a range of *Tamp* values increasing from 5 to 10°C (Fig. 6 B), while deciduous crowns (dec) demonstrated a negative linear relationship with rising *Tamp* starting in 10°C (Fig. 6 D).

## 5 DISCUSSION

### 5.1 Leafing phenological patterns across vegetations

The  $G_{cc}$  index extracted from the digital images allowed tracking the leafing seasonality of the vegetations and the definition of the growing seasons through phenological metrics detected from the derivatives of generalized additive models fitting. As expected,  $G_{cc}$  curves followed the wet periods

fluctuations from their climatic zones, leading to differences on phenological dates and the growing seasons among vegetations, mainly between the caatinga vegetation and the three cerrado vegetations.

Within sites, SOS and EOS presented more discrepancies in the Caatinga (28 and 31 days of difference between years, respectively) and the woody cerrado (38 and 36 days difference among years, respectively). For the caatinga, the phenomenon of the Atlantic Dipole (a temperature variation of the Atlantic Ocean) can cause a high interannual variability in the precipitation rates (GUTIÉRREZ et al., 2014), which would lead to the seasonality dynamics of the growing seasons among years. Given that plant species from this ecosystem are influenced mainly by the water availability, there is an immediately response of the reproductive and vegetative phenophases to rainfall events (CARVALHO and BARBOSA, 1989; ARAÚJO et al., 2007).

Despite the differences among years, the woody cerrado site was the more dissimilar to the other savanna vegetations regarding the SOS and EOS detected dates. Studies in cerrado vegetations usually report the start of the community leaf flushing (SOS) for the transition period from the dry to the wet season, around the month of September (e.g., MONASTERIO and SARMIENTO, 1976; WILLIAMS et al., 1997; PIRANI et al., 2009; MUNHOZ and FELFILI, 2005, CAMARGO et al., 2018). We relate the high variations of SOS and EOS among years (from 36 to 38 days) in this vegetation to two main reasons. One could be related to the smoothing procedures over parts of the gap-filled  $G_{cc}$  time series, what could be responsible for the earlier SOS and EOS in the cycles of 2013/2014 and 2014/2015, while the second to the massive presence, in the camera field of view, of crowns from species flushing out the community flushing, during dry season, influencing the overall outcomes of  $G_{cc}$  curve patterns.

The shape of the growing season also differed among vegetations, clearly influenced by the LOS, much shorter for the Caatinga and longer for the cerrado vegetations. The green-up and green-down curves were more abrupt for the caatinga, explained by the predominance and high synchrony of strongly seasonal and many fast deciduous species in this vegetation, as pointed out by few dry forest studies (MURPHY and LUGO, 1986; PEZZINI et al., 2014). On the other hand, the moister cerrado vegetations were composed of a different proportion of deciduous, semideciduous and evergreen, maintaining partially green coverage of the vegetation even during the dry season and smoothing  $G_{cc}$

curve changes along the wet season as supporting direct observations of leaf exchange patterns and the definition of the Cerrado as a semideciduous vegetation (MORELLATO et al., 2013; CAMARGO et al., 2018).

## 5.2 Environmental cues of leafing phenology

The models' predictions found non-linear relationships between phenology and the most recurrent significant variables, day-length and *CWD*. Day length was the most present variable to explain the  $G_{cc}$  time series of vegetation communities. As expected, daylength was more important for the cerrado vegetations than caatinga. In this context, light-related changes that precede the wet season, such as the photoperiod seasonality, could be triggering leaf flushing in the cerrado communities. Photoperiod has been reported to trigger the start of leaf flushing for seasonal dry tropical vegetations (BORCHERT; RIVERA and HAGNAUER, 2002; RIVERA et al., 2002; HIGGINS et al., 2011; ROSSATTO et al., 2013; GARCIA et al., 2017). The consistent signal has been suggested to trigger and synchronize leaf flushing for tropical seasonal ecosystems despite the species leaf exchange strategy (BORCHERT and RIVERA, 2001; RIVERA et al., 2002; ROSSATTO et al., 2013). The peak of the community flushing before the onset of the wet season supports the hypothesis that cerrado trees have access to underground water due their deep root system or their capability to use the precedent leaf fall for rehydration for an early leaf production (EAMUS and PRIOR, 2001; GOLDSTEIN et al., 2008). The community leaf flushing before the rainy season would also avoid nutrient loss by leaching during leaf development and the threat of high herbivory rates to young leaves (SARMIENTO et al., 1985; ROSSATTO et al., 2009).

The skewness pattern of the  $G_{cc}$  curves from Caatinga indicates a link between time and duration of the irregular leafing cycles, restricted within the wet period, following the precipitation pulses in the system. A similar pattern has been detected by digital cameras for dry grasslands, confirming the high dependency of the interannual precipitation variability (BROWN et al., 2016; RICHARDSON et al., 2018). The likely thresholds indicated in the plant-water relationships in the caatinga community shown low rates of accumulated precipitation stimulating  $G_{cc}$  time series changes, what could explain the fast response pattern of leaf flushing, reflected in the growing season curve oscillations of this site.



The cumulative water deficit (*CWD*) relationships, explained the seasonality of leaf production in the four tropical seasonal vegetations investigated in this study. This variable can be considered of major biological meaningful to the understand of physiological plant responses, given that it integrates water and energy interactions, primary effects of climate on plants (STEPHENSON, 1998). According to our results, *CWD* influenced leaf phenological responses of all four vegetations. Among the leaf exchange strategies groups, *CWD* was the most recurrent variable to better explain leaf phenology patterns.

Thermal amplitude had a positive relationship with the community pattern of  $G_{cc}$  in the woody cerrado. This variable was also positive correlated with the rates of green-up and senescence across a gradient of snow-free mountain vegetations (STREHER et al., 2017). The amplitude of temperature at the woody cerrado reached 20°C, with high values found in the periods of transition between dry and wet seasons. Temperature would play a significant role speeding plant development and their organs (KORNER, 2006), what could be influencing the rates of green-up and green-down in the cerrado curves.

Regarding the leafing patterns according to the leaf exchange strategies, variables of day-length and *CWD* were also the most influential factors across sites. Our results indicated that both predictors are about the same across the vegetations, except for the short cumulative seven-day rainfall necessary for leaf flushing in the caatinga. The relationship between predictors-response varied and became more heterogenous from the highest to the least seasonal sites. Woodland cerrado vegetations have shown more discrepancies among leaf exchange strategies and predictors in their smooth function. For instance, deciduous ROIs from the Dense and Woody cerrado were explained by thermal amplitude, but the relationship established between the covariates were opposite, one being positive and the other negative (Fig. 6 C and D). We could notice that different phenological behaviors presented variations on timing and rate of  $G_{cc}$  values among groups and within vegetations (Fig. 4 C and D). This pattern was less marked for the caatinga and the cerrado shrubland, where phenological behaviors from ROIs groups were more similar in terms of  $G_{cc}$  time series patterns and relationship response to predictors. This phenological dynamic can be explained by the fact that high seasonal constrained environments tend to be more synchronic, due species (caatinga) or life forms (open cerrado scrubland) adapted to

the limited favorable time for plant development (wet season). As long as the environment becomes less constrained by the climate, leaf exchange patterns would become more independent from seasonal environmental constraints, given that soil water sources availability increases (BORCHERT, 1998), as we observed across our four vegetation biomes.

At the Itirapina Ecological Station (cerrado scrubland site), different physiognomies from open grassland to woodland cerrado occur over a groundwater depth lower than 4 m, and a recent study has found that soil fertility did not define the occurrence of woody physiognomies (LEITE et al., 2018). Besides, grasses typically require rainfall events to start leaf growth after rains (ANDREW and MOTT, 1983; COOK et al., 2002). However, leaf phenology of the grassland layer (grass ROI) in the cerrado shrubland was not significantly predicted by water relationships, which contradicted our expectations about different response between woody and grassy dominated vegetations in accordance with the temporal niche separation hypothesis (SCHOLLES and WALKER, 1993). Grass ROI model reached around 50% of explanation by day-length and thermal amplitude. The Brazilian cerrado is considered a “wet” neotropical savanna, with regions of South America reaching up to 2,500 mean annual precipitation (MAP), contrasting in more than 500 mm from the African and Australian savannas, and where the influence of fire frequency would be an important determinant of the grasslands and closed savannas distribution, besides climate seasonality (LEHMANN et al., 2011).

Woodland cerrado vegetation communities (woody cerrado and dense cerrado) presented discrepancies regarding their leaf phenology patterns and environmental predictors. In fact, dense cerrado demonstrated to be more similar with the cerrado shrubland than with the woody cerrado. We suggest that this difference may be related to the species composition and the leaf exchange strategies predominant within each vegetation community.

In conclusion, water and light were the most important predictors for the leaf phenological patterns across the sites. Water-plant relationships were more important for the caatinga community, and light effects, through day-length seasonality, had more influence in the leafing patterns of the cerrado communities. The *CWD* variable appeared as an important predictor for the drought effects on the leafing responses, although the previous 30 days of accumulated precipitation and thermal amplitude had also significant contributions. Phenological signals and predictor-response relationships have

increased in variability across sites, where woodland cerrado physiognomies have shown increased capability to sustain a greater complexity in their species leafing strategies than caatinga. One of the major benefits that came from the near-surface remote phenology, using digital cameras, is the reliability of acquiring continuous good quality phenological data from multiple sites and the potential to establish long-term phenological datasets. Through long-term monitoring, we will be able to consent in the main drivers influencing plant communities and forecasting shifts in the face of climate change scenarios. For now, with this study, we can collaborate with phenology for seasonal tropical vegetations, corroborate hypothesis from literature and have more insights about tropical vegetation dynamics.

Acknowledgments - the present study was supported by São Paulo Research Foundation FAPESP (grants #2009/54208-6, #2010/52113-5 and #2013/50155-0), Microsoft Research and CNPq. We thank the Instituto Florestal for the permissions to work at the cerrado shrubland and dense cerrado sites, and Embrapa for all the support and collaboration in the Caatinga site. We thank Marina Muller Corrêa and Carolina Crivelin for the help in the image processing of the cerrado shrubland and woody cerrado sites. BA receives fellowship from FAPESP (#2014/00215-0 and #2016/01413-5). LPCM, RST, and HR receive a research productivity fellowship from CNPq.

## 6 REFERENCES

- ABERNETHY, K. et al. Current issues in tropical phenology: a synthesis. **Biotropica**, v. 50 (3), p. 477-482, 2018.
- AHRENDT, H.E. et al. Tree phenology and carbon dioxide fluxes: Use of digital photography for process-based interpretation at the ecosystem scale. **Climate Research**, v. 39(3), p. 261–274, 2009.
- ALBERTON, B.C. et al. Introducing digital cameras to monitor plant phenology in the tropics: Applications for conservation. **Perspectives in Ecology and Conservation**, v. 15, p. 82-90, 2017.
- ALBERTON, B.C. et al. Using phenological cameras to track the green up in a cerrado savanna and its on-the-ground validation. **Ecological Informatics**, v. 19, p. 62–70, 2014.
- ANDREW, M.H.; MOTH, J.J. Annuals with transient seed banks: the population biology of indigenous *Sorghum* species of tropical north-west Australia. **Australian Journal of Ecology**, v. 8 (3), p. 265-276, 1983.
- ARAÚJO, E.L.; CASTRO, C.C. and ALBUQUERQUE, U.P. Dynamics of Brazilian Caatinga – A Review Concerning the Plants, Environment and People. **Functional Ecosystems and Communities**, 1(October 2015), p.15–28, 2007.

ARCHIBALD, S. and SCHOLLES, R.J. Leaf green-up in a semi-arid African savanna –separating tree and grass responses to environmental cues. **Journal of Vegetation Science**, v. 18 (4), p.583, 2007.

BATALHA, M.A. and MANTOVANI, W. Reproductive Phenological Patterns of Cerrado Plant Species At the Pé-De-Gigante Reserve (Santa Rita Do Passa Quatro, SP, Brazil): a Comparision Between the Herbaceous and Woody Floras. *Revista Brasileira de Biologia*, v. 60 (1), p.129–145, 2000.

de BEURS, K. and HENEGBRY, G.M. Spatial-Temporal statistical methods for modelling land surface phenology. In I. L. Hudson & M. R. Keatley, eds. **Phenological Research: Methods for Environmental and Climate Change Analysis**. Springer Netherlands, p. 177–208, 2010.

BORCHERT, R. et al. Insolation and photoperiodic control of tree development near the equator. **New Phytologist**, v. 205 (1), p.7–13, 2015.

BORCHERT, R. Responses of tropical trees to rainfall seasonality and its long-term changes. **Climatic Change**, v. 39 (2), p.381–393, 1998.

BORCHERT, R. Soil and stem water storage determine phenology and distribution of tropical dry forest trees. **Ecology**, v. 75 (5), p. 1437-1449, 1994.

BORCHERT, R.; RIVERA, G. and HAGNAUER, W. Modification of vegetative phenology in a tropical semi-deciduous forest by abnormal drought and rain. **Biotropica**, v. 34 (1), p.27–39, 2002.

BROWN, T.B. et al. Using phenocams to monitor our changing earth: Toward a global phenocam network. **Frontiers in Ecology and the Environment**, v. 14 (2), p.84–93, 2016.

CAMARGO, M.G.G. et al. Leafing patterns and leaf exchange strategies of a cerrado woody community. **Biotropica**, v. 50 (3), p.442–454, 2018.

CARVALHO, D. and BARBOSA, D.A. Dados fenológicos de 10 espécies arbóreas de uma área de caatinga (Alagoinha-PE). **Acta bot. bras.**, v. 3 (2), p.109–117, 1989.

CHAMBERS, L.E. et al. Phenological Changes in the Southern Hemisphere. **PLoS ONE**, v. 8 (10), 2013.

COOK, G.D. et al. Variation in vegetative water use in the savannas of the North Australian Tropical Transect. **Journal of Vegetation Science**, v. 13 (3), p. 413-418, 2002.

CRIMMINS, M.A.; CRIMMINS, T.M. Monitoring plant phenology using digital repeat photography. **Environmental management**, v. 41 (6), p. 949-958, 2008.

EAMUS, D. Ecophysiological traits of deciduous and evergreen woody species in the seasonally dry tropics. **Trends in Ecology and Evolution**, 14(1), pp.11–16, 1999.

EAMUS, D. and PRIOR, L. **Ecophysiology of trees of seasonally dry tropics**: Comparisons among phenologies, 2001.

ELLIOTT, S.; BAKER, P.J. and BORCHERT, R. Leaf flushing during the dry season: The paradox of Asian monsoon forests. **Global Ecology and Biogeography**, v. 15 (3), p.248–257, 2006.

ESCOBAR, D.F.E; SILVEIRA, F.A.O and MORELLATO, L.P.C. Timing of seed dispersal and seed dormancy in Brazilian savanna: two solutions to face seasonality. **Annals of botany**, v. 121 (6), p. 1197-1209, 2018.

FRESCINO, T.S.; EDWARDS, T.C. and MOISEN, G.G. Modeling spatially explicit forest structural attributes using Generalized Additive Models. **Journal of Vegetation Science**, v. 12 (1), p.15–26, 2001.

- GARCIA, L.C.; BARROS, F. V. and LEMOS-FILHO, J.P. Environmental drivers on leaf phenology of ironstone outcrops species under seasonal climate. **Anais da Academia Brasileira de Ciências**, v. 89 (1), p.131–143, 2017.
- GILLESPIE, A.R.; KAHLE, A.B. and WALKER, R.E. Color enhancement of highly correlated images. II. Channel ratio and “chromaticity” transformation techniques. **Remote Sensing of Environment**, v. 22 (3), p.343–365, 1987.
- GOLDSTEIN, G. et al. Water economy of Neotropical savanna trees: Six paradigms revisited. **Tree Physiology**, v. 28 (3), p.395–404, 2008.
- GUTIÉRREZ, A.P.A. et al. Drought preparedness in Brazil. **Weather and Climate Extremes**, v. 3, p. 95-106, 2014.
- HIGGINS, S.I. et al. Is there a temporal niche separation in the leaf phenology of savanna trees and grasses? **Journal of Biogeography**, v. 38 (11), p.2165–2175, 2011.
- JAMES, R. et al. Implications of global warming for the climate of African rainforests. **Phil. Trans. R. Soc. B**, v. 368 (1625), p. 20120298, 2013.
- JÖNSSON, P. and EKLUNDH, L. TIMESAT—a program for analyzing time-series of satellite sensor data. **Computers & Geosciences**, v. 30 (8), p. 833-845, 2004.
- Kill, L.H.P. Caracterização da vegetação da reserva legal da embrapa semiárido. **Documentos online**, v. 5 (2003), p.121–124, 2017.
- KÖPPEN, W.P. **Grundriss der klimakunde**. 1931.
- KÖRNER, C. Significance of temperature in plant life. **Plant growth and climate change**, p. 48-69, 2006.
- LEITE, M.B. et al. Groundwater depth as a constraint on the woody cover in a Neotropical Savanna. **Plant and Soil**, v. 426 (1-2), p. 1-15, 2018.
- LEHMANN, C.E.R et al. Deciphering the distribution of the savanna biome. **New Phytologist**, v. 191 (1), p. 197-209, 2011.
- MARRA, G. and WOOD, S.N. Practical variable selection for generalized additive models. **Computational Statistics and Data Analysis**, v. 55 (7), p.2372–2387, 2011.
- MIGLIAVACCA, M. et al. Using digital repeat photography and eddy covariance data to model grassland phenology and photosynthetic CO<sub>2</sub> uptake. **Agricultural and Forest Meteorology**, v. 151 (10), p.1325–1337, 2011.
- MONASTERIO, M. and SARMIENTO, G. Phenological strategies of plants species in the tropical savanna and semi-deciduous forest of the Venezuelan Llanos. **Journal of Biogeography**, v. 3 (4), p.325–356, 1976.
- MOORE, C.E. et al. Tree – grass phenology information improves light use efficiency modelling of gross primary productivity for an Australian tropical savanna. **Biogeosciences**, v. 14, p.111–129, 2017.
- MORELLATO, L.P.C. et al. Linking plant phenology to conservation biology. **Biological Conservation**, v. 195, p.60–72, 2016.
- MORELLATO, L.P.C.; CAMARGO, M.G.G. and GRESSLER, E. A review of plant phenology in South and Central America. In: **Phenology: An integrative environmental science**. Springer, Dordrecht, p. 91-113, 2013.

- MORELLATO, L.P.C. et al. Phenology of Atlantic Rain Forest Trees: A Comparative Study **Biotropica**, v. 32(4), p.811–823, 2000.
- MORELLATO, L.P.C. et al. Estudo comparativo da fenologia de espécies arbóreas de floresta de altitude e floresta mesófila semidecídua na Serra do Japi, Jundiaí, São Paulo. **Revista brasileira de Botânica**, v. 12 (1), p. 85-98, 1989.
- MORISSETTE, J.T. et al. Tracking the rhythm of the seasons in the face of global change: Phenological research in the 21 st century. **Frontiers in Ecology and the Environment**, v. 7 (5), p.253–260, 2009.
- MOULIN, S. et al. Global-scale assessment of vegetation phenology using NOAA/AVHRR satellite measurements. **Journal of Climate**, v. 10 (6), p. 1154-1170, 1997.
- MUNHOZ, C.B.R. and FELFILI, J.M. Fenologia do estrato herbáceo-subarbustivo de uma comunidade de campo sujo na Fazenda Água Limpa no Distrito Federal, Brasil. **Acta Botanica Brasilica**, v. 19 (4), p.979–988, 2005.
- MURPHY, P.G. and LUGO, A.E. Ecology of Tropical Dry Forest. **An. Rev. Ecol. Syst.**, v. 17, p.67–88, 1986.
- MURRAY-TORTAROLO, G. et al. Changes in the dry season intensity are a key driver of regional NPP trends. **Geophysical Research Letters**, 2016.
- OLIVEIRA-FILHO, A.T. and RATTER, J.A. Vegetation physiognomies and woody flora of the cerrado biome. **The cerrados of Brazil: ecology and natural history of a neotropical savanna**, p. 91-120, 2002.
- OLSON, D.M. et al. Terrestrial Ecoregions of the World: A New Map of Life on Earth A new global map of terrestrial ecoregions provides an innovative tool for conserving biodiversity. **BioScience**, v. 51 (11), p. 933-938, 2001.
- PEZZINI, F.F. et al. Changes in tree phenology along natural regeneration in a seasonally dry tropical forest. **Plant Biosystems**, v. 148 (5), p.965–974, 2014.
- PIRANI, F.R.; SANCHEZ, M. and PEDRONI, F. Fenologia de uma comunidade arbórea em cerrado sentido restrito, Barra do Garças, MT, Brasil. **Acta Botanica Brasilica**, v. 23 (4), p.1096–1110, 2009.
- PIVELLO, V. et al. Proposta de zoneamento ecológico para a reserva de cerrado Pé-de-Gigante (Santa Rita do Passa Quatro, SP). **Brazilian Journal of Ecology**, v. 2 (2), p. 108-118, 1998.
- POLGAR, C.A.; PRIMACK, R.B. Leaf-out phenology of temperate woody plants: from trees to ecosystems. **New Phytologist**, v. 191 (4), p. 926-941, 2011.
- QUESADA, M. et al. Succession and management of tropical dry forests in the Americas: Review and new perspectives. **Forest Ecology and Management**, v. 258 (6), p. 1014-1024, 2009.
- REICH, P.B. Phenology of tropical forests: patterns, causes, and consequences. **Canadian Journal of Botany**, v. 73(2), p. 164-174, 1995.
- REICH, P.B. and BORCHERT, R. Water Stress and Tree Phenology in a Tropical Dry Forest in the Lowlands of Costa Rica. **The Journal of Ecology**, v. 72 (1), p.61–74, 1984.
- REYS, P. et al. Estrutura e composição florística de um Cerrado sensu stricto e sua importância para propostas de restauração ecológica. **Hoehnea**, p. 449-464, 2013.
- RIBEIRO, J.F.; WALTER, B.M.T. Fitofisionomias do bioma Cerrado. **Embrapa Cerrados (ALICE)**, 1998.

- RICHARDSON, A.D. et al. Use of digital webcam images to track spring green-up in a deciduous broadleaf forest. **Oecologia**, v. 152 (2), p.323–334, 2007.
- RICHARDSON, A.D.R. et al. Near-surface remote sensing of spatial and temporal variation. **Ecological Applications**, v. 19(6), p.1417–1428, 2009.
- RICHARDSON, A.D. et al. Climate change, phenology, and phenological control of vegetation feedbacks to the climate system. **Agricultural and Forest Meteorology**, v. 169, p.156–173, 2013.
- RICHARDSON, A.D. et al. Tracking vegetation phenology across diverse North American biomes using PhenoCam imagery. **Scientific Data**, v. 5, p.180028, 2018.
- R Core Team. **A language and environment for statistical computing**. R Foundation for Statistical Computing, Vienna, Austria, 2017.
- RIVERA, G. et al. Increasing day-length induces spring flushing of tropical dry forest trees in the absence of rain. **Trees - Structure and Function**, v. 16 (7), p.445–456, 2002.
- ROSSATTO, D.R. et al. Seasonal variation in leaf traits between congeneric savanna and forest trees in Central Brazil: Implications for forest expansion into savanna. **Trees - Structure and Function**, v. 27 (4), p.1139–1150, 2013.
- ROSSATTO, D.R.; HOFFMANN, W.A. and FRANCO, A.C. Differences in growth patterns between co-occurring forest and savanna trees affect the forest–savanna boundary. **Functional Ecology**, v. 23 (4), p. 689–698, 2009.
- RÖTZER, T.; GROTE, R. and PRETZSCH, H. The timing of bud burst and its effect on tree growth. **International Journal of Biometeorology**, v. 48 (3), p.109–118, 2004.
- SARMIENTO, G.; GOLDSTEIN, G. and MEINZER, F. Adaptive strategies of woody species in neotropical savannas. **Biological Reviews**, v. 60 (3), p. 315–355, 1985.
- SCHOLES, R.J. and ARCHER, S.R. Tree-grass interactions in savannas. **Annual review of Ecology and Systematics**, v. 28 (1), p. 517–544, 1997.
- SINGH, J.S. and SINGH, V.K. Phenology of seasonally dry tropical forest. **Current science**, p. 684–689, 1992.
- SINGH, K.P. and KUSHWAHA, C.P. Emerging paradigms of tree phenology in dry tropics. **Current Science**, p. 964–975, 2005.
- SONNENTAG, O. et al. Digital repeat photography for phenological research in forest ecosystems. **Agricultural and Forest Meteorology**, v. 152 (1), p.159–177, 2012.
- STEPHENSON, N.L. Climatic control of vegetation distribution: the role of the water balance. **The American Naturalist**, v. 135 (5), p. 649–670, 1990.
- STEPHENSON, N. Actual evapotranspiration and deficit: biologically meaningful correlates of vegetation distribution across spatial scales. **Journal of Biogeography**, v. 25 (5), p. 855–870, 1998.
- STREHER, A.S. et al. Land Surface Phenology in the Tropics: The Role of Climate and Topography in Snow-Free Mountain. **Ecosystems**, v. 20 (8), p. 1436–1453, 2017.
- TANNUS, J.L.S.; ASSIS, M.A. and MORELLATO, L.P.C. Fenologia reprodutiva em campo sujo e campo úmido numa área de cerrado no sudeste do Brasil, Itirapina-SP. **Biota Neotropica**, 2006.

- VAN SCHAIK, C.P.; TERBORGH, J.W. and WRIGHT, S.J. the Phenology of Tropical Forests - Adaptive Significance and Consequences for Primary Consumers. **Annual Review of Ecology and Systematics**, v. 24 (1993), p.353–377, 1993.
- VELOSO, H.P.; FILHO, A.L.R.R. & LIMA, J.C.A. Classificação da vegetação brasileira, adaptada a um sistema universal. Instituto Brasileiro de Geografia e Estatística, Diretoria de Geociências, Departamento de Recursos Naturais e Estudos Ambientais, 1991.
- WILLIAMS, R.J. et al. Leaf phenology of woody species in a north Australian tropical savanna. **Ecology**, v. 78 (8), p. 2542-2558, 1997.
- WILLIAMS, L.J.; BUNYAVEJCHEWIN, S. and BAKER, P.J. Deciduousness in a seasonal tropical forest in western Thailand: interannual and intraspecific variation in timing, duration and environmental cues. **Oecologia**, v. 155 (3), p. 571-582, 2008.
- WHITECROSS, M.A.; WITKOWSKI, E.T.F. and ARCHIBALD, S. Savanna tree-grass interactions: A phenological investigation of green-up in relation to water availability over three seasons. **South African Journal of Botany**, v. 108, p. 29-40, 2017.
- WOEBBECKE, D.M. et al. Color indices for weed identification under various soil, residue, and lighting conditions. **Transactions of the ASAE**, v. 38 (1), p.259–269, 1995.
- WOOD, S.N. Fast stable restricted maximum likelihood and marginal likelihood estimation of semiparametric generalized linear models. Journal of the Royal Statistical Society. **Series B: Statistical Methodology**, v. 73 (1), p.3–36, 2001.
- WRIGHT, S.J. and VAN SCHAIK, C.P. Light and the Phenology of Tropical Trees. **The American Naturalist**, v. 143 (1), p.192–199, 1994.
- YANG, L. et al. Using a generalized additive model with autoregressive terms to study the effects of daily temperature on mortality. **BMC Medical Research Methodology**, v. 12, 2012.
- ZHANG, X. al. Monitoring vegetation phenology using MODIS. **Remote sensing of environment**, v. 84 (3), p. 471-475, 2003.



## Figures legends

**Figure 1** Geographic distribution of study sites according to the Biome (following OLSON et al., 2011) denoted by the background color, and the vegetation types considered in this study: caatinga, cerrado shrubland and woody cerrado: cerrado and dense cerrado.

**Figure 2** Month average of local environmental variables of day-length, maximum and minimum temperature ( $T_{max}$  and  $T_{min}$ ), thermal amplitude ( $T_{amp}$ ) and rainfall for each vegetation site of this study – A, B and C caatinga; D, E, and F cerrado shrubland; G, H, and I woody cerrado; J, K, and L dense cerrado.

**Figure 3** Three-day 90<sup>th</sup> percentil  $G_{cc}$  time series of the xeric (A) and savanna (B – D) vegetations fitted by generalized additive models. (A) caatinga, (B) cerrado shrubland, (C) woody cerrado and (D) dense cerrado. Derivatives were calculated for the growing seasons detection. Green lines represent the start of the growing season and red lines the end of the growing season. Black line represents the model fitted, gray shadow the confident interval and dark dots the observed data.

**Figure 4** Three-day 90<sup>th</sup> percentil  $G_{cc}$  time series of the community and the selected ROIs for xeric (A) and savanna (B – D) vegetations fitted by generalized additive mixed models (GAMM). (A) caatinga, (B) cerrado shrubland, (C) woody cerrado, and (D) dense cerrado. Continuous colored lines represent the GAM model fitting, gray shadow represent the confidence interval and dark dots the observed data. Light blue lines represent the crowns for woody deciduous ROIs, yellow line for fast-response deciduous, green line for evergreen, blue line for spring flushing semideciduous, and dark orange for the winter flushing semideciduous; pink line represents the GAMM fit for dominant grassy vegetation, and orange for the community ROI of each vegetation site.

**Figure 5** Response of fitted generalized additive mixed models for the three-day 90<sup>th</sup> percentil  $G_{cc}$  community time-series to each environmental variable: *day-length*, *rainfall\_lag7* (rainfall of the previous seven days), *rainfall\_cum30* (accumulated precipitation of the last 30 days), *CWD* (cumulative water deficit) and *Tamp* (thermic amplitude) and vegetation– caatinga (A), cerrado shrubland (B), and woody cerrado (C), dense cerrado (D).

**Figure 6** Response of fitted generalized additive mixed models for the three-day 90<sup>th</sup> percentil  $G_{cc}$  of species' leaf strategies and life-form time-series to the environmental variables: (*day-length*,

*rainfall\_lag7*, *rainfall\_cum30*, *CWD* and *Tamp*) of each vegetation site – caatinga (A), cerrado shrubland (B), woody cerrado (D), and dense cerrado (C). deciduous = dec; fast-response deciduous = dec\_fast; wet flushing semideciduous = semi\_wet; dry flushing semideciduous = semi\_dry; evergreen = ever; grassy layer = grass.

**Table 1** Study sites summary description including the general vegetation name (Name), site designation and coordinates, location in Brazil (City, state and region), vegetation type, period of study (phenocam monitoring), mean annual total precipitation according to the normal climate and length of dry season in months (for estimation, see methods)

Name	Study site designation Lat/Long.	Location	Vegetation type	Phenocam Monitoring	Mean Annual Total Precipitation (mm)	Dry Season Length (months)
caatinga	Embrapa Semi-árido - 9°05'S / 40°19' W	Petrolina, PE, Northeast Brazil	Xeric shrubland (Caatinga)	10/May/2013 to 31/Dec/2015	510 mm	8
cerrado shrubland	Itirapina Ecological Station - 22°13'23"S / 47°53'02.67"W	Itirapina, SP, Southeastern, Brazil	grasslands, savannas and shrublands (Cerrado <i>campo sujo</i> )	28/Mar/2013 to 28/May/2015	1,524 mm	6
woody cerrado	Botelho Farm - 22°10'49.18"S / 47°52'16.54"W	Itirapina, SP, Southeastern, Brazil	grasslands, savannas and shrublands (Cerrado <i>sensu stricto</i> )	02/Sep/2011 to 03/Feb/2015	1,524 mm	6
dense cerrado	Pé de Gigante - 47° 34' - 47° 41' W / 21° 36' - 21° 44' S	Santa Rita do Passa Quatro, SP, Southeastern Brazil	grasslands, savannas and shrublands (Cerrado <i>sensu stricto denso</i> )	26/Aug/2013 to 31/Dec/2015	1499 mm	6

**Table 2** Phenological metric dates (day of year) derived from digital cameras  $G_{cc}$  time series for each vegetation. SOS = Start of growing season, POS = Peak of growing season, EOS = End of growing season and LOS = Length of growing season.

<b>SITE/YEAR</b>	<b>SOS</b>	<b>POS</b>	<b>EOS</b>	<b>LOS</b>
<i>caatinga</i>				
2013/2014	296	6	183	252
2014/2015	282	360	214	297
2015/2016	310	364	NA	NA
<i>cerrado shrubland</i>				
2013/2014	NA	NA	230	NA
2014/2015	239	317	219	345
2015/2016	228	309	NA	NA
<i>woody cerrado</i>				
2011/2012	NA	NA	170	NA
2012/2013	185	284	134	314
2013/2014	158	254	135	342
2014/2015	147	240	NA	NA
<i>dense cerrado</i>				
2013/2014	NA	290	204	NA
2014/2015	213	279	223	345
2015/2016	229	298	NA	NA

**Table 3** Approximate significance of smooth terms from the generalized additive models (GAM) between the  $G_{cc}$  time series from the ROIs of each vegetation and the environmental predictors. Effective degrees of freedom (edf) and F-test values are presented for each variable: Day-length, Cumulative water deficit (CWD), Precipitation lagged seven days (Rainfall\_lag7), Cumulative precipitation from the last 30 days (Rainfall\_Cum30), Temperature amplitude (Tamp), followed by the coefficient of determination ( $R^2$ ) of each model. All variables were significant at  $P$  values  $< 0.001$ . deciduous = dec; fast-response deciduous = dec\_fast; wet flushing semideciduous = semi\_wet; dry flushing semideciduous = semi\_dry; evergreen = ever; grassy layer = grass.

Site location	ROI	Day-length (hours)		CWD (mm)		Rainfall_lag7 (mm)		Rainfall_Cum_30 (mm)		ampT (°C)		$R^2$
		edf	F-test	edf	F-test	edf	F-test	edf	F-test	edf	F-test	
caatinga	comu	7.83	12.324	8.559	28.565	1.0	36.02	6.91	16.36	N.S	N.S	<b>0.86</b>
	dec	1.599	14.34	8.302	23.169	1.818	18.289	7.681	9.731	N.S	N.S	<b>0.79</b>
	dec_fast	7.388	6.045	6.33	15.276	1.0	30.309	7.143	13.125	N.S	N.S	<b>0.74</b>
cerrado shrubland	comu	5.726	39.535	6.678	13.189	N.S	N.S	3.907	4.617	N.S	N.S	<b>0.88</b>
	grass	2.114	9.535	N.S	N.S	N.S	N.S	N.S	N.S	1.00	19.53	<b>0.56</b>
	dec	5.948	41.807	5.216	7.841	N.S	N.S	3.773	6.384	1.434	8.575	<b>0.87</b>
woody cerrado	comu	5.218	22.436	7.097	8.484	N.S	N.S	N.S	N.S	3.558	17.05	<b>0.51</b>
	ever	1.00	7.441	4.569	21.991	N.S	N.S	N.S	N.S	N.S	N.S	<b>0.29</b>
	semi_wet	3.602	21.105	7.881	40.59	N.S	N.S	5.32	12.9	3.7	7.288	<b>0.75</b>
	semi_dry	2.693	32.952	7.309	18.228	N.S	N.S	N.S	N.S	3.184	19.95	<b>0.66</b>
	dec	N.S	N.S	7.665	5.904	N.S	N.S	N.S	N.S	3.663	25.49	<b>0.42</b>
dense cerrado	comu	7.773	36.383	7.94	8.317	N.S	N.S	6.745	3.156	N.S	N.S	<b>0.79</b>
	ever	7.288	38.316	8.163	16.224	N.S	N.S	5.671	5.699	N.S	N.S	<b>0.76</b>
	semi_wet	7.837	19.284	8.717	29.203	N.S	N.S	5.138	10.109	1.00	9.502	<b>0.82</b>
	dec	7.144	30.9	8.264	28.548	2.719	6.734	5.884	3.857	1.00	6.772	<b>0.82</b>

Figure 1

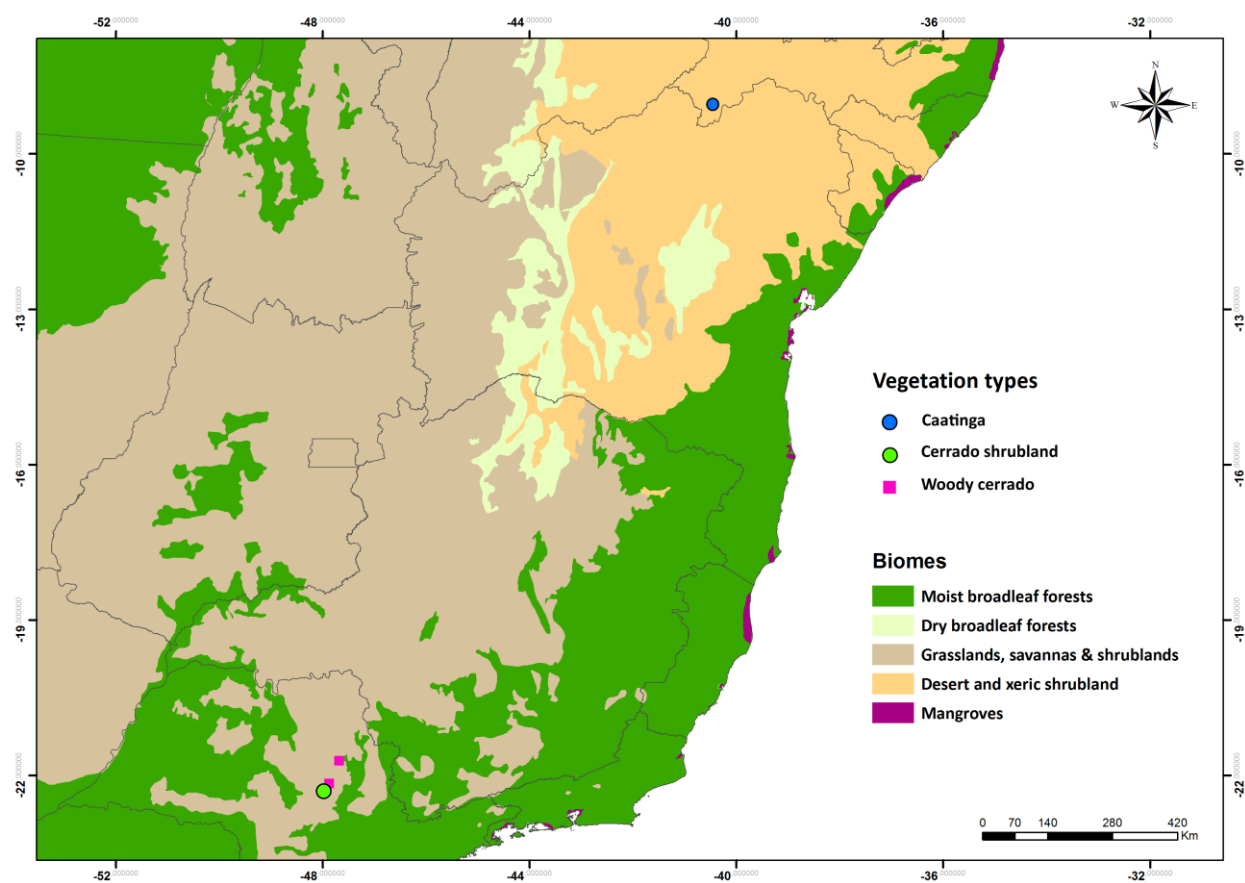


Figure 2

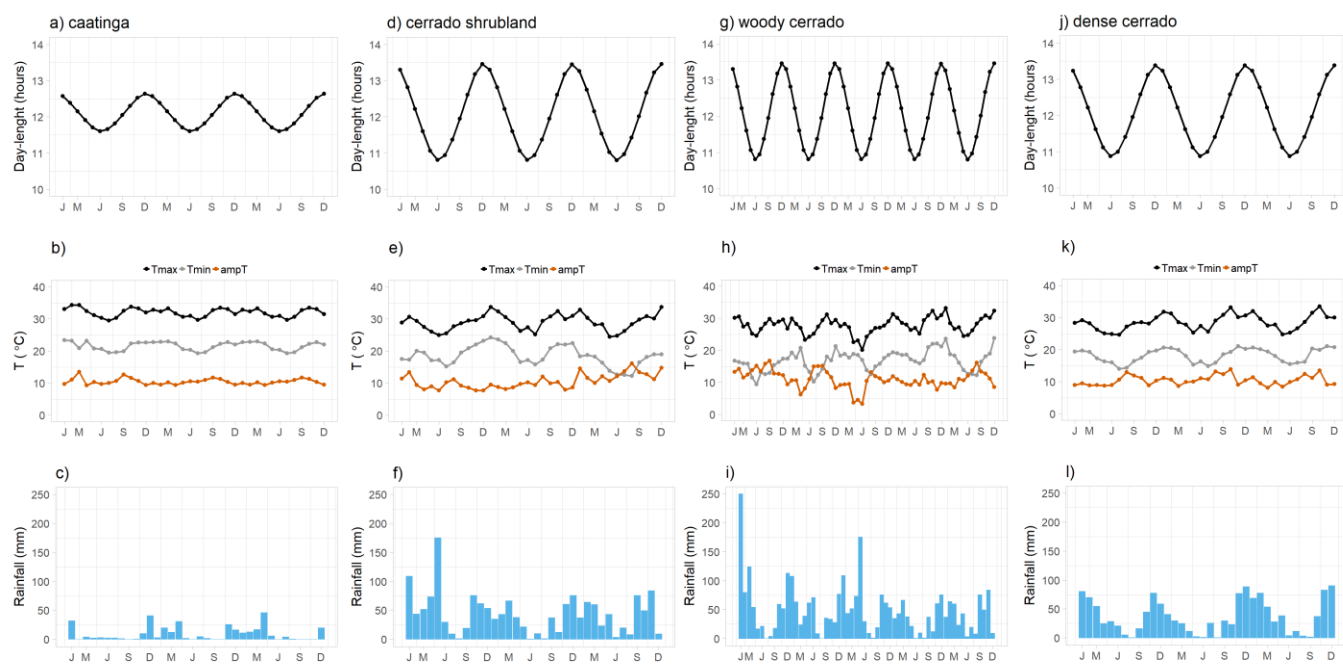


Figure 3

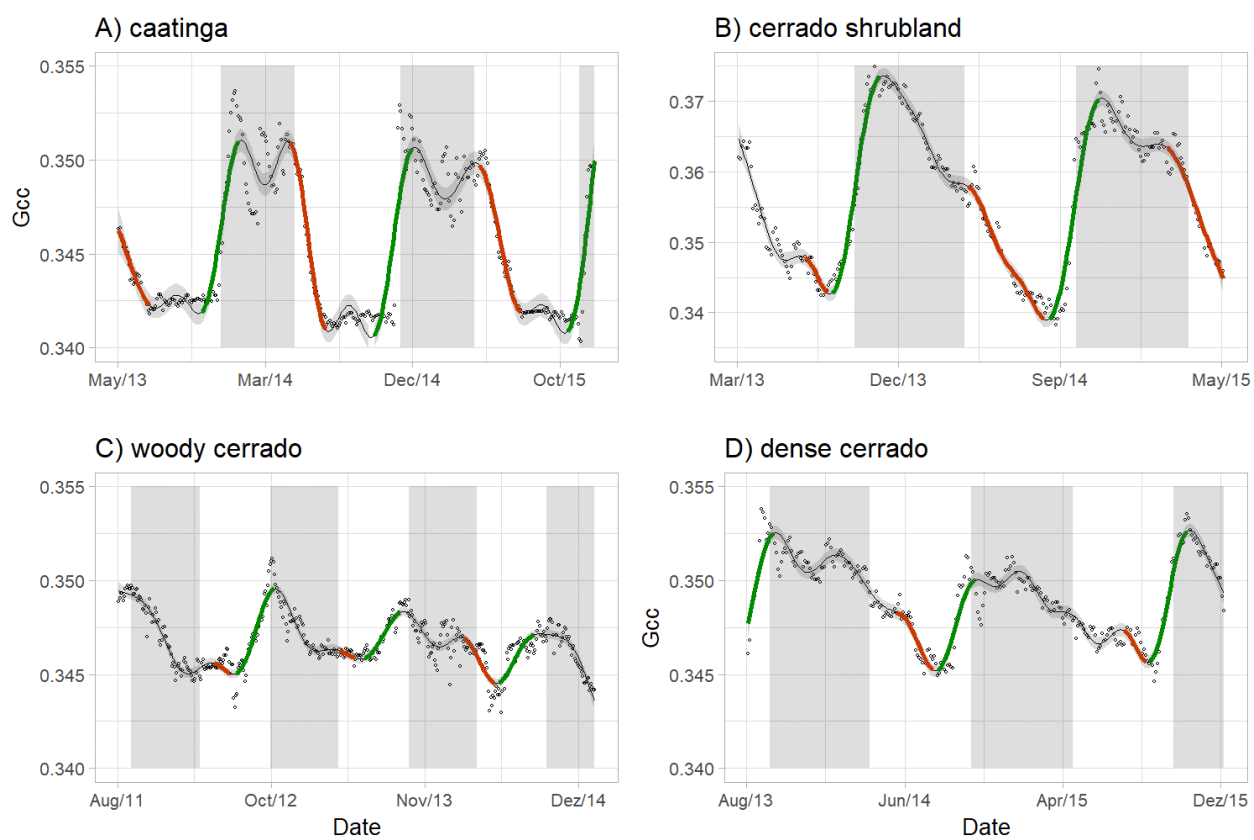




Figure 4

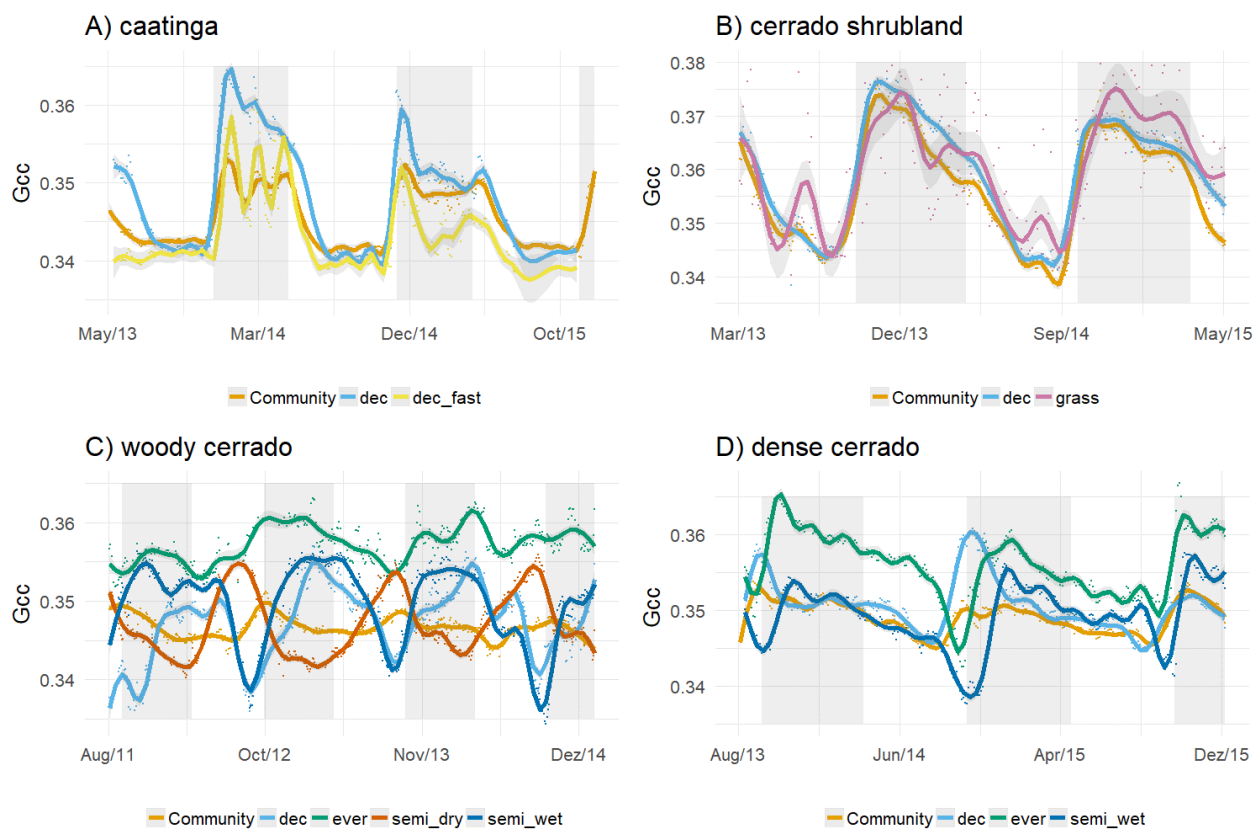


Figure 5

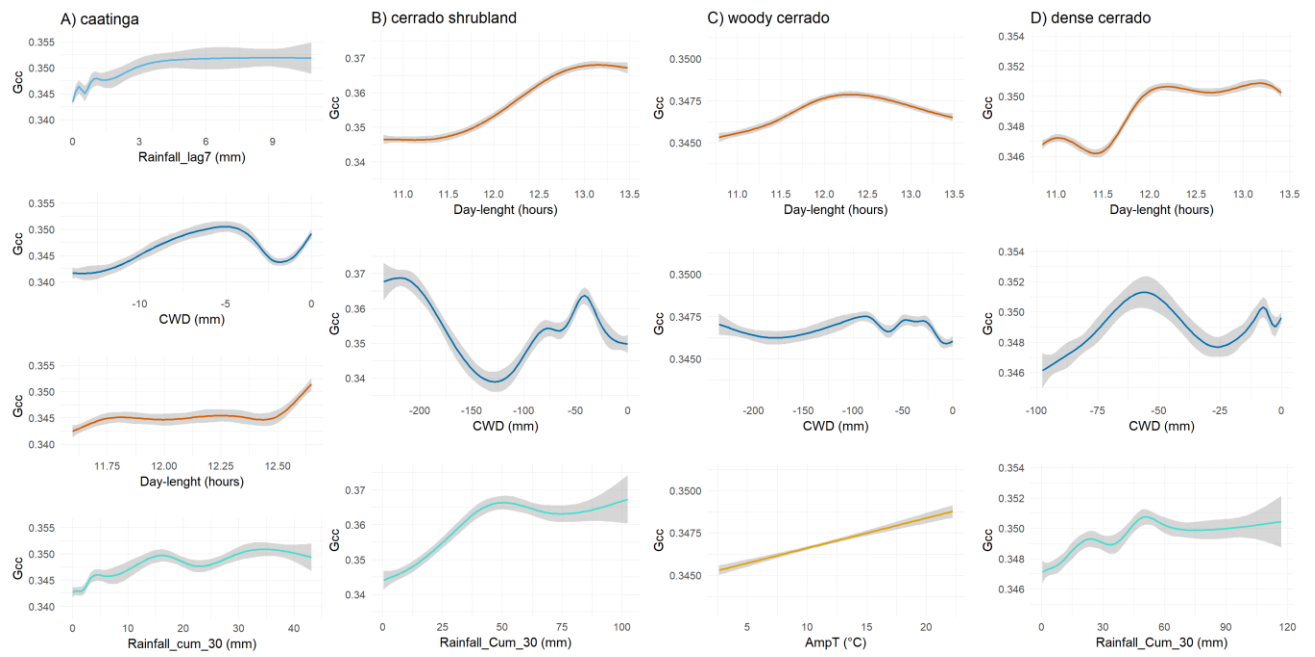
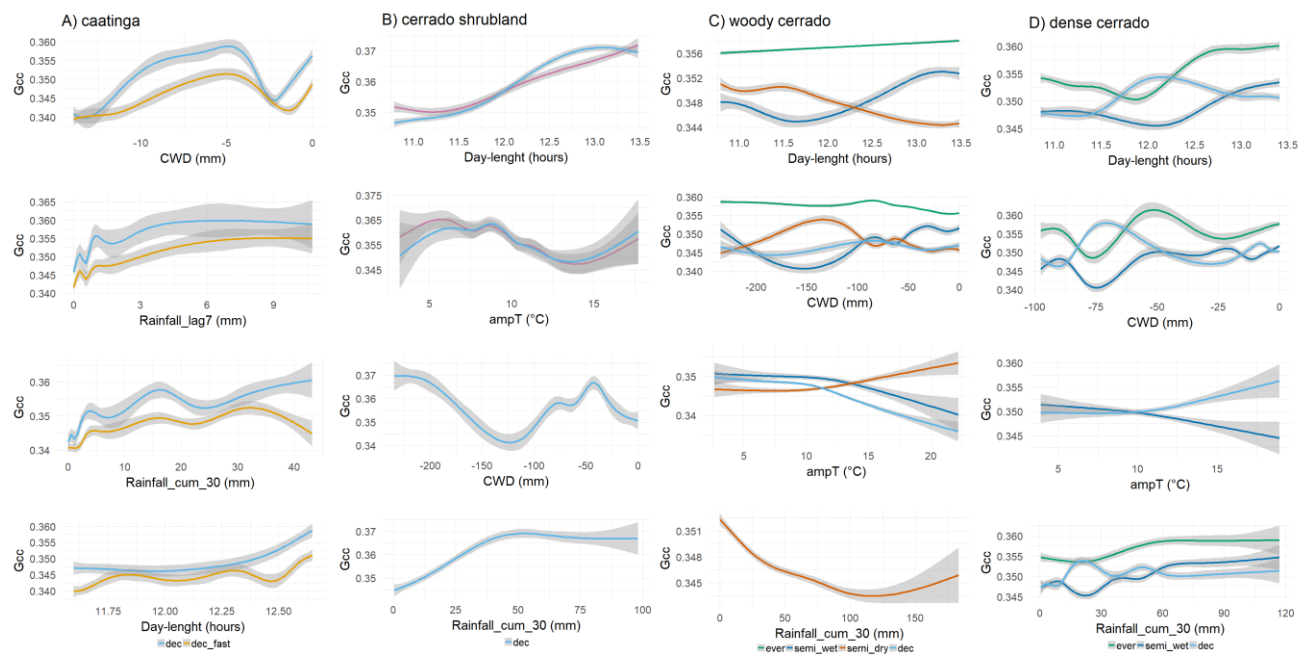


Figure 6



## Supplementary Material

**LEAFING PATTERNS AND ENVIRONMENTAL DRIVERS ACROSS SEASONAL TROPICAL COMMUNITIES**

Bruna Alberton, L. Humberto Rocha, Magna Soelma, Thiago S. F. Silva, Ricardo S. Torres, Patricia C. Morellato

Figure S1 Performance of the gap-filling algorithm on the daily  $G_{cc}$  time-series of the woody cerrado site. The algorithm created, based on an Auto-regressive moving average model (ARMA) fitting over the  $G_{cc}$  time-series, consists of three steps: first, the optimal order of the ARMA model is chosen based on physical principles; secondly, data segments before and after a given gap are fitted using an ARMA model of the order selected in the first step; and next, the gap is interpolated using a weighted function of a forward and a backward prediction based on the models of the selected data segments. The second and third steps are repeated for each gap contained in the entire time series.

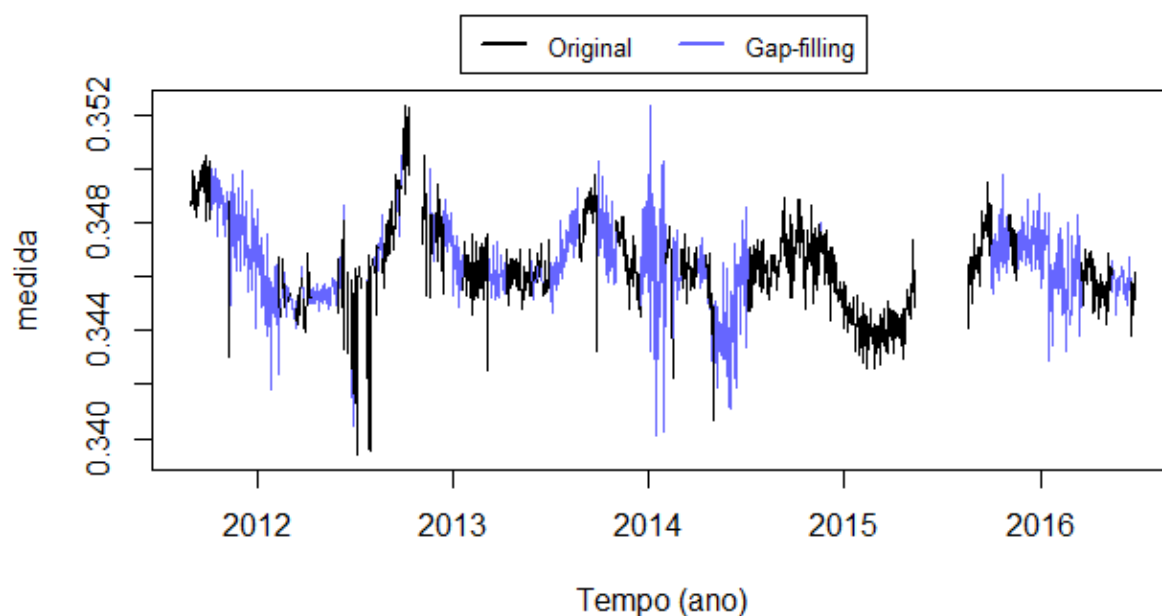


Table S1 List of plant species identified in the field of view of the digital camera from the Dry forest vegetation site.

<b>Family</b>	<b>Scientific name</b>	<b>Life form</b>
Anacardiaceae	<i>Spondias tuberosa</i> Arruda	Shrub Tree
Anacardiaceae	<i>Myracrodruon urundeuva</i> Allemão	Tree
Anacardiaceae	<i>Schinopsis brasiliensis</i> Engl.	Tree
Apocynaceae	<i>Aspidosperma pyrifolium</i> Mart. & Zucc.	Tree
Bignoniaceae	<i>Handroanthus spongiosus</i> (Rizzini) S.Grose	Tree
Burseraceae	<i>Commiphora leptophloeos</i> (Mart.) J.B.Gillett	Shrub Tree
Cactaceae	<i>Pilosocereus</i> Byles & Rowley	NA
Euphorbiaceae	<i>Sapium argutum</i> (Müll.Arg.) Huber	Shrub Tree
Euphorbiaceae	<i>Sapium glandulosum</i> (L.) Morong	Shrub Tree
Euphorbiaceae	<i>Cnidoscolus quercifolius</i> Pohl	Shrub Tree
Euphorbiaceae	<i>Manihot pseudoglaziovii</i> Pax & K.Hoffm.	NA
Euphorbiaceae	<i>Croton conduplicatus</i> Kunth	Shrub Sub-Shrub
Fabaceae	<i>Mimosa tenuiflora</i> (Willd.) Poir.	Shrub Tree Sub-Shrub
Fabaceae	<i>Poincianella microphylla</i> (Mart. ex G.Don) L.P.Queiroz	Shrub Tree
Fabaceae	<i>Senegalia piauiensis</i> (Benth.) Seigler & Ebinger	Shrub Tree
Fabaceae	<i>Poincianella pyramidalis</i> (Tul.) L.P.Queiroz	Tree
Malvaceae	<i>Pseudobombax simplicifolium</i> A.Robyns	Tree

Table S2 List of plant species identified in the field of view of the digital camera from the Grassland savanna vegetation site.

Family	Scientific name	Life form
Apocynaceae	<i>Aspidosperma tomentosum</i> Mart.	Tree
Asteraceae	<i>Gochnatia pulchra</i> Cabrera	Shrub   Tree
Bignoniaceae	<i>Jacaranda decurrens</i> Cham.	Shrub
Caryocaraceae	<i>Caryocar brasiliense</i> Cambess.	Tree
Cyperaceae	<i>Bulbostylis</i> Kunth	Herb
Erythroxylaceae	<i>Erythroxylum suberosum</i> A.St.-Hil.	Shrub Tree Sub-Shrub
Fabaceae	<i>Machaerium acutifolium</i> Vogel	Tree
Fabaceae	<i>Andira humilis</i> Mart. ex Benth.	Shrub Tree
Lamiaceae	<i>Aegiphila verticillata</i> Vell.	Shrub Tree Sub-Shrub
Malpighiaceae	<i>Byrsonima intermedia</i> A.Juss.	Shrub
Myrtaceae	<i>Eugenia pyriformis</i> Cambess.	Shrub Tree Sub-Shrub
Myrtaceae	<i>Campomanesia pubescens</i> (Mart. ex DC.) O.Berg	Shrub Tree
Arecaceae	<i>Syagrus petraea</i> (Mart.) Becc.	Herb   Palm
Poaceae	<i>Andropogon</i> L.	Herb
Poaceae	<i>Loudetiopsis</i> Conert	Herb
Poaceae	<i>Trachypogon spicatus</i> (L.f.) Kuntze	Herb
Sapotaceae	<i>Pouteria torta</i> (Mart.) Radlk.	Shrub Tree
Sapotaceae	<i>Pradosia brevipes</i> (Pierre) T.D.Penn.	SubShrub
Verbenaceae	<i>Lippia origanoides</i> Kunth	Shrub Sub-Shrub
Vochysiaceae	<i>Qualea grandiflora</i> Mart.	Shrub Tree
Vochysiaceae	<i>Vochysia tucanorum</i> Mart.	Tree

Table S3 List of plant species identified in the field of view of the digital camera from the PDG woodland savanna site.

<b>Family</b>	<b>Scientific name</b>	<b>Life form</b>
Annonaceae	<i>Xylopia aromatica</i> (Lam.) Mart.	Shrub Tree
Caryocaraceae	<i>Caryocar brasiliense</i> Cambess.	Tree
Fabaceae	<i>Pterodon pubescens</i> (Benth.) Benth.	Tree
Fabaceae	<i>Leptolobium dasycarpum</i> Vogel	Tree
Fabaceae	<i>Diptychandra aurantiaca</i> Tul.	Tree
Fabaceae	<i>Anadenanthera peregrina</i> var. <i>falcata</i> (Benth.) Altschul	Shrub Tree
Fabaceae	<i>Copaifera langsdorffii</i> Desf.	Tree
Fabaceae	<i>Vatairea macrocarpa</i> (Benth.) Ducke	Tree
Sapotaceae	<i>Pouteria ramiflora</i> (Mart.) Radlk.	Shrub Tree

Table S4 List of plant species identified in the field of view of the digital camera from the CORE woodland savanna site.

<b>Family</b>	<b>Scientific name</b>	<b>Life form</b>
Annonaceae	<i>Xylopia aromatica</i> (Lam.) Mart.	Shrub Tree
Apocynaceae	<i>Aspidosperma tomentosum</i> Mart.	Tree
Caryocaraceae	<i>Caryocar brasiliense</i> Cambess.	Tree
Fabaceae	<i>Pterodon pubescens</i> (Benth.) Benth.	Tree
Fabaceae	<i>Bowdichia virgilioides</i> Kunth	Shrub Tree
Melastomataceae	<i>Miconia rubiginosa</i> (Bonpl.) DC.	Shrub Tree
Myrtaceae	<i>Myrcia splendens</i> (Sw.) DC.	Tree
Myrtaceae	<i>Myrcia guianensis</i> (Aubl.) DC.	Tree
Sapotaceae	<i>Pouteria torta</i> (Mart.) Radlk.	Shrub Tree
Sapotaceae	<i>Pouteria ramiflora</i> (Mart.) Radlk.	Shrub Tree
Vochysiaceae	<i>Qualea grandiflora</i> Mart.	Shrub Tree



### **Section 3**

## **LEAF PHENOLOGY CORRELATES TO GROSS PRIMARY PRODUCTIVITY: AN INTER-COMPARISON ACROSS SEASONALLY CONTRASTING TROPICAL BIOMES**

Bruna Alberton<sup>1</sup>, Andrew Richardson<sup>2,3</sup>, Ricardo da S. Torres<sup>4</sup>, Humberto Rocha<sup>5</sup>, Magna S. B. De Moura<sup>6</sup>, Leonor Patricia Cerdeira Morellato<sup>1</sup>

<sup>1</sup> Laboratório de Fenologia, Universidade Estadual Paulista (Unesp), Instituto de Biociências, Rio Claro, São Paulo, Brazil

<sup>2</sup> School of Informatics, Computing and Cyber Systems, Northern Arizona University, Flagstaff, AZ, USA

<sup>3</sup> Center for Ecosystem Science and Society, Northern Arizona University, Flagstaff, AZ, USA.

<sup>4</sup> Institute of Computing, University of Campinas, Brazil

<sup>5</sup> Departamento de Ciências Atmosféricas, IAG, Universidade de São Paulo, Brazil

<sup>6</sup> Empresa Brasileira de Pesquisa Agropecuária, Embrapa Semiárido, Brazil

\* Corresponding author

Email address: [bru.alberton@gmail.com](mailto:bru.alberton@gmail.com)

### **1 ABSTRACT**

Tropical forests play a key role in the global carbon budget, but temporal patterns of productivity, their drivers, and constraints remain under discussion. Leaf phenology, the temporal patterns of leaf flushing and senescence, is essential to the understanding of ecosystems processes and has a key role in the seasonality of ecosystems productivity. Understanding the interplay of water and light, the main climatic drivers over tropical vegetation, and the importance of leaf phenology controlling ecosystem productivity under seasonal climates are still on debate. Monitoring phenology over multi-sites may be infeasible, especially for high diverse tropical sites, what motivated the search for new tools. The use of phenocams has been proven an accurate method to monitor leaf phenology continuously over time and simultaneously at different sites or vegetations, tracking vegetation greenness seasonality through

vegetation indices extracted from repeated photographs. Recent studies have reported the correlation between greenness index with GPP curves. Here we proposed a study to investigate the key role of leaf phenology defining temporal patterns of gross primary productivity across contrasting seasonal tropical extra-Amazonian vegetations: the nearly non-seasonal, light limited, evergreen Atlantic Forest; the Cerrado, a neotropical savanna under a wet – dry alternated seasons and; the Caatinga, a xeric vegetation exclusive from Brazil, representing a water-limited, extreme seasonally dry ecosystem. Our main questions are: (i) Does leaf phenology explain GPP patterns across seasonally contrasting biomes? (ii) what is the relative importance of water and light over leaf phenology controlling GPP seasonality? and (iii) How can spatial-temporal dynamics of crown's leafing behaviors contribute to the community leafing patterns? Do these relationships change over contrasting environments that are under different seasonality constraints? We monitored temporal patterns of leaf phenology (leaf flushing and senescence phenophases) derived from digital repeated photograph and partitioned gross primary productivity (GPP) from eddy covariance measurements of CO<sub>2</sub> fluxes. We describe the temporal patterns of leaf production and ecosystem productivity of the three biomes and modeled the relative importance of phenology and the environmental factors over the productivity across sites. The significance of phenology, water and light cues, changes across biomes. Coupled effects of phenology and water availability are observed on the caatinga, while environmental variability and phenology are equally contributing in the cerrado productivity, and phenology is the better explaining factor of GPP in the rainforest vegetation. Through this inter-comparison analysis, we could uncover temporal patterns and drivers of ecosystem productivity across seasonal tropical biomes and disentangle the interplay between phenology and water relations across contrasting seasonal sites, with phenology imposing different influences on vegetations according to their dominant leafing exchange strategies.

## 2 INTRODUCTION

Tropical forests play a key role in the global carbon budget, but we still need to understand some uncertainties regarding the temporal patterns, drivers, and constraints of tropical forests photosynthetic seasonality, a topmost issue in the climate change research agenda, essential to forecast and mitigate effects of the changing climate on carbon cycles. Temporal patterns of leaf development

and senescence are essential to the understanding of ecosystems processes and how the global carbon balance may respond to shifts in climate and atmospheric composition (WILLIAMS et al., 1998; GASH et al., 2004; POLGAR and PRIMACK, 2011; RICHARDSON et al., 2013).

Plant leaf exchange patterns define the seasonality of vegetation communities, which is evident in the proportion of deciduous and evergreen species (REICH, 1995; CAMARGO et al., 2018). Furthermore, leaf phenology, can be related to the vegetation physiology, temporal variations of biomass, leaf area index (LAI), leaf age, deciduousness, length of growing season (LOS), (MIGLIAVACCA et al., 2011; RICHARDSON et al., 2013; PEICHL; SONNENTAG; NILSSON, 2014) and ultimately, driving ecosystem photosynthetic metabolism and carbon budget (RESTREPO-COUBE et al., 2013; SALESKA et al., 2003; WU et al., 2016).

Light and water are the key factors related to the control of photosynthetic seasonality and primary production in the tropics (SALESKA et al., 2003; HUETE et al., 2006; MYNENI et al., 2007; BRANDO et al., 2010), generating a debate around the interplay between water and light limitations depending on the duration and intensity of the dry season. Spatial analysis reported water supply demands as the main constrain controlling seasonal productivity in tropical vegetations globally (KANNIAH et al., 2011; GUAN et al., 2015; WAGNER et al., 2016), and across biomes (ROCHA et al., 2009; RESTREPO-COUBE et al., 2013), defining the boundaries of ecosystems and the transition zones between wet and drylands (OLSON et al., 2001; OLIVEIRAS and MAHLI, 2017). A mean annual precipitation around 2,000 mm yr<sup>-1</sup> was proposed as a threshold that would distinguish water limited systems from those responsive to daylength or other non-environmental cues (GUAN et al., 2015; WAGNER et al., 2016). The importance of leaf phenology controlling ecosystem productivity under seasonal climates are still on debate, since plants respond mainly to climatic variability, but leaf exchange strategies combined with plant functional adaptations, rather than their physiology, are capable of dominating plant-water-carbon relations (VICO et al., 2015).

Near-surface phenology, the use of repeated photographs taken by digital cameras to track vegetation greenness, has been proven an accurate method to monitor leaf phenology continuously over time and simultaneously at different sites or vegetations (RICHARDSON et al., 2007; RICHARDSON et al., 2009; AHRENDTS et al., 2009; MORISETTE et al., 2009; MIGLIAVACCA et

al., 2011; ALBERTON et al., 2017). A handful of studies have demonstrated that camera-derived  $G_{cc}$  index, a measure of vegetation greenness, characterizes the changes in canopy leaf phenology and are temporally related to the ecosystem gross primary productivity (GPP) curves estimated from local eddy flux measurements in temperate forests and grasslands (RICHARDSON et al., 2010; MIGLIAVACCA et al., 2011; KLOSTERMAN et al., 2014; KEENAN et al., 2014; TOOMEY et al., 2015). Leaf phenology has therefore been regarded as the main driver of ecosystem gross primary productivity (GPP) but, contrasting to temperate zones, for high-diverse tropical vegetations the seasonality of photosynthetic activity is not always evident, and environmental drivers and cues for leaf flush and senescence are still unclear and may not be related only to the environmental variability (BORCHERT, 1998; WRIGHT and VAN SCHAIK, 1994; RESTREPO-COUBE et al., 2013; MORTON et al., 2014; CAMARGO et al., 2018).

Phenocams monitoring tropical ecosystems are still sparse when compared with temperate zones, but its use is growing widely. For studies in seasonally dry tropical ecosystems, camera-derived information was able to track leaf seasonal changes for the community and individual species of savanna vegetations (ALBERTON et al., 2014; MOORE et al., 2017). For low seasonal tropical areas as the rainforests of Borneo (NAGAI et al., 2016) or Amazon basin in Brazil (LOPES et al., 2016),  $G_{cc}$  index was less sensitive at the whole community level, but instead, was able to track seasonal vegetation changes when each individual crown at a time were analyzed (LOPES et al., 2016; NAGAI et al., 2016).

Here we proposed a study to investigate the key role of leaf phenology defining temporal patterns of gross primary productivity across contrasting seasonal tropical extra-Amazonian vegetations. Study sites represent three tropical biomes contrasting in the amount and distribution of precipitation along the year, with marked differences regarding the wet and dry season intensity and duration (Fig. 1). Therefore, sites may characterize well the hydroclimate control on tropical vegetations (GUAN et al., 2015) and were used to verify the relative importance of the interplay water and light defining seasonal patterns of gross primary productivity. They are (Fig. 1): the nearly non-seasonal, light limited evergreen Atlantic Forest; the Cerrado, a neotropical savanna under a wet – dry alternated seasons and; the Caatinga, a xeric vegetation exclusive from Brazil, representing a water-limited,

extreme seasonally dry ecosystem (Fig. 1) (OLSON et al., 2001; VELOSO et al., 1991). Since we are analyzing three high diverse vegetations under distinct climatic pressures, we also investigated the role of the crowns leafing behaviors that compose the plant community patterns, by assessing their spatial-temporal dynamics during leafing season.

We monitored temporal patterns of leaf phenology (leaf flushing and senescence phenophases) derived from digital repeated photograph and performed eddy covariance measurements of CO<sub>2</sub> fluxes at three sites of caatinga vegetation, cerrado woodland, and Atlantic rainforest. Our main questions are: (i) Does leaf phenology explain GPP patterns across seasonally contrasting biomes? We expect that camera-derived pattern of leaf production and senescence would be the primary factors explaining ecosystem productivity (GPP) across all sites despite their seasonal status. (ii) what is the relative importance of water and light over leaf phenology controlling GPP seasonality? We expect a light demand response and dry season leaf flush in the rainforest and an increasing water limitation towards cerrado and caatinga. The hydroclimate constrains would interact more with the GPP patterns from the driest to the wettest ecosystems; and (iii) How can spatial-temporal dynamics of crown's leafing behaviors contribute to the community leafing patterns? Do these relationships change over contrasting environments that are under different seasonality constraints? We expect high synchronicity among Caatinga species under extreme water-limited climate and a lower degree of synchrony towards cerrado and rainforest; we aimed to incorporate this approach into the context of the ecosystem productivity patterns, evaluating how phenological dynamics among tropical communities can influence the relationship between  $G_{cc}$  and GPP.

## 1 METHODS

### Sites description

Sites belong to different vegetation types geographically distributed across three main tropical biomes (VELOSO et al., 1991; OLSON et al., 2001): the Caatinga or the desert and xeric shrubland biome, the Cerrado or the grasslands, savannas and shrublands biome, and the tropical rainforest or the moist broadleaf forests biome (Fig. 1). Camera-derived monitoring were conducted in thee extra-Amazonian sites, where flux towers with ongoing eddy covariance measurements were placed (Table

1) measuring leaf phenology and carbon fluxes: caatinga, cerrado woodland, and rainforest.

**Caatinga** – the first site is the exclusive Brazilian vegetation named caatinga, a xeric sclerophyllous vegetation from the Semi-Arid region, mostly distributed in the Northeastern Brazil. The study area has approximately 600 ha, at 342 m a.s.l, and belongs to the *Reserva Legal da Embrapa Semiárido* (9°05'S; 40°19' W), Petrolina municipality, Pernambuco State, Northeastern Brazil (KILL, 2017). According to the 30 years of normal climate data (from 1960 to 1990), compiled from the WorldClim database v.1.0, mean temperature is 24.7°C with minimum of 15.9°C and maximum temperature of 32.9°C, and a mean annual precipitation of 566 mm. Dry season extends along 8 months (May to December), and the wet season is usually from January to April, when precipitation surpass 100 mm (Fig.1). Local vegetation presents a 5 m high canopy composed by xerophilous trees and shrubs and a continuous herbaceous layer adapted to the xeric and harsh conditions, and the richest botanical families are Fabaceae, Euphorbiaceae, Poaceae and Cactaceae (KILL, 2017).

**Cerrado** – the second site is a woody cerrado formation located in the Reserva Ecológica Pé-de-Gigante (PEG) (47° 34' – 47° 41' W; 21° 36' – 21° 44' S) at 649 m a.s.l. The area belongs to the Parque Estadual do Vassununga, at Santa Rita do Passa Quatro county, São Paulo State, Southeastern Brazil. According to the 30 years of normal climate data (1960-1990), mean annual temperature is of 21.1°C, with minimum and maximum ranges of 10.7°C and 29.0°C, respectively. Mean annual precipitation is of 1421 mm, with a wet season extended from October to March (precipitation above 100 mm), and a dry season from April to September (Fig. 1). The PEG Reserve comprehends a heterogenous landscape, covered by open grasslands to woody dense cerrado formations. The vegetation where the flux tower is installed along with the phenocamera system corresponds to the physiognomy classified as a dense cerrado (LATANSIO-AIDAR et al., 2010). This formation is characterized by a dense, dominant woody component, with a high density of shrubs and trees, a discontinuous canopy and a sparse herbaceous layer (RIBEIRO and WALTER, 1998). The dense cerrado dominant woody layer reaches 10 m to 15 m high and are composed mainly of the species *Pterodon pubescens* (Benth.) Benth., *Copaifera langsdorffii* Desf., and *Anadenanthera peregrina* var. *falcata* (Benth.) Altschul from the Fabaceae family. The nearly-closed canopy results in a shaded and cooler understory and the scattered herbaceous component (PIVELLO et al., 1998; LATANSIO-

AIDAR et al., 2010).

**Rainforest** – the last site belongs to the Atlantic Forest or moist broadleaf biome (OLSON et al., 2001; VELOSO et al., 1991; OLIVEIRA-FILHO and FONTES, 2000). Site is located at the Núcleo Santa Virginia (SVG) (coordinates between 23°17'-23°24'S and 45°03'-45°11'W), 1056 m a.s.l, within the area of the Parque Estadual da Serra do Mar, São Paulo State, Southeastern Brazil. The 30-year normal climate data (1960-1990) show a mean annual temperature of 16°C, with minimum of 5.8°C and maximum temperature of 23.8°C, and a mean annual precipitation of 1,692 mm. There is an 8-month wet season extended from September to April and a 4-month drier and colder season from May to August (Fig. 1) but accompanied by a constant mist the stays late in the morning, up to 9:00-10:00 hs and is back around 16:00 – 17:00 hs in the afternoon (pers. obs.). According to the phytosociological survey carried out in the footprint area of the flux tower where phenocamera is installed, the study site is characterized as a mature vegetation, preserved from disturbances for the last 35 years, and under the influence of fog events. The closed canopy is about 20 to 30 m high, Lauraceae and Myrtaceae are the richest plant families, with the occurrence of a high percentage of palm trees represented only by *Euterpe edulis* Mart. species and ferns from the Cyatheaceae family and a rich, dense, herbaceous understory (MARCHIORI et al., 2016).

#### Local climate and environmental variables

For the local climate description, we collected three years of data (2013-2015) from sensors of the meteorological stations located at the flux towers of each site. Environmental variables summarized or extracted from local meteorological sensors were: mean air temperature ( $T_{\text{air}}$ ), cumulative precipitation (P), photosynthetically active radiation (PAR), evapotranspiration (ET), and vapor pressure deficit (VPD). To evaluate dry season intensity, we calculated the cumulative water deficit (CWD), based on the cumulative difference of  $ET-P$ . Every time the result from  $ET-P$  is positive, CWD is set to zero (more details in JAMES et al., 2013; MURRAY-TORTAROLO et al., 2016). Time series of environmental variables were weekly aggregated for data analysis.

To further characterize the dry season experienced by each ecosystem studied, we calculated the dry season precipitation (DSP), as the three-year average of total accumulated precipitation along



the dry season months; and the dry season length (DSL), defined as the consecutive number of months where evapotranspiration (ET) surpass the precipitation (P) (Table 1). Three -year monthly average of environmental variables presented in Figure 2 were confronted with the 30-year normal climate data across each site and were used in the models.

The three-year monthly average of local climatic data from the caatinga vegetation were hotter and drier than the 30-year normal climate (Fig. S 1A E 2A). Local annual mean precipitation was 260 mm and annual mean temperature 27,05°C (Fig. 2 A). Interannual variability of precipitation in the semi-arid region tends to be very high and is mainly attributed to the temperature variation of the Atlantic Ocean, caused by the Atlantic Dipole. This phenomenon can lead to a displacement of the Intertropical Convergence Zone (ITCZ), responsible for the rainfall regime of this region (GUTIÉRREZ et al., 2014). For the cerrado site, local climate data presented a mean annual temperature of 22.5°C and a lower mean annual precipitation of 1,150 mm, when compared with the 30-year normal climate (1,421 mm). The year 2014 was atypical, with a summer much drier than usual, with precipitation reaching just 152 mm between January to February, substantially below the same months during the years of 2013 and 2015 (374 mm and 403 mm, respectively) or the normal precipitation. Dry season length (DSL) extended from May to October. The tree-year monthly average of local climatic data from the rainforest site presented an expected mean annual temperature of 16.7°C but a higher mean annual precipitation of 1,800 mm than the 30-year normal climate (1,692 mm). The 2014 was the rainiest year with 1,965 mm of accumulated precipitation. In addition, DSL was only 1 month long, with August as the driest month (annual average of 45 mm).

#### Eddy covariance measurements

At each one of the study sites previously described, we have a flux tower with an instrumental platform including automatic measurements of climate variables and turbulent atmospheric fluxes. An eddy covariance device measures the atmospheric turbulent fluxes of sensible heat, evapotranspiration, momentum flux, and total CO<sub>2</sub> flux. The eddy correlation method calculates the vertical flux of atmospheric carbon dioxide, a term usually referred to as the net ecosystem exchange (NEE), which in theory means the sum of gross primary productivity, plant respiration, and soil respiration. With

half-hourly data provided from each site's operators, we calculated NEE (in  $\text{mol CO}_2\text{m}^{-2} \text{ s}^{-1}$ ). The partitioning of the  $\text{CO}_2$  NEE flux measurements into Respiration and Gross Primary Productivity (GPP) was calculated following the nighttime approach using the Lloyd-Taylor function (REICHSTEIN et al., 2005). The MDS algorithm (REICHSTEIN et al., 2005) was applied for gap-filling of the variables: net ecosystem exchange (NEE), air temperature ( $T_{\text{air}}$ ), and vapor pressure deficit (VPD). All the eddy covariance data processing and analysis were developed in R (R CORE TEAM, 2017), using the package ReddyProc (REICHSTEIN et al., 2016). Daily sum of GPP time-series were weekly aggregated.

#### Digital camera monitoring

For each one of the study sites, a digital hemispherical lens camera Mobotix Q 24 (Mobotix AG—Germany) was placed at the top of the Flux Tower attached to an extension arm facing northeast at a mean vertical distance of 10 m from the tree canopy. Energy supply is a 12V battery charged by a solar panel. Cameras were configured to automatically take a daily sequence of five JPEG images (at  $1280 \times 960$  pixels of resolution) in the first 10 min of each hour, from 6:00 to 18:00 h (UTC-3; Universal Time Coordinated). The installation of each camera occurred at different times (see Table1). For data analysis, we used a time series spanning from 2013 to 2015 for the caatinga and the cerrado sites. Due to a sequence of gaps in data collection since camera setup, we decided to use only one year and three months of data from the rainforest site. We filled gap sequences of more than 7 days with no images recorded using the StructTS algorithm with a structure model fitted by maximum likelihood (see HYNDMAN and KHANDAKAR, 2008) in R language (R CORE TEAM, 2017) with package imputeTS.

Image data analysis was conducted by defining regions of interest (ROI), as described by Richardson et al. (2007, 2009) and Alberton et al. (2014). For our main analysis, ROIs were based on a community approach, which encompasses the entire image excluding the portion of the field of view obstructed by the tower. A second approach was used to select our ROIs based on the trees crowns within the community ROI (see ALBERTON et al., 2014, 2017). Each individual crown selected from the original image was processed separately (Fig. S1). As high diverse tropical ecosystems may

encompass dozens of species in one single image, we aimed with this approach to verify and scrutinize the greening signals or the crowns leafing behaviors within the community pattern among sites. The spatial and temporal variation of the crowns leafing behavior was considered to evaluate their influence in the camera-derived phenological pattern and in the context of the GPP analysis among sites. Time series associated with crowns (ROIs within the images) belonging to a given vegetation domain were analyzed in function of time, by evaluating their synchronicity, and rate of the  $G_{cc}$  curve values. We highlight that this perspective is based on analyzing tree crowns for the understanding of the overall community pattern. We did not examine species by species, since high diverse tropical forests may have not sufficient replicates for a meaningful interpretation of species behavior in the community fraction represented by the single image.

#### Vegetation index time-series

ROIs were analyzed in terms of the contribution of the relative brightness of the green, red, and blue color channels (RGB chromatic coordinates in WOEBBECKE et al., 1995) in relation to the primary colors (red, green, and blue). The normalized RGB chromatic coordinate ( $RGB_{cc}$ ) index is referred to as the most suitable index to detect leaf color changes, and the most efficient to suppress light variation (GILLESPIE et al., 1987; WOEBBECKE et al., 1995). We calculate the normalized index of the green and red color channels ( $G_{cc}$  and  $R_{cc}$ ), as:

$$Total_{avg} = Red_{avg} + Green_{avg} + Blue_{avg}$$

$$\% \text{ of Green} = \frac{Green_{avg}}{Total_{avg}}$$

$$\% \text{ of Red} = \frac{Red_{avg}}{Total_{avg}}$$

Vegetation indexes were calculated for each of the five hourly images taken by the camera at each day, with a daily measurement extracted by taking the 90<sup>th</sup> percentile of all calculated daytime values. This procedure has been shown to minimize noise in the color channels series ( $RGB_{cc}$ ) related to the illumination effects of seasonal changes and time of the day (adapted by SONNENTAG et al., 2012). Finally, time series were weekly aggregated.

## Data Analysis

### Temporal models

We examined temporal dynamics of leaf phenology and productivity, as well the effects between them and with the environmental factors, using additive mixed models (GAMM), applying a normal distribution, and an identity-link function. As initial scatterplots indicated, response variables GPP and  $G_{cc}$  (y-axis) presented multiple non-linear relationships with the covariates (time and environmental cues). As inherent to time series structure, we tested our data for some temporal autocorrelation among observations. Then, we nest our models with an Auto-Regressive Moving Average (ARMA) time series model, meaning that instead of assuming that errors are independently distributed, we assume that they are indeed correlated. Importantly, generalized additive models (GAM) or smoothing models are considered highly useful for modelling nonparametric responses. Their main assumption is that additive functions can be of smoothing, linear, step, quadratic or other function (HASTIE and TIBSHIRANI, 1990). We did not presume an *a priori* model for the association between response and predictors but instead allowed the data to inform this relationship. Also, the degree of smoothing of an additive model is expressed by the effective degrees of freedom (edf), which mean that the higher the edf, the lower is the linearity of the curve interaction.

To describe the temporal patterns of the variables representing leaf phenology ( $G_{cc}$  and  $R_{cc}$ ) and productivity (GPP) across the biomes, we fitted models using time as the smooth explanatory term. To investigate our main question, we first fitted single-variable models between GPP and the biotic ( $G_{cc}$  and  $R_{cc}$ ) and abiotic (precipitation, CWD, PAR, and  $T_{air}$ ) explanatory variables to evaluate the contribution of each factor separated on the productivity. Then, to understand the relative importance of phenology and the environmental variability over GPP across contrasting seasonal biomes, we fitted two multivariate full models: an abiotic model using the explanatory terms related to water ( $P$  and CWD), light demands (PAR), and mean air temperature ( $T_{air}$ ), and a biotic-abiotic model by adding phenology as an explanatory term. All terms included in the multivariate models were previously checked for multicollinearity. By assessing the approximate significance parameters of the smooth and/or linear terms and the coefficient of determination from the models, we could compare the

performance between the single-variable, abiotic, and the biotic-abiotic models. All analysis were run in R language (R CORE TEAM, 2017) using base package mgcv (WOOD, 2006) for the generalized additive models.

### Spatial-temporal phenological dynamics

To answer our third question, we carried out a visual analysis into the complete set of crowns ROIs in order to extract the onset date of phenological stages transitions. We select the leaf flushing onset as the phenophase to test the degree of synchrony of the crowns time series greening, and we analyze all the ROIs crowns in function of time to evaluate timing and rate of the Gcc time series within each vegetation site. We applied circular statistics to calculate the mean angle or date correspondent to the most frequent date of leaf flushing onset (see MORELLATO et al., 2000; MORELLATO et al., 2010). We divided the 360° of a circumference by 12 and each month of the year is represented by a range of 30° starting on January (midpoint 15°, see MORELLATO et al., 2010 for details). Then, we tested whether the mean onset data are significantly concentrated around the mean angle or date, as a proxy of seasonality by applying the Rayleigh test ( $Z$ ), as suggested by Morellato et al. (2000, 2010). If the mean onset data are significantly concentrated around the mean angle or date, we consider the leafing pattern seasonal. The degree of synchrony represented by the length of the vector  $r$  has no unity and ranges from 0 (no synchronicity) to 1 (perfect synchrony). We performed circular analyses per study site, for all the crowns using Oriana 4.0 (Kovach Computing Services).

## 3 RESULTS

### 3.1 Temporal patterns of phenology and productivity across sites

Phenocam indices revealed seasonal patterns for all sites despite their degree of seasonality (Fig. 3). In general,  $G_{cc}$  and  $R_{cc}$  indexes showed inverse relationship, with  $G_{cc}$  presenting higher values from the late dry season towards the wettest months, which are related to the leaf flushing of the vegetation community, while  $R_{cc}$  highest values were prevalent along the driest periods, which are mainly related to the process of senescence and the decrease of green biomass. Curve oscillations, which means the peaks and valleys of  $G_{cc}$  and  $R_{cc}$  values along time, presented different patterns across

sites.

The  $G_{cc}$  pattern for the caatinga vegetation presented marked seasonality, with an abrupt green-up precisely at the beginning of the wet season and a relatively abrupt green-down starting at the end of the wet season. During the dry season, low values of  $G_{cc}$  were nearly constant giving a flat pattern to the curve. Within the wet period,  $G_{cc}$  showed oscillations with peaks and valleys that followed precipitation events (Fig 3 A). The rest season corresponding to the driest months was long (from April to November) presenting few or none  $G_{cc}$  oscillations, but not reaching zero, which indicates the presence of some green biomass. Cactaceae family species as the Facheiro (*Pilosocereus pachycladus* F.Ritter) can be found through all the year in the images and are likely responsible for sustaining  $G_{cc}$  values during dry season. In the cerrado vegetation,  $G_{cc}$  presented a marked green-up earlier, yet in the dry season, and a slower green-down, in comparison to the caatinga site. The cerrado green-down started by the end of the wet season and extended until the end of the dry season (Fig. 3 C). For the rainforest, green-up started right in the driest month with a progressive increase towards the wet period (Fig. 3 E). Green-down started from the middle of the wet season and was less abrupt than the caatinga but with a higher decrease in a shorter time if compared with the cerrado site.

$R_{cc}$  curves demonstrated an inverse pattern to  $G_{cc}$  in the wet seasons across all sites. Within the dry periods,  $R_{cc}$  for the caatinga peaked at the beginning of the dry season followed by a linear decrease towards the mid to the end of the dry season (Fig. 3 B). Inversely, in the cerrado site,  $R_{cc}$  time series increased by the end of the wet season peaking by the end of the dry season (Fig. 3D). In the late dry season (August), red increasing did not follow the inverse pattern with  $G_{cc}$ ; in fact, they increased together (Fig. 2C and D). This pattern is linked to the colorful, reddish new leaves, produced right at the start of the community leaf flushing.  $R_{cc}$  curve from rainforest site was higher for winter time, just when  $G_{cc}$  scores have decreased, and showed the lowest range of values of all sites (min= 0.3074/max= 0.3176). This may indicate an absence of a massive leaf senescence in the community. Instead, species leaf turnover may be occurring along the all year.

As occurred for the camera-vegetation indices, sites also presented differences regarding GPP seasonality (Fig. S4). Productivity started to increase within the wet season in the caatinga and cerrado sites (Fig. S4 A and B), while in the rainforest GPP, curve oscillations did not present a tightly link

with the precipitation events (Fig. S4 C). There were discrepancies regarding amplitude and range of GPP values among sites, with caatinga presenting the lowest values (min=0/max=5.88  $\mu\text{mol CO}_2 \text{ m}^{-2} \text{ s}^{-1}$ ), followed by cerrado (min=0.40  $\mu\text{mol CO}_2 \text{ m}^{-2} \text{ s}^{-1}$  / max=11.00  $\mu\text{mol CO}_2 \text{ m}^{-2} \text{ s}^{-1}$ ) and rainforest (min=2.39  $\mu\text{mol CO}_2 \text{ m}^{-2} \text{ s}^{-1}$ /max=11.02  $\mu\text{mol CO}_2 \text{ m}^{-2} \text{ s}^{-1}$ ). The cerrado vegetation presented the highest range of productivity (10.60  $\mu\text{mol CO}_2 \text{ m}^{-2} \text{ s}^{-1}$ ).

### 3.2 Camera-derived phenology and GPP relationships

Temporal models were significant between GPP and  $G_{cc}$  for all vegetations, and between GPP and  $R_{cc}$  for the cerrado and rainforest sites (Table 2).  $G_{cc}$  and GPP from the caatinga site presented the most coincident pattern, with both time series demonstrating similar oscillations during growing season, but with  $G_{cc}$  never reaching zero (Fig. 4 A). Single variable model fitted between GPP and  $G_{cc}$  in the caatinga site showed an exponential high relationship ( $R^2 = 0.70$ ), while the relationship between GPP and  $R_{cc}$  was not significant (Fig. 5A and B). In the cerrado, there was a displacement between GPP and  $G_{cc}$  curves (Fig. 4B). While  $G_{cc}$  presented its marked green-up and peak in the transition from dry to the wet season, GPP started increasing within the wet season, reaching its peak in the mid of the wet period. Green-down and decreasing of productivity were less coincident during the year cycle of 2014/2015 than the ones observed for previous years (Fig. 4B). GPP and  $G_{cc}$  presented a sigmoidal function relationship ( $R^2 = 0.30$ ) and the strongest relationship with  $R_{cc}$  ( $R^2 = 0.44$ ) among all sites (Fig. 5 C and D).  $G_{cc}$  green-down pattern in the rainforest occurred in delay when compared to the GPP curve, and the green-up started ahead to the productivity increases (Fig. 4C). GPP pattern was significantly explained through sigmoid curves (Fig. 5 E and F) by  $G_{cc}$  ( $R^2 = 0.40$ ) and  $R_{cc}$  ( $R^2 = 0.36$ ).

### 3.2 Environmental cues and GPP relationships

Among all sites, GPP presented significant relationships with environmental cues (Table 2). In the caatinga, significant relationships were found only for water related variables. The cumulative water deficit (CDW) was the most important climatic factor ( $R^2 = 0.32$ ), showing an inverse sigmoid interaction with decline values of GPP (Fig. 6A), followed by the precipitation ( $R^2 = 0.24$ ). Between the two multivariate models, biotic-abiotic performed better ( $R^2 = 0.78$ ) than the abiotic model ( $R^2 =$

0.67). In the cerrado, precipitation was the best predictor of GPP ( $R^2 = 0.36$ ) with a polynomial function and a low threshold of precipitation values (until 10 mm) for GPP increase (Fig. 6B), followed by  $T_{\text{air}}$  ( $R^2 = 0.19$ ), PAR ( $R^2 = 0.17$ ), and CWD ( $R^2 = 0.15$ ). The biotic-abiotic model obtained the best performance in predicting GPP ( $R^2 = 0.76$ ). GPP patterns from the rainforest site presented significant interactions only with the variable mean air temperature ( $T_{\text{air}} - R^2 = 0.25$ ) that showed a sigmoidal curve of interaction with GPP reaching highest values above 17.5 °C (Fig. 6C) and, like the other sites, the biotic-abiotic models had the best relationship with productivity ( $R^2 = 0.40$ ).

### 3.3 Spatial-temporal crowns greening dynamics

A total of 212 ROIs representing plant crowns from the images were selected among all sites, distributed along 35 ROIs for the caatinga, 72 ROIs for the cerrado and 105 ROIs for the rainforest (Fig. S1). From these number of ROIs, we were able to extract the onset day of the leaf flushing phenophase for a reduced number, due the loss of plant individuals for mortality and coverage by nearby crowns or lianas across the years. At the end, visual inspection was carried out for 31 ROIs from caatinga, 46 ROIs from the cerrado and 94 ROIs from the rainforest. Onset dates from these individuals generated the synchronicity index represented by the Rayleigh test (Fig. S2). Caatinga was the vegetation community that reached the highest synchronicity among their ROIs crowns leafing behaviors ( $r = 0.98$ , mean angle = 334°), followed by the cerrado ( $r = 0.89$ , mean angle = 261°) and the rainforest ( $r = 0.37$ , mean angle = 333°).

The high degree of synchrony by the caatinga and the cerrado vegetations is demonstrated by the temporal patterns of crowns ROIs greening signals in Figure 7. Nearly all crowns from the caatinga presented similar timing regarding leaf phenological transitions, with coincident greening patterns by the start and end of the wet period (Fig. 7 A). In the cerrado site,  $G_{\text{cc}}$  crowns green-up were concentrated at the end of the dry season, and with groups of individuals green-up entering the wet period, demonstrating groups flushing at different times along the wet season (Fig. 7B). Greening signals related to crowns from the rainforest showed the less synchronic patterns, with not concentrations of marked  $G_{\text{cc}}$  transitions along the period. Instead,  $G_{\text{cc}}$  curves presented a flatter shape or seasonal changes more distributed at different times of the year, not only during dry season (Fig.



7C).

## 4 DISCUSSION

### 4.1 Leaf phenology, water/light relationship and the GPP across contrasting tropical biomes

Temporal patterns of tropical ecosystem productivity and leaf phenology production were significantly correlated across all vegetations studied, and presented the strongest relationships, when compared with the GPP and environmental variables interactions. Across our contrasting biomes, we reported a much stronger coupled relation between GPP and  $G_{cc}$  for the caatinga site ( $R^2 = 0.70$ ), when compared to the cerrado ( $R^2 = 0.30$ ) and rainforest ( $R^2 = 0.40$ ). The only comparable study on seasonal tropics reporting GPP- $G_{cc}$  relationships for an Australian savanna (MOORE et al., 2017) showed that community  $G_{cc}$  had different performances for understory and overstory layers, with the grasslands component better coupled with carbon fluxes ( $R^2 = 0.65$ ) than shrubs and trees ( $R^2 = 0.23$ ). Studies investigating GPP prediction by camera-derived indices are concentrated on the north hemisphere (e.g.: RICHARDSON et al., 2007; AHRENDT et al., 2009; MIGLIAVACCA et al., 2011; PEICHL et al., 2014).  $G_{cc}$  index performed well by correlating with GPP across temperate deciduous forests, explaining over 80% of the carbon fluxes seasonality (RICHARDSON et al., 2007; AHRENDT et al., 2009; TOOMEY et al., 2015).

We confirmed the strong relationships between GPP and phenology in our results. In spite of that, there was also an important influence of climatic constraints over productivity on the seasonal ecosystems of caatinga and cerrado. In fact, when we compared abiotic (just environmental factors) and biotic-abiotic models (environmental factors and greening), we notice an improvement of explanation when phenology and environmental terms are added together in the model. For the caatinga vegetation, the GPP patterns closely following the precipitation presented similarity to the few records of productivity rates derived from MODIS products, also characterized by the fast vegetation response to moisture pulses (SILVA et al., 2013; MORAIS et al., 2017). The caatinga greening and GPP curve oscillations during the wet season have been also described for carbon fluxes from other high seasonal ecosystems, such as temperate grasslands (BROWN et al., 2016; MURRAY-TORTAROLO et al., 2016).

The cerrado productivity observed here followed the expected pattern for wet savannas (MIRANDA et al., 1997; CHEN et al., 2003), with GPP likely constrained by a wet-dry climate, high rates of GPP along the wet season, and a steep decrease in the driest months. For savannas, seasonal patterns of rainfall and changes in soil water content have been tightly coupled with productivity indices as GPP (CHEN et al., 2003). Rainfall plays a critical role in determining the distribution of GPP of distinct tropical vegetation types, ranging from rainforests to arid grasslands (KANNIAH et al., 2010).

We did not find any previous publications reporting GPP patterns from Atlantic Forest. However, for evergreen tropical sites across the world as well as Central Amazon forests, seasonality increases photosynthetic capacity during dry season, indicating not prevalent climatic constraints (BRANDO et al., 2010; GUAN et al., 2015; WU et al., 2016). In the case of our Atlantic rainforest, we notice a decrease of ecosystem photosynthesis during the coldest and driest months, characterized by a lowest mean air temperature when compared with other tropical evergreen forests, which are explained by the local elevated altitude of 1,056 m a.s.l (MARCHIORI et al., 2016). Ground biomass studies carried out in the same site indicated an increase in the stocks of carbon and nitrogen along a gradient of elevation, suggesting a relationship of decreasing temperature with reduced photosynthetic activity, since colder soil temperatures would tend to lose less carbon to the atmosphere (RAICH et al., 2002; VIEIRA et al., 2011; MARCHIORI et al., 2016). Also, temperature has been reported as an important factor influencing several biogeochemical terrestrial processes (WU et al., 2011). The interaction of temperature and rainfall and its influence on tropical productivity has been recently reported, where high rainfall can decrease C cycling rates when interacting with cool temperatures ( $< 20^{\circ}\text{C}$ ), while in warm forests ( $> 20^{\circ}\text{C}$ ), rainfall and temperature interaction produces the opposite effect (TAYLOR et al., 2017).

#### 4.2 Leaf phenology spatiotemporal dynamics and ecosystem productivity across seasonal biomes

Through the crowns greening analysis carried out in the present study, we teased apart the composite greening signals of the vegetation communities and indicated, for each vegetation, the dominant patterns that represent the community and affect carbon fluxes, providing us insights about how phenological dynamics were triggering or dampening photosynthesis dynamics of each

ecosystems. The evaluation of the spatial and temporal phenological dynamics from individual crowns greening patterns within digital images have been reported for other studies involving camera-derived leafing patterns description and spatial variability (RICHARDSON, 2009; LOPES et al., 2016; NAGAI et al., 2016), as well as to investigate GPP patterns (AHRENDT et al., 2009).

Caatinga and cerrado, the most seasonal sites, presented higher synchronicity in terms of time and rate of crowns greening signals, while rainforest has demonstrated a non-seasonal pattern with crowns  $G_{cc}$  curves distributed along the all period or with no marked seasonality and synchronicity among crowns. Based on theories of community and phenology dynamics, we made inferences regarding the synchronicity dynamics across sites. Shorter growing seasons would concentrate species occurrence at the same time, while longer growing seasons would facilitate species life cycles to different times of the year. This could affect the way competition influence species dynamics as well, swinging from a relative strength of interspecific competition in the first case, to a intraspecific competition in the latter (see more in MITTELBACH, 2017). Climatic constrains appear to underlie this effect with more strength from the Equator towards higher latitudes (USINOWICZ et al., 2017).

Due the high variation of seasonal and inter-annual climatic conditions in tropical vegetations, there is a high diversity of physiological and phenological strategies of plants to cope with changes in water availability (MURPHY and LUGO, 1986; LEHMANN et al., 2009; VICO et al., 2015). While evergreen species would be favored by short dry seasons length or by the ability to access groundwater or water stores, on the other hand, high inter-annual seasonality of wetter periods would be favoring the occurrence of different deciduous phenological strategies (REICH, 1995; RIVERA et al., 2002; VICO et al., 2015; CAMARGO et al., 2018).

There is a lack of knowledge regarding the mechanisms controlling leaf phenology strategies of individual plants due their complexity (BORCHERT and RIVERA, 2001; CAMARGO et al., 2018) and the high diversity of plant species and strategies in the tropics. Nevertheless, we can classify our plants into three main leaf phenological strategies (EAMUS and PRIOR, 2001; SINGH and KUSHWAHA, 2005; ELLIOT et al., 2006): (i) opportunistic drought deciduous species, mainly driven by water availability and leaf flushing following the first rainfall events indicating the start of the wet season; (ii) schedule drought deciduous species, independent of water availability and mainly driven

by photoperiod, temperature, or radiation, with leaf flushing before or early the wet season; and (iii) evergreen species, able to shed new leaves asynchronously throughout the year. Each strategy imposes its own risks to plants given the ecological tradeoffs of each case. That is why a nuanced of species strategies may be found in the tropics rather than the prevalence of one, given the variation in changes of rainfall availability and predictability (VICO et al., 2015; CAMARGO et al., 2018).

Hereafter, we discuss based on the climatic seasonality imposed on each biome and by assessing the crowns leafing behavior within the vegetation communities, how leaf phenology controlling productivity may change across the biomes.

#### 4.2.1 High synchronic leaf phenology and productivity in seasonally constrained vegetation: the caatinga case

The temporal patterns of leaf production and ecosystem productivity in the caatinga were very coincident with both presenting multiple seasonal cycles within the wet period. This irregular pattern visually followed shortly the moisture pulses) or tracked the reduced deficit of water as by the temporal models. Similar patterns were detected by cameras across other ecosystems such as the grasslands, where there is a vegetation dependent on the inter-annual variation of precipitation rates (BROWN et al., 2016; RICHARDSON et al., 2018). Phenological direct observations of caatinga commonly recorded flowering and flushing phenophases as a consequence of precipitation with formation of new leaves immediately after the rainfall event (CARVALHO and BARBOSA, 1989; MACHADO et al., 1997; ARAÚJO; CASTRO; ALBUQUERQUE, 2007).

High synchronicity among crowns leafing behaviors suggests a common high influence of climatic factors triggering leaf phenophases. The harsh seasonal conditions lead the caatinga to be mainly composed of opportunistic drought deciduous species described above, avoiding dry season stress and constrained their leafing to periods of water availability (see VICO et al., 2015). Leaf flushing in opportunistic drought deciduous species are usually synchronous and responsive to water availability. There are cases, where species may respond to other precedent cues such as atmospheric water decreases, but in general still associated with small rainfall events (MURPHY and LUGO, 1986; BORCHERT, 1994; WILLIAMS et al., 1997). Year-to-year high interannual variability in the

precipitation rates contribute to the variability of the onset community leaf flushing and occasionally to be more or less intense (MACHADO et al., 1997). Thus, climatic constraints in the caatinga and leaf phenology are tightly coupled and then varying together, what mostly explains the high correlation between phenology and GPP in a very water dependent ecosystem. Despite that, we highlight the model improvement when phenology is added in the biotic-abiotic model ( $R^2 = 0.78$ ).

#### 4.2.2 Leaf phenology synchronicity and productivity in a mid-seasonal ecosystem

The woodland cerrado temporal patterns of leaf production and productivity demonstrated a marked seasonality with a lower degree of asynchrony between crowns compared to caatinga. Green-up onset occurred yet in the late dry season, a pattern shared by savannas, with the input of new leaves preceding the massive rainfall events (e.g.: MONASTERIO and SARMIENTO, 1976; WILLIAMS et al., 1999; PIRANI et al., 2009; MUNHOZ and FELFILI, 2005; RYAN et al., 2016; ADOLE et al., 2016). The onset of GPP occurred after entering the wet season and demonstrated to be mainly correlated with the seasonal patterns of precipitation, following the leaf flushing.

Plant species from less harsh climatic conditions, as our study cerrado, may be able to cope with water limitations and find longer and wetter periods to produce new leaves still during the dry season (BORCHERT, 1998). Cerrado trees, for example, may use deep roots to exploit deeper soil water sources and be able to flush new leaves in the late dry season (EAMUS, 1999; SCHOLZ et al., 2008; ROSSATO et al., 2012). A high synchronic pattern was demonstrated by the crowns greening behaviors from the studied cerrado community and a timing concentration of leafing onset at the end of the dry season in September. This behavior characterizes schedule drought deciduous species, or those capable of enduring droughts by developing adaptations to maximize their carbon gains without experiencing stress (SCHOLZ et al., 2002; VICO et al., 2015; ELLIOT et al., 2006). Schedule drought deciduous are mainly driven by consistent factors such as photoperiod and demonstrate high interspecific synchronicity and low inter-annual variability on the leaf flushing dates (VICO et al., 2015; CAMARGO et al., 2018).

We conclude from our results that both: climate, mainly through water relations, and phenology, represented by a larger range of leaf strategies including schedule drought deciduous

species, contribute to the seasonal patterns of GPP in the cerrado. Our finding concurs with general expectation that savanna productivity would be predicted by a complex interaction of climatic and phenological factors (KANNIAH et al., 2011; WHITLEY et al., 2011; MA et al., 2013, 2014; MOORE et al., 2017).

#### 4.2.3 Leaf phenology asynchrony explains productivity of less seasonal ecosystems

The degree of synchronicity of rainforest crowns greening, calculated based on the visual inspection of the crowns greening signals was the lowest among the three ecosystems studied, typical for a non-seasonal vegetation. In fact, leaf flushing dates were concentrated in two main periods (December and March), demonstrating a bimodal pattern. The production of new leaves slowed down during the colder and driest months, with most of  $G_{cc}$  curves presented a flat pattern in the driest month (August). Seasonality in the phenological transitions of leafing and flowering were demonstrated by other Atlantic Rainforest locations, belonging to the same latitude of our study site (e.g.: MORELLATO et al., 2000; BENCKE and MORELLATO, 2002; PEREIRA et al., 2008). The driest months are also the colder ones, concentrated in June, July, and August, and the community leaf flushing increase is marked in the transition from the driest to the wettest months, during September and October (MORELLATO et al., 2000), which coincides with the pattern tracked by the cameras in our study.

The  $G_{cc}$  and  $R_{cc}$  values detected for our rainforest were the highest and lowest, respectively, among our three vegetations. This outcome, in association with the low degree of synchronicity of the crowns greening are explained by the predominance of evergreen species in this vegetation biome (MORELLATO et al., 2000; BENCKE and MORELLATO, 2002). The dominance of evergreen species strategists, or plants retaining their foliage year-round and simultaneously exchanging new foliage and senescing old ones, may sustain vegetation indices values due persistent green biomass along the all year (see RICHARDSON et al., 2018). The evergreen species show asynchronous activity throughout the year, without apparent seasonal changes in their leaf area index (LAI) and, therefore, endure drought by physiological adaptations that are not yet well clear in the literature (BORCHERT, 1994; NEPSTAD et al., 1994; REICH, 1995; BORCHERT, 1998).

Despite the influence of low temperatures in the GPP patterns, the Atlantic rainforest showed a reduced influence of environmental factors. Given that evergreen species tend to be more independent from seasonal environmental constraints (BORCHERT, 1998), we suggest that leafing phenology is exerting the main control over the temporal patterns of ecosystem productivity in the less seasonal biome of Atlantic rainforest.

We also suggest that the moderate effect between phenology and GPP in the rainforest vegetation is partially influenced by the seasonal low ranges of temperature during dryer months. We also recognize the fact that evergreen phenological patterns may be underestimated for being more complicated to be tracked by camera-derived indices (TOOMEY et al., 2015; NAGAI et al., 2016; LOPES et al., 2016; RICHARDSON et al., 2018). Also, the vegetation index here applied, derived from RGB color channels sensors as the phenocams, may not be able to follow the stages of leaf maturation precisely, since that the chromatic coordinates are more sensitive to light colors and would better indicate the seasonality of leaf production (see LOPES et al., 2016). The importance to consider leaf aging stages on the response of productivity has been reported for tropical evergreen forests (WU et al., 2016).

## 5 CONCLUSIONS

A fine-scale phenological monitoring using the repeated photograph technic is unprecedented for the Caatinga dry forest, Brazilian savanna and the Atlantic Rainforest. In the case of the Cerrado, cameras have already been applied for species and community levels of tropical savannas, used in the context of method validation with ground observations for woody cerrado (ALBERTON et al., 2014) and in ecosystem productivity studies in Australian savannas (MOORE et al., 2017). The addressed questions in this study, involving tropical sites under different seasonality constraints, are a significant step towards the understanding of ecosystem functionality. Accordingly, phenology and its confident representation is a key parameter to be considered in climate e biogeochemical cycle models (MA et al., 2013). Carbon fluxes relationships with the canopy development are still underexplored and not well described for the tropics. Despite the existence of record from GPP seasonality and dynamics for tropical seasonal sites, the actual knowledge about how phenology and GPP covary is still limited, and

we offer the first strong evidence of leafing phenology shaping GPP patterns across seasonally dry tropical biomes. Even considering GPP patterns and controls still need further investigation, the data analyzed here, combining hourly digital images and high frequency eddy covariance measurements, is unprecedented for the tropics and brings the first modeling of biotic and abiotic controls of productivity and photosynthesis seasonality.

We bring evidences of a complex interaction of both environmental and phenology controlling productivity in tropical ecosystems. Temporal patterns of GPP across biomes varied and presented distinct differences that at some extent confirmed the hydroclimate hypothesis initially proposed. Caatinga vegetation was constrained by the strong dry season and leafing and GPP patterns were coupled in a climatic-phenological interaction, while reduced influence of climatic and phenological seasonality defined GPP seasonality for the cerrado, and a strong relation of GPP and phenology in the less seasonal rainforest. Camera-derived phenology is, therefore, a good proxy for productivity in high synchronic and seasonal tropical ecosystems, as the caatinga.

Importantly, the outcomes reported on this study were only possible due a multi-site comparison analysis, enabling the observation of the nuances of the leaf phenology dynamics and GPP patterns across biomes. We highlight the impacts of future changes on water regimes for the tropics over the productivity of seasonal vegetations, also affecting phenological responses of species, on seasonal tropical ecosystems (VICO et al., 2015; MORELLATO et al., 2016, RESTREPO-COUPÉ et al., 2017).

**Acknowledgments** – the present study was supported by São Paulo Research Foundation - FAPESP (grants #2009/54208-6, #2010/52113-5 and #2013/50155-0), Microsoft Research and CNPq. We thank the Instituto Florestal for the permissions to work at the Cerrado and Atlantic Rainforest sites, and Embrapa for all the support and collaboration in the Caatinga site. BA receives fellowship from FAPESP (#2014/00215-0 and #2016/01413-5). LPCM, RST and HR receive a research productivity fellowship from CNPq.

## 6 REFERENCES



ADOLE, T.; JADU, D.; ATKINSON, P.M. A systematic review of vegetation phenology in Africa. **Ecological informatics**, v. 34, p. 117-128, 2016.

AHREND, H.E. et al. Tree phenology and carbon dioxide fluxes: Use of digital photography for process-based interpretation at the ecosystem scale. **Climate Research**, v. 39(3), p. 261–274, 2009.

ALBERTON, B.C. et al. Introducing digital cameras to monitor plant phenology in the tropics: Applications for conservation. **Perspectives in Ecology and Conservation**, v. 15, p. 82-90, 2017.

ALBERTON, B.C. et al. Using phenological cameras to track the green up in a cerrado savanna and its on-the-ground validation. **Ecological Informatics**, v. 19, p. 62–70, 2014.

ARAÚJO, E.L.; CASTRO, C.C.; ALBUQUERQUE, U.P. Dynamics of Brazilian Caatinga – A Review Concerning the Plants, Environment and People. **Functional Ecosystems and Communities**, v. 1, p. 15–28, 2007.

BENCKE, C.S.C.; MORELLATO, L.P.C. Estudo comparativo da fenologia de nove espécies arbóreas em três tipos de floresta atlântica no sudeste do Brasil. **Revista Brasileira de Botânica**, v. 25(2), p. 237–248, 2002.

BORCHERT, R. Water status and development of tropical trees during seasonal drought. **Trees**, v. 8 (3), p. 115-125, 1994.

BORCHERT, R. Responses of tropical trees to rainfall seasonality and its long-term changes. **Climatic Change**, v. 39(2), p. 381–393, 1998.

BORCHERT, R.; RIVERA, G. Photoperiodic control of seasonal development and dormancy in tropical stem-succulent trees. **Tree Physiology**, v. 21 (4), p. 213-221, 2001.

BRANDO, P. M. et al. Seasonal and interannual variability of climate and vegetation indices across the Amazon. **Proc. Natl Acad. Sci., USA**, v. 107, p. 14685–14690, 2010.

BROWN, T.B. et al. Using phenocams to monitor our changing earth: Toward a global phenocam network. **Frontiers in Ecology and the Environment**, v. 14(2), p. 84–93, 2016.

CAMARGO, M.G.G. et al. Leafing patterns and leaf exchange strategies of a cerrado woody community. **Biotropica**, v. 50 (3), p. 442-454, 2018.

CARVALHO, D.; BARBOSA, D.A. Dados fenológicos de 10 espécies arbóreas de uma área de caatinga (Alagoinha-PE ). **Acta bot. bras.**, v. 3(2), p. 109–117, 1989.

CHEN, X.; HUTLEY, L.B.; EAMUS, D. Carbon balance of a tropical savanna of northern Australia. **Oecologia**, v. 137(3), p. 405–416, 2003.

EAMUS, D. Ecophysiological traits of deciduous and evergreen woody species in the seasonally dry tropics. **Trends in Ecology and Evolution**, v. 14(1), p. 11–16, 1999.

EAMUS, D.; PRIOR, L. Ecophysiology of trees of seasonally dry tropics: comparisons among phenologies. **Advances in Ecological Research**, v. 32, p. 113-197, 2001.

ELLIOTT, S.; BAKER, P.; BORCHERT, R. Leaf flushing during the dry season: the paradox of Asian monsoon forests. **Global Ecology and Biogeography**, v. 15 (3), p. 248-257, 2006.

GASH, J.H.C. et al. Amazonian climate: Results and future research. **Theoretical and Applied Climatology**, v. 78(1-3), p. 187-193, 2004.

GILLESPIE, A.R.; KAHLE, A.B.; WALKER, R.E. Color enhancement of highly correlated images. II. Channel ratio and “chromaticity” transformation techniques. **Remote Sensing of Environment**, v. 22(3), p. 343-365, 1987.

GUAN, K. et al. Photosynthetic seasonality of global tropical forests constrained by hydroclimate. **Nature Geosci**, v. 8(4), p. 284-289, 2015. Available at: <http://dx.doi.org/10.1038/ngeo2382>.

GUTIÉRREZ, A.P.A. et al. Drought preparedness in Brazil. **Weather and Climate Extremes**, v. 3, p. 95-106, 2014. Available at: <http://dx.doi.org/10.1016/j.wace.2013.12.001>.

HASTIE, T.J.; TIBSHIRANI, R. Generalized additive models. **Statistical Science**, v. 1(3), p. 297-318, 1990.

HUETE, A.R. et al. Amazon rainforests green-up with sunlight in dry season. **Geophys. Res. Lett.**, v. 33, 2006.

HYNDMAN, R.J.; KHANDAKAR, Y. Automatic time series forecasting: The forecast package for R. **Journal Of Statistical Software**, v. 27(3), p. C3-C3, 2008. Available at: <http://www.robjhyndman.com/papers/forecastpackage.pdf>.

JAMES, R. et al. Implications of global warming for the climate of African rainforests. **Phil Trans R Soc B**, 2013

KANNIAH, D. et al. The comparative role of key environmental factors in determining savanna productivity and carbon fluxes: A review, with special reference to northern Australia. **Progress in Physical Geography**, v. 34 (4), p. 459-490, 2010.

KANNIAH, K.D.; BERINGER, J.; HUTLEY, L.B. Environmental controls on the spatial variability of savanna productivity in the Northern Territory, Australia. **Agricultural and Forest Meteorology**, v. 151(11), p. 1429-1439, 2011.

KEENAN, T.; GRAY, J.; FRIEDL, M. Net carbon uptake has increased through warming-induced changes in temperate forest phenology. **Nature Climate Change**, v. 4 (June), p. 598-604, 2014.

KILL, L.H.P. Caracterização da vegetação da reserva legal da Embrapa semiárido. **Documentos online**, v. 5, p. 121-124, 2017

KLOSTERMAN, S.T. et al. Evaluating remote sensing of deciduous forest phenology at multiple

spatial scales using PhenoCam imagery. **Biogeosciences**, v. 11(16), p. 4305–4320, 2014.

LEHMANN, C.E.R.; PRIOR, L.D.; BOWMAN, D.M.J.S. Decadal dynamics of tree cover in an Australian tropical savanna. **Austral Ecology**, v. 34 (6), p. 601–612, 2009.

LOPES, A.P. et al. Leaf flush drives dry season green-up of the Central Amazon. **Remote Sensing of Environment**, v. 182, p. 90–98, 2016. Available at: <http://dx.doi.org/10.1016/j.rse.2016.05.009>.

MA, X. et al. Spatial patterns and temporal dynamics in savanna vegetation phenology across the North Australian Tropical Transect. **Remote sensing of Environment**, v. 139, p. 97–115, 2013.

MA, X. et al. Parameterization of an ecosystem light-use-efficiency model for predicting savanna GPP using MODIS EVI. **Remote Sensing of Environment**, v. 154, p. 253–271, 2014.

MACHADO, I.C.S.; BARROS, L.M.; SAMPAIO, E.V.S.B. Phenology of Caatinga Species at Serra Talhada, PE, Northeastern Brazil. **Biotropica**, v. 29(1), p. 57–68, 1997.

MARCHIORI, N.M. et al. Tree Community Composition and Aboveground Biomass in a Secondary Atlantic Forest, Serra Do Mar State Park, São Paulo, Brazil. **Cerne**, v. 22(4), p. 501–514, 2016.

MIGLIAVACCA, M. et al. Using digital repeat photography and eddy covariance data to model grassland phenology and photosynthetic CO<sub>2</sub> uptake. **Agricultural and Forest Meteorology**, v. 151(10), p. 1325–1337, 2011.

MIRANDA, A.C. et al. Fluxes of carbon, water and energy over Brazilian cerrado: an analysis using eddy covariance and stable isotopes. **Plant, Cell & Environment**, v. 20 (3), p. 315–328, 1997.

MITTELBACH, G.G. A matter of time for tropical diversity. **Nature**, v. 550(7674), p. 51–52, 2017.

MONASTERIO, M.; SARMIENTO, G. Phenological strategies of plants species in the tropical savanna and semi-deciduous forest of the Venezuelan Llanos. **Journal of Biogeography**, v. 3(4), p. 325–356, 1976.

MOORE, C.E. et al. Tree – grass phenology information improves light use efficiency modelling of gross primary productivity for an Australian tropical savanna. **Biogeosciences**, v. 14, p.111–129, 2017.

MORAIS, Y. et al. Análise do sequestro de carbono em áreas de Caatinga do Semiárido pernambucano. **Revista Brasileira de Meteorologia**, v. 32 (4), p. 585–599, 2017.

MORELLATO, L.P.C. et al. Linking plant phenology to conservation biology. **Biological Conservation**, v. 195, p. 60–72, 2016.

MORELLATO, L.P.C. et al. Phenology of Atlantic Rain Forest Trees: A Comparative Study. **Biotropica**, v. 32(4b), p.811–823, 2000.

MORELLATO, L.P.C.; ALBERTI, L.F.; HUDSON, I.L. Applications of circular statistics in plant

phenology: a case studies approach. In I. L. Hudson & M. R. Keatley, eds. *Phenological Research*. Springer Netherlands, p. 339–359, 2010.

MORISSETTE, J.T. et al. Tracking the rhythm of the seasons in the face of global change: Phenological research in the 21 st century. **Frontiers in Ecology and the Environment**, v. 7(5), p. 253–260, 2009.

MORTON, D.C. et al. Amazon forests maintain consistent canopy structure and greenness during the dry season. **Nature**, v. 506(7487), p.221–224, 2014.

MUNHOZ, C.B.R.; FELFILI, J.M. Fenologia do estrato herbáceo-subarbusivo de uma comunidade de campo sujo na Fazenda Água Limpa no Distrito Federal, Brasil. **Acta Botanica Brasilica**, v. 19(4), p. 979–988, 2005.

MURPHY, P.G.; LUGO, A.E. Ecology of Tropical Dry Forest. **Annual Review of Ecology and Systematics**, v. 17, p. 67–88, 1986.

MURRAY-TORTAROLO, G. et al. Changes in the dry season intensity are a key driver of regional NPP trends. **Geophysical Research Letters**, 2016.

MYNENI, R.B. et al. Large seasonal swings in leaf area of Amazon rainforests. **Proc. Natl Acad. Sci., USA**, v. 104, p. 4820–4823, 2007.

NAGAI, S. et al. Usability of time-lapse digital camera images to detect characteristics of tree phenology in a tropical rainforest. **Ecological Informatics**, v. 32, p. 91–106, 2016.

NEPSTAD, D.C. et al. The role of deep roots in the hydrological and carbon cycles of Amazonian forests and pastures. **Nature**, v. 372 (6507), p. 666, 1994.

OLIVEIRA-FILHO, A.T.; FONTES, M.A.L. Patterns of floristic differentiation among Atlantic Forests in Southeastern Brazil and the influence of climate. **Biotropica**, v. 32(4b), p. 793-810, 2000.

OLSON, D.M. et al. Terrestrial Ecoregions of the World: A New Map of Life on Earth A new global map of terrestrial ecoregions provides an innovative tool for conserving biodiversity. **BioScience**, v. 51 (11), p. 933-938, 2001.

PEICHL, M.; SONNENTAG, O.; NILSSON, M.B. Bringing Color into the Picture: Using Digital Repeat Photography to Investigate Phenology Controls of the Carbon Dioxide Exchange in a Boreal Mire. **Ecosystems**, v. 18(1), p. 115–131, 2014.

PEREIRA, T.S. et al. Fenologia de espécies arbóreas em Floresta Atlântica da Reserva Biológica de Poço das Antas, Rio de Janeiro, Brasil. **Iheringia, Série Botânica**, Porto Alegre, v. 63(2), p. 329–339, 2008.

PIRANI, F.R., SANCHEZ, M. & PEDRONI, F. Fenologia de uma comunidade arbórea em cerrado sentido restrito, Barra do Garças, MT, Brasil. **Acta Botanica Brasilica**, v. 23(4), p. 1096–1110, 2009.

PIVELLO, V. et al. Proposta de zoneamento ecológico para a reserva de cerrado Pé-de-Gigante (Santa Rita do Passa Quatro, SP). **Brazilian Journal of Ecology**, v. 2 (2), p. 108-118, 1998.

POLGAR, C.A.; PRIMACK, R.B. Leaf-out phenology of temperate woody plants: from trees to ecosystems. **New Phytologist**, v. 191 (4), p. 926-941, 2011.

REICH, P.B. Phenology of tropical forests : patterns, causes, and consequences. **Canadian Journal of Botany**, v. 73(2), p. 164-174, 1995.

REICHSTEIN, M. et al. On the separation of net ecosystem exchange into assimilation and ecosystem respiration: Review and improved algorithm. **Global Change Biology**, v. 11(9), p. 1424–1439, 2005.

REICHSTEIN, M. et al. REddyProc: Data processing and plotting utilities of (half-) hourly eddy-covariance measurements. R package version 0.8-2/r15, 2016

RESTREPO-COUBE, N. et al. Do dynamic global vegetation models capture the seasonality of carbon fluxes in the Amazon basin? A data-model intercomparison. **Global Change Biology**, v. 23(1), p. 191–208, 2017.

RESTREPO-COUBE, N. et al. What drives the seasonality of photosynthesis across the Amazon basin? A cross-site analysis of eddy flux tower measurements from the Brasil flux network. **Agricultural and Forest Meteorology**, v. 182–183, p. 128–144, 2013.

RIBEIRO, J.F.; WALTER, B.M.T. Fitofisionomias do bioma Cerrado. **Embrapa Cerrados (ALICE)**, 1998.

RICHARDSON, A.D. et al. Climate change, phenology, and phenological control of vegetation feedbacks to the climate system. **Agricultural and Forest Meteorology**, v. 169, p. 156–173, 2013.

RICHARDSON, A.D. et al. Intercomparison of phenological transition dates derived from the PhenoCam Dataset V1.0 and MODIS satellite remote sensing. **Scientific Reports**, p. 1–12, 2018.

RICHARDSON, A.D. et al. Use of digital webcam images to track spring green-up in a deciduous broadleaf forest. **Oecologia**, v. 152(2), p.323–334, 2007.

RICHARDSON, A.D.A.D. et al. Influence of spring and autumn phenological transitions on forest ecosystem productivity. **Philosophical Transactions of the Royal Society B: Biological Sciences**, v. 365(1555), p. 3227–3246, 2010.

RICHARDSON, A.D.R. et al. Near-surface remote sensing of spatial and temporal variation. **Ecological Applications**, v. 19(6), p.1417–1428, 2009.

RIVERA, G. et al. Increasing day-length induces spring flushing of tropical dry forest trees in the absence of rain. **Trees - Structure and Function**, v. 16(7), p.445–456, 2002.

R Core Team. A language and environment for statistical computing. R Foundation for Statistical Computing, Vienna, Austria, 2017.

ROCHA, H.R. et al. Patterns of water and heat flux across a biome gradient from tropical forest to savanna in Brazil. *Journal of Geophysical Research: Biogeosciences*, v. 114 (G1), 2009.

ROSSATTO, D.R. et al. Depth of water uptake in woody plants relates to groundwater level and vegetation structure along a topographic gradient in a neotropical savanna. ***Environmental and Experimental Botany***, v. 77, p. 259-266, 2012.

SALESKA, S.R. et al. Carbon in Amazon forests: unexpected seasonal fluxes and disturbance-induced losses. ***Science***, v. 302 (5650), p. 1554-1557, 2003

SCHOLZ, F.G. et al. Biophysical and life-history determinants of hydraulic lift in Neotropical savanna trees. ***Functional Ecology***, v. 22(5), p.773–786, 2008.

SILVA, B.B. et al. Determinação por sensoriamento remoto da produtividade primária bruta do perímetro irrigado São Gonçalo–PB. ***Revista Brasileira de Meteorologia***, v. 28 (1), p. 57-64, 2013.

SCHOLZ, F.G. et al. Hydraulic redistribution of soil water by neotropical savanna trees. ***Tree Physiology***, v. 22(9), p.603–612, 2002.

SONNENTAG, O. et al. Digital repeat photography for phenological research in forest ecosystems. ***Agricultural and Forest Meteorology***, v. 152(1), p.159–177, 2012.

TAYLOR, P.G. et al. Temperature and rainfall interact to control carbon cycling in tropical forests. ***Ecology Letters***, v. 20(6), p.779–788, 2017.

TOOMEY, M. et al. Greenness indices from digital cameras predict the timing and seasonal dynamics of canopy-scale photosynthesis. ***Ecological Applications***, v. 25(1), p.99–115, 2015.

USINOWICZ, J. et al. Temporal coexistence mechanisms contribute to the latitudinal gradient in forest diversity. ***Nature***, v. 550(7674), p.105–108, 2017.

VELOSO, H.P.; FILHO, A.L.R.R.; LIMA, J.C.A. Classificação da vegetação brasileira, adaptada a um sistema universal. Instituto Brasileiro de Geografia e Estatística, Diretoria de Geociências, Departamento de Recursos Naturais e Estudos Ambientais, 1991.

VIEIRA, S.A. et al. Stocks of carbon and nitrogen and partitioning between above-and belowground pools in the Brazilian coastal Atlantic Forest elevation range. ***Ecology and Evolution***, v. 1 (3), p. 421-434, 2011.

WAGNER, F.H. et al. Climate seasonality limits leaf carbon assimilation and wood productivity in tropical forests. ***Biogeosciences***, v. 13 (8), p. 2537-2562, 2016.

WHITLEY, R.J. et al. Is productivity of mesic savannas light limited or water limited? Results of a simulation study. ***Global Change Biology***, v. 17 (10), p. 3130-3149, 2011.

WILLIAMS, R.J. et al. Leaf phenology of woody species in a north Australian tropical savanna. ***Ecology***, v. 78 (8), p. 2542-2558, 1997.

WILLIAMS, M. et al. Seasonal variation in net carbon exchange and evapotranspiration in a Brazilian rain forest: A modelling analysis. **Plant, Cell and Environment**, v. 21(10), p.953–968, 1998.

WILLIAMS, R.J. et al. Reproductive Phenology of Woody Species in a North Australian Tropical Savanna. **Biotropica**, v. 31, pp.626–636, 1999.

WOEBBECKE, D.M. et al. Color indices for weed identification under various soil, residue, and lighting conditions. **Transactions of the ASAE**, v. 38(1), p.259–269, 1995.

WOOD, S.N. Generalized additive models: an introduction with R. **Texts in statistical science**, Chapman and Hall/CRC, p. 392, 2006.

WRIGHT, S.J.; VAN SCHAIK, C.P. Light and the Phenology of Tropical Trees. **The American Naturalist**, v. 143(1), p.192–199, 1994.

WU, Z. et al. Responses of terrestrial ecosystems to temperature and precipitation change: a meta-analysis of experimental manipulation. **Global Change Biology**, v. 17 (2), p. 927–942, 2011.

WU, J. et al. Leaf development and demography explain photosynthetic seasonality in Amazon evergreen forests. **Science**, v. 351(6276), p.972–976, 2016.

## Figure legends

**Figure 1** Map showing the location of the study sites and flux towers (circles) of each vegetation type belonging to a biome (following of Olson et al. 2001 classification) with its respective Walter & Lieth climate diagram. A) caatinga; B) cerrado; C) rainforest

**Figure 2** Mean monthly time series across the ecosystem sites with contrasting seasonality conditions. From upper to bottom panels: Photosynthetic Active Radiation (PAR  $\mu\text{mol m}^{-2} \text{s}^{-1}$ ) on the primary y axis, with mean air temperature ( $T_{\text{air}}$  °C) and vapor pressure deficit (VPD kPa) on the secondary y axis; followed by, on the primary y axis, cumulative precipitation (Precipitation  $\text{mm/mo}^{-1}$ ), Evapotranspiration (ET  $\text{mm/mo}^{-1}$ ), and cumulative water deficit (CWD mm).

**Figure 3** Weekly time series of the camera-derived color indices,  $G_{\text{cc}}$  and  $R_{\text{cc}}$ , for each vegetation community site: caatinga (A and B panels), cerrado (C and D panels) and rainforest (D and E panels). Blue bars represent weekly cumulative precipitation time series (Precipitation mm), and gray shaded areas, the dry season length.

**Figure 4.** Weekly Time series of gross primary productivity (GPP - black circles,  $\mu\text{mol CO}_2 \text{m}^{-2} \text{s}^{-1}$ ) and  $G_{\text{cc}}$  (green chromatic coordinate, green circles) for the (a) caatinga; (b) cerrado; and (c) rainforest. All data period of measurements of each variable is featured in each plot.

**Figure 5** Partial fits of the temporal additive mixed models between the GPP and the explanatory variables of  $G_{\text{cc}}$  and  $R_{\text{cc}}$  across the vegetation sites with contrasting seasonality conditions: caatinga (A and B), cerrado (C and D), rainforest (D and E).

**Figure 6** Partial fits of the temporal additive mixed models from the best relationships between GPP and the environmental terms of CWD, Precipitation and mean air temperature ( $T_{\text{air}}$ ) across the vegetation sites with contrasting seasonality conditions: caatinga (A and B), cerrado (C and D), rainforest (D and E).

**Figure 7** Temporal additive mixed models representing the crowns ROIs  $G_{\text{cc}}$  time series of each vegetation site: caatinga (A); cerrado (B); and rainforest (C).



**Table 1** Sites descriptions.

Vegetation type	Site name – Lat/Long.	Location	Canopy height	Biome	Measurement period		Mean Annual Precipitation (MAP) (mm year <sup>-1</sup> )	Dry Season Precipitation (DSP) (mm month <sup>-1</sup> )	Dry Season Length (DSL) (months)
					Eddy Covariance	Phenocam			
Caatinga	Embrapa Semi-árido - 9°05'S; 40°19' W	Petrolina, PE, Northeast Brazil	5 m	desert and xeric shrubland	01/Jan/2013 to 31/Dec/2015	10/May/2013 to 31/Dec/2015	260 mm	75 mm	8
Cerrado	Pé de Gigante - 47° 34' – 47° 41' W, 21° 36' – 21° 44' S	Santa Rita do Passa Quatro, SP, Southeastern Brazil	12 m	grasslands, savannas & shrublands	01/Jan/2013 to 31/Dec/2015	26/Aug/2013 to 31/Dec/2015	1,150 mm	289 mm	6
Rainforest	Santa Virgínia - 23°17'-23°24'S; 45°03'-45°11'W	São Luiz do Paraitinga, SP	30 m	Moist broadleaf forest	01/Jan/2013 to 31/Dec/2015	17/Out/2014 to 31/Dec/2015	1,800 mm	45 mm	1

**Table 2** Temporal additive mixed models analysis of variables (that is, Green chromatic coordinate,  $G_{cc}$ ; Red chromatic coordinate,  $R_{cc}$ ; Cumulative Precipitation, Rain; Cumulative water deficit, CWD; Photosynthetic active radiation, PAR; mean air temperature,  $T_{air}$ ) explaining Gross Primary Productivity (GPP) for each ecosystem site. All the  $p$  values were  $< 0.001$ .

Models	Sites								
	caatinga			cerrado			rainforest		
	edf	F test	Adj. $R^2$	edf	F test	Adj. $R^2$	edf	F test	Adj. $R^2$
<i>Single-variable model</i>									
GPP = s( $G_{cc}$ )	3.57	65.91	<b>0.71</b>	2.90	14.84	<b>0.30</b>	3.18	10.44	<b>0.40</b>
GPP = s( $R_{cc}$ )	<i>n.s</i>	<i>n.s</i>	<i>n.s</i>	3.14	25.02	<b>0.45</b>	2.77	3.90	<b>0.36</b>
GPP = s(Rain)	3.79	10.75	<b>0.25</b>	3.24	7.84	<b>0.37</b>	<i>n.s</i>	<i>n.s</i>	<i>n.s</i>
GPP = s(CWD)	3.46	16.22	<b>0.32</b>	2.89	2.44	<b>0.15</b>	<i>n.s</i>	<i>n.s</i>	<i>n.s</i>
GPP = s( $T_{air}$ )	<i>n.s</i>	<i>n.s</i>	<i>n.s</i>	2.69	3.19	<b>0.19</b>	2.21	2.30	<b>0.25</b>
GPP = s(PAR)	<i>n.s</i>	<i>n.s</i>	<i>n.s</i>	2.93	2.52	<b>0.18</b>	<i>n.s</i>	<i>n.s</i>	<i>n.s</i>
<i>Abiotic model</i>	-	-	<b>0.67</b>	-	-	<b>0.57</b>	-	-	<b>0.25</b>
<i>Biotic-abiotic model</i>	-	-	<b>0.78</b>	-	-	<b>0.76</b>	-	-	<b>0.40</b>

Adj.  $R^2$  = adjusted coefficient of determination; *n.s* = not significant at  $P < 0.001$

Abiotic final models: caatinga, GPP = s(CWD) + s(rain); cerrado, GPP = s(rain) + s(PAR) + s( $T_{air}$ ); rainforest, GPP = s( $T_{air}$ ).

Biotic-abiotic final models: caatinga, GPP = s( $G_{cc}$ ) + s(rain); cerrado, GPP = s( $G_{cc}$ ) + s( $R_{cc}$ ) + s(rain) + s( $T_{air}$ ); rainforest, GPP = s( $G_{cc}$ ) + s( $R_{cc}$ ) + s( $T_{air}$ ).

Fig. 1

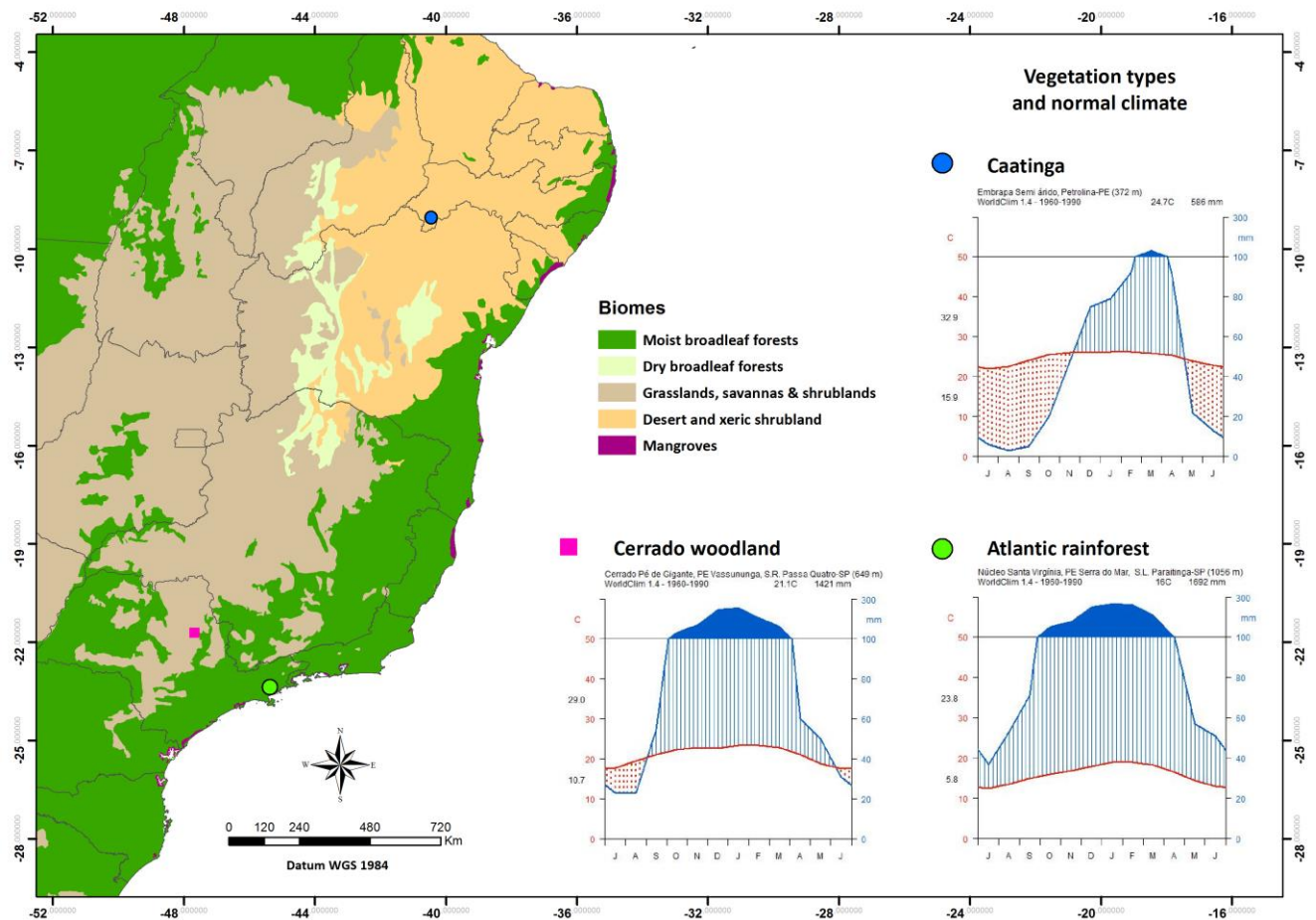


Fig.2

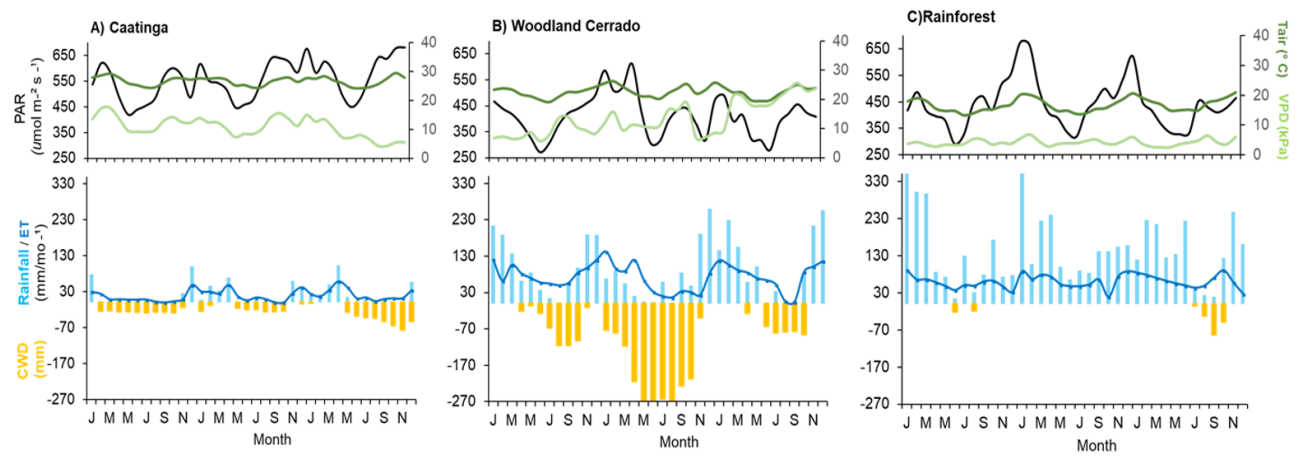


Fig.3

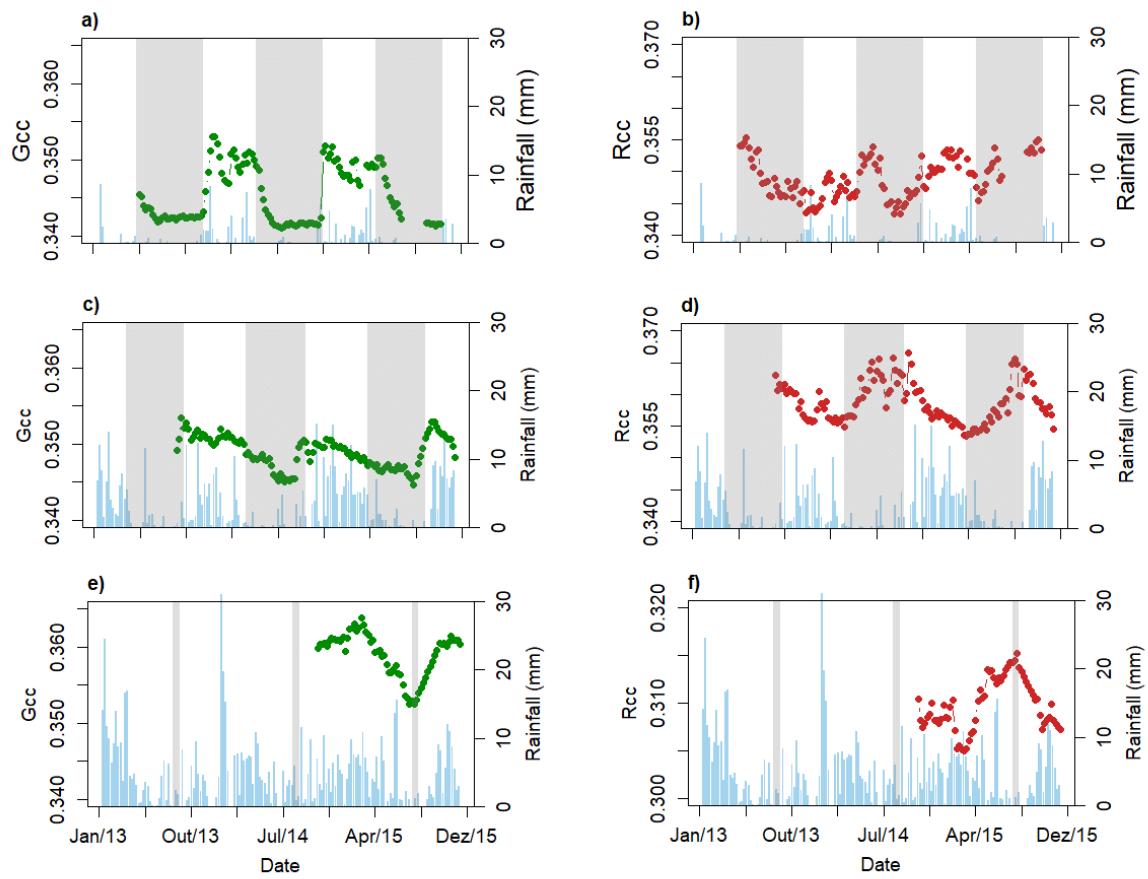


Fig. 4

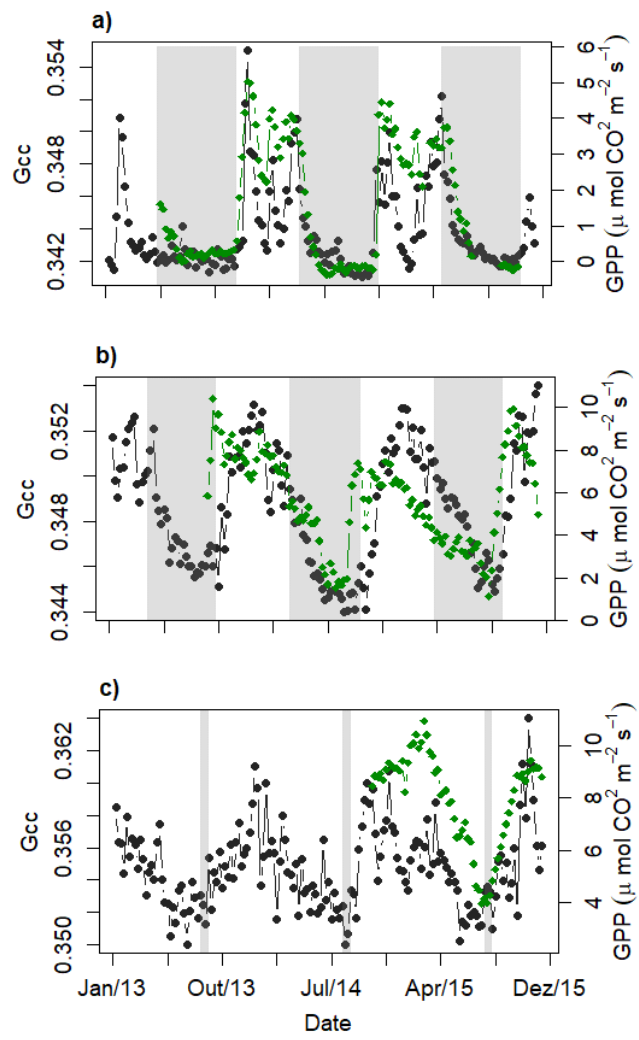


Fig. 5

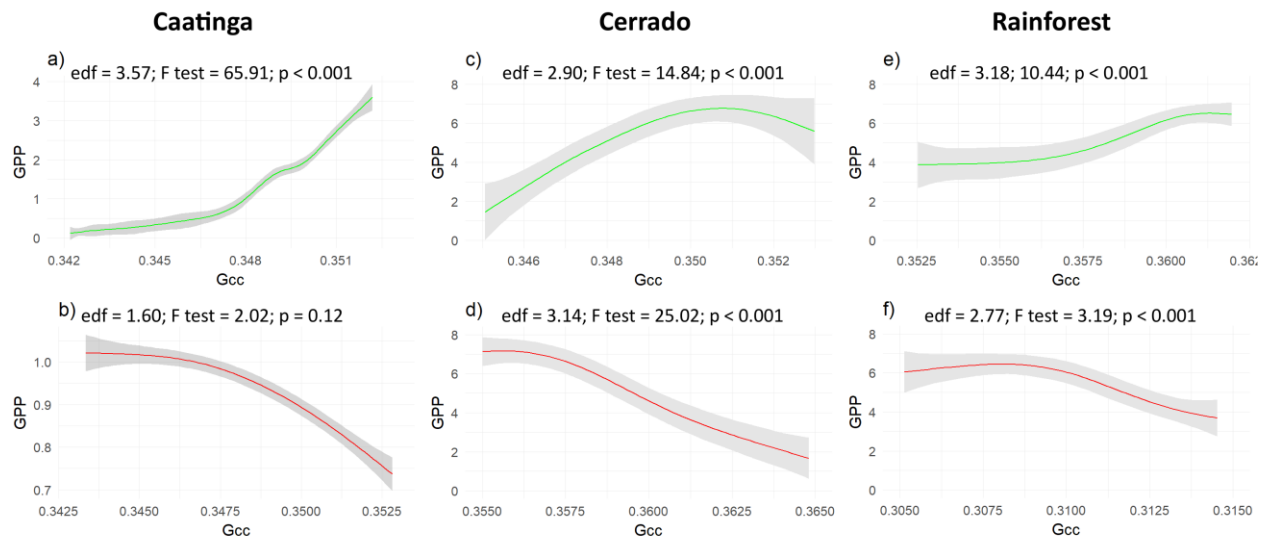


Fig.6

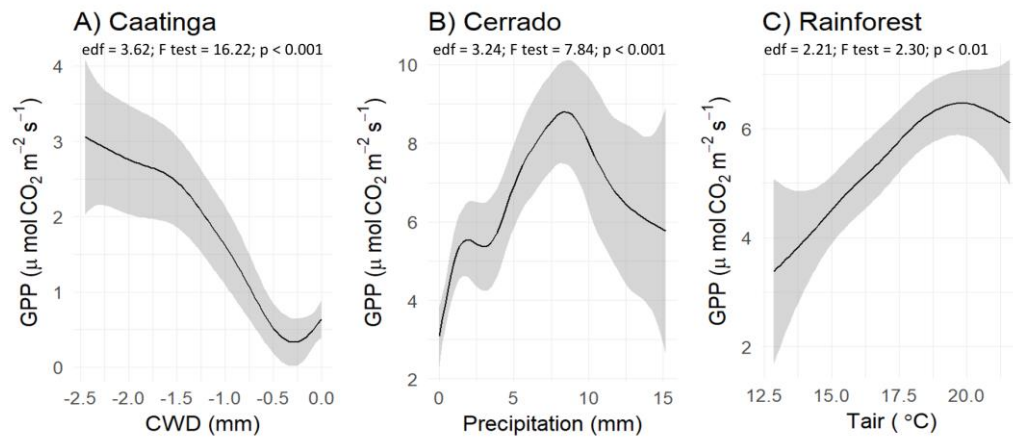
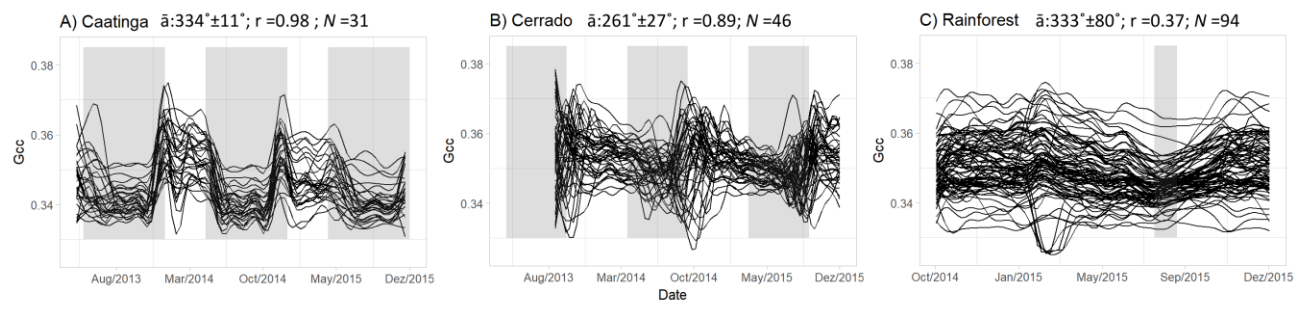




Fig. 7



## Supplementary Material

**LEAF PHENOLOGY CORRELATES TO GROSS PRIMARY PRODUCTIVITY: AN INTER-COMPARISON ACROSS SEASONALLY CONTRASTING TROPICAL BIOMES**

Bruna Alberton<sup>1\*</sup>, Andrew Richardson<sup>2,3</sup>, Ricardo Torres<sup>4</sup>, Humberto Rocha<sup>5</sup>, Magna S. B. De Moura<sup>6</sup>, Leonor Patricia Cerdeira Morellato<sup>1</sup>

**Figure S1** Original hemispherical images showing the single crowns manually selected within each one of the vegetation sites. A - caatinga with 31 crowns ROIs selected; B - cerrado with 46 crowns ROIs selected; and C -rainforest with 94 crowns ROIS selected in the image.

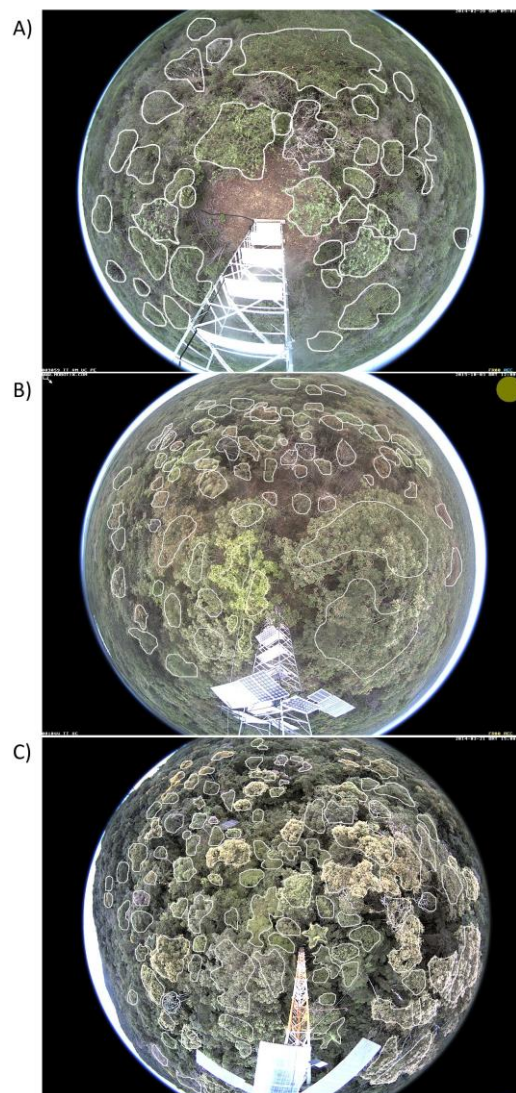


**Figure S2** Circular histograms of leaf flushing onset for the years of study from the crowns ROIs selected within the images of each site: a) caatinga; b) cerrado; and c) rainforest. The arrows point to the mean angle or date ( $\bar{\alpha}$ ) where most of the crowns' ROIs were considering flushing new leaves from the visual inspection; the length of the arrow indicates the value of the  $r$  vector and represents the synchronicity of the crowns ROIs leafing around the mean date. The  $r$  variable has no units and varies from zero to one (when all the data are concentrated at the same direction or angle; see Methods for details).  $N$  represents the number of crowns ROIs observed during visual inspection.

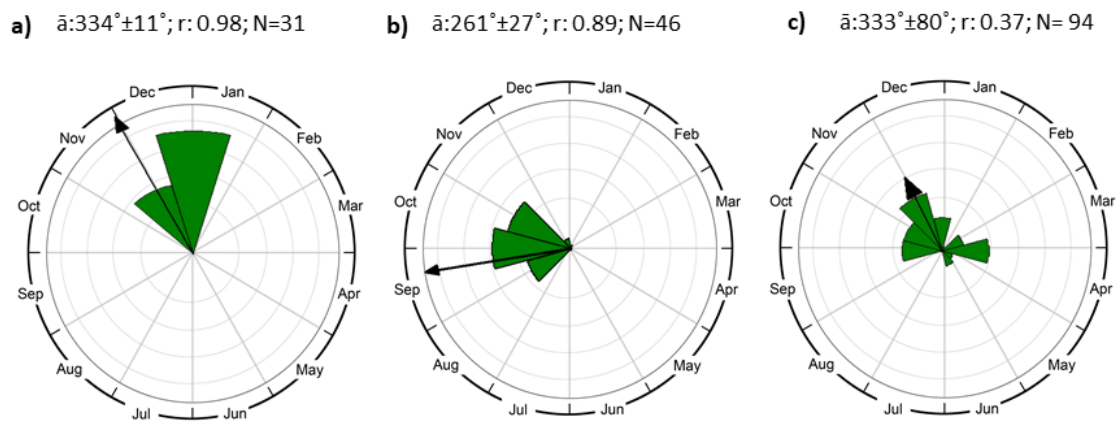


**Figure S3** A sample of the original hemispherical images taken during wet (upper panels) and dry season (below panels) for each vegetation site representing a different biome – A Caatinga – B Cerrado – C Atlantic Rainforest.

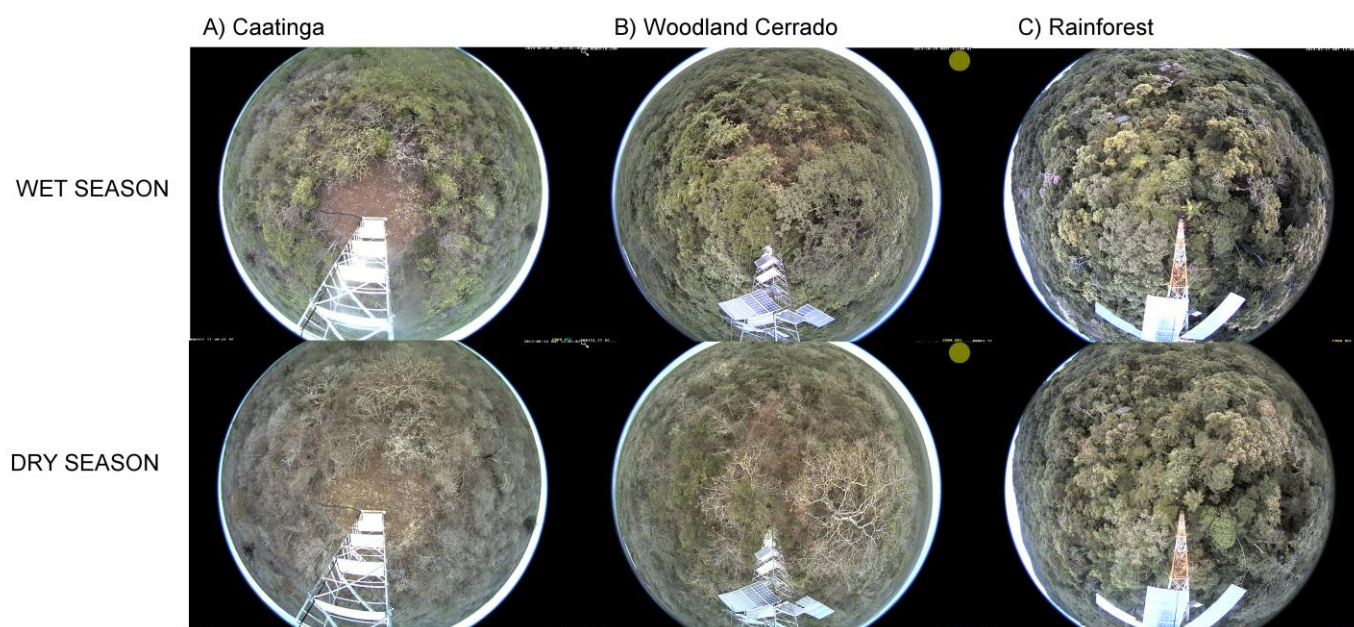


**Figure S4** Weekly time series of daily sums of Gross Primary Productivity (GPP  $\mu\text{mol CO}_2 \text{ m}^{-2} \text{ s}^{-1}$ ) patterns for the ecosystem sites of caatinga (A), cerrado (b) and rainforest (C). Blue bars represent weekly cumulative precipitation time series (Rainfall mm), and gray shaded areas, the dry season length.

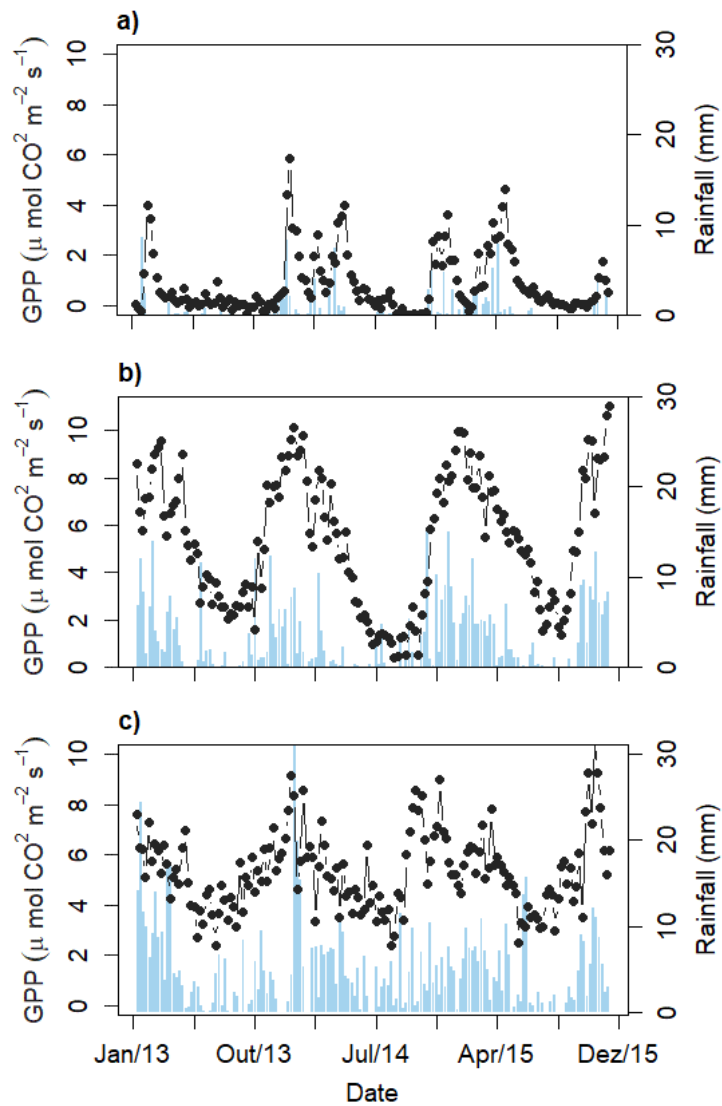


**Figure S5** Temporal additive mixed models of the crowns ROIs daily  $G_{cc}$  time series from the caatinga vegetation site.

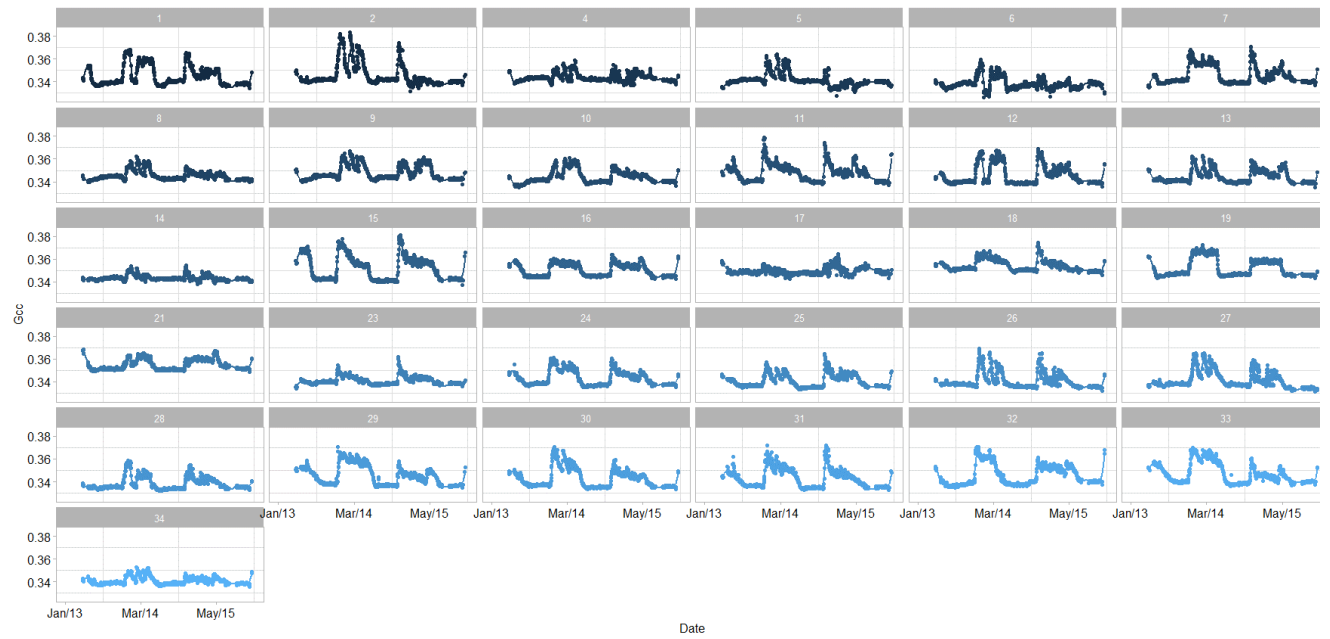
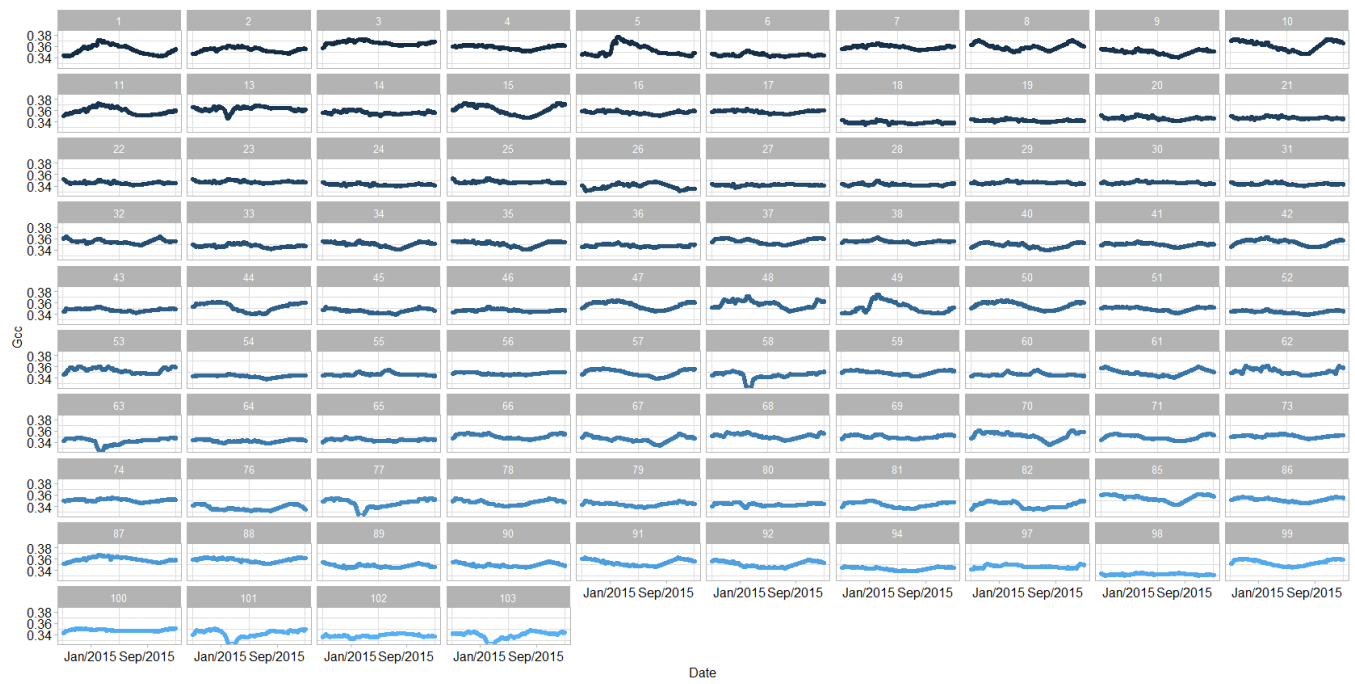


**Figure S6** Temporal additive mixed models of the crowns ROIs daily  $G_{cc}$  time series from the cerrado vegetation site.





**Figure S7** Temporal additive mixed models of the crowns ROIs daily  $G_{cc}$  time series from the rainforest site.





## Section 4

Here, I present the key results, developed during my doctoral thesis, related to the e-science framework where my thesis was developed. Our studies were conducted in the context of the e-phenology project (see Mariano et al., 2016) and were associated with the e-phenology phenocam network.

First, the development of a phenological database was one of the first devised goals, due to the need of organize the enormous bulk of information generated and aggregated to the e-phenology project. The database was delineated in the context of the e-phenology network and it is the starting point of the management of our high-volume imagery and ecological and phenological associated dataset (Mariano et al. 2016). It integrates the ground-based direct phenological observations carried out in a long-term monitoring program (Long-term Cerrado Phenology project – <http://www.recod.ic.unicamp.br/ephenology/>) and the repeated daily imagery from the digital cameras. It also includes site base information, sensor derived-data from the site's weather stations and plant ecological traits from individuals and species.

The automatization of data processing was also an important step to make analysis of thousands of hundreds of images faster and to create a standard protocol of image processing. A Java interface, called PhenoViewer (unpublished software), was created by the computer scientists team (J. Almeida Jr and collaborators) and optimized by the user group according to the user's feedbacks and tasks needed along the last years. The image processing tool was developed with the purpose of pre-processing (organization with unfold and renaming tasks) and processing (vegetative indexes calculation) the high volume of images of the e-phenology network.

The further steps relate to several analytical tool explored to the analyses of phenocam images. The use of machine learning algorithms to plant species identification in the image data provides important steps of image analysis, which is the automatic identification of each plant crown of the within the vegetation image (Almeida et al., 2014). Through the years, several approaches have been proposed to support the identification of individuals of particular species from phenocam imagery (Almeida et al., 2014; Almeida et al., 2015, Almeida et al., 2016; Faria et al., 2016a; Faria et al., 2016b). Works related to this task can be divided into two main groups: those based on the use of machine learning fusion approaches, and those based on time series representations. Examples of initiatives of the first

group are the works of Almeida et al., (2014) and Faria et al., (2016a). Almeida et al., (2014), for example, proposed an Adaboost-based framework for combining multiscale classifiers with the objective of recognizing plant species within vegetation images. The other trend is focused on time series representations (Almeida et al., 2016, Faria et al., 2016b). Almeida et al., (2016), for example, proposed two different time-series-based visual rhythm representations to support plant species identification. These representations are more efficient to be processed and yielded effective results in plant species identification tasks. All those works use general-purpose color and texture descriptors to represent image regions.

Regarding the visualization of phenological time-series, the PhenoVis, a visual analytics tool, was developed to provide a more insightful way to deal with camera-derived phenological time-series. Its application is based on the problematization of using average pixels values for the vegetation index (e.g.:  $G_{cc}$ ) calculated from a given Region of interest (ROI) in the image. Different images representing distinct phenological stages of the vegetation may share the same average of  $G_{cc}$  values. In the work of Leite et al., (2016), we introduced the Chronological Percentage Maps (CPMs), a visual mapping technique that combines pixels derived distribution from all images of a given time period to create a normalized stacked bar chart. Thus, the PhenoVis tool encompasses the CPMs, designed for a more expressive representation of phenological time series combined with a color-coded information, and supports comparative analysis of phenological data for multiple years with algorithms allowing search for phenological patterns similarity and filters for specific time periods or regions.

List of published articles originated from the e-science collaborations described above:

ALMEIDA J., SANTOS, JA, ALBERTON, B., MORELLATO, L.P.C., TORRES, R.S. Phenological visual rhythms: compact representations for fine-grained plant species Identification. **Pattern Recognition Letters**, v. 81, p. 90-100, 2016. (APPENDIX B)

FARIA F. A., ALMEIDA, J., ALBERTON, B., MORELLATO, L.P.C., ROCHA, A., TORRES, R.S. Time series-based classifier fusion for fine-grained plant species recognition. **Pattern Recognition Letters**, v. 81, p. 101-109, 2016. (APPENDIX C)

FARIA F. A., ALMEIDA, J., ALBERTON, B., MORELLATO, L.P.C., TORRES, R.S. Fusion of Time Series Representations for Plant Recognition in Phenology Studies. **Pattern Recognition Letters**, v. 83, p. 205-214, 2016. (APPENDIX D)

LEITE, R.A., SCHNORR, L, ALMEIDA JR, TORRES, R.S., ALBERTON, B., MORELLATO, LPC, COMBA, J. PhenoVis – Visual Phenological Analysis of Forest Ecosystems. **Information Sciences**, v. 372, p. 181-195, 2016. (APPENDIX E)

ALMEIDA, J., PEDRONETTE, D., ALBERTON, B., MORELLATO, L.P.C., TORRES, R.S. Unsupervised distance learning for plant species identification. **JSTARS Journal of Selected Topics in Applied Earth Observations and Remote Sensing**, v. 9 (12), p. 5325-5338, 2016. (APPENDIX F)

## CONCLUSIONS

In the present thesis, I intended to incorporate a novel approach as a consistent tool for the monitoring of the vegetative phenology in tropical ecosystems. In the first section, I established a first-step protocol with main guidelines for the camera system method and setup in the tropics. We demonstrated that the establishment of phenocam networking is a powerful tool for biological conservation through its capability of fine temporal resolution data associated with wide spatial monitoring coverage. Besides, phenocams applications can bring new information for management and restoration practices at several sites and environments and contribute for the education for conservation and citizen science initiatives.

Next sections (2 and 3), I approached ecological questions to be tested applying repeated digital photographs on tropical ecosystems. In section 2, leaf phenology derived by digital cameras were used in an analytical procedure to unravel the main drivers influencing  $G_{cc}$  time series across seasonally dry vegetations. Water and light were the most important predictors for the leaf phenological patterns across the sites. Water-plant relationships were more important for the Caatinga community, and light, through day-length seasonality, had more influence in the leafing patterns of the cerrado communities. An interesting outcome was the increasing variability of phenological signals (leafing behaviors) and predictor-response relationships (distinct smooth functions) across sites where seasonality was less pronounced and/or distinct species life-form were capable of overcoming drought-effects, such as deep root systems trees from woodland cerrado compared to grassy cerrado. Following this idea, section 3 has shown a novel approach to relate leaf phenology to seasonality of ecosystems productivity. The phenological dynamics regarding the variability of species phenological signals, and how they are built in into each contrasting vegetation communities explains drivers of leaf phenology and productivity. Besides, the comparison of tropical biomes under different hydroclimatic conditions is essential to the understanding of ecosystem functionality and access future responses to climate change.

The so-called near-surface remote phenology using digital cameras is an opportunity to obtain an impartial and comparable assessment of leaf seasonal changes in tropical environments and has becoming more and more common for phenological research. The arrivals of novel technologies followed by the advance of e-science methods for dealing with large data sets are changing the scenario

of plant ecology studies, from species to ecosystems. Next challenges to be addressed are the continuity of the e-phenology network and the spread of new cameras covering new vegetation types; and the development of bottom-up studies, integrating on-the-ground observations, cameras, drones, and satellites, inter-comparing them and placing camera-derived phenology in its own scale, by understanding how much and what kind of information can be retrieved from ecosystems. I believe the thesis innovates by providing original ecological research outcomes from an e-science perspective, which led to a unique research profile for a young scientist.

## REFERENCES

- ALBERTON, B. et al. Using phenological cameras to track the green up in a cerrado savanna and its on-the-ground validation. **Ecological Informatics**, v. 19, p. 62–70, 2014.
- BALDOCCHI, D. D. et al. Predicting the onset of net carbon uptake by deciduous forest with soil temperature and climate data: A synthesis of FLUXNET data. **International Journal of Biometereology**, v. 49, p. 377–387, 2005.
- CHAMBERS, L.E. et al. Phenological Changes in the Southern Hemisphere. **Plos One**, v. 8, p. 1–12, 2013.
- CRIMMINS, M.A.; CRIMMINS, T.M. Monitoring plant phenology using digital repeat photography. **Environ. Manage.**, v. 41, p. 949–958, 2008.
- FIELD, C.B. et al. Primary production of the biosphere: integrating terrestrial and oceanic components. **Science**, v. 281, p. 237–240, 1998.
- GRAHAM, E.A. et al. Public Internet-connected cameras used as a cross-continental ground-based plant phenology monitoring system. **Glob. Change Biol.** v. 16, p. 3014–3023, 2010.
- HEY, T.; HEY, J.e-Science and its implications for the library community. **Libr.Hi Tech**, v. 24, p. 515–528, 2006.
- KEENAN, T. F. et al. Tracking forest phenology and seasonal physiology using digital repeat photography: a critical assessment. **Ecological Applications**, v. 24(6), p. 1478–1489, 2014.
- LOPES, A.P. et al. Leaf flush drives dry season green-up of the Central Amazon. **Remote Sensing of Environment**, v. 182, p. 90–98, 2016.
- MIGLIAVACCA, M. et al. Using digital repeat photography and eddy covariance data to model grassland phenology and photosynthetic CO<sub>2</sub> uptake. **Agricultural and Forest Meteorology**, v. 151(10), p. 1325–1337, 2011.
- MARIANO, G., MORELLATO, LPC, ALMEIDA J. ALBERTON, B., CAMARGO, MGG; & TORRES, RS. Modeling plant phenology database: blending near-surface remote phenology with on-the-ground observations. **Ecological Engineering**, v. 91, p. 396–408, 2016.
- MOORE, C.E. et al. Tree – grass phenology information improves light use efficiency modelling of gross primary productivity for an Australian tropical savanna. **Biogeosciences**. v. 14, p. 111–129, 2017.
- MORELLATO, L.P.C.; GRESSLER, E.; CAMARGO, M.G.G. A review of plant phenology in South and Central America. In: M.D. Schwartz (ed.). **Phenology: An Integrative Environmental Science**, Springer, New York, 91–113, 2013.
- MORELLATO, L.P.C. et al. Linking plant phenology to conservation biology. **Biological Conservation**, v. 195, p. 60–72, 2016.
- MORISSETTE, J.T. et al. Tracking the rhythm of the seasons in the face of global change: phenological research in the 21st century. **Front. Ecol. Environ.** v. 7, p. 253–260, 2009.

NAGAI, S. et al. Usability of time-lapse digital camera images to detect characteristics of tree phenology in a tropical rainforest. **Ecological Informatics**, v. 32, p. 91–106, 2016.

OMETTO, J.P.H.B. et al. Amazonia and the modern carbon cycle: Lessons learned. **Oecologia**, v. 143(4), p. 483–500, 2005.

POLGAR, C.A.; PRIMACK, R.B. Leaf-out phenology of temperate woody plants: From trees to ecosystems. **New Phytologist**, v. 191(4), p. 926–941, 2011.

REICH, P.B. Phenology of tropical forests: patterns , causes , and consequences. **Can. J. Bot.** v. 73, p. 164–174, 1995.

RESTREPO-COUBE, N. et al. What drives the seasonality of photosynthesis across the Amazon basin? A cross-site analysis of eddy flux tower measurements from the Brasil flux network. **Agricultural and Forest Meteorology**, v. 182–183, p.128–144, 2013.

RESTREPO-COUBE, N. et al. Do dynamic global vegetation models capture the seasonality of carbon fluxes in the Amazon basin? A data-model intercomparison. **Global Change Biology**, v. 23(1), p.191–208, 2017.

RICHARDSON, A.D. et al. Influence of spring and autumn phenological transitions on forest ecosystem productivity. **Philosophical Transactions of the Royal Society B: Biological Sciences**, v. 365(1555), p.3227–3246, 2010.

TOOMEY, M. et al. Greenness indices from digital cameras predict the timing and seasonal dynamics of canopy-scale photosynthesis. **Ecological Applications**, v. 25(1), p.99–115, 2015.

WU, J. et al. Leaf development and demography explain photosynthetic seasonality in Amazon evergreen forests. **Science**, v. 351(6276), p.972–976, 2016.

WU, J. et al. The phenology of leaf quality and its within-canopy variation is essential for accurate modeling of photosynthesis in tropical evergreen forests, **New Phytologist**, p.1–14, 2017.



## Appendix A

Article published in the Journal Biotropica:

CAMARGO, M.G.G. et al. Leafing patterns and leaf exchange strategies of a cerrado woody community. **Biotropica**, v. 50 (3), p.442–454, 2018.

LRH: Camargo *et al.*

RRH: Leafing Patterns of a Cerrado Community

**Leafing patterns and leaf exchange strategies of a cerrado woody community**

Maria Gabriela Gutierrez de Camargo<sup>1</sup>, Gustavo Henrique de Carvalho<sup>1</sup>, Bruna de Costa Alberton<sup>1,2,4</sup>, Paula Reys<sup>1,3</sup>, Leonor Patrícia Cerdeira Morellato<sup>1</sup>

1. UNESP — Universidade Estadual Paulista, Instituto de Biociências, Departamento de Botânica, Laboratório de Fenologia, Rio Claro, São Paulo, Brasil; 2. UNESP — Universidade Estadual Paulista, Instituto de Biociências, Programa de Pós-graduação em Ecologia e Biodiversidade, Rio Claro, São Paulo, Brasil; 3. Universidade de Rio Verde, Campus I, Rio Verde, Goiás, Brasil; 4. brualberton@gmail.com

## ABSTRACT

The deciduousness of tropical trees and communities depend on ecosystems characteristics such as plant species diversity, and strength of the dry season. Based on seven-years of phenological observations we provide the first long-term description of leafing patterns of a woody cerrado community, aiming to investigate: (i) the leaf exchange strategies considering the inter-annual variation on the degree of deciduousness of individuals and species and quantify the community deciduousness; (ii) the relationship between inter-annual patterns of leaf fall and leaf flush according to the species' leaf exchange strategies and climate; (iii) the onset of cerrado growing season and its relation to climate seasonality. To detect seasonality and leafing onset we applied circular statistics and to understand the relationships between environmental predictors and leaf exchange strategies, we used generalized additive models. From 106 species observed, we classified 69 as deciduous (26 species), semi-deciduous (25) or evergreen (18) and defined the studied cerrado as a semi-deciduous vegetation. Leaf phenology was markedly seasonal, and similar among years. Leaf fall peaked in the dry season, and leaf flush in the dry-to-wet transition. Leaf fall patterns related to temperature and leaf flush to day length and rainfall. Semi-deciduous and deciduous species were more constrained by climate than the evergreen ones. The cerrado growing season started in the dry-to-wet season transition. Inter-annual variations in rainfall and temperature affected the individuals' and, consequently, species' degree of deciduousness, highlighting individual and species variability, and suggesting that cerrado leafing patterns is likely susceptible to future climate change scenarios.

**Key-words:** climatic drivers; deciduous; evergreen; generalized additive models; growing season; leaf phenology; savanna; seasonality; semi-deciduous.

## RESUMO

A deciduidade das árvores e comunidades tropicais depende de características do ecossistema como a diversidade de espécies de plantas e a intensidade da estação seca. Baseados em sete anos de observações fenológicas, apresentamos uma descrição de longo prazo de padrões vegetativos de uma comunidade lenhosa de cerrado com o objetivo de investigar: (i) as estratégias de trocas foliares considerando a variação interanual no grau de deciduidade dos indivíduos e espécies e quantificar a deciduidade da comunidade; (ii) as relações entre padrões interanuais de queda e brotamento foliar conforme a estratégia de trocas foliares das espécies e o clima; (iii) o início da estação de crescimento da comunidade de cerrado estudada e sua relação com a sazonalidade climática. Utilizamos estatística circular para analisar a sazonalidade fenológica e o início do brotamento foliar na comunidade, e modelos aditivos generalizados para entender as relações entre variáveis ambientais e as estratégias de trocas foliares. Dentre as 106 espécies observadas, 69 foram classificadas como decíduas (26 espécies), semi-decíduas (25) ou sempre-verdes (18) e definimos o cerrado estudado como uma vegetação semi-decídua. A fenologia vegetativa foi marcadamente sazonal e similar entre anos. O pico de queda foliar ocorreu na estação seca e o de brotamento na transição entre as estações seca e chuvosa. O padrão de queda de folhas foi relacionado à temperatura e o de brotamento ao comprimento do dia e pluviosidade. As espécies decíduas e semi-decíduas foram mais afetadas pelo clima do que as sempre-verdes. A estação de crescimento no cerrado começou na transição entre as estações seca e úmida. As variações interanuais na precipitação e temperatura afetaram o grau de deciduidade de indivíduos e consequentemente das espécies, ressaltando a alta variabilidade individual e específica, sugerindo que os padrões de troca foliar das espécies do cerrado podem ser afetados por mudanças climáticas futuras.

DECIDUOUSNESS, DEFINED AS EITHER A PARTIAL OR A FULL LOSS OF LEAVES, IS A KEY FUNCTIONAL trait dependent on ecosystems characteristics such as soils and species diversity,

essential for estimating dry season length and intensity in tropical ecosystems (Condit *et al.* 2000). Leaf development and senescence, as well as leaf exchange strategies of plant species, are recognized to have important effects at the ecosystem scale because they are linked to a range of processes, including carbon uptake, water and energy fluxes, resource availability, and nutrient cycling (Reich 1995, Lavorel *et al.* 2007, Polgar & Primack 2011, Richardson *et al.* 2013). Additionally, the degree of deciduousness of a community is an indicator of shifts in the intensity and timing of species activities due to inter-annual shifts in the weather, for instance, leaf loss can be more intense during severe dry seasons (Reich 1995, Condit *et al.* 2000, Williams *et al.* 1997). Since savannas are the world's second most important type of vegetation, contributing to carbon flux and storage (Archibald & Scholes 2007), studies of the vegetative phenology in these ecosystems have a global reach.

The Brazilian Cerrado, a neotropical savanna, is the second largest vegetation type in the Brazilian territory and presents a gradient of physiognomies, ranging from grasslands to tall woodlands (Overbeck *et al.* 2015, Durigan & Ratter 2016, Coutinho 2006). The cerrado harbors the world's highest woody plant diversity among savannas (Ratter *et al.* 1996, Sarmiento 1984, Munhoz & Felfili 2006), and is generally under a seasonal climate with well-defined wet and dry seasons (Ratter *et al.* 1996). The seasonal climate is known to influence the phenology of plant populations and communities (Monasterio & Sarmiento 1976, Morellato *et al.* 2013, 2016). To reduce transpiration and avoid plant collapse related to water status, plants subjected to seasonal climates tend to lose their leaves during the dry season, facilitating the re-hydration process for the growing season (Reich & Borchert 1984, Franco *et al.* 2005). Most cerrado trees produce new leaves and flowers at the end of the dry season, just before the start of the raining season, indicating that individuals have access to water at greater depth to permit their maintenance even when rainfall is low (Monasterio & Sarmiento 1976, Williams *et al.* 1997, Jackson *et al.* 1999, Batalha & Mantovani 2000,

Batalha & Martins 2004, Lenza & Klink 2006, Tannus *et al.* 2006, Pirani *et al.* 2009).

Few studies have addressed leaf exchange patterns in cerrado communities (Miranda 1995, Munhoz & Felfili 2005, Lenza & Klink 2006, Alberton *et al.* 2014, Pirani *et al.* 2009). Most of them either focused on reproductive phenophases or in describing general aspects of the community phenology, providing only inferences about the relationship between leafing patterns and environmental cues (e.g. Mantovani & Martins 1988, Batalha *et al.* 1997, Batalha & Mantovani 2000, Batalha & Martins 2004, Damascos *et al.* 2005, Tannus *et al.* 2006, Bulhão & Figueiredo 2002, Dalmolin *et al.* 2015). Others, however, have found negative correlations between leaf fall and precipitation (Munhoz & Felfili 2005, Pirani *et al.* 2009). The investigation of vegetative phenology, its causes, and the quantification of leaf exchange strategies at a community level in the cerrado are, thus, still missing. In addition, leaf exchange strategies in communities are mainly defined based on the leafing patterns of few species and in short-term phenological observations (Franco *et al.* 2005, Lenza & Klink 2006), which may include bias related to some punctual plant response to local weather conditions. Therefore, the use of long-term phenology leafing data series is essential to the definition of the species' leaf exchange strategies.

Here, we describe, for the first time, the seven-year long leaf phenology of a cerrado community, aiming to (i) identify the leaf exchange strategies considering the inter-annual variation in the degree of deciduousness of individuals and species and quantify the community deciduousness; (ii) investigate the relationship between inter-annual patterns of leaf fall and leaf flush according to the species' leaf exchange strategies and the climate conditions; (iii) uncover the onset of the cerrado growing season and the relation to climate seasonality.

We expect to find a dominance of leaf-exchange species (deciduous and semi-deciduous) and a higher deciduousness degree over years due to the length and severity of

the dry season (Reich & Borchert 1984, Franco *et al.* 2005, Reich 1995, Condit *et al.* 2000, Williams *et al.* 1997). Based on few short-term phenology studies describing leaf exchange strategies of woody cerrado species (Alberton *et al.* 2014, Pirani *et al.* 2009, Lenza & Klink 2006), we expected leaf fall during the dry season and leaf flush peaking in the transition between dry and wet seasons, defining the onset of the growing season. We also expected rainfall and day length as the main environmental factors related to leafing seasonality, as previously suggested for tropical seasonal vegetations (Condit *et al.* 2000, Borchert & Rivera 2001).

## METHODS

**STUDY SITE** — We developed our study in an area of woody cerrado in the municipality of Itirapina, São Paulo state, Southeastern Brazil (22°10'31"S; 47°52'26"W). The study site is located 770 m above sea level and covers an area of 260 ha. The climate is characterized by two markedly regular seasons: a dry (winter) season from April to September and a wet (summer) season from October to March (Fig. 1). Average annual total rainfall was 1524 mm and the mean annual temperature was 20.7 °C between 1972 and 2011 (Camargo *et al.* 2011). The vegetation is a woody savanna classified as a cerrado *sensu stricto* (Coutinho 1978), with a discontinuous woody layer reaching 6 to 8 m high and a continuous herbaceous stratum. A woody species survey in the area indicated that Myrtaceae, Fabaceae, and Malpighiaceae are the richest families and *Bauhinia rufa*, *Xylopia aromatica*, *Miconia rubiginosa*, *Virola sebifera*, and *Myrcia guianensis* the most abundant species (Reys *et al.* 2013).

**PHENOLOGICAL DATA** — To describe and analyze woody species leafing patterns we used a phenological dataset of monthly surveys conducted from January 2005 to December 2011. During this period, we directly observed leaf fall and leaf flush (following Morellato *et al.* 1989) in 2112 marked individuals with at least 30 cm of stem circumference on the ground

level, sampled over 36 transects (25 m x 2 m) (see Reys *et al.* 2013, Vogado *et al.* 2016). We took circumference and height measurements of all individuals sampled.

To estimate leaf fall and leaf flush phenophases, we monthly recorded the phenological activity of each individual in a qualitative binary scale, with “0” indicating absence of the phenophase and “1” the phenophase presence. We also estimated the intensity of leaf fall and flush based on a semi-quantitative scale with three classes in which “0” indicates the absence of a phenophase, “1” indicates the presence of a phenophase with low to intermediate intensity (up to 50% of the crown flushing new leaves or of the crown with no leaves or senescent leaves) and “2” the presence of a phenophase with high intensity (more than 50% of the crown flushing new leaves or with senescent leaves) (Opler *et al.* 1980, Morellato *et al.* 2000, Vogado *et al.* 2016). Despite the use of a monthly frequency of observations to record and classify the leaf exchange strategies in this study, it is unlikely that we have missed the occurrence of the total absence of leaves in an individual (a 100% deciduous event, see below) or a leaf fall increase from one month to another that, of course, we could also infer from the coverage of newly emerged leaves. We recorded for all years of observations when individuals were totally leafless (100% of leaf fall). The definition of 100% fall category also helped us to define the occurrence of leaf flush, since sometimes one month of leaf fall was followed by new young leaves on the subsequent month. From March 2007 to December 2008, we did not score leafing intensity; we only recorded phenological activity using the qualitative scale. The qualitative and semi-quantitative individual observations were independently collected and provide complementary information which improve the analyses of phenological patterns (Bencke & Morellato 2002).

To calculate the intensity index, we adapted the Fournier index (Fournier 1974), considering “2” as the class of maximum intensity (Vogado *et al.* 2016). We choose to use only three intensity classes instead of five, as suggested by Fournier (1974), and commonly



used in tropical plant phenology, to facilitate the definition of phenological changes at monthly intervals.

LEAF EXCHANGE STRATEGIES AND THE DEGREE OF DECIDUOUSNESS — We classified the individual and species leaf exchange strategy for each of the five years we scored leaf fall intensity (2005, 2006, 2009 to 2011). For each individual, we classified as **deciduous** the individual recorded with no leaves (100% leaf fall) in at least one month, in a year. We classified as **semi-deciduous** the individual recorded with more than half of the branches without leaves (intensity score “2”) in at least one month in a year. Finally, we classified as **evergreen** the individual observed with up to half of the branches without leaves (“0” or “1” intensity score) throughout a given year. To estimate the degree of deciduousness, we calculated the proportion of deciduous, semi-deciduous and evergreen individuals in the community in each of the five years we evaluated leaf fall intensity.

We classified all species with more than five individuals sampled as deciduous, semi-deciduous, or evergreen based on the above individual’s annual leaf exchange strategies. A species was classified as **deciduous** if more than half of all individuals sampled were classified as deciduous in at least one of the five years; **semi-deciduous** if more than half of all individuals were classified as semi-deciduous in at least one of the five years; and as **evergreen** all the remaining species.

DATA ANALYSES — Since we scored the intensity of phenology using an ordinal scale ranging from 0 to 2, we applied ordinal multinomial regressions to assess the drivers of leaf fall and flush. We fitted two models (leaf fall and flush) for species grouped according with leaf exchange strategies, analyzing the number of individuals with 0, 1, 2, and 100% of leaf fall intensities and 0, 1, and 2 of leaf flush intensities. We also fitted multinomial models

for the whole community, regardless of leaf strategies. All models had monthly rainfall, mean temperature, monthly day length difference (longest minus shortest day within the month), and an interaction between rainfall and temperature as predictors. Monthly rainfall, maximum, mean, and minimum temperatures for the study period (January 2005 to December 2011) were obtained from the climatic station at Estação Climatológica do Centro de Recursos Hídricos e Ecologia Aplicada (CRHEA – Universidade de São Paulo), 4 km from the study site. We used day length data for the latitude  $-22^{\circ}17'S$ ;  $-47^{\circ}87'W$  (*maptools* package for R).

To better understand the nature of the relationships between predictors and leaf exchange strategies, we further fitted generalized additive models (GAM) using intensity data. These models allowed us to identify threshold regions in environmental variables and long-term trends for leaf fall (number of individuals with 100% leaf fall) and presenting leaf flushing. We fitted all additive models with a correlation structure based on years. We evaluated the ordinal models by looking at the significance of each variable and the generalized additive models with  $R^2$  and variable significance. We carried out all analyses in R (R Core Team 2017) using base packages ordinal (Christensen 2016) for the ordinal regressions and mgcv (Wood 2011) for the generalized additive models.

Considering that recurrent temporal events, such as phenological data, are circular in nature, with no true starting point (Zar 1999), to infer the beginning of the growing season, we applied circular statistics to the individuals' onset month of leaf flush following Morellato *et al.* (2000, 2010). To do that, first we define the start of leafing season of each individual and year as the first month we recorded leaf flush in each year. Then we divided the  $360^{\circ}$  of a circumference by 12 and each month of the year is represented by a range of  $30^{\circ}$  starting on January (mid point  $15^{\circ}$ , see Morellato *et al.* 2010, for details). Then we calculate the angle or date (month) correspondent to the most frequent leaf flush onset (circular mode), the mean

angle or onset date (the mean angle or mean onset data of the frequency distribution of individuals around the circle). Finally, we tested whether the mean onset data are significantly concentrated around the mean angle or date, as a proxy of seasonality by applying the Rayleigh test ( $Z$ ) as suggested by Morellato *et al.* 2000, 2010. If the mean onset data is significantly concentrated around the mean angle or date, we consider the leafing pattern seasonal and the degree of synchrony or seasonality is represented by the length of the vector  $r$ . The vector  $r$  has no unity and ranges from 0 (no seasonality or synchronicity) to 1 (perfect seasonal or synchronous), (Morellato *et al.* 2010). We performed circular analyses per study year, for all the community, and by leaf exchange strategies using Oriana 4.0 (Kovach Computing Services).

## RESULTS

We sampled 2112 individuals and 106 species (Table S1). Over the seven years of observations, some individuals died or were lost, leading to the final sample of 1651 individuals and 102 species. The community phenological patterns were described based on the total number of individuals observed per month, in each year.

Out of the 106 species initially surveyed, 69 species presented more than five individuals and were classified as deciduous (26 species; total basal area= 1.46 m<sup>2</sup>), semi-deciduous (25 species; total basal area= 6.10 m<sup>2</sup>) and evergreen (18 species; total basal area= 2.29 m<sup>2</sup>) (Fig. 2; Table S1). Species and individual's degree of deciduousness varied among years (Fig. 2). Only five species presented the same deciduousness degree over the five years: *Jacaranda caroba*, which reached deciduity in all the years (most of individuals with no leaves or 100% leaf fall) and, *Anadenanthera peregrina* var. *falcata*, *Byrsonima coccolobifolia*, *Campomanesia pubescens* and *Dalbergia miscolobium*, which reached semi-deciduity in all the years (most individuals lose more than half of their leaves). Individuals

and consequently, the species, rarely lose all their leaves, maintaining at least half of the leaves in most of the years (Fig. 2). We observed the lowest deciduousness degree in the community in 2005 and the highest one in 2010, (Fig. 2). The number of deciduous individuals responded to both: mean temperature and total rainfall when intra and inter-annual seasonality components were considered ( $R^2=0.70$ ;  $P<0,01$ ).

Leafing patterns were seasonal and similar among years and within leaf exchange strategies (Fig. 3 and 4). Leaf fall predominated in the dry season, peaking in July (Fig. 3), while leaf flush was concentrated in the transition between dry to wet seasons, peaking in September (Fig. 4). We observed an unexpected increase of leaf fall on December 2009 and, on 2010 mainly in the middle of the wet season, related to a larger number of individuals losing leaves but at a low intensity (Fig. 3).

Leafing patterns according to the leaf exchange strategies were similar among years, overlapping during the periods of higher activity and intensity in the community (Fig. 3 and 4). Deciduous species presented a seasonal leaf exchange patterns highly constricted to the one period of the year, concurrent with the highest phenological activity and intensity in the community (Fig. 3 and 4). During the peaks of leaf fall and leaf flush in the community, deciduous species presented the highest synchrony among individuals and phenophases intensity followed by semi-deciduous and evergreen species. Conversely, semi-deciduous, and mainly evergreen species, presented more individual's activity outwith the community peaks of leaf exchange (Fig. 3 and 4).

In general, for both phenophases, leaf fall and flush, the effects of abiotic variables increased from evergreen to deciduous species (Table 1). The exceptions were the influence of the day length difference on the leaf fall, almost the same for all leaf exchange strategies; and the rainfall on the leaf flush, similar between evergreen and semi-deciduous species, but higher for deciduous species (Table 1). Leaf fall patterns of all strategies were negatively

related to the rainfall and temperature, and positively related to the day length difference (Table 1). The strongest relations were among leaf fall and temperature and temperature-rainfall interaction (Table 1).

When analyzing the variables separately with generalized additive models, we confirm a higher climatic influence and seasonality in the deciduity of semi and, mainly, deciduous species (Fig.5). All leaf fall models had high coefficients of determination (evergreen  $R^2 = 0.53$ ; semi-deciduous  $R^2 = 0.70$ ; deciduous  $R^2 = 0.77$ ). Similarly, all variables but rainfall in the evergreen model presented a significant nonlinear effect on leaf fall. A higher proportion of individuals lost leaves when the rainfall was around 50 mm, the temperature between 16 and 19°C and the day length between 11 and 11.5 h (Fig. 5), which corresponds to the dry season conditions (see Fig. 1). Individuals deciduity decreased when precipitation was around 100 mm, the temperature 22°C and the day length 12 h (Fig. 5), corresponding to the transition from dry to wet seasons.

Leaf flush patterns were positively related to the day length difference, but also to the rainfall, and negatively related to the temperature (Table 1). Even with a stronger effect of abiotic variables on deciduous and semi-deciduous species (Table 1), when analyzed separately with generalized additive models, individuals of species with different leaf exchange strategies responded in a similar way to the environmental variables, showing seasonality over the 7 y of observations. Leaf flush for all strategies responded non-linearly to the abiotic variables (evergreen  $R^2 = 0.55$ ; semi-deciduous  $R^2 = 0.56$ ; deciduous  $R^2 = 0.62$ ; Fig. 6). We observed the first increase in leaf flush activity when precipitation was around 100 mm, and the day length about 11.5 h, in the transition from dry to wet season. The proportion of individuals flushing peaked at around 200 mm, 19°C and a day length close to 12 h (Fig. 6), which corresponds, to the middle of the wet season, when the differences in the amount of sunlight are highest (see Fig. 1). Particularly, rainy months (> 300mm) also seem

to trigger flushing, although months with such amounts of accumulated rain are rare (Fig. 6A).

We determined the leaf flush onset for half of the individuals observed (Table 2), with no evident onset for all remaining trees. The community growing season started in early September in four out the seven years and otherwise in late August, with the mean angle between 20 August and 10 September (Table 2). When analyzed by leaf exchange strategy, the beginning of the growing season was observed mainly on September for deciduous species and between August and September for semi-deciduous and evergreen species (Table S2). Individuals synchronicity or concentration around the mean onset date were higher for deciduous species, with  $r$  vector around 0.82, followed by semi-deciduous and evergreen species, with the length of vector  $r$  around 0.69 and 0.62, respectively (Table S2).

## DISCUSSION

Cerrado is the most species-rich savanna in the world and second largest Brazilian vegetation type, after Amazonia (Overbeck *et al.* 2015, Durigan & Ratter 2016, Coutinho 2006). However, the studies investigating cerrado seasonal patterns are still sparse, representing less than 10% of the phenological studies surveyed for neotropical region (Mendoza *et al.* 2017), and less than half of those include leafing phenology (Morellato *et al.* 2013, unpublished data). Based on our unique seven-year phenological data we showed the predominance of deciduous and semi-deciduous leaf exchange strategies and established the woody cerrado as an overall seasonal, semi-deciduous vegetation. The individual's degree of deciduousness was highly explained by the climate conditions, with individuals rarely reaching the full deciduity. The cerrado leaf exchanging patterns were consistently seasonal and similar among the years, confirming the expected seasonality described by short-term studies on savannas and other tropical seasonal vegetation (Miranda 1995, Williams *et al.*

1999, Munhoz & Felfili 2005, Lenza & Klink 2006, Pirani *et al.* 2009). Leaf fall and flush of cerrado species were related to all abiotic variables, but mainly to temperature and day length difference, and semi-deciduous and deciduous species were the most constrained by the climate. The onset of the community growing season, here defined based on a subset of the species, started in the transition from dry to wet season (August-September), and it is sustained by the overall larger number of individuals putting out new leaves at this time in the community.

In the cerrado community studied, the predominance of deciduous or semi-deciduous species (74%), in relation to the evergreen ones (26%), was related to the climate seasonality with a marked dry season, and has also been associated to soil properties and species' leaf-economy strategies (Franco *et al.* 2005, Souza, Franco, *et al.* 2015). Studies in cerrado *sensu stricto* sites in Brazil Central, also found a high proportion of deciduous and semi-deciduous woody species (Rossatto *et al.* 2009, Pirani *et al.* 2009), while in West African and Australian savannas the strategies are more evenly distributed in the community (Eamus & Prior 2001). Semi-deciduous species predominate in Australia, and evergreen and semi-deciduous species in West Africa, (Williams *et al.* 1997, De Bie *et al.* 1998). Different definitions have been used to classify leaf exchange strategies, constraining the comparisons regarding to the amount of deciduity of cerrado savanna and other seasonal dry vegetation (e.g. Reich 1995, Eamus & Prior 2001). A common definition brings deciduous, brevi-deciduous (differing in the length of total leafless period) and evergreen with short or long leaf flush strategies or low or no deciduity (Williams *et al.* 1997, Franco *et al.* 2005, Lenza & Klink 2006), but their analyses are usually performed contrasting deciduous and evergreens. Reich (1995) propose deciduous with synchronous leaf flush, deciduous with asynchronous leaf flush and evergreens. We chose the large accepted, more inclusive, deciduous class including both, brevi- and deciduous species, all losing all leaves or 100% regardless the length of leafless

phase and leaf flushing at the end of dry season; a semi-deciduous strategy that implies in the loss of a representative amount of leaves, never above a 50% canopy cover, and evergreens that retain all or almost all leaves year round (Eamus and Prior 2001). That choice facilitates our comparisons and fit well to our monthly direct observations (see also Williams *et al.* 1997).

Here we demonstrated, based on our long-term phenology data, that independently of the leaf exchange strategy, individuals and, consequently, species' deciduousness degree vary among years according to the climate conditions, mostly the inter-annual rainfall variability. That variability is expected for seasonally dry forest and savannas (Reich 1995, Eamus & Prior 2001, Goldstein *et al.* 2008), but has never been demonstrated for tropical savannas based on individual long-term leaf exchange patterns. Therefore, it is necessary exercise caution when classification of species leaf exchange strategies is derived from short-term observation of vegetative phenology, since it can be underestimated whether the survey is conducted in a "wet" year. Considering the number of leaf exchangers species, their basal area and on the fact that individuals' deciduousness degrees rarely reached 100% leaf fall, we classified the studied cerrado community as a semi-deciduous vegetation and that assumption might apply for general cerrado woodlands (cerrado *sensu stricto*).

The consistent seasonal leafing patterns observed over seven years for the studied cerrado community substantiated the patterns described for other cerrado vegetation based on short-term observations, with leaf fall largely in the middle of the dry season and the leaf flush in the transition from dry to wet season, beginning at the end of dry season, after the first shower rains, but before the period of high rainfall intensity (Lenza & Klink 2006, Rossatto *et al.* 2009, Silvério & Lenza 2010, Alberton *et al.* 2014, Pirani *et al.* 2009). This leafing pattern is also found for the Australian savannas (Prior *et al.* 2004, Williams *et al.* 1997). The observed peak of leaf fall in the dry season is expected for seasonally dry



vegetations and species, since it is a strategy to improve water use and avoid water losses by transpiration (Monasterio & Sarmiento 1976, Reich & Borchert 1984, Reich 1995, Pedroni *et al.* 2002, Lenza & Klink 2006, Goldstein *et al.* 2008). Other effects acting as drivers of leaf fall such as seasonal dust accumulation and herbivory, were not assessed in this study. Despite this being a less explored topic, a few studies investigated the effects of biomass harvesting by leaf-cutter ants, showing partial or total defoliation in some cerrado's plant species (Costa *et al.* 2008, Mundim *et al.* 2012). Also, the damage by insects was also more intense in young leaves during the late dry season, corresponding to the main period of leaf flushing in the cerrado (Marquis *et al.* 2001). Therefore, herbivory might change leaves exchanges patterns by accelerating leaf aging due to damage or reducing photosynthetic activity. Moreover, insect-related damage and parasitism have negative effects on plant reproduction (Marquis *et al.* 2002, Franco 1998), factors that could lead to changes on cerrado phenological dynamics.

The peak of leaf flush preceding the start of the rainy season, observed in cerrado woody plants, is still an intriguing pattern. The predominance of species flushing at the end of the dry season supports the hypothesis that cerrado trees have constant access to the water in the soil due to the deep root system of most species, and that the preceding leaf fall contributes to rehydration and the early production of new leaves (Goldstein *et al.* 2008, Eamus & Prior 2001). The positive correlations with the rainfall and day length difference may indicate the favorable conditions in the transition season to the production of cerrado new leaves. Day length difference was the main factor positively predicting the leaf flushing pattern of cerrado, mainly for deciduous species, and explains the certainty of the leafing season. For tropical seasonal dry vegetation, day length is suggested as the main trigger for leaf flush, independently of the leaf exchange strategy (Borchert 2000, Borchert & Rivera 2001, Rivera *et al.* 2002, Higgins *et al.* 2011, Rossatto *et al.* 2013, but see Reich 1995,

Goldstein *et al.* 2008). Flushing before the more intense rainfall can also avoid loss of nutrient by leaching during the leaf development and favor nutrient uptake before the rainy season, the flowering and fruiting time of many species, due to the high luminance and photosynthetic activity of emerging new leaves (Rossatto *et al.* 2009, Sarmiento *et al.* 1985).

Deciduous species presented leaf fall mostly constrained to the middle of the dry season and leaf flush to the transition between dry to wet seasons. Although semi-deciduous and evergreen species also presented a seasonal leafing pattern, some individuals showed leaf exchange activity out of these periods. These results agree with the individual's response to abiotic variables, since we found a gradual response from deciduous to evergreen species, with evergreens significantly, but less constrained, by the climate and day length difference, mainly for leaf fall. Leaf fall restricted to the dry season has been described for several short-term savanna studies (e.g. Lenza & Klink 2006, Williams *et al.* 1997, Pirani *et al.* 2009). Rossatto *et al.* (2013) also observed a coincident leaf flush onset in cerrado species, but with an extended leaf flush into the wet season for cerrado evergreen species. At some savannas, the evergreen species seem to have a more diversified leaf exchange strategy, some flushing new leaves all year long while others concentrating the leaf production in the dry-to-wet season transition (Reich 1995, Franco *et al.* 2005).

Independent of the leaf strategy, if we simulate the GAM analyses with abiotic variables constant over time, the cerrado leafing pattern is still seasonal (Fig. 5 D and 6 D). This resilient seasonal pattern in addition to the high correlation with all the abiotic variables, makes it hard to establish the triggers and constraints of vegetative patterns in cerrado, as for other savanna communities (Higgins *et al.* 2011). Some authors suggest that the predominance of woody deciduous or semi-deciduous species, that seasonally change completely or partially their leaves, is an adaptation to the seasonal water restrictions, not directly related to the rainfall but also to the soil water availability and air humidity (Borchert

1994a, 1994b, Reich 1995, Eamus and Prior 2001, Franco *et al.* 2005a). Apart from abiotic factors, the cerrado woody species leafing patterns have been related to herbivory avoidance strategies and plant physiology, according to the different leaf exchange strategies or for aluminum accumulating or non-accumulating species (Franco *et al.* 2005, Borges & Prado 2014, Souza *et al.* 2015b).

We defined the community growing season onset as the dry to wet season, transition (August-September). This finding was based on a subset of the community' species showing a well-defined rest season and flushing onset, but also in the overall community significant seasonality and, increase of leaf flushing on early September. The observed decrease in the leaf fall activity, mainly for deciduous and semi-deciduous species, and the peak of leaf flush activity, for all strategies, when the climatic conditions corresponds to the dry-to-wet season transition also indicates the end of the cerrado resting season and start of the growing season (Table 1; Fig. 5). The absence of a marked resting season for half of the species was related to the fact that, even for deciduous species, individuals rarely lose all their leaves (100% leaf fall), and that leaf fall, for some semi-deciduous and mainly evergreen species, is observed in small intensities all year long. Another point is that, the absence of a community wide, well-defined leaf flush onset for all species is not expected for tropical communities, due to the high diversity of species and phenological patterns (Morellato *et al.* 2013, 2016), even for seasonal dry vegetations. Alberton *et al.* (2014), working with digital cameras daily repeated photographs or near surface phenology at the same cerrado site, detected an identical timing of the growing season as revealed in the present study. Their cross-validation with the direct monthly observations rules out any inherent subjectivity of our leaf exchange direct observations.

The predominance of a distinct leaf flushing season was demonstrated for some seasonal dry vegetations around the world, the marked dry seasons favoring fast response,

opportunistic species flushing new leaves at the end of dry season, after the first rains (Vico *et al.* 2015). We argue that cerrado could integrate the ecohydrological framework proposed by Vico *et al.* (2015) for seasonally dry ecosystems. Considering the interannual variability in the degree of deciduousness of cerrado individuals and, consequently species over this 7y study, the importance of temperature and rainfall as drivers of leaf fall and flush, and the similarity to other seasonally dry ecosystems, the cerrado leaf exchange phenology is likely susceptible to future climate changes scenarios of raising temperature and reduced rainfall (Vico *et al.* 2015, Reich 1995, Eamus & Prior 2001, IPCC 2004).

## ACKNOWLEDGMENTS

We thank the owners of Fazenda São José and the Instituto Arruda Botelho (IAB) for allowing us to conduct field work at the farm. We also thank all the former and actual members of Phenology Laboratory for their invaluable contribution to phenological data collection in the field and for the many fruitful discussions. Our research was supported by São Paulo Research Foundation (FAPESP) grants #2007/59779-6; FAPESP-Microsoft Research #2013/50155-0 and #2010/52113-5; FAPESP-VALE-FAPEMIG #2010/51307-0 and #2009/54208-6. LPCM holds a research productivity fellowship from CNPq (National Council for Scientific and Technological Development). BA (#2014/00215-0 and #2016/01413-5), MGGC (#2010/01762-3 and #2015/10754-8) and GHC (#2015/14292-9) receive fellowships from FAPESP.

**Data Availability:** The data used in this study are archived at the Dryad Digital Repository

## LITERATURE CITED

ALBERTON, B., J. ALMEIDA, R. HELM, R. S. TORRES, A. MENZEL, and L. P. C. MORELLATO.

2014. Using phenological cameras to track the green up in a cerrado savanna and its on-

- the-ground validation. *Ecol. Inform.* 19: 62–70.
- ARCHIBALD, S., and R. J. SCHOLES. 2007. Leaf green-up in a semi-arid African savanna—separating tree and grass responses to environmental cues. *J. Veg. Sci.* 18: 583–594.
- BALDOCCHI, D., E. FALGE, L. GU, R. OLSON, D. HOLLINGER, S. RUNNING, P. ANTHONI, C. BERNHOFER, K. DAVIS, and R. EVANS. 2001. FLUXNET: A new tool to study the temporal and spatial variability of ecosystem—scale carbon dioxide, water vapor, and energy flux densities. *Bull. Am. Meteorol. Soc.* 82: 2415–2434.
- BATALHA, M. A., S. ARAGAKI, and W. MANTOVANI. 1997. Phenological variations of the cerrado species in Emas - Pirassununga, SP. *Acta Bot. Bras* 11: 61–78.
- BATALHA, M. A., and W. MANTOVANI. 2000. Reproductive phenological patterns of cerrado plant species at the Pé-De-Gigante Reserve (Santa Rita Do Passa Quatro, SP, Brazil): a comparison between the herbaceous and woody floras. *Rev. Bras. Biol.* 60: 129–145.
- BATALHA, M. A., and F. R. MARTINS. 2004. Reproductive phenology of the cerrado plant community in Emas National Park (Central Brazil). *Aust. J. Bot.* 52: 149–161.
- BENCKE, C. S. C., and L. P. C. MORELLATO. 2002. Comparison of two methods of plant phenology estimation, their interpretation and representation. *Rev. Bras. Botânica* 25: 269–275.
- DE BIE, S., P. KETNER, M. PAASSE, and C. GEERLING. 1998. Woody plant phenology in the West Africa savanna. *J. Biogeogr.* 25: 883–900.
- BORCHERT, R. 2000. Organismic and environmental controls of bud growth in tropical trees. *Garden* 87–108.
- BORCHERT, R., and G. RIVERA. 2001. Photoperiodic control of seasonal development and dormancy in tropical stem-succulent trees. *Tree Physiol.* 21: 213–221.
- BORGES, M. P., and C. H. B. A. PRADO. 2014. Relationships between leaf deciduousness and flowering traits of woody species in the Brazilian neotropical savanna. *Flora Morphol.*

- Distrib. Funct. Ecol. Plants 209: 73–80.
- BULHÃO, C. F., and P. S. FIGUEIREDO. 2002. Phenology of leguminous trees in an area of cerrado in the northeast of Maranhão. *Rev. Bras. Botânica* 25: 361–369.
- CAMARGO, M. G. G., R. M. SOUZA, P. REYS, and L. P. C. MORELLATO. 2011. Effects of environmental conditions associated to the cardinal orientation on the reproductive phenology of the cerrado savanna tree *Xylopia aromatica* (Annonaceae). *An. Acad. Bras. Cienc.* 83: 1007–1019.
- CHRISTENSEN, R. H. B. 2016. Regression Models for Ordinal Data [R package ordinal version 2015.6-28].
- CONDIT, R., K. WATTS, S. A. BOHLMAN, R. PÉREZ, R. B. FOSTER, and S. P. HUBBELL. 2000. Quantifying the deciduousness of tropical forest canopies under varying climates. *J. Veg. Sci.* 11: 649–658.
- COSTA, A. N., H. L. VASCONCELOS, E. H. M. VIEIRA-NETO, and E. M. BRUNA. 2008. Do herbivores exert top-down effects in Neotropical savannas? Estimates of biomass consumption by leaf-cutter ants. *J. Veg. Sci.* 19: 849–854.
- COUTINHO, L. M. 1978. The concept of Cerrado. *Rev. Bras. Bot* 1: 17–23.
- COUTINHO, L. M. 2006. The biome concept. *Acta Bot. Brasilica* 20: 13–23.
- DALMOLIN, Â. C., F. DE ALMEIDA LOBO, G. VOURLITIS, P. R. SILVA, H. J. DALMAGRO, M. Z. ANTUNES, and C. E. R. ORTÍZ. 2015. Is the dry season an important driver of phenology and growth for two Brazilian savanna tree species with contrasting leaf habits? *Plant Ecol.* 216: 407–417.
- DAMASCOS, M. A., C. H. B. A. PRADO, and C. C. RONQUIM. 2005. Bud composition, branching patterns and leaf phenology in Cerrado woody species. *Ann. Bot.* 96: 1075–1084.
- DURIGAN, G., and J. A. RATTER. 2016. The need for a consistent fire policy for Cerrado

- conservation. *J. Appl. Ecol.* 53: 11–15.
- EAMUS, D., and L. PRIOR. 2001. Ecophysiology of trees of seasonally dry tropics: comparisons among phenologies. *Adv. Ecol. Res.* 32: 113–197.
- FOUNIER, L. 1974. Un método cuantitativo para la medición de características fenológicas en árboles. *Turrialba* 24: 422–423.
- FRANCO, A. C. 1998. Seasonal patterns of gas exchange, water relations and growth of it *Roupala montana*, an evergreen savanna species. *Plant Ecol.* 136: 69–76.
- FRANCO, A. C., M. BUSTAMANTE, L. S. CALDAS, G. GOLDSTEIN, F. C. MEINZER, A. R. KOZOVITS, P. RUNDEL, and V. T. R. CORADIN. 2005. Leaf functional traits of Neotropical savanna trees in relation to seasonal water deficit. *Trees - Struct. Funct.* 19: 326–335.
- GOLDSTEIN, G., F. C. MEINZER, S. J. BUCCI, F. G. SCHOLZ, A. C. FRANCO, and W. A. HOFFMANN; 2008. Water economy of Neotropical savanna trees: six paradigms revisited. *Tree Physiol.* 28: 395–400.
- HIGGINS, S. I., M. D. DELGADO-CARTAY, E. C. FEBRUARY, and H. J. COMBRINK. 2011. Is there a temporal niche separation in the leaf phenology of savanna trees and grasses? *J. Biogeogr.* 38: 2165–2175.
- IPCC. 2004. Climate change 2014: impacts, adaptation, and vulnerability. Part A: global and sectoral aspects C. of working G. I. to the F. A. R. of the I. P. on C. Change (Ed.). Cambridge University Press, Cambridge, United Kingdom and New York, NY, USA.
- JACKSON, P. C., F. C. MEINZER, M. BUSTAMANTE, G. GOLDSTEIN, A. FRANCO, P. W. RUNDEL, L. CALDAS, E. IGLER, and F. CAUSIN. 1999. Partitioning of soil water among tree species in a Brazilian Cerrado ecosystem. *Tree Physiol.* 19: 717–724.
- LAVOREL, S., S. DÍAZ, J. H. C. CORNELISSEN, E. GARNIER, S. P. HARRISON, S. MCINTYRE, J. G. PAUSAS, N. P. CATHERINE, and R. CARLOS. 2007. Plant functional types : are we

- getting any closer to the Holy Grail? *In* Terrestrial ecosystems in a changing world. pp. 149–164, Springer Berlin, Heidelberg.
- LENZA, E., and C. A. KLINK. 2006. Phenological behavior of woody species in a “cerrado” sensu stricto of Brasília, DF. *Brazilian J. Bot.* 29: 627–638.
- MANTOVANI, W., and F. R. MARTINS. 1988. Phenological variations in species of the “cerrado” of the Moji Guaçu Biological Reserve, São Paulo State. *Revta. Bras. Bot* 11: 101–112.
- MARQUIS, R. J., I. R. DINIZ, and H. C. MORAIS. 2001. Patterns and correlates of interspecific variation in foliar insect herbivory and pathogen attack in Brazilian cerrado. *J. Trop. Ecol.* 17: 127–148.
- MARQUIS, R. J., H. C. MORAIS, and I. R. DINIZ. 2002. Interactions among cerrado plants and their herbivores: unique or typical. *The cerrados of Brazil* 306–328.
- MENDOZA, I., C. A. PERES, L. PATRÍCIA, and C. MORELLATO. 2017. Continental-scale patterns and climatic drivers of fruiting phenology : A quantitative Neotropical review. *Glob. Planet. Change* 148: 227–241.
- MIRANDA, I. S. 1995. Phenology of the arboreal stratum of a savanna community at Alter-do-Chão, PA. *Rev. Bras. Botânica* 18: 235–240.
- MONASTERIO, M., and G. SARMIENTO. 1976. Phenological strategies of plants species in the tropical savanna and semi-deciduous forest of the Venezuelan Llanos. *J. Biogeogr.* 3: 325–356.
- MORELLATO, L. P. C., L. F. ALBERTI, and I. L. HUDSON. 2010. Applications of circular statistics in plant phenology: a case studies approach. *In* I. L. Hudson and M. R. Keatley (Eds.) *Phenological Research*. pp. 339–359, Springer Netherlands.
- MORELLATO, L. P. C., B. ALBERTON, S. T. ALVARADO, B. BORGES, E. BUISSON, M. G. G. CAMARGO, L. F. CANCIAN, D. W. CARSTENSEN, D. F. E. ESCOBAR, P. T. P. LEITE, I.



- MENDOZA, N. M. W. B. ROCHA, N. C. SOARES, T. S. F. SILVA, V. G. STAGGEMEIER, A. S. STREHER, B. C. VARGAS, and C. A. PERES. 2016. Linking plant phenology to conservation biology. *Biol. Conserv.* 195.
- MORELLATO, L. P. C., M. G. G. CAMARGO, and E. GRESSLER. 2013. A review of plant phenology in south and central america.
- MORELLATO, L. P. C., and H. F. LEITÃO-FILHO. 1989. Estratégias fenológicas de espécies arbóreas em floresta mesófila na Serra do Japi, Jundiaí, São Paulo. *Rev. Bras. Biol.* 50: 163–173.
- MORELLATO, L. P. C., D. C. TALORA, A. TAKAHASI, C. C. BENCKE, E. C. ROMERA, and V. B. ZIPPARRO. 2000. Phenology of Atlantic Rain Forest Trees: A Comparative Study. *Biotropica* 32: 811–823.
- MUNDIM, F. M., E. M. BRUNA, E. H. M. VIEIRA-NETO, and H. L. VASCONCELOS. 2012. Attack frequency and the tolerance to herbivory of Neotropical savanna trees. *Oecologia* 168: 405–414.
- MUNHOZ, C. B. R., and J. M. FELFILI. 2005. Phenology of the herbaceous layer in a campo sujo community in the Fazenda Água Limpa, Federal District, Brazil. *Acta Bot. Brasilica* 19: 979–988.
- MUNHOZ, C. B. R., and J. M. FELFILI. 2006. Phytosociology of the herb-subshrub layer in an area of campo sujo, Distrito Federal, Brazil. *Acta Bot. Brasilica* 20: 671–685.
- OPLER, P. A., G. W. FRANKIE, H. G. BAKER, S. JOURNAL, N. MAR, H. G. BAKER, D. C. RICA, C. UNIVERSITARIA, S. JOSE, and C. RICA. 1980. Comparative phenological studies of treelet and shrub species in tropical wet and dry forests in the lowlands of Costa Rica. *Biotropica* 12: 167–188.
- OVERBECK, G. E., E. VÉLEZ-MARTIN, F. R. SCARANO, T. M. LEWINSOHN, C. R. FONSECA, S. T. MEYER, S. C. MÜLLER, P. CEOTTO, L. DADALT, G. DURIGAN, G. GANADE, M. M.

- GOSSNER, D. L. GUADAGNIN, K. LORENZEN, C. M. JACOBI, W. W. WEISSER, and V. D. PILLAR. 2015. Conservation in Brazil needs to include non-forest ecosystems. *Divers. Distrib.* 21: 1455–1460.
- PEDRONI, F., M. SANCHEZ, and F. A. M. SANTOS. 2002. Phenology of copaíba (*Copaifera langsdorffii* Desf. – Leguminosae, Caesalpinioideae) in a semideciduous forest, southeastern Brazil. *Rev. Bras. Botânica* 25: 183–194.
- PIRANI, F. R., M. SANCHEZ, and F. PEDRONI. 2009. Phenology of a tree community in a cerrado sensu stricto, Barra do Garças, Mato Grosso state, Brasil. *Acta Bot. Brasilica* 23: 1096–1110.
- POLGAR, C. A., and R. B. PRIMACK. 2011. Leaf-out phenology of temperate woody plants: from trees to ecosystems. *New Phytol.* 191: 926–941.
- PRIOR, L. D., D. M. J. S. BOWMAN, and D. EAMUS. 2004. Seasonal differences in leaf attributes in Australian tropical tree species: Family and habitat comparisons. *Funct. Ecol.* 18: 707–718.
- RATTER, J. A., S. BRIDGEWATER, R. ATKINSON, and J. F. RIBEIRO. 1996. Analysis of the floristic composition of the Brazilian cerrado vegetation II: comparison of the woody vegetation of 98 areas. *Edinburgh J. Bot.* 53: 153–180.
- REICH, P. B. 1995. Phenology of tropical forests: patterns, causes, and consequences. *Can. J. Bot.* 73: 164–174.
- REICH, P. B., and R. BORCHERT. 1984. Water stress and tree phenology in a tropical dry forest in the lowlands of Costa Rica. *J. Ecol.* 61–74.
- REYS, P., M. G. G. CAMARGO, M. T. GROMBONE-GUARATINI, A. D. P. TEIXEIRA, M. A. ASSIS, and L. P. C. MORELLATO. 2013. Structure and floristic composition of a Cerrado sensu stricto and its relevance to ecological restoration. *Hoehnea* 40: 449–464.
- RICHARDSON, A. D., T. F. KEENAN, M. MIGLIAVACCA, Y. RYU, O. SONNENTAG, and M.

- TOOMEY. 2013. Climate change, phenology, and phenological control of vegetation feedbacks to the climate system. *Agric. For. Meteorol.* 169: 156–173.
- RIVERA, G., S. ELLIOTT, L. S. CALDAS, G. NICOLOSSI, V. T. CORADIN, and R. BORCHERT. 2002. Increasing day-length induces spring flushing of tropical dry forest trees in the absence of rain. *Trees-Structure Funct.* 16: 445–456.
- ROSSATTO, D. R., W. A. HOFFMANN, and A. C. FRANCO. 2009. Differences in growth patterns between co-occurring forest and savanna trees affect the forest-savanna boundary. *Funct. Ecol.* 23: 689–698.
- ROSSATTO, D. R., W. A. HOFFMANN, L. DE C. R. SILVA, M. HARIDASAN, L. S. L. STERNBERG, and A. C. FRANCO. 2013. Seasonal variation in leaf traits between congeneric savanna and forest trees in Central Brazil: implications for forest expansion into savanna. *Trees* 27: 1139–1150.
- SARMIENTO, G. 1984. *The ecology of neotropical savannas*. Harvard University Press.
- SARMIENTO, G., G. GOLDSTEIN, and F. MEINZER. 1985. Adaptive strategies of woody species in neotropical savannas. *Biol. Rev.* 60: 315–355.
- SILVÉRIO, D. V., and E. LENZA. 2010. Phenology of woody species in a typical cerrado in the Bacaba Municipal Park, Nova Xavantina, Mato Grosso, Brazil. *Biota Neotrop.* 10: 205–216.
- SOUZA, M. C. DE, P. C. P. BUENO, L. P. C. MORELLATO, and G. HABERMANN. 2015. Ecological strategies of Al-accumulating and non-accumulating functional groups from the cerrado sensu stricto. *An. Acad. Bras. Cienc.* 87: 813–823.
- SOUZA, M. C., A. C. FRANCO, M. HARIDASAN, D. R. ROSSATTO, J. F. ARAÚJO, L. P. C. MORELLATO, and G. HABERMANN. 2015. The length of the dry season may be associated with leaf scleromorphism in cerrado plants. *An. Acad. Bras. Cienc.* 87: 1691–1699.
- TANNUS, J. L. S., M. A. ASSIS, and L. P. C. MORELLATO. 2006. Reproductive phenology in

dry and wet grassland in an area of Cerrado at Southeastern Brazil, Itirapina - SP. *Biota Neotrop.* 6: 0–0.

VICO, G., S. E. THOMPSON, S. MANZONI, A. MOLINI, J. D. ALBERTSON, J. S.

ALMEIDA-CORTEZ, P. A. FAY, X. FENG, A. J. GUSWA, and H. LIU. 2015. Climatic, ecophysiological, and phenological controls on plant ecohydrological strategies in seasonally dry ecosystems. *Ecohydrology* 8: 660–681.

VOGADO, N. O., M. G. G. CAMARGO, G. M. LOCOSSELLI, and L. P. C. MORELLATO. 2016.

Edge effects on the phenology of the guamirim, *Myrcia guianensis* (Myrtaceae), a cerrado tree, Brazil. *Top. Conserv. Sci.* 9: 291–312.

WILLIAMS, R. J., B. A. MYERS, W. MÜLLER, G. A. DUFF, and D. EAMUS. 1997. Leaf

phenology of woody species in a north Australian tropical savanna. *Ecology* 78: 2542–2558.

WOOD, S. N. 2011. Fast stable restricted maximum likelihood and marginal likelihood

estimation of semiparametric generalized linear models. *J. R. Stat. Soc. Ser. B (Statistical Methodol.* 73: 3–36.

ZAR, J. H. 1999. *Biostatistical analysis* 4th ed. Pearson Education India.

TABLE 1. Results of the ordinal multinomial models for the relation between leaf fall and leaf flush (individuals' activity) and total rainfall, mean temperature, monthly day length difference and rainfall-temperature interaction, according to species leaf exchange patterns.

All the  $p$  values were  $< 0.001$ .

Leaf exchange pattern	Models	Estimate	Standard error	Z value
<b>Leaf fall</b>				
Evergreen	Total rainfall	-0.031	0.009	-3.313
	Mean temperature	-0.271	0.009	-30.755
	Day length difference	0.067	0.006	10.655
	Rainfall * temperature	0.258	0.010	25.372
Semi-deciduous	Total rainfall	-0.151	0.008	-19.896
	Mean temperature	-0.352	0.007	-49.048
	Day length difference	0.051	0.005	9.957
	Rainfall * temperature	0.375	0.008	45.301
Deciduous	Total rainfall	-0.287	0.010	-28.350
	Mean temperature	-0.416	0.010	-43.700
	Day length difference	0.068	0.007	10.040
	Rainfall * temperature	0.469	0.011	42.940
<b>Leaf flush</b>				
Evergreen	Total rainfall	0.135	0.010	13.010
	Mean temperature	-0.086	0.010	-8.780
	Day length difference	0.317	0.008	42.023
	Rainfall * temperature	-0.095	0.012	-8.001
Semi-deciduous	Total rainfall	0.093	0.009	10.265
	Mean temperature	-0.290	0.009	-33.285
	Day length difference	0.424	0.007	62.288
	Rainfall * temperature	-0.075	0.010	-7.185
Deciduous	Total rainfall	0.351	0.012	28.760
	Mean temperature	-0.385	0.012	-32.030
	Day length difference	0.567	0.010	55.570
	Rainfall * temperature	-0.307	0.015	-20.220

TABLE 2. Circular statistics analyses of the leaf flush onset, per year, in the individuals of a cerrado woody community, Southeastern Brazil. Individuals with marked onset: number of individuals, from the total of observed individuals, for which we could define the leaf flush onset date and include in the circular analyses; (n) number of individuals which presented the leaf flush onset in the indicated month; onset mean angle: mean angle of data distribution around the circle; onset mean date: month correspondent to the mean angle; \* $p < 0.05$ .

	2005	2006	2007	2008	2009	2010	2011
Observed individuals	2112	2111	2100	2046	1979	1947	1891
Individuals with marked onset	1300	1384	1000	876	816	778	994
Most frequent onset month (n)	Sep (665)	Aug (537)	Sep (447)	Aug (423)	Sep (348)	Sep (290)	Aug (359)
Onset mean angle ( $\mu$ )	236.4°	229.6°	249.8°	238.3°	245.8°	248.4°	236.0°
Onset mean date	Aug	Aug	Sep	Aug	Sep	Sep	Aug
Length of mean vector ( $r$ )	0.69	0.64	0.59	0.82	0.76	0.72	0.74
Rayleigh test (Z)	617.21*	560.45*	346.05*	583.44*	468.37*	399.08*	550.24*

## FIGURE LEGENDS

FIGURE 1. Climate between 2005 and 2011 in Itirapina, São Paulo, Brazil. The rainfall as daily (circles) and monthly (bars) accumulated precipitation. Temperature as monthly mean (line) and daily means (black circles). Day length is shown as daily values and monthly difference.

FIGURE 2. Percentage of species (A) and individuals (B) per deciduousness degree in each year according to the leaf fall intensity and the percentage of species per leaf exchange strategy (C) in a cerrado woody community, Southeastern Brazil. Deciduous: individuals or species which more than half of individuals reached 100% of leaf fall; semi-deciduous: individuals or species which more than half of individuals reached “2” of leaf fall intensity; evergreen individuals or species which the individuals reached only “1” of leaf fall intensity.

FIGURE 3. Leaf fall phenology on percent of individuals (A) and percent of intensity (B) in a cerrado woody community according to the species’ leaf exchange strategy: deciduous (26 species), semi-deciduous (25 species) and evergreen (18 species). The blue bars indicate the wet season.

FIGURE 4. Leaf flush phenology on percent of individuals (A) and percent of intensity (B) in a cerrado woody community according to the species’ leaf exchange strategy: deciduous (26 species), semi-deciduous (25 species) and evergreen (18 species). The blue bars indicate the wet season.

FIGURE 5. Fitted generalized additive models’ responses of the proportion of individuals without leaves to the abiotic variables - rainfall (A), temperature (B) and day length difference (C) - and since the first phenological observation in the field (D).

FIGURE 6. Fitted generalized additive models’ responses of the proportion of individuals flushing new leaves to the abiotic variables - rainfall (A), temperature (B) and day length difference (C) - and since the first phenological observation in the field (D).

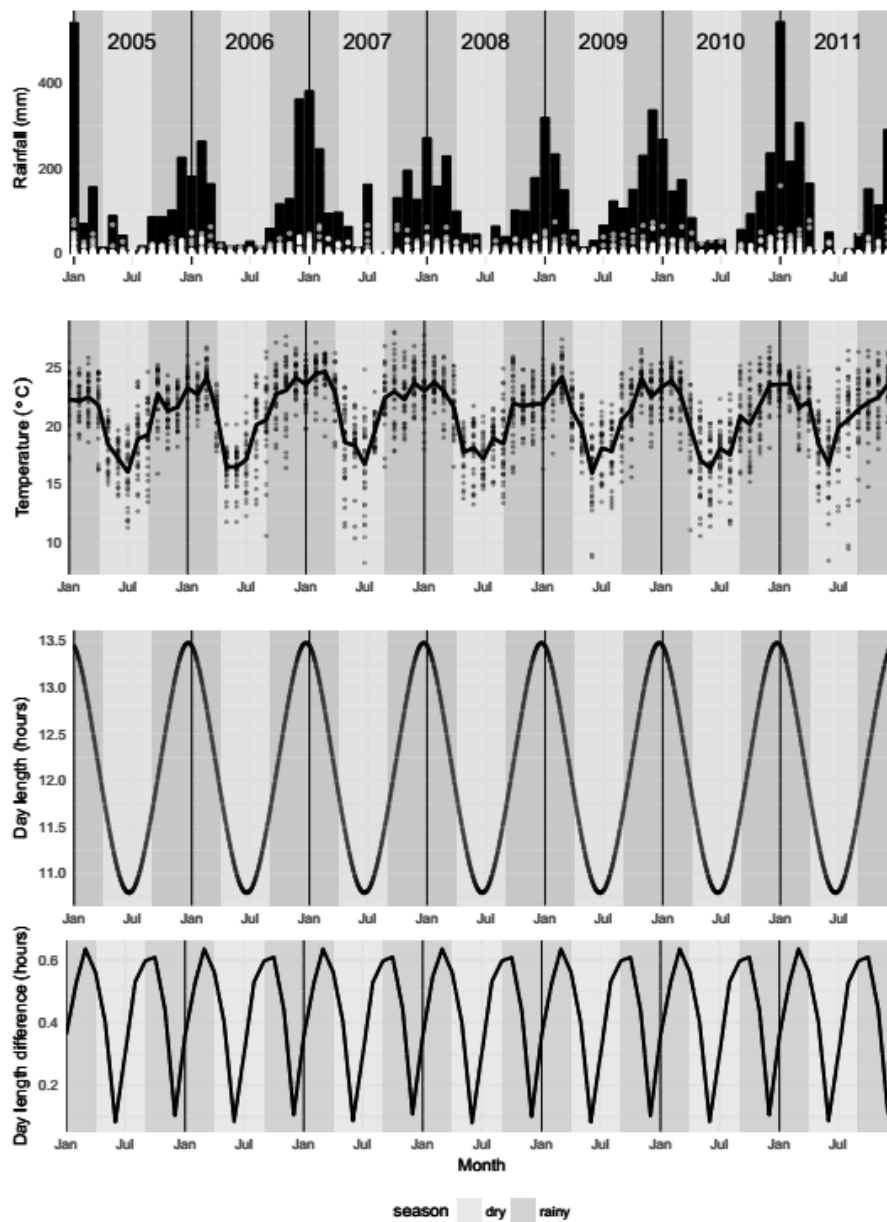


Figure 1



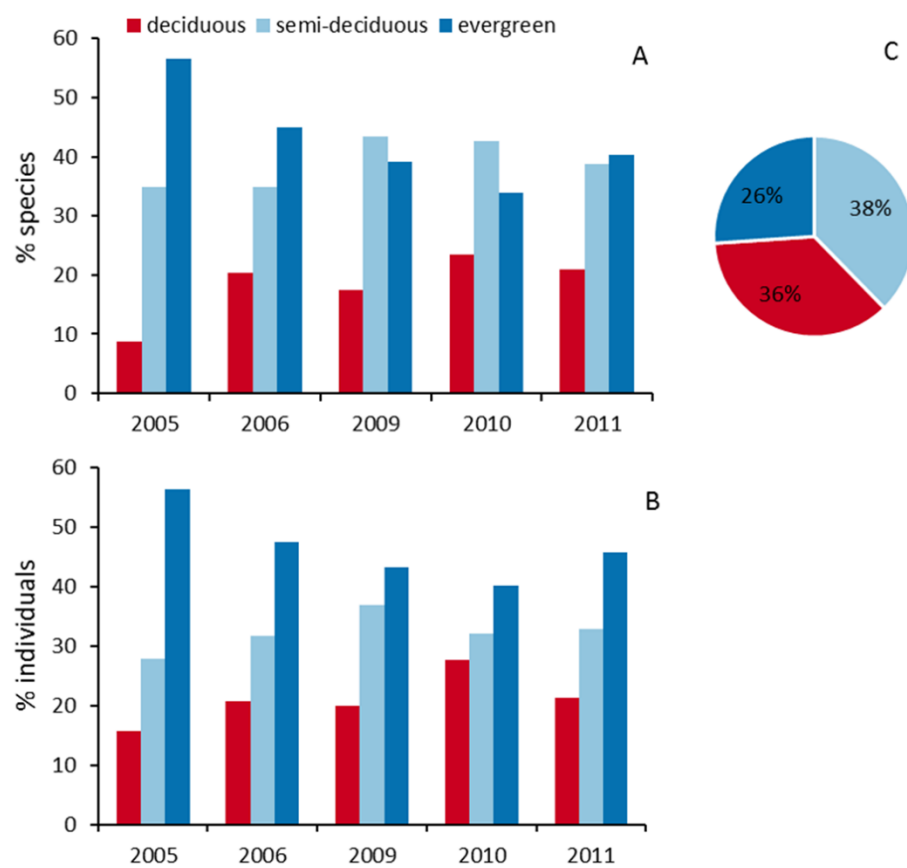


Figure 2

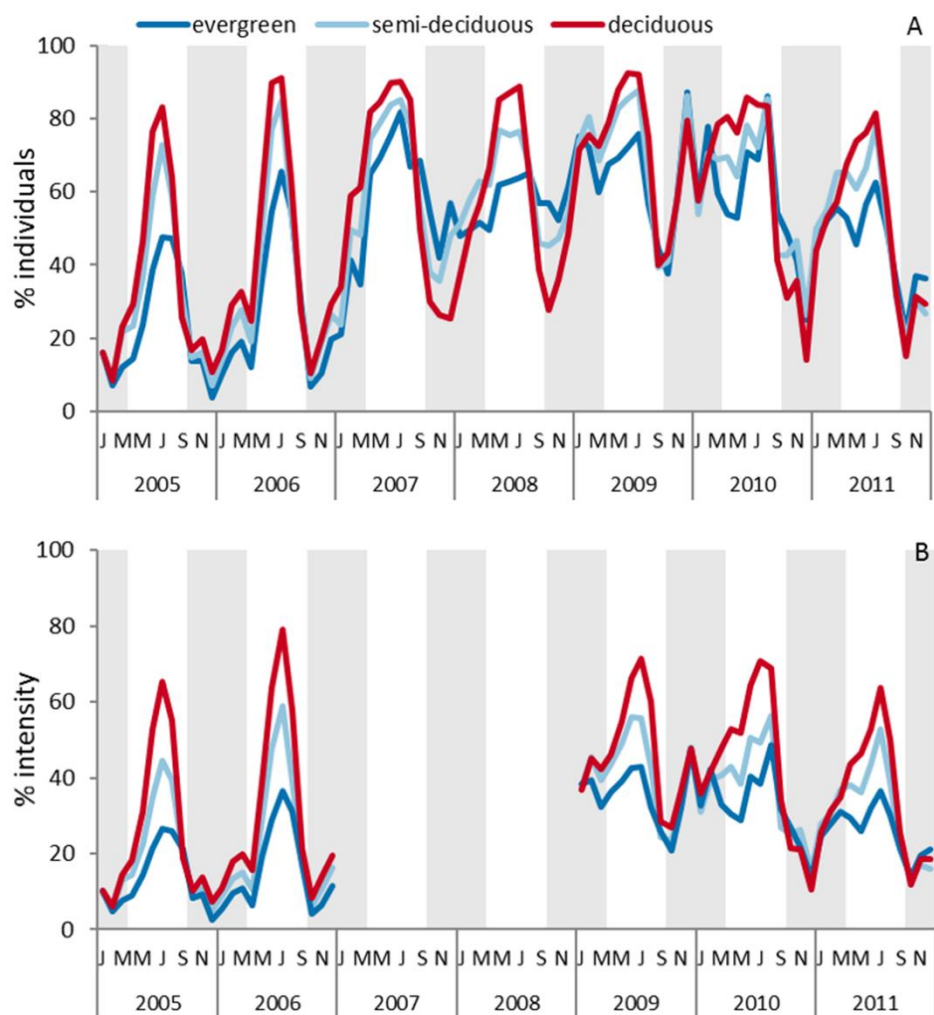


Figure 3

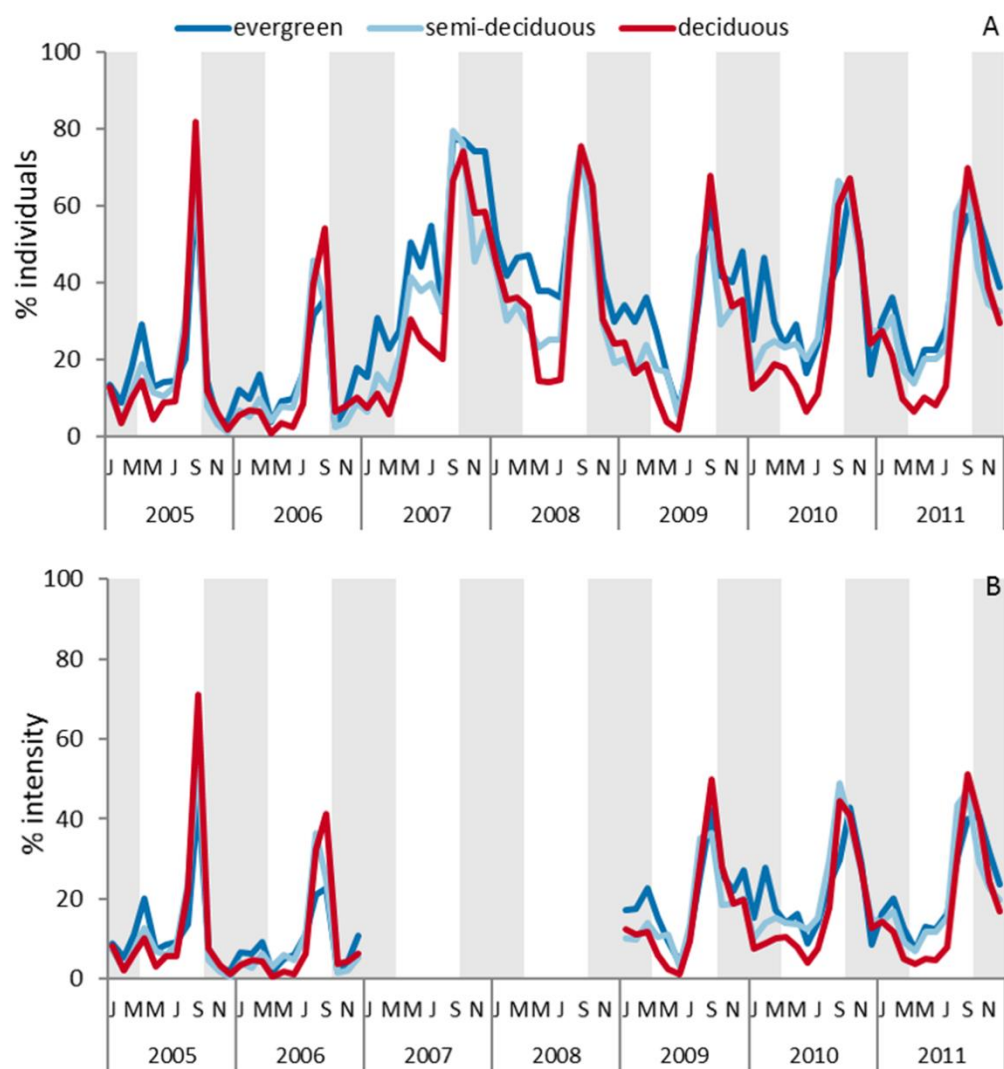


Figure 4

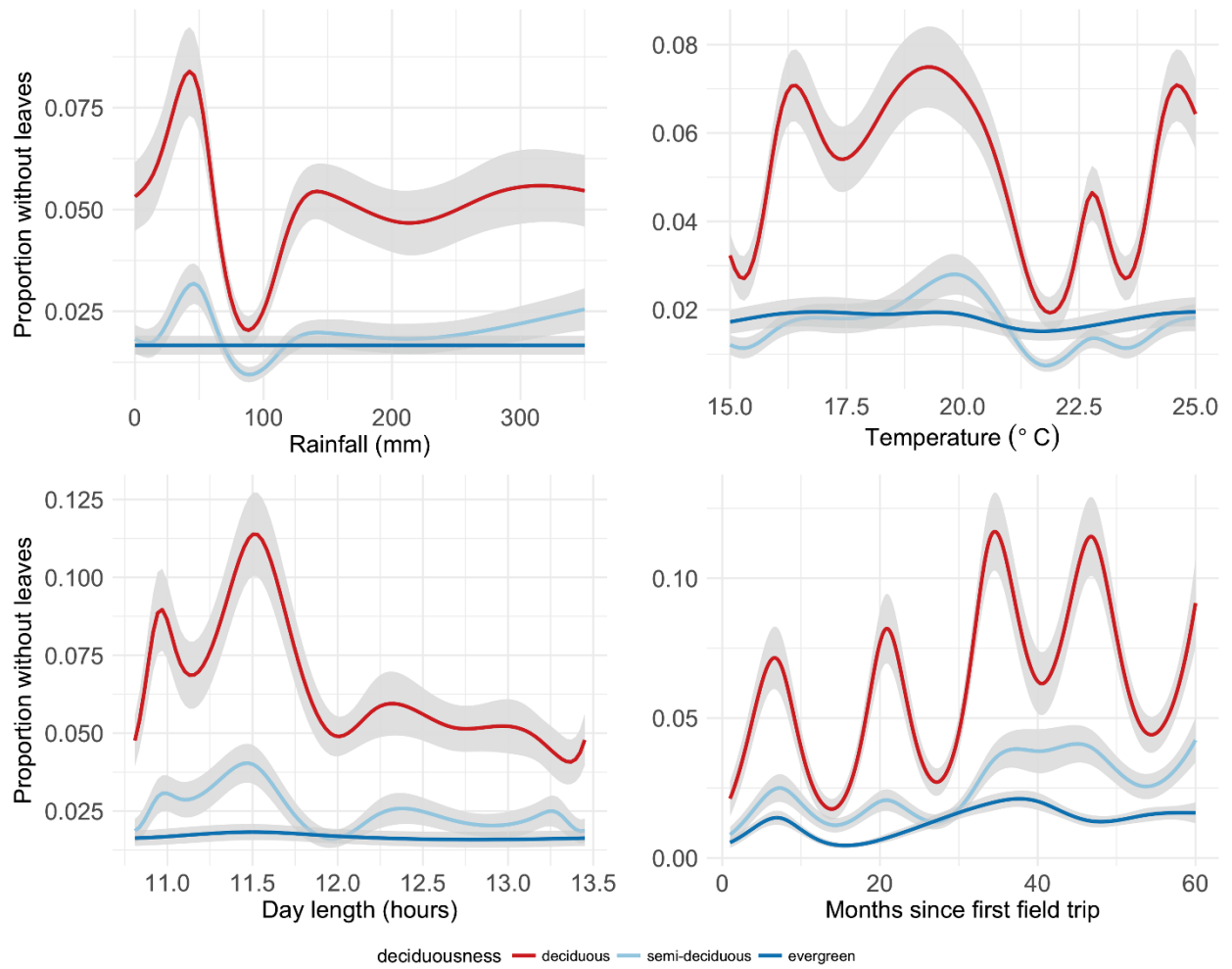


Figure 5

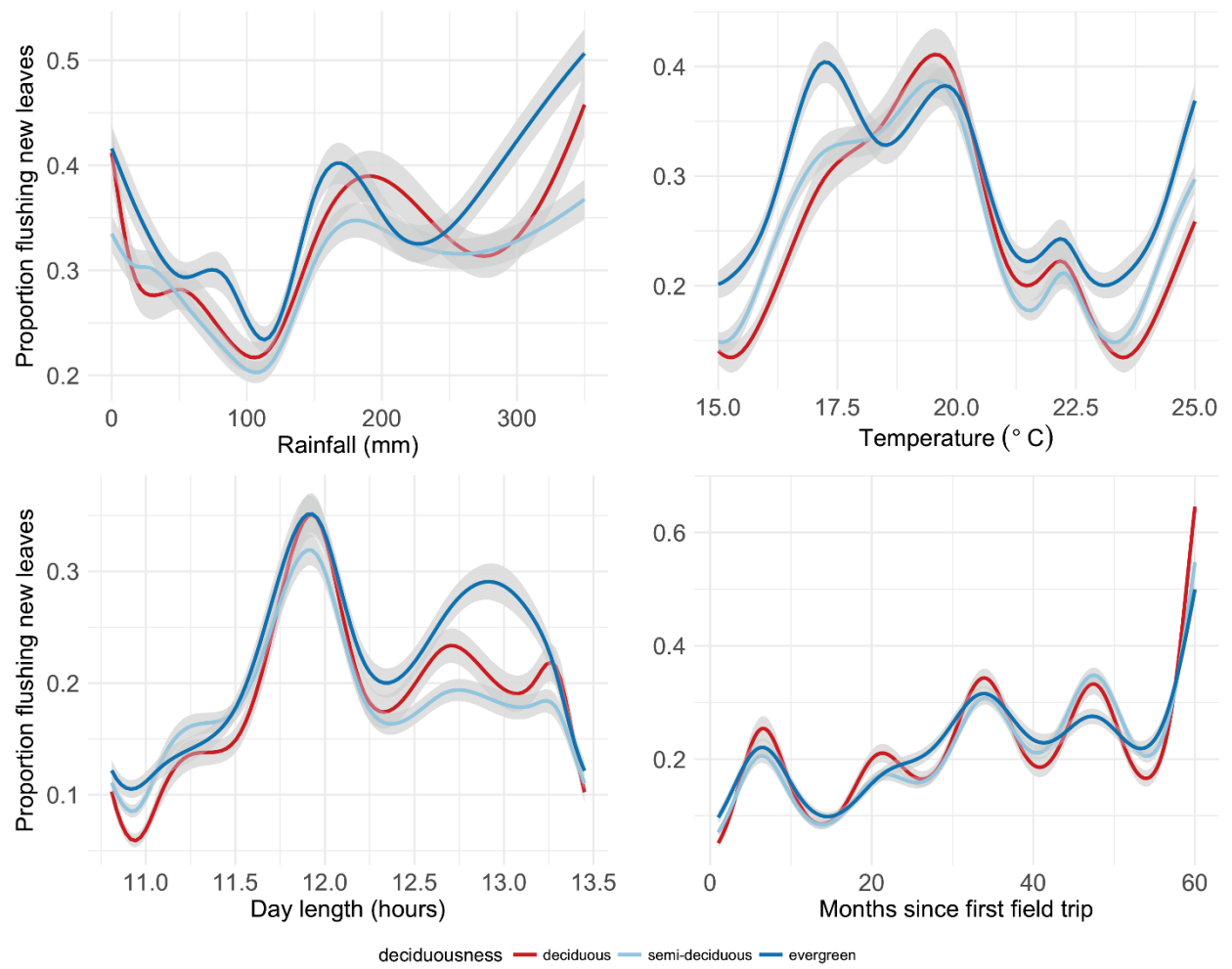


Figure 6

### **Appendix B**

Article published in the Journal Pattern Recognition Letters:

ALMEIDA J., SANTOS, JA, ALBERTON, B., MORELLATO, L.P.C., TORRES, R.S. Phenological visual rhythms: compact representations for fine-grained plant species Identification. **Pattern Recognition Letters**, v. 81, p. 90-100, 2016.

## Phenological visual rhythms: Compact representations for fine-grained plant species identification

Jurandy Almeida <sup>a,d,\*</sup>, Jefersson A. dos Santos <sup>b</sup>, Bruna Alberton<sup>c</sup>, Leonor Patricia C. Morellato<sup>c</sup>, Ricardo da S. Torres <sup>d</sup>

<sup>a</sup> Institute of Science and Technology, Federal University of São Paulo – UNIFESP, 12247-014 São José dos Campos, SP, Brazil

<sup>b</sup> Department of Computer Science, Federal University of Minas Gerais – UFMG, 31270-010 Belo Horizonte, MG, Brazil

<sup>c</sup> Department of Botany, Institute of Biosciences, São Paulo State University – UNESP, 13506-900 Rio Claro, SP, Brazil

<sup>d</sup> Institute of Computing, University of Campinas – UNICAMP, 13083-852 Campinas, SP, Brazil

## Abstract

Plant phenology, the study of recurrent life cycles events and its relationship to climate, is a key discipline in climate change research. In this context, digital cameras have been effectively used to monitor leaf flushing and senescence on vegetations across the world. A primary condition for the phenological observation refers to the correct identification of plants by taking into account time series associated with their crowns in the digital images. In this paper, we present a novel approach for representing phenological patterns of plant species. The proposed method is based on encoding time series as a visual rhythm. Here, we focus on applications of our approach for plant species identification. In this scenario, visual rhythms are characterized by image description algorithms. A comparative analysis of different descriptors is conducted and discussed. Experimental results show that our approach presents high accuracy on identifying individual plant species from its specific visual rhythm. Additionally, our representation is compact, making it suitable for long-term data series.

## Keywords:

Remote phenology, Plant identification, Image analysis, Time series, Visual rhythm

## 1. Introduction

Plant phenology, the study of recurrent life cycles events and its relationship to climate, is a key discipline in climate change research [34]. One key component of phenology research is the leaf exchange patterns from leaf budding to senescence, due to its relevance to comprehend ecosystem processes, such as growth, water and gas exchange, and nutrient cycling [24]. The dynamics of plant growing seasons define the spatial and temporal patterns of carbon balance and water exchange, and ultimately the productivity of terrestrial ecosystems [22,35].

Recently, digital cameras have been effectively applied as multi-channel imaging sensors to estimate color changes (RGB channels) that are related to leaf flushing and senescence phenology [1,2,30]. The technique allows to increase the range of study sites and

species and the accuracy of phenological observations, and a clear perception of the start and end of the growing season [2,16].

We have monitored leaf changing patterns of a tropical cerrado-savanna vegetation by taking daily digital images [2]. We extracted image color information from the RGB (red, green, and blue) channels and correlated the changes in pixel levels over time with leaf phenology patterns [2]. The analysis was conducted after we defined regions of interest (ROI) based on the random selection of plant species crowns identified in the digital image [29]. We obtained a time series associated with each ROI, raising the need of using appropriate tools for mining patterns of interest in a given digital image [7,11,32,33].

The plant species identification is a key issue for the phenological observation of tree crowns using phenocams, especially in tropical vegetations where one single image may include a high number of species [2,6,7]. This task is time consuming since first each crown in the image has to be matched to the tree in the soil and then the tree is identified at species level. In this sense, we have developed and deployed computational methods to find similar patterns in the digital images and then we checked if they correspond to similar species or leaf functional groups [5,6].

The major challenge of designing automatic tools for addressing the plant identification task is to deal with fine-grained

\* Corresponding author at: Institute of Science and Technology, Federal University of São Paulo – UNIFESP, 12247-014 São José dos Campos, SP, Brazil. Tel.: +55 12 3309 9500; fax: +55 12 3921 8857.

E-mail addresses: [jurandy.almeida@unifesp.br](mailto:jurandy.almeida@unifesp.br) (J. Almeida), [jefersson@dcc.ufmg.br](mailto:jefersson@dcc.ufmg.br) (J.A. dos Santos), [bru.alberton@gmail.com](mailto:bru.alberton@gmail.com) (B. Alberton), [pmorella@rc.unesp.br](mailto:pmorella@rc.unesp.br) (L.P.C. Morellato), [rtorres@ic.unicamp.br](mailto:rtorres@ic.unicamp.br) (R. da S. Torres).

recognition, where the categories are visually similar. In general, different plant species may have an analogous behavior with respect to leaf color change and, hence, the differences between their time series are quite subtle and hard to be detected, even for humans without careful training. Usually, plant identification is based on the analysis of huge volumes of sequential vegetation images, i.e., vegetation images obtained over time. In this scenario, another challenge refers to efficiency aspects, both in terms of storage requirements and processing time. Typical existing solutions for plant identification based on vegetation images [6,28] do not scale properly for handling ever-growing collections.

In this paper, we present an effective and efficient approach for capturing phenological patterns from time series generated by digital images. Our strategy consists of encoding time series as a visual rhythm [25]. This simple, yet effective, approach offers rich information regarding spatio-temporal data, which is useful in many fields of applicability. Here, we focus on applications of the proposed method to identify and distinguish the behavior of plant species. In this scenario, visual rhythms are characterized by traditional and recently proposed image description algorithms. Such methods are able to codify key image features into fixed-size representations.

The proposed method was evaluated in a dataset recorded during the main leaf flushing season composed of about 2,700 images [2]. We performed a detailed experimental comparison of several image descriptors. The results show that our approach presents high accuracy on identifying regions in the images belonging to a same plant species. In addition, our strategy provides a compact representation for time series. The improvement of the computation makes it suitable for long-term data sets.

This paper extends substantially our preliminary works presented in [3,4]. Here, we introduce several innovations. First, we present a review of the state-of-the-art approaches for processing spatio-temporal data. In addition, we discuss new strategies of generating visual rhythms from time series. Finally, after a much more thorough presentation of the proposed method, we extend the experimental evaluation of our technique, including a statistical analysis of its performance.

The remainder of this paper is organized as follows. Section 2 briefly describes related work. Section 3 discusses the methodology adopted for acquiring time series. Section 4 presents our approach and shows how to apply it to characterize time series. Section 5 presents the adopted experimental protocol, while Section 6 reports the results of our experiments and compares our technique with other methods. Finally, we offer our conclusions and directions for future work in Section 7.

## 2. Related work

The increasing accessibility to data with high spatio-temporal resolution has enabled a detailed analysis of vegetation properties. At the same time, it requires feature extraction techniques able to represent such properties, taking into account storage aspects.

Time series-based vegetation indices from remote sensing images (RSIs) are widely used for phenological and land cover change studies [10,13,17,31]. Rodrigues et al. [31] presented a software to extract phenological parameters (e.g., maturity and senescence) from Normalized Difference Vegetation Index (NDVI) time series. Foster et al. [13] also applied NDVI time series to detect grassland vegetation. Brooks et al. [10], in turn, proposed a Fourier-based algorithm to fit NDVI multitemporal curves and reduce missing data effects in the analysis. Hmimina et al. [17] exploited NDVI time-series to evaluate the potential use of MODerate resolution Imaging Spectroradiometer (MODIS) remote sensing data for monitoring phenological patterns in a African savanna.

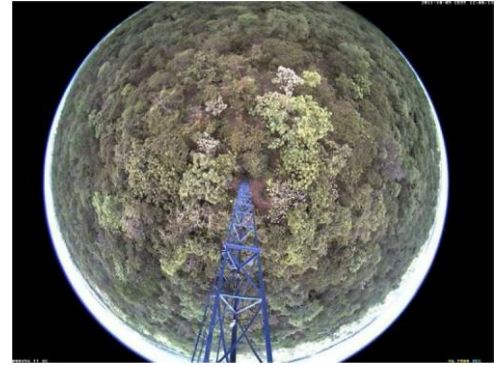


Fig. 1. Sample image of the cerrado savanna recorded by the digital camera on October 5th, 2011.

In [6,8,23,28], the authors consider not only temporal but also spatial properties. For that, they extract time series from segmented regions. Petitjean et al. [28] proposed a strategy to encode spatial data over time. Their strategy consists of segmenting each image of the series in order to characterize each pixel of the data with spatial properties. The time series are computed for each pixel based on the properties extracted from the segmented regions. Ardila et al. [8], in turn, used time series based on spatial properties, from pre-defined regions to monitor urban trees. Almeida et al. [6] exploited a multiscale segmentation structure to compute time series with spatial information, which were used to detect phenological patterns in a cerrado-savanna vegetation. Ma et al. [23] analyzed spatial and temporal patterns in savanna vegetation phenology in Australia by comparing image datasets from different spatial resolutions.

In spite of all the advances, existing strategies for processing spatio-temporal data usually require a considerable amount of storage space. A traditional phenology database storing information from just one event per individual per year, for several species and observation stations may encompass a enormous amount of data. For instance, the data set of phenological observations of plant species from Central Europe, largely Germany, from about 9000 stations, covering 130 years (1880–2009), includes more than 16 millions observations [12]. This paper aims to fill such a gap. Here, we introduce a compact representation for identifying and characterizing plant species in time series obtained from phenological observations.

## 3. Time series acquisition

The near-remote phenological system was set up in an 18 m tower in a Cerrado *sensu stricto*, a savanna-like vegetation located at Itirapina, São Paulo State, Brazil. We set up the camera to automatically take a daily sequence of five JPEG images (at  $1280 \times 960$  pixels of resolution) in the first 10 min of each hour, from 6:00 to 18:00 h (UTC3), totaling 65 images per day. The present study was based on the analysis of over 2,700 images (Fig. 1), recorded at the end of the dry season, between August 29th and October 3rd 2011, day of year (DOY) 241 to 278, during the main leaf flushing season [2].

The image analysis was conducted by defining different regions of interest (ROI), as described in [1,2,29,30]. For each ROI, a binary image with the same dimensions of the original image was created. These images are later used as masks. A mask of white pixels indicates the ROI, and the remaining area is filled by black pixels. As defined in [2], we selected six ROIs (Fig. 2) of six plant species described as follow: (1) *Aspidosperma tomentosum* (Fig. 2(a)), (2) *Caryocar brasiliensis* (Fig. 2(b)), (3) *Myrcia guianensis* (Fig. 2(c)), (4)



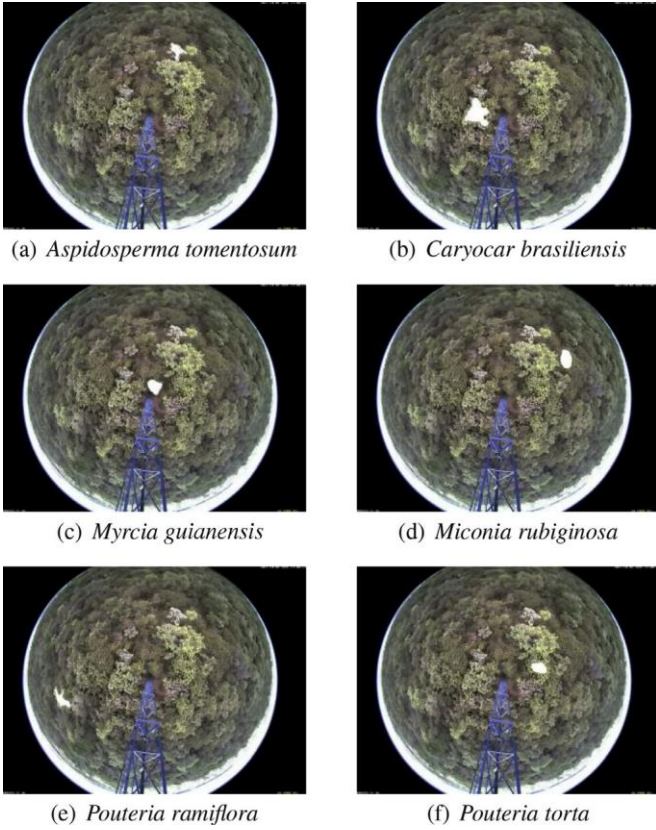


**Fig. 2.** Regions of interest (ROIs) defined for the analysis of cerrado-savanna digital images: (a) *Aspidosperma tomentosum*, (b) *Caryocar brasiliensis*, (c) *Myrcia guianensis*, (d) *Miconia rubiginosa*, (e) *Pouteria ramiflora*, and (f) *Pouteria torta*.

*Miconia rubiginosa* (Fig. 2(d)), (5) *Pouteria ramiflora* (Fig. 2(e)), and (6) *Pouteria torta* (Fig. 2(f)).

According to the leaf exchange data from the on-the-ground field observations on leaf fall and leaf flush at our study site, those species were classified into three functional groups [2]: (i) deciduous: *Aspidosperma tomentosum* and *Caryocar brasiliensis*; (ii) evergreen: *Myrcia guianensis* and *Miconia rubiginosa*; and (iii) semideciduous: *Pouteria ramiflora* and *Pouteria torta*.

#### 4. Visual rhythm-based description

Visual rhythms [25] are an effective way to analyze temporal properties from video data. It consists of an abstraction of a video that encodes the temporal change of pixel values along a specific sampling line [21], as illustrated in Fig. 3(a). In this example, the central column of a set of images are put together to create a single image, the visual rhythm. A clear advantage of this approach is the reduction of the storage space of the extracted features. Therefore, it also speeds up data processing.

Formally, a visual rhythm is a simplification of a video  $V = \{f_t\}$ ,  $t \in [1, T]$ , in domain  $2D + t$ , with  $T$  frames of dimensions  $W_V \times H_V$ , in which each frame  $f_t$  is transformed into a vertical line on an image  $R$ , in domain  $1D + t$ , such that,

$$R(t, z) = f_t(r_x \times z + a, r_y \times z + b), \quad t \in [1, W_R], \quad z \in [1, H_R],$$

where  $W_R$  ( $W_R = T$ ) and  $H_R$  are its width and height, respectively;  $r_x$  and  $r_y$  are the sampling rates along the horizontal and vertical directions;  $a$  and  $b$  are the horizontal and vertical offsets on each frame, respectively.

Without loss of generality, a time series comprised of images taken by digital cameras at fixed time intervals can be viewed as a

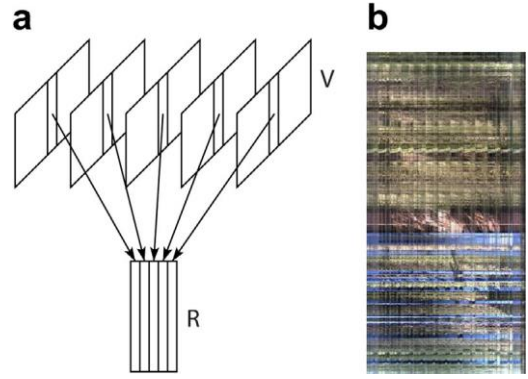


**Fig. 3.** Visual rhythm: (a) simplification of a video content by mapping each frame into one column of an image; (b) a real example produced by sampling the central vertical line of the digital images.

video of the vegetation. Therefore, a visual rhythm can be used to simplify a time series into a single image, as illustrated in Fig. 3(b). This example shows the visual rhythm produced by sampling the central vertical line of vegetation digital images such as the one showed in Fig. 1. The parameters  $r_x$ ,  $r_y$ ,  $a$ , and  $b$  used to generate the visual rhythm are 0, 1,  $W_V/2$ , and 0, respectively. In this paper, we propose to take advantage of existing image descriptors to identify and characterize phenological changes in visual rhythm images.

The major problem with the previous definition of visual rhythms is that it has been designed for the pixel sampling of specific lines (e.g., diagonal, horizontal, and vertical). Here, we are interested in analyzing unshapely regions related to plant species that are identified by phenology experts (see Fig. 2). However, it is impossible to adjust values for the parameters  $r_x$ ,  $r_y$ ,  $a$ , and  $b$  so that we can transform a ROI into a vertical line of a visual rhythm. The novelty of this paper is to generalize the notion of visual rhythms. From a generic point of view, this approach relies on taking samples of the information to be analyzed and then grouping them in an orderly manner. The key contribution of our idea is the mapping function we design to encode the temporal change of a ROI into a single image. In the following, we present different strategies of generating visual rhythms from time series obtained by digital images of vegetation data.

##### 4.1. Pixel-based visual rhythm

Let  $S = \{S_h\}$ ,  $h \in [1, H]$  be a set of  $H$  image sequences, in which each  $S_h = \{I_{dh}\}$ ,  $d \in [1, D]$  is composed of  $D$  images  $I_{dh}$ , with dimensions  $W_S \times H_S$ , taken by the digital camera at the day of year  $d$  and the hour  $h$ ; and  $M$  be a binary image, with the same dimensions of  $S$ , in which white pixels indicate an area of interest. Fig. 4 shows how pixel-based visual rhythm images are created.

Initially, we convert the binary image  $M$  into a list of Cartesian coordinates  $L_{xy} = \{(x, y) \mid M(x, y) = 1\}$ . Next, we use this list for computing the geometric center  $(x_c, y_c)$  of the area of interest. After that, we translate the Cartesian coordinate system of the elements in the list  $L_{xy}$  to have its origin at the point  $(x_c, y_c)$  and then we convert them to the polar coordinate system, creating a list of polar coordinates  $L_{r\theta}$ . Thereafter, we create an index  $K = \{k \mid \forall (r, \theta) \in L_{r\theta}, k = 2\pi r + \theta\}$  which assigns a unique value to each element in the list  $L_{r\theta}$ . Finally, we sort the keys in the index  $K$  in an increasing order and then we use them to arrange the elements in the list  $L_{xy}$ .

Thus, we can define a visual rhythm as a mapping of an image sequence  $S_h$  into a single image  $R_h$ , in which each image  $I_{dh}$  is a column (i.e., vertical line) at the row  $d$ , such that

$$R_h(d, z) = I_{dh}(L_{xy}(z)), \quad d \in [1, W_R], \quad z \in [1, H_R],$$

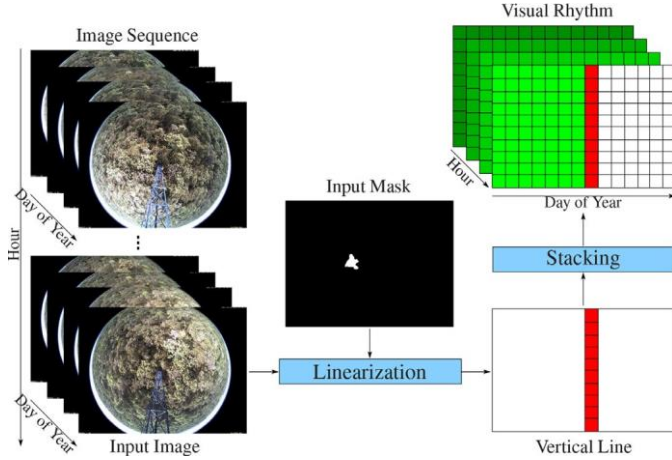


**Fig. 4.** Overview of the pixel-based strategy. For each hour, the pixel set of the segmented region is linearized. At the end of the process, the pixel values of the segmented region along the time is a column in a new image: the visual rhythm. One visual rhythm is computed for each hour of the day along the time.

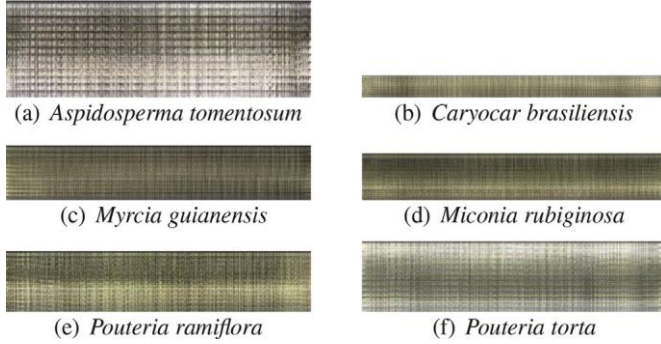


**Fig. 5.** Visual rhythms obtained for each ROI by using the pixel-based strategy.

where  $W_R = D$  and  $H_R = I_{xy}$  are its width and height, respectively. Fig. 5 presents the visual rhythms produced by the pixel sampling of the digital images using each ROI from Fig. 2.

#### 4.2. Area-based visual rhythm

Let  $S = \{I_{dh}\}$ ,  $d \in [1, D]$ ,  $h \in [1, H]$  be an image sequence composed of  $D \times H$  images  $I_{dh}$ , with dimensions  $W_S \times H_S$ , taken by the digital camera at the day of year  $d$  and the hour  $h$ ; and  $M$  be a binary image, with the same dimensions of  $S$ , in which white pixels indicate an area of interest. Fig. 6 shows how area-based visual rhythm images are created. The third-order moment is the initially, we convert the binary image  $M$  into a list of Cartesian coordinates  $L_{xy} = \{(x, y) \mid M(x, y) = 1\}$ . After that, we use this list to draw a sample of the pixels from an input image  $I_{dh}$ . Finally, we extract a feature  $F_{dh}$  that uniquely characterizes the natural distribution of all those pixels by calculating color moments of this segmented region.

Here, we use the three central moments of a color distribution [37]. The first-order moment can be interpreted as the average color intensity, and it can be calculated by using the formula:

$$\mathcal{F}_{dh} = E_{dh} = \frac{\sum_{(x,y) \in L_{xy}} I_{dh}(x, y)}{|L_{xy}|}.$$

The second-order moment is the standard deviation, which is obtained by taking the square root of the variance of the color dis-

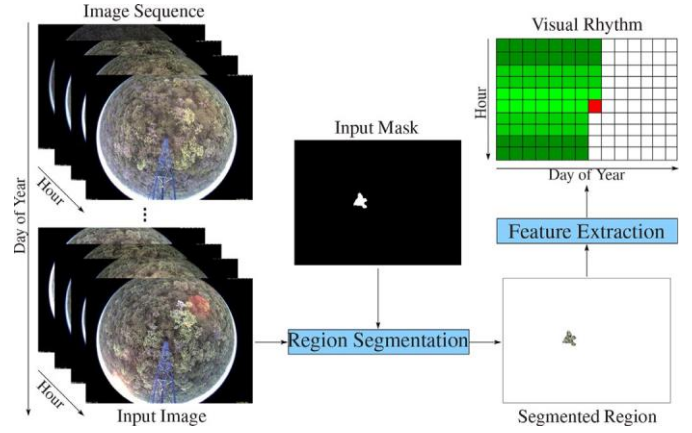


**Fig. 6.** Overview of the area-based strategy. This representation encodes the color intensity of each region in each hour (vertically) along the year (horizontally). The color intensity of a entire region is computed by using statistical moments.

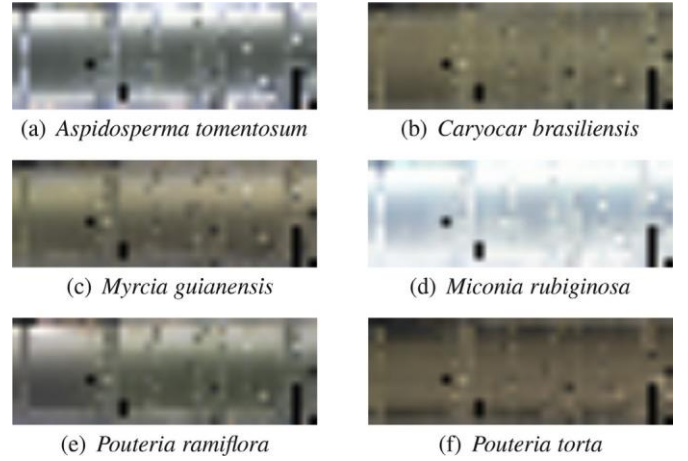


**Fig. 7.** Visual rhythms obtained for each ROI by using the area-based strategy. Each ROI was encoded by the first-order moment.

tribution, i.e.,

$$\mathcal{F}_{dh} = \sigma_{dh} = \sqrt{\frac{\sum_{(x,y) \in L_{xy}} [I_{dh}(x, y) - E_{dh}]^2}{|L_{xy}|}}.$$

skewness. It measures how asymmetric the color distribution is, and thus it gives information about the shape of the color distribution. It can be computed with the following formula:

$$\mathcal{F}_{dh} = S_{dh} = \sqrt[3]{\frac{\sum_{(x,y) \in L_{xy}} [I_{dh}(x, y) - E_{dh}]^3}{|L_{xy}|}}.$$

Thus, we can define a visual rhythm as a mapping of an image sequence  $S$  into a single image  $R$ , in which each feature  $F_{dh}$  is a pixel at the position  $(d, h)$ , i.e.,

$$R(d, h) = F_{dh}, d \in [1, W_R], h \in [1, H_R],$$

where  $W_R = D$  and  $H_R = H$  are its width and height, respectively. Figs. 7–9 present the visual rhythms produced by the pixel sampling of the digital images using each ROI from Fig. 2, where each ROI was encoded by the first-order, second-order, and third-order moments, respectively.



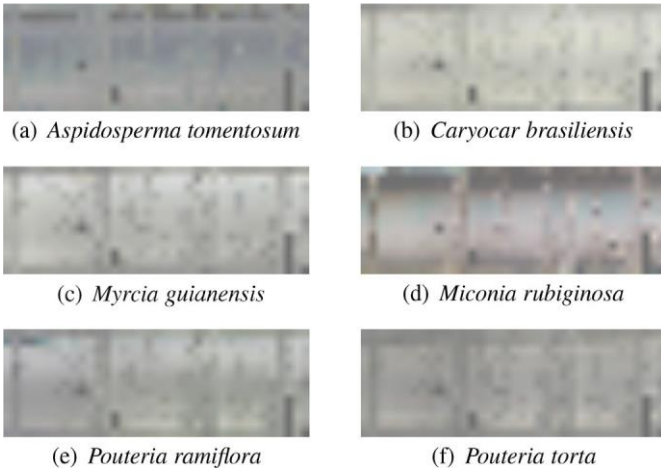


**Fig. 8.** Visual rhythms obtained for each ROI by using the area-based strategy. Each ROI was encoded by the second-order moment.

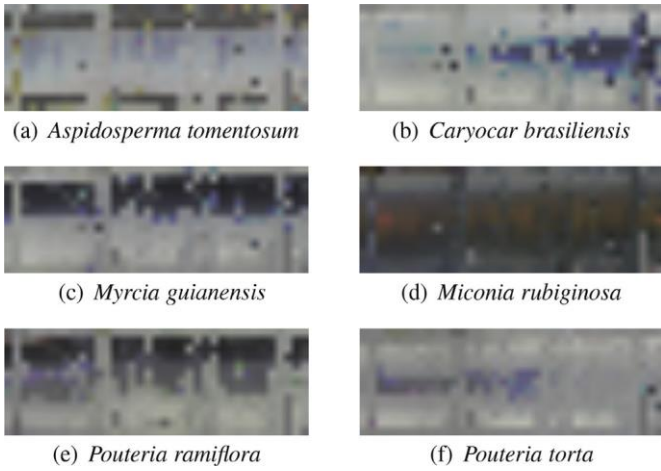


**Fig. 9.** Visual rhythms obtained for each ROI by using the area-based strategy. Each ROI was encoded by the third-order moment.

## 5. Experimental protocol

This section presents the adopted experimental protocol. First, we introduce the region-based image retrieval scenario used in our evaluation in Section 5.1. Next, we present the used evaluation metrics and the baseline considered in our study in Sections 5.2 and 5.3, respectively.

### 5.1. Image retrieval protocol

We carried out experiments to identify plant species in the image using the proposed visual rhythm representations. In this work, we approach the plant identification as an image retrieval problem, in contrast to some initiatives that have addressed this task in the context of image classification [5,6]. Our objective is to use the proposed representations in search services that could leverage the understanding of phenological changes over time by providing areas of plant individuals whose visual features are similar to those of a region of interest defined as input.

We adopted a content-based region retrieval approach in our evaluation protocol. This approach relies on the execution of *similarity searches* [41], according to which image regions are ranked in order of their distance from a given query region. From each image region, feature vectors are extracted by taking into account different representations (e.g., pixel-based or area-based visual rhythm)

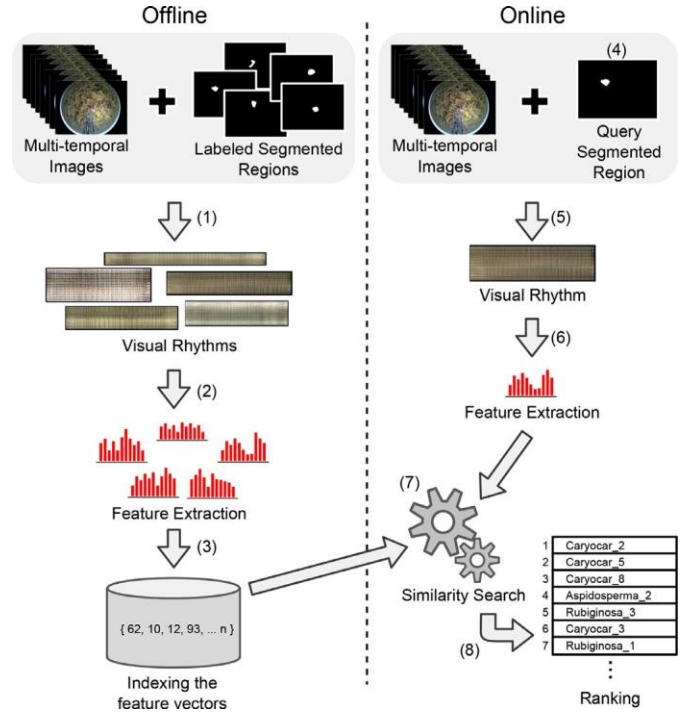


**Fig. 10.** Flowchart of a content-based region retrieval system used in the evaluation protocol.

and descriptors (e.g., Global Color Histogram). Two regions are considered similar to each other, if the distance of their feature vectors are small. The more effective a descriptor is, the more relevant image regions are ranked at top positions of the returned ranked list.

The flowchart of the content-based region retrieval system is illustrated in Fig. 10. The process is composed of offline and online steps. The offline steps comprise: (1) the representation of each labeled segmented regions in the multitemporal data by using visual rhythms; (2) the extraction of features from each visual rhythm through descriptors; and (3) the indexing of features in a data repository. The online steps consists of a query search composed of the following steps: (4) the selection of a query pattern, which is a segmented region along the multitemporal images; (5) the computation of the query's visual rhythm; (6) the extraction of features by using descriptors; (7) the search computation by similarity; and (8) the final similarity ranking, including all patterns learned at the offline stages.

In this system, we provide a time series extracted from an image area associated with a given species and we query for similar time series computed from other image areas that belong to the same species. For describing time series encoded into a visual rhythm, we used six traditional and recently proposed image descriptors: Auto Color Correlogram (ACC) [18], Color Coherent Vector (CCV) [26], Border/Interior pixel Classification (BIC) [36], and Global Color Histogram (GCH) [38], for encoding color information; Generic Fourier Descriptor (GFD) [42] and Haar-Wavelet Descriptor (HWD) [20], for analyzing spectral properties. The distance function used for feature comparison is the Manhattan ( $L_1$ ) distance. For more details regarding those image descriptors, refer to [27].

Our strategy to evaluate image descriptors in the context of time series description is based on assessing the similarity among regions associated with individuals of a same species. For that, we used the Guigues algorithm [15] to segment the hemispheric image into small polygons, obtaining 8, 849 segmented regions (SR). Then, we associated each SR with a single ROI aiming to label it. A

**Table 1**

MAP scores obtained by each of the image descriptors along all the available periods of the day.

Hour	Pixel-based visual rhythm						Baseline		
	<i>ACC</i>	<i>BIC</i>	<i>CCV</i>	<i>GCH</i>	<i>GFD</i>	<i>HWD</i>	<i>RGB</i>	<i>ExG</i>	<i>NDI</i>
6	0.587	0.601	<b>0.601</b>	0.608	0.338	0.374	0.739	<b>0.523</b>	0.490
7	0.561	0.555	0.549	0.545	0.353	0.377	0.720	0.515	0.569
8	0.571	0.555	0.554	0.546	0.355	0.385	0.716	0.480	0.532
9	0.572	0.574	0.548	0.569	0.353	0.380	0.733	0.422	0.619
10	<b>0.620</b>	<b>0.612</b>	0.588	<b>0.614</b>	0.354	0.382	0.741	0.407	0.644
11	0.607	0.586	0.562	0.585	0.345	0.372	<b>0.744</b>	0.398	0.640
12	0.535	0.528	0.519	0.534	0.342	0.356	0.731	0.381	0.632
13	0.542	0.526	0.506	0.513	0.334	0.364	0.718	0.407	0.628
14	0.577	0.577	0.553	0.554	0.341	0.387	0.723	0.419	0.625
15	0.567	0.562	0.542	0.542	0.346	<b>0.395</b>	0.718	0.427	0.633
16	0.558	0.548	0.530	0.524	0.347	0.386	0.700	0.434	0.615
17	0.554	0.555	0.531	0.548	<b>0.358</b>	0.388	0.686	0.464	0.610
18	0.576	0.590	0.596	0.595	0.338	0.376	0.688	0.498	<b>0.656</b>

**Table 2**

P@5 scores obtained by each of the image descriptors along all the available periods of the day.

Hour	Pixel-based visual rhythm						Baseline		
	<i>ACC</i>	<i>BIC</i>	<i>CCV</i>	<i>GCH</i>	<i>GFD</i>	<i>HWD</i>	<i>RGB</i>	<i>ExG</i>	<i>NDI</i>
06	0.761	0.795	0.769	0.767	0.451	0.502	0.878	<b>0.779</b>	0.728
07	0.779	0.778	0.729	0.782	0.495	0.523	<b>0.922</b>	0.764	0.848
08	0.805	0.742	0.713	0.749	<b>0.506</b>	0.513	0.878	0.724	0.777
09	0.778	0.757	0.706	0.735	0.500	0.521	0.856	0.661	0.800
10	0.807	<b>0.824</b>	<b>0.788</b>	<b>0.818</b>	0.494	0.532	0.834	0.642	0.816
11	<b>0.833</b>	0.817	0.765	0.770	0.466	0.503	0.852	0.639	0.806
12	0.785	0.743	0.728	0.749	0.471	0.449	0.860	0.620	0.809
13	0.810	0.788	0.743	0.775	0.463	0.466	0.835	0.675	0.792
14	0.780	0.768	0.763	0.794	0.475	0.517	0.872	0.702	0.814
15	0.714	0.711	0.751	0.736	0.466	0.523	0.862	0.700	0.798
16	0.697	0.729	0.732	0.725	0.480	0.518	0.866	0.676	0.800
17	0.738	0.740	0.724	0.762	0.505	<b>0.538</b>	0.866	0.676	0.817
18	0.798	0.787	0.788	0.777	0.432	0.520	0.906	0.720	<b>0.908</b>

labeled region is created if there is at least 80% of overlapped area between a SR and a ROI. In the remainder of this paper, when we refer to regions of interest related to tree crowns of plant species identified manually in the digital image, we use the acronym ROI; and when we refer to segmented regions obtained from the segmentation algorithm, we use the acronym SR. The similarity between two SRs is computed as a function of the distance between the feature vectors extracted from their visual rhythms. An image descriptor is better than another if it ranks more SRs belonging to the same ROI of a query SR at the first positions.

For each ROI, we randomly selected twenty percent of its total number of SRs to be used as queries. Five replications were performed in order to ensure statistically sound results. Presented results consider the average performance of the evaluated image descriptors, which were computed based on the mean and standard deviation of each replication.

## 5.2. Evaluation metrics

We assess the effectiveness of each approach using the metrics of Precision and Recall. Precision is the ratio of the number of relevant SRs retrieved to the total number of irrelevant and relevant SRs retrieved. Recall is the ratio of the number of relevant SRs retrieved to the total number of relevant SRs in the database. Here, a given SR is considered as relevant only if it belongs to the same ROI of a query SR. However, there is a trade-off between Precision and Recall. Greater Precision decreases Recall and greater Recall leads to decreased Precision. So, we choose to report the results using unique-value measurements: Mean Average Precision (MAP), which is the mean of the precision scores obtained at the ranks of each relevant SR; and Precision at 5, which is the average precision after 5 SRs are returned. These metrics combine Preci-

sion and Recall into a single measure, which makes the comparison easier.

## 5.3. Baseline

We compare the visual rhythm-based techniques against three approaches widely used by phenology experts for characterizing leaf-changing patterns of plant species from digital images. The first approach is a normalized index called RGB chromatic coordinates (RGBcc), which was developed by Gillespie et al. [14] and is considered the most efficient index to detect the color of plants in relation to their background [40]. The normalized RGBcc index undergoes a nonlinear transform, as follows:

$$r = R/(R + G + B), g = G/(R + G + B), b = B/(R + G + B);$$

where  $R$ ,  $G$ , and  $B$  are the average pixel intensity of the red, green, and blue bands, respectively.

The second approach is a contrast index named as Excess Green (ExG), which was introduced by Woebbecke et al. [40] and is commonly applied to separate green plants from soil and residue background. The ExG index is defined as:  $ExG = 2g - r - b$ . Similarly, the third approach, known as Normalized Difference Index (NDI), uses only green and red channels and is given by [39]:

$$NDI = (G - R)/(G + R).$$

## 6. Experimental results

The objective of our evaluation is to confirm that the use of the proposed visual rhythm representations yields comparable results, in terms of search result effectiveness, when compared with the traditional RGBcc index. The evaluation results are discussed in Sections 6.1 and 6.2, for the pixel-based and area-based visual rhythm representations, respectively. The correlation analysis and feature combination between different approaches is discussed in

**Table 3**

Differences between MAP of the different image descriptors by considering the best result of each approach.

Approach	Confidence interval (99%)	
	Min.	Max.
RGB@11h - ACC@10h	-0.236	0.401
RGB@11h - BIC@10h	-0.291	0.461
RGB@11h - CCV@06h	-0.290	0.475
RGB@11h - GCH@10h	-0.282	0.441
RGB@11h - GFD@17h	0.022	0.744
RGB@11h - HWD@15h	-0.045	0.757

**Table 4**

Differences between P@5 of the different image descriptors by considering the best result of each approach.

Approach	Confidence interval (99%)	
	Min.	Max.
RGB@07h - ACC@11h	0.012	0.378
RGB@07h - BIC@10h	0.085	0.298
RGB@07h - CCV@10h	-0.001	0.316
RGB@07h - GCH@10h	-0.006	0.207
RGB@07h - GFD@08h	0.201	0.750
RGB@07h - HWD@17h	0.109	0.730

**Section 6.3.** Finally, in **Section 6.4**, we discuss on efficiency aspects of the visual rhythm-based techniques, highlighting the main advantages of using the proposed approaches.

#### 6.1. Pixel-based visual rhythm

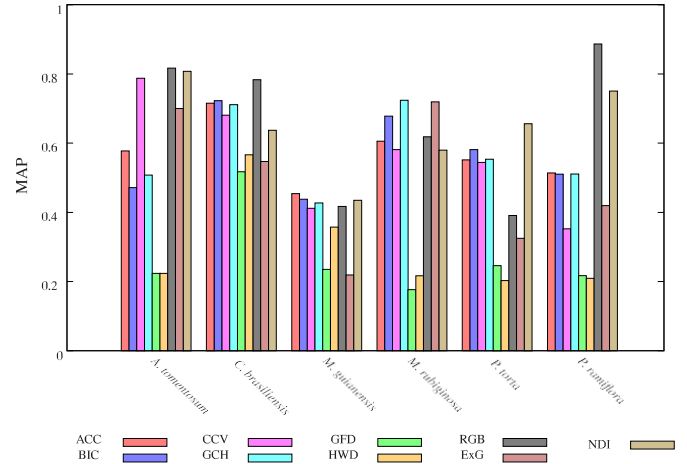
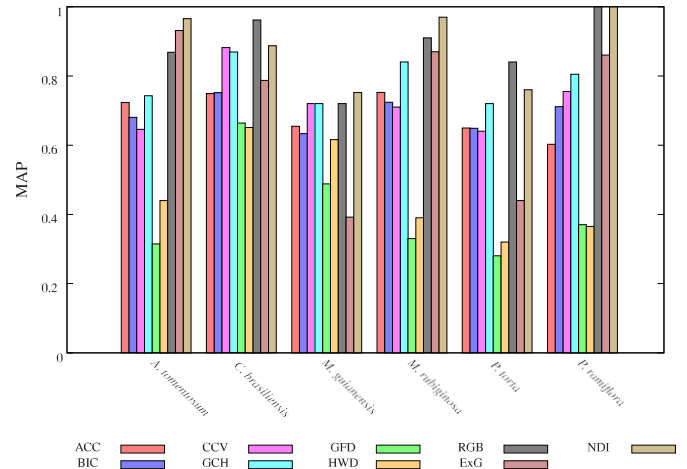
**Tables 1 and 2** compare the pixel-based visual rhythm techniques and the baseline methods with respect to the MAP and P@5 measures, respectively. MAP is a good indication of the effectiveness considering all positions of obtained ranked lists. P@5, in turn, focuses on the effectiveness of the methods considering only the first positions of the ranked lists. For each approach, we highlight the hour of day that provided the best result.

Those results indicate that the performance of the different evaluated approaches is similar, with a small advantage to the RGB-based baseline. Notice that early hours (from 8h to 11h) are better to characterize the phenological changes of plant species by using color descriptors. As we can observe, the best performances were achieved using the digital images taken at ten in the morning. This finding disagrees with the general suggestion of extracting color information from midday hours (from 11h to 14h) for ecological studies [1,19,29].

Paired *t*-tests were performed to verify the statistical significance of those results. For that, the confidence intervals for the differences between paired means of each ROI were computed to compare every pair of approaches. If the confidence interval includes zero, the difference is not significant at that confidence level. If the confidence interval does not include zero, then the sign of the difference indicates which alternative is better.

**Tables 3 and 4** present the 99% confidence intervals of the differences between the RGB-based baseline and the pixel-based visual rhythm techniques for the MAP and P@5 measures, respectively. For simplicity and readability purposes, we report only the results for the hour of day that provided the best result of each approach. Such analyses confirm that the pixel-based visual rhythm techniques and the RGB-based baseline exhibit similar performance. Notice that the confidence intervals include zero and, hence, the differences between those approaches are not significant at that confidence level.

**Figs. 11 and 12** compare the individual scores obtained for each ROI considering the best results of the evaluated methods in terms

**Fig. 11.** MAP scores obtained for each ROI.**Fig. 12.** P@5 scores obtained for each ROI.

of the MAP and P@5 measures, respectively. It is interesting to note the differences in responsiveness of the different approaches with respect to each of the species individually. The main reason for those results is the different patterns of the leaf color change of each species. In general, different image descriptors are designed to capture different visual features.

#### 6.2. Area-based visual rhythm

In **Fig. 13**, we compare the effectiveness of the baseline methods and the area-based visual rhythm techniques by considering different image descriptors. The graphs present the individual scores obtained for visual rhythms encoded by the first-order (first column), second-order (second column), and third-order (third column) moments. We show the results for the MAP (top row) and P@5 (bottom row) measures.

In general, those graphs demonstrate that visual rhythms encoded by lower order moments (left column) outperform the higher order ones (right column). On the other hand, for a same statistics, the performance of different image descriptors of a same type (color or texture) is similar. Unlike the results obtained for the pixel-based visual rhythm techniques, the texture descriptors (GFD and HWD) are more effective than the color ones (ACC, BIC, CCV, and GCH).

**Table 5** presents the 99% confidence intervals of the differences between the RGB-based baseline and the area-based visual rhythm

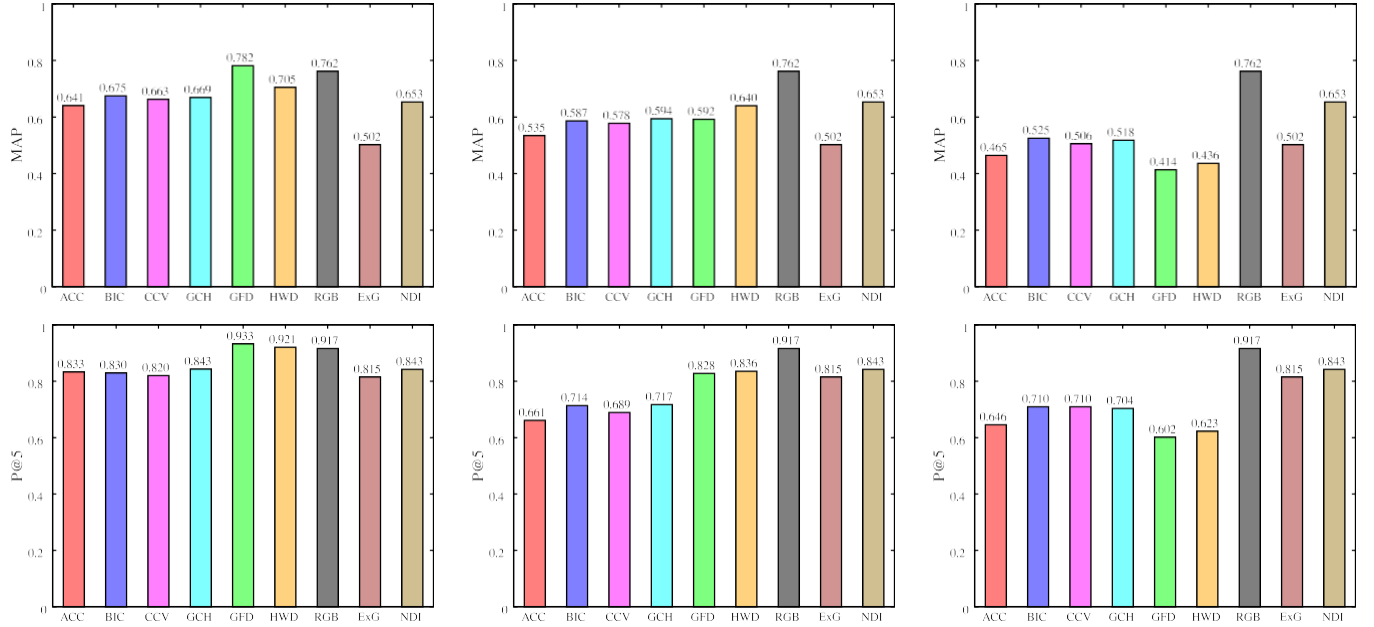


**Fig. 13.** Comparison between the effectiveness measures obtained by the evaluated approaches. These graphs present the results for visual rhythms encoded by the first-order (first column), second-order (second column), and third-order (third column) moments. They report the MAP (top row) and P@5 (bottom row) scores.

**Table 5**

Differences between MAP and P@5 scores of the different image descriptors by considering visual rhythms encoded by different color moments.

Method		MAP		P@5	
		Min.	Max.	Min.	Max.
First-Order	RGB - ACC	-0.062	0.311	-0.084	0.407
	RGB - BIC	-0.087	0.267	-0.047	0.314
	RGB - CCV	-0.048	0.276	-0.097	0.437
	RGB - GCH	-0.086	0.306	-0.093	0.360
	RGB - GFD	-0.181	0.145	-0.094	0.059
Second-Order	RGB - HWD	-0.134	0.198	-0.141	0.161
	RGB - ACC	0.010	0.475	-0.020	0.654
	RGB - BIC	-0.066	0.434	0.001	0.513
	RGB - CCV	-0.089	0.445	-0.031	0.529
	RGB - GCH	-0.105	0.457	-0.015	0.494
Third-Order	RGB - GFD	-0.134	0.444	-0.066	0.265
	RGB - HWD	-0.199	0.361	-0.125	0.239
	RGB - ACC	0.082	0.520	0.131	0.518
	RGB - BIC	0.087	0.384	0.035	0.496
	RGB - CCV	0.098	0.414	0.041	0.511
	RGB - GCH	0.083	0.386	0.071	0.471
	RGB - GFD	0.029	0.566	0.050	0.550
	RGB - HWD	-0.002	0.540	0.065	0.570

techniques for the MAP and P@5 measures, respectively. Such analyses confirm that the area-based visual rhythm techniques and the RGB-based baseline exhibit similar performance. Note that the confidence intervals include zero and, hence, the differences between those approaches are not significant at that confidence level.

In Fig. 14, we compare the individual scores obtained for each ROI in terms of the MAP (top row) and P@5 (bottom row) measures, respectively. We show the results for visual rhythms encoded by the first-order (first column), second-order (second column), and third-order (third column) moments by considering different image descriptors. Notice the differences in responsiveness of the evaluated methods with respect to each of the species individually. For instance, despite the overall performance of the first-order visual rhythms outperform the second-order ones, these latter have achieved the best results for the *Pouteria torta*. On the other hand, they have obtained the worst results for the *Myrcia guianensis*.

This behavior reflects their contrasting leaf phenology [2]: the *Myrcia guianensis* is an evergreen species and, therefore, the leaf senescence is a continuous process and color changes are more subtle over time; in contrast, the *Pouteria torta* is semideciduous, thus the color change reflects the rapid leaf senescence and the flush of new leaves.

### 6.3. Correlation analysis and descriptor combination

One important issue with regard the evaluation of multiple representations and descriptors concerns the investigation of their correlation. The objective is to somehow confirm if the different representations/descriptions provide complementary information regarding the image visual properties.

Figs. 15 (a) and 16(a) present the correlation among the ranked lists defined by the most effective descriptors associated with the pixel-based and area-based visual rhythm representations, respectively. The correlation score is computed using the Kendall rank correlation coefficient, defined as:

$$\tau(x, y) = \frac{(P - Q)}{(P + Q + T) \times (P + Q + U)}$$

where  $P$  is the number of concordant pairs,  $Q$  the number of discordant pairs,  $T$  the number of ties only in rank  $x$ , and  $U$  the number of ties only in rank  $y$ . If a tie occurs for the same pair in both  $x$  and  $y$ , it is not added to either  $T$  or  $U$ .

The RGB-based baseline is referred at the first line and column in both figures. Notice that the proposed descriptors are not correlated to each other. More importantly, they are not correlated to the RGB-based baseline. That opens a novel possibility of investigation concerning their combination.

In this sense, we have combined the ranked lists associated with the two best descriptors for the pixel-based and area-based visual rhythm representations with the RGB-based baseline using the traditional Borda Count rank aggregation approach [9]. The Borda Count algorithm is an order-based method, according to which a score is assigned to an element  $x$  in the ranked list  $r_i$ , equal to  $|r_i| - r_i(x)$ , where  $r_i(x)$  is the position of the element  $x$  in  $r_i$ . The final score of an element is the sum of the scores obtained in each ranked list.

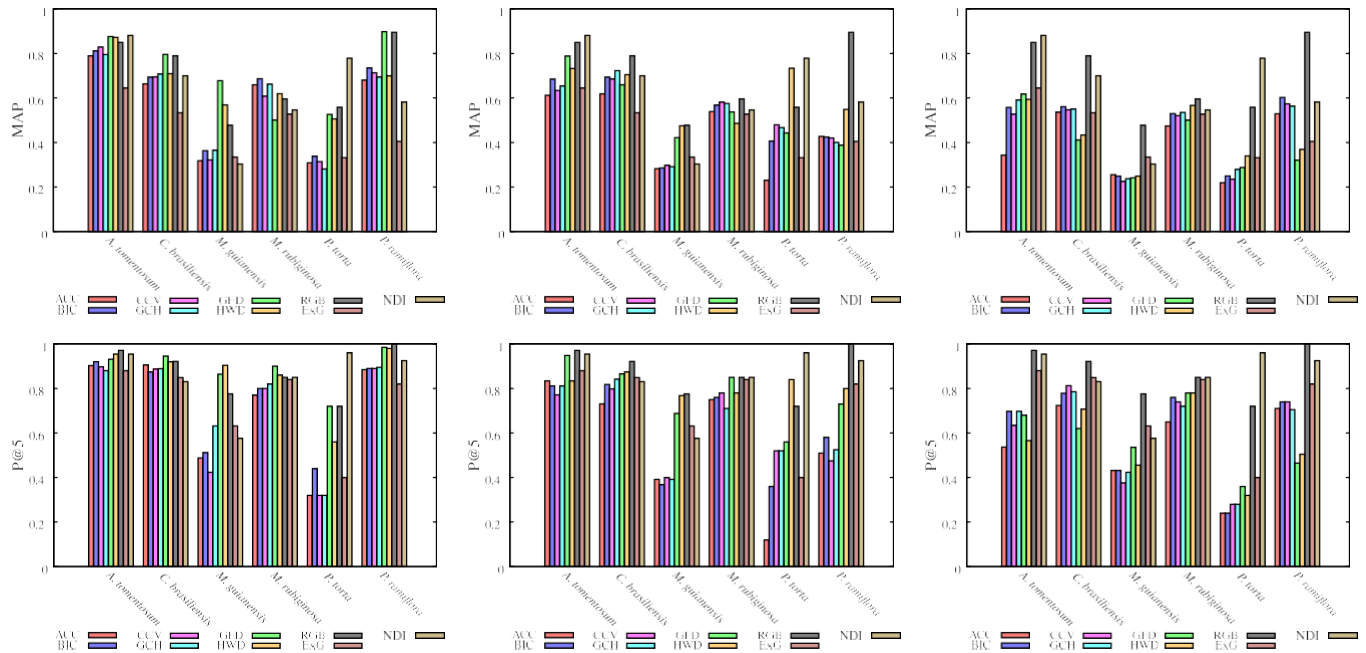


**Fig. 14.** Individual scores obtained for each ROI. These graphs present the results for visual rhythms encoded by the first-order (first column), second-order (second column), and third-order (third column) moments. They report the MAP (top row) and P@5 (bottom row) measures.

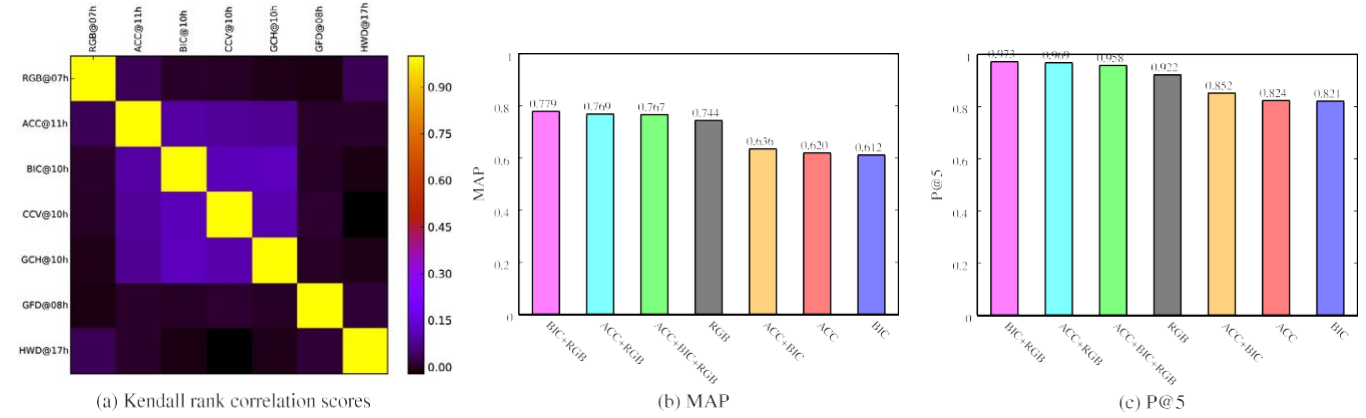


**Fig. 15.** (a) Correlation scores and (b and c) Combination results of the two best pixel-based descriptions with the RGB-based baseline.

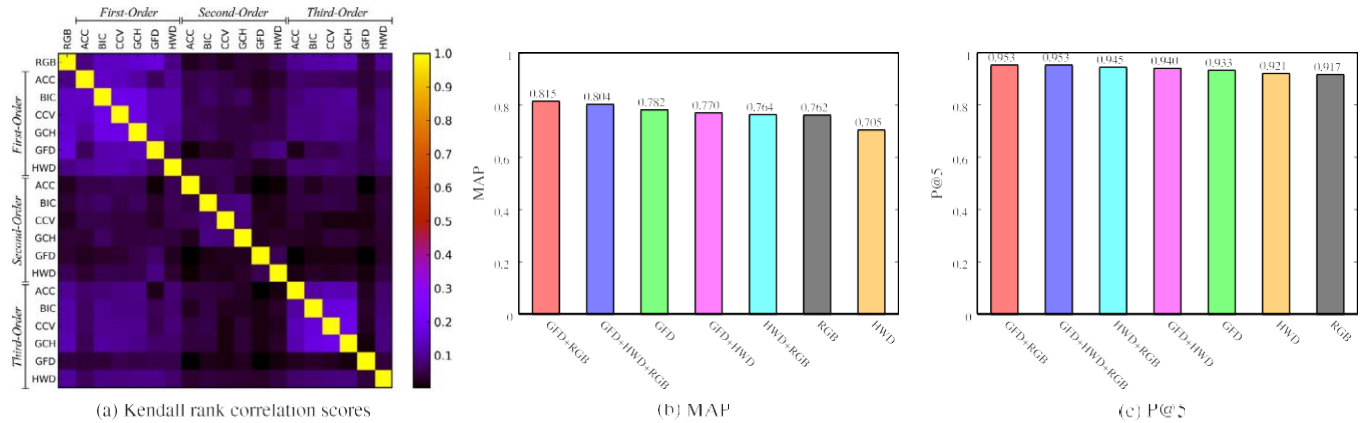


**Fig. 16.** (a) Correlation scores and (b and c) Combination results of the two best area-based descriptions with the RGB-based baseline.



**Table 6**  
Computational costs and space requirements of each of the evaluated approaches.

Method		Computational cost		Space requirements
		Extraction	Matching	
Visual rhythm	VR + ACC	$O(n)$	$O(1)$	$O(1)$
	VR + BIC	$O(n)$	$O(1)$	$O(1)$
	VR + CCV	$O(n)$	$O(1)$	$O(1)$
	VR + GCH	$O(n)$	$O(1)$	$O(1)$
	VR + GFD	$O(n \log n)$	$O(1)$	$O(1)$
	VR + HWD	$O(n \log n)$	$O(1)$	$O(1)$
Baseline	RGB	$O(n)$	$K(n)$	$K(n)$
	ExG	$O(n)$	$K(n)$	$K(n)$
	NDI	$O(n)$	$K(n)$	$K(n)$

Figs. 15 (b and c) and 16(b and c) present the MAP and P10 scores achieved by the most promising combinations for the pixel-based and area-based visual rhythm representations, respectively. As we can observe, even considering a fairly simple approach, the combination of the proposed methods with the RGB-based baseline improved the effectiveness results both in terms of MAP and P@5. These results show the potential of the idea, opening a new world of research possibilities.

#### 6.4. Computational efficiency

The key advantage of our technique is its computational efficiency. Table 6 presents the computational cost and the space requirements (in terms of the length  $n$  of the time series) of all the compared methods. In this way, we can investigate the relative difference of performance among different approaches.

Clearly, the visual rhythm-based techniques are much more efficient than the current solutions. This improvement makes our approach suitable for long-term collections of image data.

Note also that the larger the time series, the bigger would be the visual rhythm image generated, independently of the representation considered (either the pixel-based or area-based approach). For larger time series, the feature extraction process will probably take more time. Note, however, that the size of the final feature vector generated is not dependent on the size of the input image. It only depends on the descriptor used to characterize the visual properties of the visual rhythm images.

## 7. Conclusions

In this paper, we have presented a novel approach for capturing phenological patterns from time series and distinguishing the behavior of plant species. Our technique relies on encoding time series as a visual rhythm, which is characterized by image descriptors. The improvement of the computational efficiency makes our method suitable for long-term temporal data.

We have validated our technique using about 2700 images, taken from a tropical cerrado-savanna vegetation, including a high diversity of plant species. Experimental results obtained by the application of our method with several image descriptors show that it presents high accuracy and computational speed when identifying regions that belong to the same species.

Future work includes the evaluation of other visual features for image retrieval. In addition, the proposed method can be augmented to consider temporal segmentation and/or summarization methods. Finally, we also plan to consider learning-to-rank methods (e.g., genetic programming) for combining different descriptors.

## Acknowledgments

This research was supported by São Paulo Research Foundation FAPESP–Microsoft Research Virtual Institute (grants #2010/52113-

5, #2013/50169-1 and #2013/50155-0), CNPq (grant 449638/2014-6), FAPESP (grants #2007/52015-0, #2007/59779-6, #2009/18438-7, #2010/51307-0), and FAPEMIG (grant APQ-00768-14). BA received a doctoral fellowship from FAPESP (grant #2014/00215-0); LPCM and RST receive a Productivity Research Fellowship from CNPq (grants 310761/2014-0 and 306587/2009-2) and CNPq PVE (grant 400717/2013-1).

## References

- [1] H. Ahrends, S. Etzold, W. Kutsch, R. Stoeckli, R. Bruegger, F. Jeanneret, H. Wanner, N. Buchmann, W. Eugster, Tree phenology and carbon dioxide fluxes: Use of digital photography for process-based interpretation at the ecosystem scale, *Climate Res.* 39 (2009) 261–274.
- [2] B. Albetton, J. Almeida, R. Henneken, R. da S. Torres, A. Menzel, L.P.C. Morellato, Using phenological cameras to track the green up in a cerrado savanna and its on-the-ground validation, *Ecol. Inform.* 19 (2014) 62–70.
- [3] J. Almeida, J.A. dos Santos, B. Albetton, L.P.C. Morellato, R. da S. Torres, Plant species identification with phenological visual rhythms, in: *Proceedings of the IEEE International Conference on eScience (eScience'13)*, 2013a, pp. 148–154.
- [4] J. Almeida, J.A. dos Santos, B. Albetton, L.P.C. Morellato, R. da S. Torres, Visual rhythm-based time series analysis for phenology studies, in: *Proceedings of the IEEE International Conference Image Process. (ICIP'13)*, 2013b, pp. 4412–4416.
- [5] J. Almeida, J.A. dos Santos, B. Albetton, R. da S. Torres, L.P.C. Morellato, Remote phenology: Applying machine learning to detect phenological patterns in a cerrado savanna, in: *Proceedings of the IEEE International Conference on eScience'12*, 2012, pp. 1–8.
- [6] J. Almeida, J.A. dos Santos, B. Albetton, R. da S. Torres, L.P.C. Morellato, Applying machine learning based on multiscale classifiers to detect remote phenology patterns in cerrado savanna trees, *Ecol. Inform.* 23 (2014) 49–61.
- [7] J. Almeida, J.A. Santos, W.O. Miranda, B. Albetton, L.P.C. Morellato, R.S. Torres, Deriving vegetation indices for phenology analysis using genetic programming, *Ecol. Inform.* 26 (2015) 61–69.
- [8] J.P. Ardila, W. Bijker, V.A. Tolpekin, A. Stein, Multitemporal change detection of urban trees using localized region-based active contours in vhr images, *Remote Sens. Environ.* 124 (2012) 413–426.
- [9] J.C. Borda, Mémoire sur les élections au scrutin, *Histoire de l'Académie Royale des Sciences*, 1781.
- [10] E.B. Brooks, V.A. Thomas, R.H. Wynne, J.W. Coulston, Fitting the multitemporal curve: A fourier series approach to the missing data problem in remote sensing analysis, *IEEE Trans. Geosci. Remote Sens.* 50 (2012) 3340–3353.
- [11] J.C. Cont, F.A. Faria, J. Almeida, B. Albetton, L.P.C. Morellato, L. Camolesi Jr., R. da S. Torres, Evaluation of time series distance functions in the task of detecting remote phenology patterns, in: *Proceedings of the IEEE International Conference on Pattern Recognition (ICPR'14)*, 2014, pp. 3126–3131.
- [12] J. Dierenbach, F.W. Badeck, J. Schaber, The plant phenological online database (ppodb): An online database for long-term phenological data, *Int. J. Biometeorol.* 57 (2013) 805–812.
- [13] M. Forster, T. Schmidt, C. Schuster, B. Kleinschmit, Multi-temporal detection of grassland vegetation with rapideye imagery and a spectral-temporal library, in: *Proceedings of the IEEE International Geoscience and Remote Sensing Symposium (IGARSS'12)*, 2012, pp. 4930–4933.
- [14] A.R. Gillespie, A.B. Kahle, R.E. Walker, Color enhancement of highly correlated images. ii. channel ratio and “chromaticity” transformation techniques, *Remote Sens. Environ.* 22 (1987) 343–365.
- [15] L. Guigues, J. Cocquerez, H. Le Men, Scale-sets image analysis, *Intl. J. Comput. Vis.* 68 (2006) 289–317.
- [16] R. Henneken, V. Dose, C. Schlep, A. Menzel, Detecting plant seasonality from webcams using bayesian multiple change point analysis, *Agr. Forest Meteorol.* 168 (2013) 177–185.
- [17] G. Hmimina, E. Dufrêne, J.Y. Pontailier, N. Delpierre, M. Aubinet, B. Caquet, A. de Grandcourt, B. Burban, C. Flechard, A. Granier, P. Gross, B. Heinesch, B. Longdoz, C. Moureaux, J.M. Ourcival, S. Rambal, L.S. Andr, K. Soudani, Evaluation of the potential of MODIS satellite data to predict vegetation phenology in different biomes: An investigation using ground-based NDVI measurements, *Remote Sens. Environ.* 132 (2013) 145–158.
- [18] J. Huang, R. Kumar, M. Mitra, W.J. Zhu, R. Zabih, Image indexing using color correlograms, in: *Proceedings of the IEEE International Conference on Computer Vision and Pattern Recognition (CVPR'97)*, 1997, pp. 762–768.
- [19] R. Ide, H. Oguma, A cost-effective monitoring method using digital time-lapse cameras for detecting temporal and spatial variations of snowmelt and vegetation phenology in alpine ecosystems, *Ecol. Inform.* 16 (2013) 25–34.
- [20] C.E. Jacobs, A. Finkelstein, D. Salesin, Fast multiresolution image querying, in: *Proceedings of the International Conference on Computer Graphics and Interactive Techniques (SIGGRAPH'95)*, 1995, pp. 277–286.
- [21] J.S. Lee, T. Ebrahimi, Perceptual video compression: A survey, *IEEE J. Sel. Topics Signal Process.* 6 (2012) 684–697.
- [22] D. Loustau, A. Bosc, A. Colin, H. Davi, C. François, E. Dufrêne, M. Équé, E. Cloppet, D. Arrouays, C. Le Bas, N. Saby, G. Pignard, N. Hamza, A. Granier, N. Breda, P. Ciais, N. Viovy, J. Ogée, J. Delage, Modeling the climate change effects on the potential reduction of french plains forests at the sub regional level, *Tree Physiol* 25 (2005) 813–823.



- [23] X. Ma, A. Huete, Q. Yu, N.R. Coupe, K. Davies, M. Broich, P. Ratana, J. Beringer, L.B. Hutley, J. Cleverly, N. Boulain, D. Eamus, Spatial patterns and temporal dynamics in savanna vegetation phenology across the north australian tropical transect, *Remote Sens. Environ.* 139 (2013) 97–115.
- [24] G.C.S. Negi, Leaf and bud demography and shoot growth in evergreen and deciduous trees of central himalaya, india, *Trees* 20 (2006) 416–429.
- [25] C.W. Ngo, T.C. Pong, R.T. Chin, Detection of gradual transitions through temporal slice analysis, in: *IEEE International Conference on Computer Vision and Pattern Recognition (CVPR'99)*, 1999, pp. 1036–1041.
- [26] G. Pass, R. Zabih, J. Miller, Comparing images using color coherence vectors, in: *Proceedings of the ACM International Conference on Multimedia (ACM-MM'96)*, 1996, pp. 65–73.
- [27] O.A.B. Penatti, E. Valle, R. da S. Torres, Comparative study of global color and texture descriptors for web image retrieval, *J. Vis. Commun. Image Represent.* 23 (2012) 359–380.
- [28] F. Petitjean, C. Kurtz, N. Passat, P. GanÅšarski, Spatio-temporal reasoning for the classification of satellite image time series, *Pattern Recognit. Lett.* 33 (2012) 1805–1815.
- [29] A.D. Richardson, B.H. Braswell, D.Y. Hollinger, J.P. Jenkins, S.V. Ollinger, Near-surface remote sensing of spatial and temporal variation in canopy phenology, *Ecol. Appl.* 19 (2009) 1417–1428.
- [30] A.D. Richardson, J.P. Jenkins, B.H. Braswell, D.Y. Hollinger, S.V. Ollinger, M.L. Smith, Use of digital webcam images to track spring greening in a deciduous broadleaf forest, *Oecologia* 152 (2007) 323–334.
- [31] A. Rodrigues, A.R.S. Marcal, M. Cunha, Phenology parameter extraction from time-series of satellite vegetation index data using phenosat, in: *Proceedings of the IEEE International Symposium on Geoscience and Remote Sensing Society (IGARSS'12)*, 2012, pp. 4926–4929.
- [32] R. da S. Torres, M. Hasegawa, S. Tabbone, J. Almeida, J.A. dos Santos, B. Alberman, L.P.C. Morellato, Shape-based time series analysis for remote phenology studies, in: *Proceedings of the IEEE International Symposium on Geoscience and Remote Sensing Society (IGARSS'13)*, 2013, pp. 3598–3601.
- [33] L.C.B. Santos, J. Almeida, J.A. dos Santos, S.J.F. Guimarães, A.A. Araújo, B. Alberman, L.P.C. Morellato, R. da S. Torres, Phenological event detection by visual rhythm dissimilarity analysis, in: *Proceedings of the IEEE International Conference on eScience (eScience'14)*, 2014, pp. 263–270.
- [34] M.D. Schwartz, *Phenology: An Integrative Environmental Science*, second, Springer, 2013.
- [35] M.D. Schwartz, B.C. Reed, M.A. White, Assessing satellite derived start-of-season measures in the coterminous, *Int. J. Climatol.* 22 (2002) 1793–1805.
- [36] R.O. Stehling, M.A. Nascimento, A.X. Falcão, A compact and efficient image retrieval approach based on border/interior pixel classification, in: *Proceedings of the ACM International Conference on Information and Knowledge Management (CIKM'02)*, 2002, pp. 102–109.
- [37] M.A. Stricker, M. Orengo, Similarity of color images, in: *Proceedings of the SPIE International Conference on Storage and Retrieval for Image and Video Databases*, 1995, pp. 381–392.
- [38] M.J. Swain, B.H. Ballard, Color indexing, *Intl J. Comput Vis* 7 (1991) 11–32.
- [39] D.M. Woebbecke, G.E. Meyer, K. Von-Bargen, A.D. Mortensen, Plant species identification, size, and enumeration using machine vision techniques on near-binary images, *SPIE Opt. Agr. For.* 1836 (1992) 208–219.
- [40] D.M. Woebbecke, G.E. Meyer, K. Von-Bargen, A.D. Mortensen, Color indices for weed identification under various soil, residue, and lighting conditions, *Trans. ASAE* 38 (1995) 259–269.
- [41] P. Zezula, G. Amato, V. Dohnal, M. Batko, *Similarity Search: The Metric Space Approach*, first, Springer Publishing Company, Incorporated, 2010.
- [42] D. Zhang, G. Lu, Shape-based image retrieval using generic fourier descriptor, *Signal Process. Image Commun.* 17 (2002) 825–848.

### Appendix C

Article published in the Journal Pattern Recognition Letters:

FARIA F. A., ALMEIDA, J., ALBERTON, B., MORELLATO, L.P.C., ROCHA, A., TORRES, R.S. Time series-based classifier fusion for fine-grained plant species recognition. **Pattern Recognition Letters**, v. 81, p. 101-109, 2016.

## Time series-based classifier fusion for fine-grained plant species recognition

Fabio A. Faria <sup>a,c,\*</sup>, Jurandy Almeida <sup>a,c</sup>, Bruna Alberton <sup>b</sup>, Leonor Patricia C. Morellato <sup>b</sup>,  
Anderson Rocha <sup>c</sup>, Ricardo da S. Torres <sup>c</sup>

<sup>a</sup> Institute of Science and Technology, Federal University of São Paulo – UNIFESP, 12247-014 São José dos Campos, SP, Brazil

<sup>b</sup> Department of Botany, São Paulo State University – UNESP, 13506-900 Rio Claro, SP, Brazil

<sup>c</sup> Institute of Computing, University of Campinas – UNICAMP, 13083-852 Campinas, SP, Brazil

**Abstract:**

Global warming and its resulting environmental changes surely are ubiquitous subjects nowadays and undisputedly important research topics. One way of tracking such environmental changes is by means of phenology, which studies natural periodic events and their relationship to climate. Phenology is seen as the simplest and most reliable indicator of the effects of climate change on plants and animals. The search for phenological information and monitoring systems has stimulated many research centers worldwide to pursue the development of effective and innovative solutions in this direction. One fundamental requirement for phenological systems is concerned with achieving fine-grained recognition of plants. In this sense, the present work seeks to understand specific properties of each target plant species and to provide the solutions for gathering specific knowledge of such plants for further levels of recognition and exploration in related tasks. In this work, we address some important questions such as: (i) how species from the same leaf functional group differ from each other; (ii) how different pattern classifiers might be combined to improve the effectiveness results in target species identification; and (iii) whether it is possible to achieve good classification results with fewer classifiers for fine-grained plant species identification. In this sense, we perform different analysis considering RGB color information channels from a digital hemispherical lens camera in different hours of day and plant species. A study about the correlation of classifiers associated with time series extracted from digital images is also performed. We adopt a successful selection and fusion framework to combine the most suitable classifiers and features improving the plant identification decision-making task as it is nearly impossible to develop just a single “silver bullet” image descriptor that would capture all subtle discriminatory features of plants within the same functional group. This adopted framework turns out to be an effective solution in the target task, achieving better results than well-known approaches in the literature.

**Keywords:**

Plant species identification, Classifier fusion, Diversity measures

**1. Introduction**

Environmental changes have emerged as an important question in the global agenda [24,29]. This has spurred important research interest in phenology, the science of studying recurrent life cycles events and its relationship to climate [8,10,31]. To increase the range of study sites and species and the accuracy of phenological observations, dig-

ital cameras have been successfully applied as multi-channel imaging sensors, providing measures to estimate changes on phenological events, such as leaf flushing and senescence [1,26,27].

Previous work of our research group has monitored leaf changing patterns of a neotropical savanna (cerrado sensu stricto vegetation) based on daily acquired digital images [2]. We extracted image color information from the RGB (red, green, and blue) channels and correlated the changes in pixel levels over time with leaf phenology patterns [2]. The analysis was conducted after we defined regions of interest (ROI) based on the random selection of plant species crowns identified in the digital image [26]. Time series associated with each ROI have been obtained, raising the need of using appropriate tools for mining patterns of interest [3,4,6,28,30].

Fine-grained species identification in digital images is a key issue for the phenological observation of tree crowns, especially in

\* Corresponding author at: Institute of Computing, University of Campinas – UNI- CAMP, 13083-852 Campinas, SP, Brazil. Tel.: +55 12 3309 9500; fax: +55 12 3921 8857.

E-mail addresses: [ffaria@ic.unicamp.br](mailto:ffaria@ic.unicamp.br), [juruna18@gmail.com](mailto:juruna18@gmail.com) (F.A. Faria), [jurandy.almeida@unifesp.br](mailto:jurandy.almeida@unifesp.br) (J. Almeida), [bru.alberton@gmail.com](mailto:bru.alberton@gmail.com) (B. Alberton), [pmorella@rc.unesp.br](mailto:pmorella@rc.unesp.br) (L.P.C. Morellato), [anderson.rocha@ic.unicamp.br](mailto:anderson.rocha@ic.unicamp.br) (A. Rocha), [rtorres@ic.unicamp.br](mailto:rtorres@ic.unicamp.br) (R. da S. Torres).

tropical vegetations where one single image may include a high number of species [2]. Usually, this task is very time consuming since it has to be done in the field, first by matching each crown in the image to the tree in the soil and then by identifying the tree at species level [5]. In this sense, we have designed and deployed machine learning methods to find similar patterns in the digital images and then we checked if they correspond to similar species or leaf functional groups [5].

Our first studies have focused on the intraspecies analysis, i.e., on detecting different individuals of the same species [5]. However, different species from the same leaf functional group may exhibit similar phenological traits, confusing the classifiers as discriminative features among the classes are more subtle, hardening the identification process. Hence many questions arise when considering interspecies interactions, i.e., the recognition of individuals from different species belonging to the same leaf functional group [2] spurring the need for the proper design and development of fine-grained recognition algorithms to tackle the problem. Therefore, in this paper, we aim at addressing the following questions: (i) how to distinguish different species from the same leaf functional group using a pattern classification scheme for proper fine-grained decision-making; (ii) how the individual responses of classifiers built upon different phenological features are correlated to each other; and (iii) how to combine such phenological features so as to improve the responsiveness of all plant species as it is unlikely that just one phenological trait would be enough for complete and proper identification.

We start by evaluating the performance of classification models built upon a single phenological feature. Thereafter we perform a correlation analysis in order to understand the responsiveness of each plant species regarding multiple phenological features. Based on the observations made, we adopted a successful fusion framework [12] to collect complementary features and better solve the multiclass classification problem. This kind of problem has never been addressed in our studies before. Finally, we analyze the impact of increasing the number of classifiers in the individual responses of each plant species.

The most important contributions of our work are: (1) A correlation analysis between different time series-based classifiers for each species. In this vein, we can identify correlations between classifiers and relationship intra/inter species, which show to be very important for the problem we are tackling in this paper; (2) The exploration and proper custom-tailoring of a classifier fusion framework [12] to im-

prove the effectiveness results in a new application (species recognition); (3) The exploration of this classifier fusion framework for combining time series-based classifiers. Unlike the previous work of ours [12], which has used visual properties (e.g., color, texture, and shape) as input data to training base classifiers, our new proposal uses time series, a much different problem with its own intrinsic particularities and reduced information when compared to images; (4) Finally, in this work, we have considered a multi-class classification problem differently from the previous work.

## 2. Time series acquisition

A digital hemispherical lens camera (Mobotix Q24) was set up in an 18 m-high tower in a Cerrado *sensu stricto*, a neotropical savanna vegetation located at Itirapina, São Paulo State, Brazil [2,25]. Fig. 1 shows all steps of the time series acquisition process used in our work.

First, we set up the RGB digital camera to take a daily sequence of five JPEG images (at  $1280 \times 960$  pixels of resolution) per hour, from 6:00 to 18:00 h (UTC-3). The present study was based on the analysis of over 2700 images (Fig. 1(a)), recorded at the end of the dry season, between August 29 and October 3, 2011, day of year 241 to 278, during the main leaf flushing season [2].

Next, the image analysis has been conducted by defining different regions of interest (ROI), as described in [26] and defined by [2] for our target species. Then, we analyzed 22 ROIs (Fig. 1(b)) obtained from a random selection of six plant species identified manually by phenology experts in the hemispheric image [2]: (i) three regions associated with *Aspidosperma tomentosum* (green areas), (ii) four regions for *Caryocar brasiliensis* (blue areas), (iii) two regions for *Myrcia guianensis* (orange areas), (iv) six regions for *Miconia rubiginosa* (magenta areas), (v) two regions for *Pouteria ramiflora* (cyan areas), and (vi) four regions for *Pouteria torta* (red areas).

We analyzed each ROI in terms of the contribution of the primary colors (R, G, and B), as proposed by [27] and described in [2]. Initially, we analyze each color channel and compute the average value of the pixel intensity (Fig. 1(c)). After that, we compute the normalized brightness of each color channel (RGB Chromatic coordinates) (Fig. 1(d)). The normalization of those values reduces the influence of the incident light, decreasing the color variability due to changes on illumination conditions [9,34]. Finally, by computing those values along the whole period (August 28 to October 3, 2011), we obtained time series to use as input data for a learning method (Fig. 1(e)).

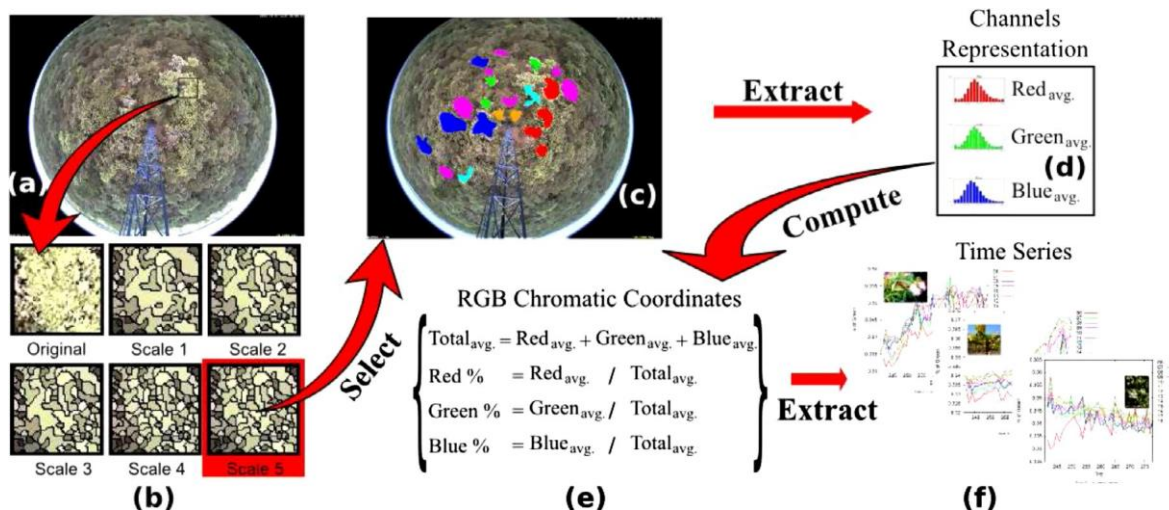


**Fig. 1.** The time series acquisition process pipeline. (a) Sample image of the Cerrado savanna; (b) Different segmentation scales are computed and the coarse scale is selected; (c) Hemispherical image with the selected ROI's species; (d) Channel representation are extracted from ROI's; (e) RGB chromatic coordinates are computed; (f) Phenological time series extracted from digital images. (For interpretation of the references to color in this figure text, the reader is referred to the web version of this article.)

According to the leaf exchange data from the on-the-ground field observations on leaf fall and leaf flush at our study site, those species were classified on three functional groups [2,23]: (i) deciduous, *A. tomentosum* and *C. brasiliensis*; (ii) evergreen, *M. guianensis* and *M. rubiginosa*; and (iii) semideciduous, *P. ramiflora* and *P. torta*.

### 3. Framework for time series-based classifier fusion

The objective of adopting a classifier fusion approach is to exploit the degree of agreement/disagreement among different classifiers, concept known as *diversity* and to improve the effectiveness results in the target task. In this sense, we adapt a successful selection and fusion framework, originally proposed for multimedia recognition, to be used as a combiner of times series-based classifier [12]. This framework selects the most suitable classifiers to be used in a meta-learning approach. In this work, we define a classifier as a tuple containing a simple learning method (e.g., *k*-Nearest Neighbors – *k*NN) and a description technique (e.g., a color channel from the RGB color channels).

#### 3.1. Classifier fusion approach

Fig. 2 illustrates the used framework [12] for plant identification. First, classifiers learn patterns from a training set (*T*) that contains samples of time series. Next,  $|C|$  classification models are created. They are applied on a validation set *V*, resulting in a matrix of classifier outcomes  $M_V$ , where  $|M_V| = |V| \times |C|$  and  $|V|$  is the number of time series extracted from a validation set *V* (Fig. 2(a)).

Thereafter, in the selection of the most appropriate time series-based classifiers to be combined,  $M_V$  is used to calculate different diversity measures (*D*). These measures compute the degree of agreement and disagreement all of  $|C|$  available classifiers [20].

The main objective of this selection process is to select a set  $C^* \subset C$  of classifiers that are more suitable to be fused/combined (Fig. 2(b)). Note that a new matrix  $M_V^* \subset M_V$  is computed. Finally, given a new time series extracted from *I*, a fusion technique (e.g., Support Vector Machines) uses the newly created matrix  $M_V^*$  to learn patterns and thus define the final class of *I* through a meta-learning approach (Fig. 2(c)).

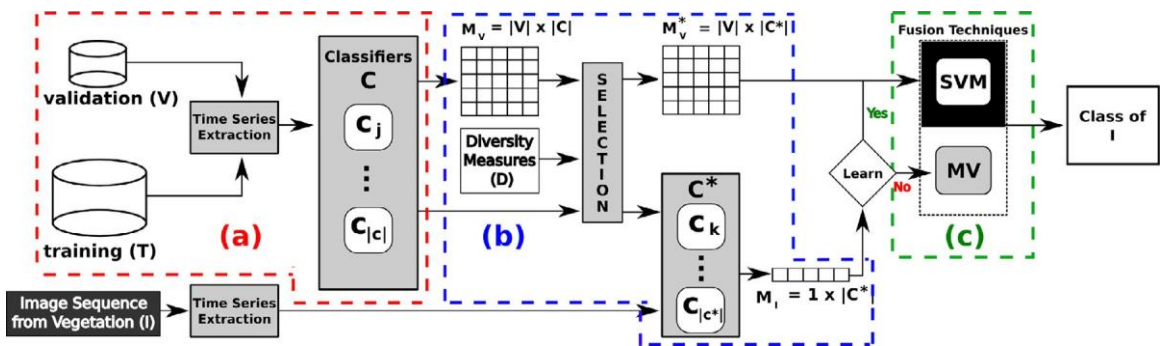


Fig. 2. Time series-based classifier selection and fusion framework adapted from [12]. In (a), given a classification problem with training examples, different classifiers are trained using data from training set *T*. In (b), the most discriminating classifiers are selected ( $C^*$ ) by taking into account diversity measures (*D*). Finally, in (c), classifiers are combined in a meta-level approach using any other classifier. In this particular example, both the SVM and Majority Voting (MV) techniques can be used as the classifier fusion technique.

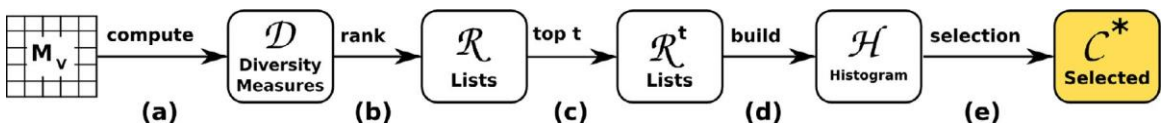


Fig. 3. The five steps for classifier selection are: (a) Computation of diversity measures from the validation matrix  $M_V$ ; (b) Ranking of pairs of classifiers by their diversity measures scores; (c) Selection of the top  $t$  ranked pairs of classifiers; (d) Computation of a histogram  $H$  that counts the number of occurrences of each classifier; (e) Select the most appropriate classifiers  $|C^*|$  based on their occurrence in  $H$  and satisfy a defined threshold  $T$ .

#### 3.2. Classifier selection approach

Fig. 3 illustrates the adopted five-step approach for selecting classifiers based on diversity measures, previously introduced in [12].

First, set *D* of diversity measures are used to assess the degree of agreement among available classifiers in *C* by taking into account the  $M_V$  matrix previously computed. In this approach, five different measures have been used (*Correlation Coefficient p*, *Double-Fault Measure*, *Disagreement Measure*, *Interrater Agreement k*, and *Q-Statistic* [20,21]). That step is represented by arrow (a) in Fig. 3. Pairs of classifiers are then ranked according to their diversity score. Each diversity measure defines a different ranked list and, at the end of this step, a set *R* of ranked lists is produced (arrow (b)). In the following, a novel set of ranked lists  $R^t$  is computed by selecting the top  $t$  pairs of classifiers from each ranked list in *R* (arrow (c)), and a histogram *H* that counts the number of occurrences of a classifier in all ranked lists of  $R^t$  is computed (arrow (d)). Finally, the most frequent classifiers in *H*, whose accuracy is greater than a given threshold *T*, are combined by a fusion approach (arrow (e)). *T* is a threshold defined in terms of the average accuracy among all classifiers using the validation set *V*.

### 4. Experimental protocol

This section presents the experimental protocol used in this work.

#### 4.1. Dataset

In this work, we have applied the same evaluation method used in [2]. It relies on the classification of time series extracted from pixels associated with individuals of a same species. For that, we used the algorithm introduced by [15] to segment the hemispheric image into small polygons, obtaining 8849 segmented regions (SR). Then, we associated each SR with a single ROI aiming to label it. A labeled region is created if there is at least 80% of overlapped area between an SR and a ROI.

Finally, we extracted a time series from each labeled region using the approach described in Section 2. In this way, we built a dataset of 892 time series separated into six classes, one for each plant species: *A. tomentosum* (96), *C. brasiliensis* (346), *M. guianensis* (36), *M. rubiginosa* (195), *P. ramiflora* (50), and *P. torta* (169).



**Table 1**

Confusion matrix. TP, TN, FP, and FN stand for true positive, true negative, false positive, and false negative, respectively.

		Predicted	
		Class A	Class B
Real	Class A	TP	FN
	Class B	FP	TN

#### 4.2. Evaluation measures

To report the effectiveness of each method in the experiments, we have used evaluation measures based on the confusion matrix: accuracy and average accuracy [32]. Given a confusion matrix as Table 1 shows, the measures can be calculated according to Eqs. (1–5).

$$\text{Total} = \text{TP} + \text{FP} + \text{FN} + \text{TN} \quad (1)$$

$$\text{Specificity} = \frac{\text{TN}}{(\text{FP} + \text{TN})} \quad (2)$$

$$\text{Sensitivity} = \frac{\text{TP}}{(\text{TP} + \text{FN})} \quad (3)$$

$$\text{Accuracy} = \frac{\text{TP} + \text{TN}}{\text{Total}} \quad (4)$$

$$\text{Average Accuracy} = \frac{\text{Specificity} + \text{Sensitivity}}{2} \quad (5)$$

In the case of multi-class classification task with unbalanced datasets, the use of Average Accuracy avoids that the evaluation of learning methods are biased towards the majority class [32]. Since in our experiments, we have used the 5-fold cross-validation protocol, all reported results are in terms of Mean Accuracy or Mean Average Accuracy.

### 5. Results and discussion

This section presents five different performed experiments and discusses the obtained results. In Section 5.1, we compare different values for the  $k$  parameter of the  $k$ NN learning method that yields better results in the target problem. Since it is impracticable to use all and any learning method from the literature, we conduct a pre-processing of simple classifiers. In Section 5.2, we analyze the relationship between hours of the day and the six different plant species. This experiments is essential to identify differences between available species. In Section 5.3, a correlation analysis between available time series- based classifiers is performed. Thus, we might measure the degree of agreement/disagreement between involved classifiers. In Section 5.4, we adapt the framework to combine different classifiers to consider the use of complementary information provided by RGB channels. Furthermore, we compare this framework to other well-known techniques from the literature (e.g., majority voting [22] and bootstrap aggregation [7]). Finally, in Section 3.2, we use the same framework with classifier selection process to reduce the number of time series-based classifiers used, while maintaining similar effectiveness results.

#### 5.1. Finding the best $k$ NN classifier

We have used eight  $k$ -Nearest Neighbors ( $k$ NN) methods [13], using  $k \in \{1, 3, 5, 7, 9, 11, 13, 15\}$ . Such methods are simple and fast, being suitable to be combined in a real-time recognition system. As in this paper we rely on the presence of several descriptors, using

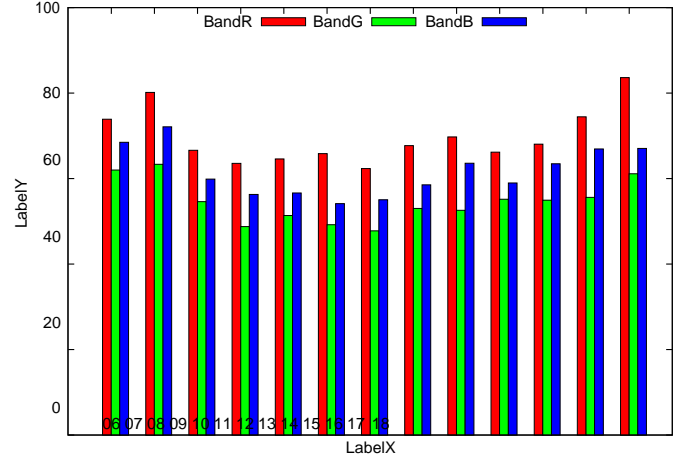


**Fig. 4.** Mean accuracy results for all hours and RGB channels using  $k$ NN-1 as learning method.

all those learning methods might be costly. Therefore, we have conducted a study to find the best parameter  $k$  that yields good results in our approach. Through experiments, we observed that the best effectiveness performance was obtained for  $k = 1$ . From now on, all the experiments reported in this work considers  $k$ NN-1 as base classifiers inside the proposed framework. Fig. 4 shows the effectiveness results of the RGB channels for each hour of the day on the validation set  $V$ .

In these experiments, we observed that the best results were achieved for red channel (R) in all hours. We also observe that all classifiers performed better in extreme hours 6, 7, 17, and 18. These results are used in the next section to guide the correlation analysis between all 39 available time series-based classifiers ( $3 \text{ channels} \times 13 \text{ h} = 39 \text{ classifiers}$ ).

#### 5.2. Relation between hour and species

In these experiments, we have analyzed the behavior of each species (*A. tomentosum*, *C. brasiliensis*, *M. guianensis*, *M. rubiginosa*, *P. ramiflora*, and *P. torta*) throughout the day using the same validation set  $V$  used in the previous section. For these species, we use the same color patterns employed for their regions in Fig. 1(c). (*A. tomentosum* – green, *C. brasiliensis* – blue, *M. guianensis* – orange, *M. rubiginosa* – magenta, *P. ramiflora* – cyan, and *P. torta* – red).

Figs. 5, 6, and 7 show the behavior of all species for each one of three different color channels (RGB). The  $x$ -axis refers to the hours of day (6, ..., 18), while the  $y$ -axis refers to the mean average accuracy. As it can be observed, although all species have the same behavior with relation to the best results in the extreme hours, these behaviors might vary for each species. In Fig. 5, notice that the *C. brasiliensis* species (blue line) has a behavior more stable than the other curves. In contrast, the *M. guianensis* species (orange line) has the highest performance decrease between ranges 7–8 and the highest increase on the ranges 6–7 and 16–18.

In Fig. 6, we can observe that the curve for the *C. brasiliensis* species is more stable over the time of day. The curve of the *A. tomentosum* species (green line) differs from the other curves. It has a “U-like” shape, which indicates that time series-based classifiers yield better results for extreme hours.

In Fig. 7, we can see that the behavior of the curve of the *P. ramiflora* species (cyan line) has the highest performance decrease between ranges 8–9. Furthermore, we can observe that there are differences between R and B color channels with relation to the best results achieved at 6 and 18 h for all species. Classifiers using R color channel at 18 h achieved better results than those at 6 h. The contrary

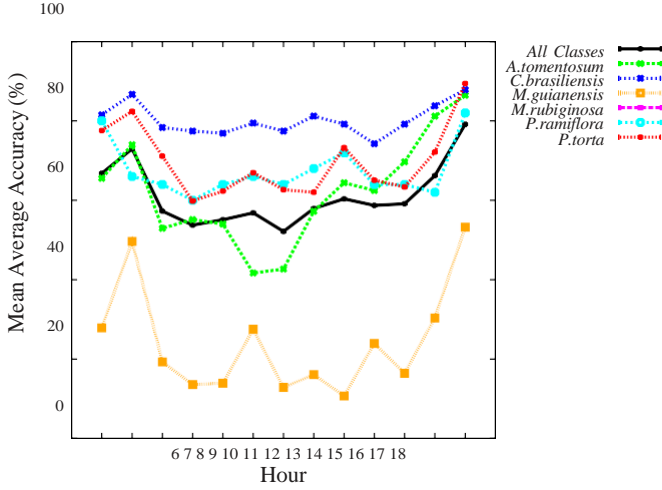


**Fig. 5.** Mean accuracy results for all hours and R color channel using kNN-1 as learning method for each class. (For interpretation of the references to color in this figure text, the reader is referred to the web version of this article.)

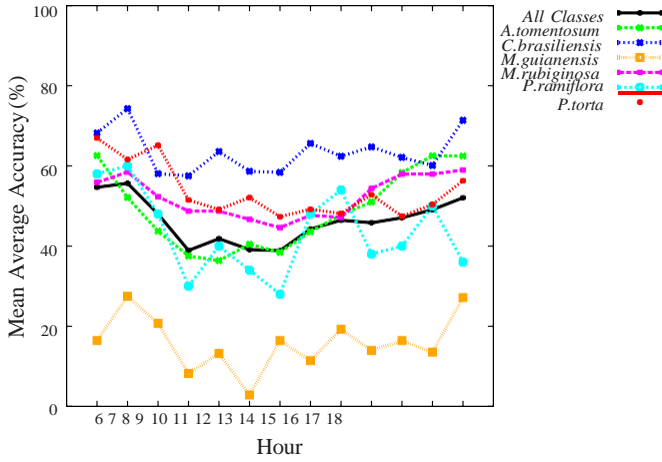


**Fig. 6.** Mean accuracy results for all hours and G channel using kNN-1 as learning method for each class. (For interpretation of the references to color in this figure text, the reader is referred to the web version of this article.)

was observed for the G channel. In this case, the best results were observed at 6 h. Note also that the curves of the species *M. guianensis* presents the lower mean average accuracy for all color channels. We might attribute these consistent difference to its leafing phenology: *M. guianensis* (orange line) is the only species reducing the percentage of green over the period of study [2].

In summary, each species has a particular behavior with regard to different RGB color channels throughout the day. This phenomenon might be justified by scattering of solar radiation and canopy reflectance [33]. Moreover, the leaf biochemical contents (e.g., chlorophyll, water, and dry matter) and canopy architecture (e.g., leaf area index, leaf angle distribution, and relative leaf size) might have impacted the spectral response of leaves [17].

This study might reinforce the importance of the R channel for the identification of these plant species as pointed out in [11]. However, the G channel has shown also to be important for some species (e.g., *M. guianensis*, *P. ramiflora*, and *P. torta*) for some hours of the day. The difference in behavior of the time series-based classifiers led us to consider their combination as a suitable alternative for improving the classification results in plant identification systems. We therefore performed a correlation analysis between all those classifiers to guide us in the time series-based classifier selection process.

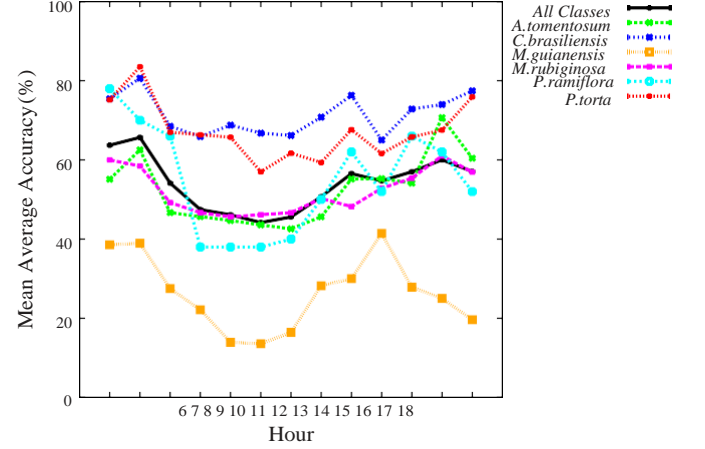


**Fig. 7.** Mean accuracy results for all hours and B channel using kNN-1 as learning method for each class. (For interpretation of the references to color in this figure text, the reader is referred to the web version of this article.)

### 5.3. Correlation analysis between time series-based classifier

This section shows a correlation analysis of each pair of classifiers for all 39 available time series-based classifiers aiming at finding which of them might be combined by the framework described in Section 3.

The Correlation Coefficient  $\rho$  (COR) [20] has been used to assess the correlation of two classifiers  $c_i$  and  $c_j$ :

$$COR(c_i, c_j) = \frac{ad - bc}{(a+b)(c+d)(a+c)(b+d)}, \quad (6)$$

where  $a$  is the percentage of time series that both classifiers  $c_i$  and  $c_j$  classified correctly in a validation set  $V$ . Value  $b$  is the percentage of time series that  $c_j$  hit and  $c_i$  missed,  $c$  is the opposite of  $b$ . The value  $d$  is the percentage of time series that both classifiers missed. The pairs of classifiers with lower COR values have greater degree of complementarity and are more likely to yield better results when combined. Range of COR is in  $[-1, +1]$ .

Fig. 8 presents the COR values for all possible combinations of pairs of classifiers considering the six classes. The lowest correlation coefficients are closer to the purple color ( $-1$ ) and the highest coefficients are closer to the yellow color ( $+1$ ). Furthermore, in this figure, there are seven important regions that have been highlighted and they are explained below.

As we can observe in Fig. 8(a), in region (1), there are few classifiers with high correlation between the channels R and G which are closer to their extreme hours (16–18 h). However, outside of region (1), the classifier from channels R and G are less correlated with channel B. We can see some points in purple, which means lower correlation coefficients. Fig. 8(b) shows a more homogeneous behavior of the classifiers, since instances of class *C. brasiliensis* are not difficult to be correctly classified. Furthermore, we can notice that there are a few yellow strips meaning high correlation of the same classifier with all other classifiers. Fig. 8(c) shows many purple points, which mean a low correlation between almost all classifiers used in this work. This phenomenon can be explained by the difficulty of classifying instances of the class *M. guianensis*. In region (2), we found the lowest correlation coefficient for all experiments. Fig. 8(d) shows a similar behavior to Fig. 8(a) with coefficients more homogeneous. We can observe in region (3) that classifiers of the same color channel G are more correlated between them. However, in region (4), R and G

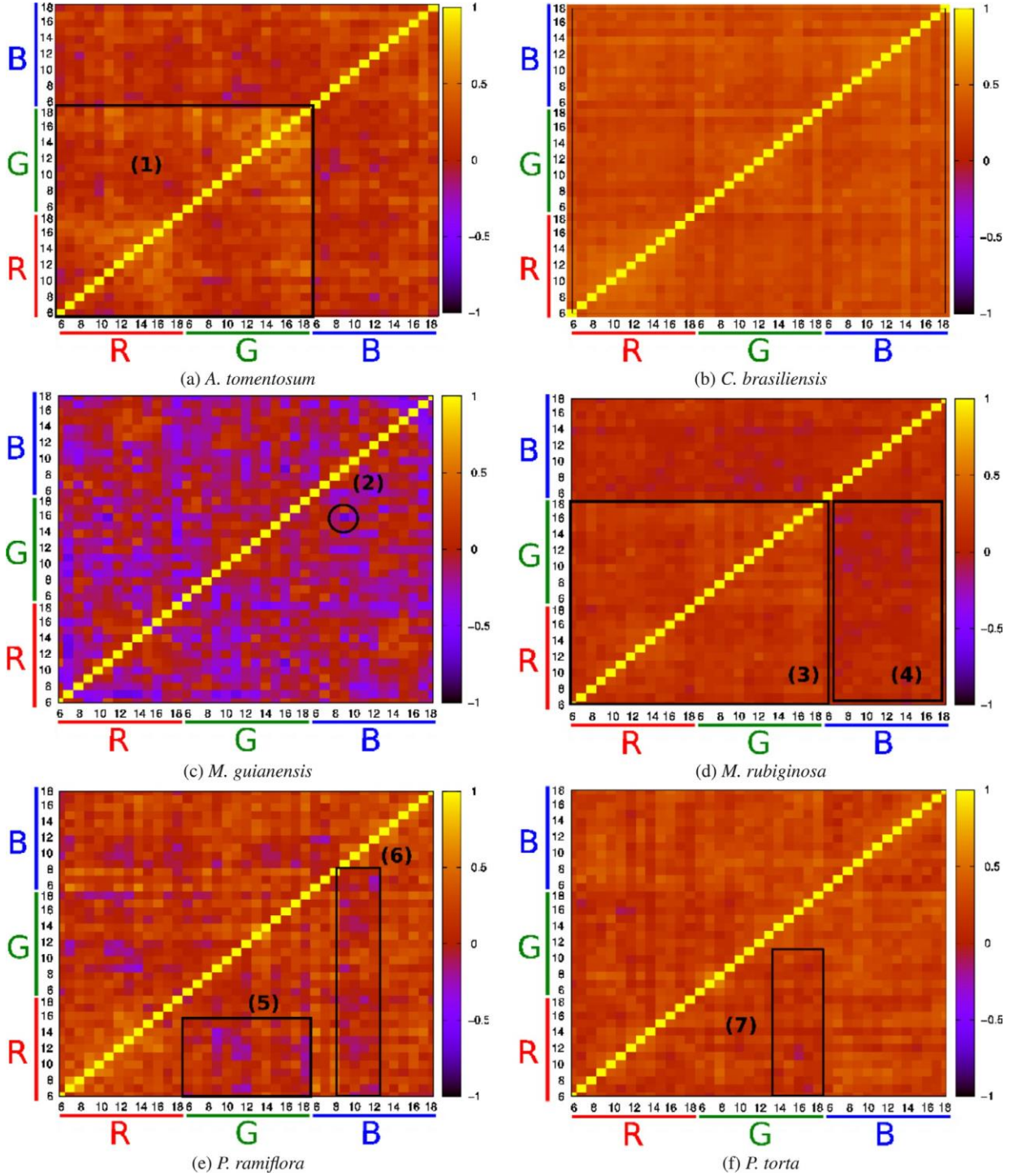


**Fig. 8.** Correlation analysis considering all 39 available time series-based classifiers (3 channels  $\times$  13 h = 39 classifiers). The lowest correlation coefficients are closer to the purple color ( $-1$ ) and the highest coefficients are closer to the yellow color ( $+1$ ). (For interpretation of the references to color in this figure legend, the reader is referred to the web version of this article.)

are less correlated with *B*. Fig. 8(e) shows the second most difficult class to be classified: *P. ramiflora*. In regions (5) and (6), we found the lowest correlation coefficients between almost all classifiers of  $R \times G$  and all classifiers of the color channels *R* and *G* with part of classifiers of channel *B* (9–12 h). Finally, in Fig. 8(f), which refers to the class *P. torta*, we can notice that the classifiers achieve similar behavior to Fig. 8(a) and (b). In region (7), there are the less correlated classifiers within Fig. 8(f).

#### 5.4. Time series-based classifier fusion

In these experiments, 12 fusion techniques were compared: four techniques that use the adopted framework [12] (FSVM-ALL-39, FSVM-R-13, FSVM-G-13, and FSVM-B-13), four majority voting techniques [22] (MV-ALL-39, MV-R-13, MV-G-13, and MV-B-13), and four bootstrap aggregation approaches [7] (BAGG-MERGE-ALL-39, BAGG-MERGE-R-13, BAGG-MERGE-G-13, and BAGG-MERGE-B-13).



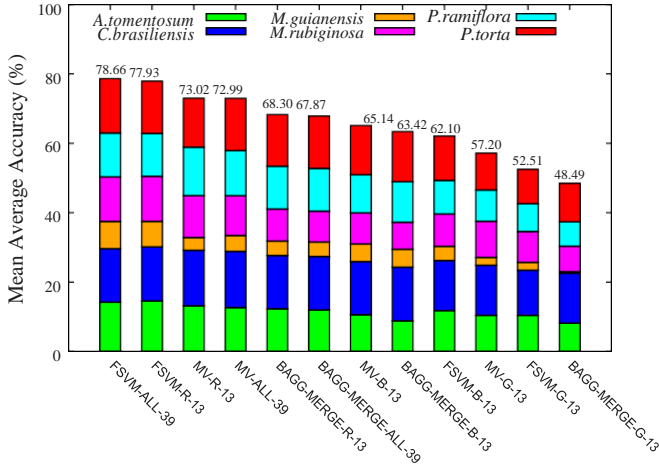


Fig. 9. Mean average accuracy of all fusion techniques.

ALL means that all color channels, hours, and features have been used. R, G, and B refer to the color channels that compose the RGB channel. Furthermore, the number after a name (e.g., 13 in FSVM-B-13) refers to amount of time series-based classifiers considered in the fusion process. MERGE denotes a binding of the all available channels, hours, and feature vectors.

The proposed framework aims at finding suitable combinations of time series-based classifiers formed by descriptors and learning methods. We have used the implementation of those learning methods available in the WEKA [16] data mining library. All learning methods were used with default parameters which means we did not optimize them.

Figs. 9 and 10 show the effectiveness results of all fusion techniques considered in this work. Two evaluation measures have been adopted, mean average accuracy (Fig. 9) and mean accuracy (Fig. 10). Balanced mean accuracy per class considers the mean accuracy of each class using the 5-fold cross validation protocol and the final effectiveness result is the average of these accuracies. Mean accuracy is the principal diagonal from confusion matrix, which counts the number of correct classification cases with respect to the total instances using the 5-fold cross validation protocol.

As it can be observed, two of our approaches (FSVM-ALL-39 and FSVM-R-13) achieved the best results among all involved fusion techniques. FSVM-ALL-39 approach obtained a mean average accuracy of

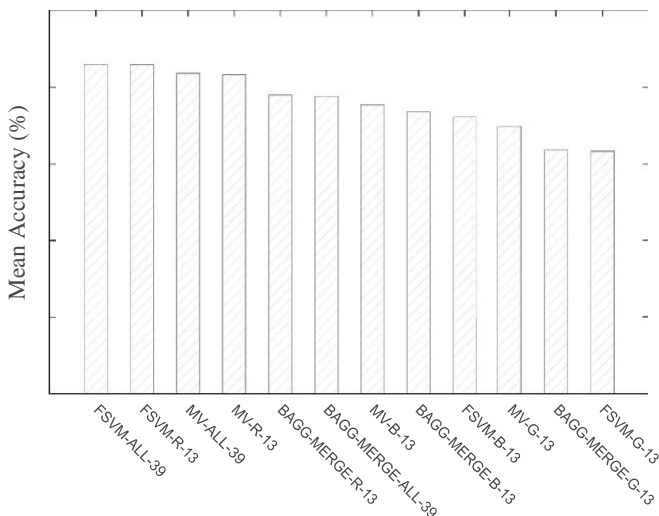


Fig. 10. Mean accuracy of all fusion techniques.

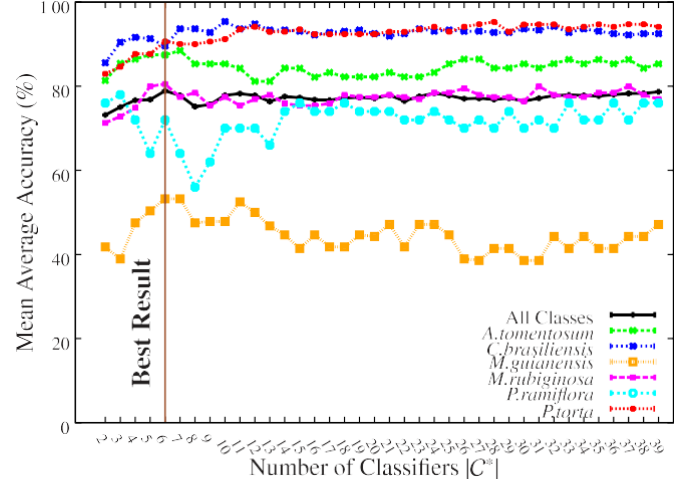


Fig. 11. Behavioral analysis of the framework for different numbers of classifiers. On the x-axis are the numbers of selected classifiers  $|C^*| = \{2, \dots, 39\}$  and y-axis are the mean accuracy achieved in the experiments. (For interpretation of the references to color in this figure text, the reader is referred to the web version of this article.)

78.66% and mean accuracy of 85.87% against the best baseline MV-R-13 that yielded 73.02% and 83.18%, respectively. A fine-grained analysis considering mean average accuracy showed that FSVM-ALL-39 approach achieved better results in two classes (*M. guianensis* and *P. torta*), FSVM-R-13 approach is the best for other two classes (*A. tomentosum* and *M. rubiginosa*). Finally, MV-ALL-39 achieved better results in the classes *C. brasiliensis* and *P. ramiflora*. Thus, our approaches achieved better results in four out of six possible classes from the dataset used.

### 5.5. Time series-based classifier selection

This section describes a behavioral analysis of the proposed framework using different numbers of time series-based classifiers  $|C^*|$  for the six classes from the dataset. Fig. 11 shows this analysis per class as well as all classes together.

In these experiments, we can notice that the classes *C. brasiliensis*, *A. tomentosum*, *M. rubiginosa*, and *P. torta* have a stable behavior with the increasing number of selected time series-based classifiers. This fact cannot be observed in the classes *M. guianensis* and *P. ramiflora*. The class *M. guianensis* achieved an increase of more than 10% of mean accuracy in the range [3, 7]. However, the curve of the class *P. ramiflora* decreases more than 15% for the same ranges. Furthermore, note that the framework using only six classifiers achieves similar results to those observed when 39 time series-based classifiers are used (see brown line in Fig. 11). In summary, the investigation for minimizing the misclassification rate per class seems to be a promising research venue and a classifier selection approach based on balanced classes might be a good solution to address this problem.

Fig. 12 depicts the histogram  $H$  created in the selection process, while Fig. 13 shows the accuracy performances of all simple/non-complex classifiers using the validation set  $V$ . We highlight in gold bars the six time series-based classifiers (see brown line in Fig. 11) that have been selected by our selection process. In Fig. 12, although classifiers *kNN1-09G*, *kNN1-09B*, and *kNN1-12G* have achieved the higher frequency than *kNN1-06R* and *kNN1-07G*, our selection approach does not choose any of those classifiers as candidate for fusion (gold bars). This is due to the policy of also considering the individual accuracy performance of classifiers in the selection process. As the accuracy performances of *kNN1-09G*, *kNN1-09B*, and *kNN1-12G* are below than the employed threshold values (dark blue line,  $T = 61.97\%$ ), these classifiers are not selected. Selected classifiers are *kNN1-06R*, *kNN1-06B*, *kNN1-07R*, *kNN1-07G*, *kNN1-07B*, and

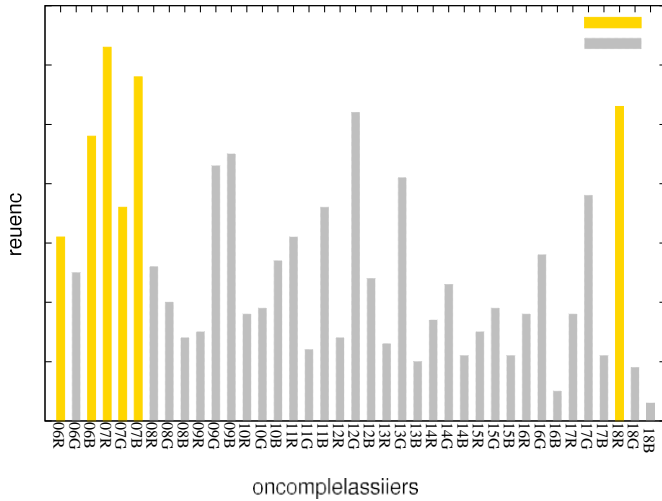


**Fig. 12.** Histogram  $H$  related to the occurrence of classifiers in the selection process. (For interpretation of the references to color in this figure text, the reader is referred to the web version of this article.)

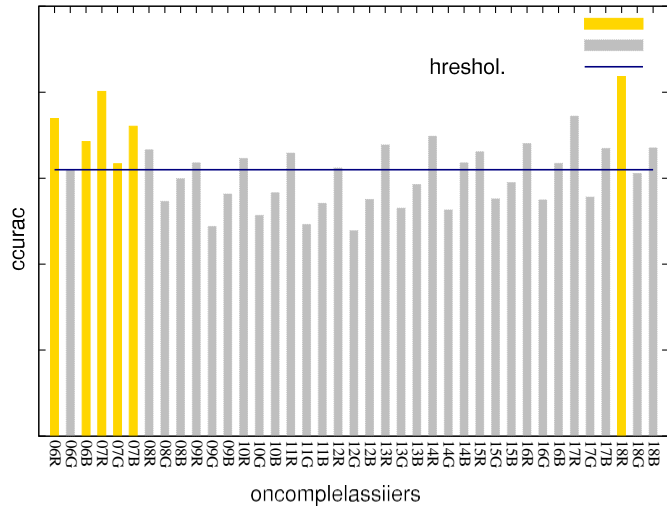


**Fig. 13.** Average accuracy performances of all non-complex classifiers used in our experiments. The dark blue line defines the employed threshold ( $T$ ) value. (For interpretation of the references to color in this figure legend, the reader is referred to the web version of this article.)

$kNN1-18R$ . In these experiments, three selected classifiers use the  $R$  channel, two classifiers use the  $B$  channel, and one classifier uses the  $G$  channel. We can observe also a huge impact of the extreme hours (06, 07, and 18) in the selection process.

## 6. Conclusions

In this paper, we proposed a time series-based classifier selection and fusion framework to address problems in fine-grained plant identification tasks. We validated such framework with phenology studies. Recalling the objectives of our work, we addressed some very important questions, such as: (i) how species from the same leaf functional group differ from each other; (ii) how different pattern classifiers might be combined to improve the effectiveness results in target fine-grained species identification as just one classifier or feature would not be discriminatory enough for the task; and (iii) whether it is possible to achieve good classification results with fewer classifiers for plant identification improving the efficiency of the whole decision-making process. To answer such questions, we have performed five different analyses: (1) Investigation of the best

value for the  $k$  parameter of the  $kNN$  learning method that yields better results in the target problem; (2) An analysis of the relationship between hours of the day and the six different plant species considered in this study; (3) A correlation analysis measuring the degree of agreement/disagreement between available time series-based classifiers; (4) Use of a classifier selection and fusion framework aiming at exploring complementary information provided by different descriptions and learning methods, thus improving the effectiveness results; (5) Investigation of the impact of using the same framework with classifier selection process to decrease the number of time series-based classifiers used, while maintaining similar effectiveness results.

The experiments performed in this work confirm that there are some differences in terms of classification performance depending on the plant species considered, as well as, the correlation that exists between RGB channels and hours of the day using  $kNN-1$  classifiers. Also, in the experiments, it was possible to note the importance of the red channel for plant species identification, in spite of the good contribution observed for the blue channel for some species (e.g., *M. guianensis*, *P. ramiflora*, and *P. torta*). Furthermore, the adopted framework achieved excellent results when compared with other well-known fusion techniques of the literature (Bootstrap Aggregation-BAGG [7] and Majority Voting-MV [22]). This framework, extended upon [12], brings an essential and important property different from those techniques in the literature: it is highly flexible and parallelizable. Regarding flexibility, our adopted approach can use any description technique or learning methods as base classifier. In addition, the method is able to use any learning method in the late fusion (meta-learning process), such as a simple majority voting or more complex techniques such as support vector machines (SVMs). As for parallelization, each combination of description and learning methods can be used in different parallel approaches (e.g., thread, processor, and GPU) due the framework structure being designed independently (in modules). With that, the more important modules are the training classifiers, the classifier selection, and the meta-learning. Furthermore, other important advantage of the adopted approach is that it considers each description and learning method as a single representation thus it does not incur in the common normalization problems and, consequently reduces the risk the “the curse of dimensionality” that may result of direct combination of features (e.g., by means of concatenating feature vectors).

A fine-grained analysis using time series-based classifier selection showed that the framework using fewer classifiers (i.e., six) achieved similar results to those observed when 39 time series-based classifiers are used. Therefore, our proposed method might be able to perform real-time plant identification in different domains such as when monitoring plants through intelligent autonomous vehicles (e.g., unmanned aerial vehicles and drones).

Another important contribution of this work is related to the use of multiclass classification approaches, which was not used in previous phenology work [5]. The main take-home message of our work is that the adopted framework might be a good solution to address complex problems such as the ones involving phenology derived from sequential digital images and fine-grained recognition of plants from the same functional leaf groups. This framework takes advantage of different and complementary information provided by RGB channels and combine them for a better decision-making process. In addition, it achieves good effectiveness results with fewer classifiers, which is paramount for efficient plant recognition.

Future work may consider the use of the proposed framework in semi-automatic plant identification tasks, in which users may provide relevance feedback that may tune the used classification models for better fine-grained categorization that always includes humans (specialists) in the loop. Also, we may consider the use of the proposed framework for real-time plant identification systems. Furthermore, other vegetation indices might be studied and combined

such as Color Index of Vegetation Extraction (CIVE) [19], Excess Green (ExG) [14], and the Plant Phenology Index (PPI) [18]. Regarding the generalization, with the proposed approach in this work for dealing with time-series based problems, we believe that other application domains, still in the realm of time series as input data, may include crop monitoring, recognizing different plant growth rates and also for plague control. Other applications also may tap on snowmelt and comparison of species or different kinds of vegetation.

## Acknowledgments

We thank the financial support of the São Paulo Research Foundation **FAPESP** (grants #2010/14910-0 and #2010/05647-4), the **FAPESP**-Microsoft Research Virtual Institute (grants #2010/52113-5, #2011/51523-8, #201313/20169-1, and #2013/50155-0), CNPq (grants #477662/2013-7 and #304352/2012-8), **CAPES** (grant #1260-12-0), and Microsoft Research. LPCM and RST receive a Productivity Research Fellowship from CNPq (grants #306243/2010-5 and #306587/2009-2). BA receives a PhD fellowship (**FAPESP** grant #2014/00215-0). Also, we have been benefited by funds from CNPq, CAPES, and FAPESP (grants #2007/52015-0, #2007/59779-6, #2009/18438-7, and #2010/51307-0). The authors thank Prof. Dr. Thiago Sanna Freire Silva for his pertinent and helpful comments on the paper.

## References

- [1] H. Ahrends, S. Etzold, W. Kutsch, R. Stoeckli, R. Bruegger, F. Jeanneret, H. Wanner, N. Buchmann, W. Eugster, Tree phenology and carbon dioxide fluxes: use of digital photography for process-based interpretation at the ecosystem scale, *Clim. Res.* 39 (2009) 261–274.
- [2] B. Alberton, J. Almeida, R. Henneken, R. da S. Torres, A. Menzel, L.P.C. Morellato, Using phenological cameras to track the green up in a Cerrado savanna and its on-the-ground validation, *Ecol. Inform.* 19 (2014) 62–70.
- [3] J. Almeida, J.A. dos Santos, B. Alberton, L.P.C. Morellato, R. da S. Torres, Plant species identification with phenological visual rhythms, in: *Proceedings of the IEEE International Conference on eScience (eScience'13)*, 2013, pp. 148–154.
- [4] J. Almeida, J.A. dos Santos, B. Alberton, L.P.C. Morellato, R. da S. Torres, Visual rhythm-based time series analysis for phenology studies, in: *Proceedings of the IEEE International Conference on Image Processing (ICIP'13)*, 2013, pp. 4412–4416.
- [5] J. Almeida, J.A. dos Santos, B. Alberton, R. da S. Torres, L.P.C. Morellato, Applying machine learning based on multiscale classifiers to detect remote phenology patterns in Cerrado savanna trees, *Ecol. Inform.* 23 (2014) 49–61.
- [6] J. Almeida, J.A. Santos, W.O. Miranda, B. Alberton, L.P.C. Morellato, R.S. Torres, Deriving vegetation indices for phenology analysis using genetic programming, *Ecol. Inform.* 26 (2015) 61–69.
- [7] L. Breiman, Bagging predictors, *Mach. Learn.* 24 (1996) 123–140.
- [8] L.E. Chambers, R. Altwegg, C. Barbraud, P. Barnard, L. Beaumont, R. Crawford, J.M. Durant, L. Hughes, M.R. Keatley, M. Low, L.P.C. Morellato, E. Poloczanska, V. Ruoppolo, R.E.T. Vanstreels, E.J. Woehler, A. Wolfaardt, Changes in southern hemisphere phenology, *PlosOne* 8 (2013) e75514.
- [9] H.D. Cheng, X. Jiang, Y. Sun, J. Wang, Color image segmentation: advances and prospects, *Pattern Recognit.* 34 (2001) 2259–2281.
- [10] E.E. Cleland, I. Chuine, A. Menzel, H.A. Mooney, M.D. Schwartz, Shifting plant phenology in response to global change, *Trends Ecol. Evol.* 22 (7) (2007) 357–365.
- [11] J.C. Conti, F.A. Faria, J. Almeida, B. Alberton, L.P.C. Morellato, L. Camolesi Jr., R. da S. Torres, Evaluation of time series distance functions in the task of detecting remote phenology patterns, in: *Proceedings of the IEEE International Conference on Pattern Recognition (ICPR'14)*, 2014, pp. 3126–3131.
- [12] F.A. Faria, J.A. dos Santos, A. Rocha, R. da S. Torres, A framework for selection and fusion of pattern classifiers in multimedia recognition, *Pattern Recognit. Lett.* 39 (2014) 52–64.
- [13] J. Friedman, T. Hastie, R. Tibshirani, *The Elements of Statistical Learning*, first ed., Springer, 2001.
- [14] C. Gée, J. Bossu, G. Jones, F. Truchetet, Crop/weed discrimination in perspective agronomic images, *Comput. Electron. Agric.* 60 (2008) 49–59.
- [15] L. Guigues, J. Cocquerez, H. Le Men, Scale-sets image analysis, *Int. J. Comput. Vis.* 68 (2006) 289–317.
- [16] M. Hall, E. Frank, G. Holmes, B. Pfahringer, P. Reutemann, I.H. Witten, The weka data mining software: an update, *ACM SIGKDD Explor. Newsl.* 11 (2009) 10–18.
- [17] S. Jacquemoud, W. Verhoef, F. Baret, C. Bacour, P.J. Zarco-Tejada, G.P. Asner, C. François, S.L. Ustin, Prospect + sail models: a review of use for vegetation characterization, *Remote Sens. Environ.* 113 (Suppl. 1) (2009) S56–S66.
- [18] H. Jin, L. Eklundh, A physically based vegetation index for improved monitoring of plant phenology, *Remote Sens. Environ.* 152 (2014) 512–525.
- [19] T. Kataoka, T. Kaneko, H. Okamoto, S. Hata, Crop growth estimation system using machine vision, in: *Proceedings of the 2003 IEEE/ASME International Conference on Advanced Intelligent Mechatronics*, vol. 2, 2003, pp. b1079–b1083.
- [20] L.I. Kuncheva, *Combining Pattern Classifiers: Methods and Algorithms*, Wiley-Interscience, 2004.
- [21] L.I. Kuncheva, C.J. Whitaker, Measures of diversity in classifier ensembles and their relationship with the ensemble accuracy, *Mach. Learn.* 51 (2003) 181–207.
- [22] L. Lam, S.Y. Suen, Application of majority voting to pattern recognition: an analysis of its behavior and performance, *IEEE Trans. Syst., Man, Cybern., Part A: Syst. Hum.* 27 (1997) 553–568.
- [23] L.P.C. Morellato, R.R. Rodrigues, H.F. Leitão Filho, C.A. Joly, Estudo comparativo da fenologia de espécies arbóreas de floresta de altitude e floresta mesófila semidecídua na serra do Iapi, Jundiá, São Paulo, Braz. J. Bot. 12 (1989) 85–98.
- [24] M. Parry, O. Canziani, J. Palutikof, P. van der Linden, C. Hanson, IPCC (2007) *Climate Change 2007: Impacts, Adaptation and Vulnerability*. Contribution of Working Group II to the Fourth Assessment Report of the Intergovernmental Panel on Climate Change, Cambridge UK: Cambridge University Press, 2007.
- [25] P. Reys, M.G.G. Camargo, A.P. Teixeira, M.A. Assis, M.T. Grombone-Guaratini, L.P.C. Morellato, Estrutura e composição florística entre borda e interior de um cerrado sensu stricto e sua importância para propostas de recuperação, *Hoennea* 40 (2013) 437–452.
- [26] A.D. Richardson, B.H. Braswell, D.Y. Hollinger, J.P. Jenkins, S.V. Ollinger, Near-surface remote sensing of spatial and temporal variation in canopy phenology, *Ecol. Appl.* 19 (2009) 1417–1428.
- [27] A.D. Richardson, J.P. Jenkins, B.H. Braswell, D.Y. Hollinger, S.V. Ollinger, M.L. Smith, Use of digital webcam images to track spring green-up in a deciduous broadleaf forest, *Oecologia* 152 (2007) 323–334.
- [28] R. da S. Torres, M. Hasegawa, S. Tabbone, J. Almeida, J.A. dos Santos, B. Alberton, L.P.C. Morellato, Shape-based time series analysis for remote phenology studies, in: *Proceedings of the IEEE International Geoscience and Remote Sensing Symposium (IGARSS'13)*, 2013, pp. 3598–3601.
- [29] R. da S. Torres, C.B. Medeiros, M.A. Gonçalves, E.A. Fox, A digital library framework for biodiversity information systems, *Int. J. Digit. Libr.* 6 (2006) 3–17.
- [30] L.C.B. Santos, J. Almeida, J.A. dos Santos, S.J.F. Guimarães, A.A. Araújo, B. Alberton, L.P.C. Morellato, R. da S. Torres, Phenological event detection by visual rhythm dissimilarity analysis, in: *Proceedings of the IEEE International Conference on eScience (eScience'14)*, 2014, pp. 263–270.
- [31] M.D. Schwartz, *Phenology: An Integrative Environmental Science*, Springer, 2013.
- [32] M. Sokolova, G. Lapalme, A systematic analysis of performance measures for classification tasks, *Inf. Process. Manag.* 45 (2009) 427–437.
- [33] M.M. Verstraete, Radiation transfer in plant canopies: scattering of solar radiation and canopy reflectance, *J. Geophys. Res.: Atmos.* 93 (1988) 9483–9494.
- [34] D.M. Woebbecke, G.E. Meyer, K. Von Bargen, D.A. Mortensen, Color indices for weed identification under various soil, residue, and lighting conditions, *Trans. ASAE* 38 (1995) 259–269.

### **Appendix D**

Article published in the Journal Pattern Recognition Letters:

FARIA F. A., ALMEIDA, J., ALBERTON, B., MORELLATO, L.P.C., TORRES, R.S. Fusion of Time Series Representations for Plant Recognition in Phenology Studies. **Pattern Recognition Letters**, v. 83, p. 205-214, 2016.

## Fusion of time series representations for plant recognition in phenology studies

Fabio A. Faria <sup>a,b,\*</sup>, Jurandy Almeida <sup>a,b</sup>, Bruna Alberton<sup>c</sup>, Leonor Patricia C. Morellato<sup>c</sup>, Ricardo da S. Torres <sup>b</sup><sup>a</sup> Institute of Science and Technology, Federal University of São Paulo – UNIFESP, São José dos Campos  
12247-014, SP, Brazil<sup>b</sup> Institute of Computing, University of Campinas – UNICAMP, Campinas 13083-852, SP, Brazil<sup>c</sup> Dept. of Botany, Sao Paulo State University – UNESP Rio Claro, 13506-900, SP, Brazil**Abstract:**

Nowadays, global warming and its resulting environmental changes is a hot topic in different biology research area. Phenology is one effective way of tracking such environmental changes through the study of plant's periodic events and their relationship to climate. One promising research direction in this area relies on the use of vegetation images to track phenology changes over time. In this scenario, the creation of effective image-based plant identification systems is of paramount importance. In this paper, we propose the use of a new representation of time series to improve plants recognition rates. This representation, called recurrence plot (RP), is a technique for nonlinear data analysis, which represents repeated events on time series into a two-dimensional representation (an image). Therefore, image descriptors can be used to characterize visual properties from this RP images so that these features can be used as input of a classifier. To the best of our knowledge, this is the first work that uses recurrence plot for plant recognition task. Performed experiments show that RP can be a good solution to describe time series. In addition, in a comparison with visual rhythms (VR), another technique used for time series representation, RP shows a better performance to describe texture properties than VR. On the other hand, a correlation analysis and the adoption of a well successful classifier fusion framework show that both representations provide complementary information that is useful for improving classification accuracies

**Keywords:**

Plant species identification, Classifier fusion, Diversity measures

**1. Introduction**

Global warming and its resulting environmental changes have raised important research topics of different disciplines. Among those is phenology that studies recurrent life cycles events and its relationship to climate [35]. To increase the range of study sites and species and the effectiveness of phenological observations, technological devices (e.g., multi-channel imaging sensors) have been successfully applied to provide metrics for estimating changes on phenological events, such as leaf development and senescence [3,4,33].

Plant species recognition in the digital images is not a trivial task, especially in tropical vegetations, where one single image

may include a huge number of species [4]. This task is very time consuming since it has to be done in the field, first by matching each crown in the image to the tree in the soil and then by identifying the tree at species level.

Our goal in this work is to support automatic plant species recognition tasks based on phenological pattern information. Different patterns correspond to different species, as well as similar patterns can be grouped in one species type or in a leaf functional group that encompasses several species. This may not just save time for phenologists but also complement the phenological interpretation of the data collected.

Almeida et al. [7] have proposed the use of machine-learning methods to find similar patterns in the digital images and then check if those patterns correspond to similar species or functional groups. Their work was focused on the intraspecies analysis, i.e., on detecting different individuals of a same species. However, different species from a same functional group may exhibit a similar phenological pattern [4], confounding the classifiers. Hence, many questions arise when considering interspecies interactions, i.e., the recognition of individuals from different species but belonging to the same functional group [4].

\* Corresponding author at: Institute of Science and Technology, Federal University of São Paulo – UNIFESP, 12247-014 São José dos Campos, SP, Brazil. Tel.: +55 12 3309 9500; fax: +55 12 3921 8857.

E-mail addresses: [ffaria@unifesp.br](mailto:ffaria@unifesp.br), [juruna18@gmail.com](mailto:juruna18@gmail.com) (F.A. Faria), [jurandy\\_almeida@unifesp.br](mailto:jurandy_almeida@unifesp.br) (J. Almeida), [bru.alberton@gmail.com](mailto:bru.alberton@gmail.com) (B. Alberton), [pmorella@rc.unesp.br](mailto:pmorella@rc.unesp.br) (L.P.C. Morellato), [rtorres@ic.unicamp.br](mailto:rtorres@ic.unicamp.br) (R. da S. Torres).



In this work, we adopt the strategy of characterizing phenological patterns from time series and distinguishing species from the same leaf functional group in plant species recognition tasks. In fact, several time series representations have been proposed in the literature. Some successful approaches include data-adaptive (e.g., SAX [26] and APCA [23]) and non-data adaptive representations (e.g., wavelets [31]). A good survey upon this subject can be found in [40].

In this work, we present a novel approach for time series representation, which is based on a technique for nonlinear data analysis called recurrence plots (RP). Different from other time series representations, RP provides a visual mechanism for pattern identification, being suitable for combining with state-of-the-art computer vision description approaches. This work has also been motivated by the results of [24] and [37]. Both studies indicate that it is possible to perform classification tasks through the use of recurrence plots and texture feature extraction approaches. RP technique has been used successfully in different application domain, such as action recognition [24], identification of diabetes analysis of epilepsy [1], and detection of financial crisis [2].

In our experiments, we performed four rigorous comparative analysis to show the robustness of RP-based representations for plant recognition tasks. We begin with an effectiveness study evaluating the performance of RP-based classifier associated with time series of different hours of day. Then, we compared the proposed approach with another time series representation proposed by [6], called Visual Rhythm (VR). Next, we performed a correlation analysis to find out agreement/disagreement between all classifiers involved between RP and VR-based representations. Finally, we adopt a successful classifier fusion framework [16] to combine the most suitable classifiers. Experimental results show that the combination of RP- and VR-based representations yields better results than their use in isolation.

In summary, the main contributions of this work are: (i) a new representation of time series based on recurrence plots technique for plant recognition; (ii) effectiveness study of the recurrence plots approach in different hours of day; (iii) effectiveness comparative study between recurrence plots and visual rhythm approaches; (iv) correlation analysis between recurrence plots and visual rhythm approaches; (v) use of a classifier fusion framework to combine the most suitable classifiers using both approaches.

The remainder of this paper is organized as follows. Section 2 presents the phenological data acquisition process considered in our study. Section 3 presents the recurrence plot approach and how to use it for phenological time series representation. Section 4 describes the experimental protocol adopted to validate the proposed approach. Section 5 reports the results of our experiments and compares the proposed approach with another time series representation. Finally, we offer our conclusions and directions for future work in Section 6.

## 2. Phenological data acquisition

A digital hemispherical lens camera (Mobotix Q24) was set up in an 18 m-high tower in a Cerrado *sensu stricto*, a neotropical savanna vegetation located at Itirapina, São Paulo State, Brazil [4,32]. Fig. 1 shows all steps of the time series acquisition process used in our work.

Firstly, we set up the camera to take a daily sequence of five JPEG images (at  $1280 \times 960$  pixels of resolution) per hour, from 6:00 to 18:00 h (UTC-3). The present study was based on the analysis of over 2700 images (Fig. 1a), recorded at the end of the dry season, between August 29th and October 3rd 2011, day of year 241 to 278, during the main leaf flushing season [4].

Next, the image analysis has been conducted by defining different regions of interest (ROI), as described in [33] and defined

by [4] for our target species. Then, we analyzed 22 ROIs (Fig. 1b) obtained from a random selection of six plant species identified manually by phenology experts in the hemispheric image [4]:

- (i) Three regions associated with *Aspidosperma tomentosum* (green areas).
- (ii) Four regions for *Caryocar brasiliensis* (blue areas).
- (iii) Two regions for *Myrcia guianensis* (orange areas).
- (iv) Six regions for *Miconia rubiginosa* (magenta areas).
- (v) Two regions for *Pouteria ramiflora* (cyan areas), and
- (vi) Four regions for *Pouteria torta* (red areas).

We analyzed each ROI in terms of the contribution of the primary colors (R, G, and B), as proposed by [34] and described in [4]. Initially, we analyze each color channel and compute the average value of the pixel intensity (Fig. 1c). After that, we compute the normalized brightness of each color channel (RGB Chromatic coordinates) (Fig. 1d). The normalization of those values reduces the influence of the incident light, decreasing the color variability due to changes on illumination conditions [4,11,41]. Finally, by computing those values along the whole period (August 28th to October 3rd, 2011), we obtained time series to use as input data for our proposed framework (Fig. 1e).

According to the leaf exchange data from the on-the-ground field observations on leaf fall and leaf flush at our study site, those species were classified on three functional groups [4,27]: (i) deciduous, *A. tomentosum* and *C. brasiliensis*; (ii) evergreen, *M. guianensis* and *M. rubiginosa*; and (iii) semideciduous, *P. ramiflora* and *P. torta*.

## 3. Recurrence plots for plant species recognition

This section introduces our approach for phenological time series representation using recurrence plots. Section 3.1 describes how to compute recurrence plots (RP) from time series, while Section 3.2 presents how we use RP for representing phenology data.

### 3.1. Recurrence plots (RP)

Recurrence plots (RP), proposed by [15] in dynamical systems, is an advanced technique of nonlinear data analysis. RP technique has been used to visualize repeated events (the recurrence of states) of higher dimensional phase spaces through projection into the two or three dimensional sub-spaces. This technique is able to investigate recurrent behavior (periodicity) at time series ( $m$ -dimensional phase space) through a two-dimensional representation, such as a distance square matrix.

Recurrence Plot might be defined by:

$$R_{i,j} = \mathbb{C}(\|x_i - x_j\|), x_i \in \mathbb{R}^m, i, j = 1 \dots N \quad (1)$$

where  $N$  is the number of considered states (dots at the time series)  $x_i$ ,  $\epsilon_i$  threshold distance,  $\|\cdot\|$  a norm between the states (e.g., Euclidean norm),  $m$  is the embedding dimension, and  $\mathbb{C}(\cdot)$  the Heaviside function. This discontinuous function has value 0 for negative argument and 1 for positive argument.

Eq. (1) provides an  $N \times N$  image, which shows us whether there are recurrent states or not, along the target trajectory. This created image might be binary or grayscale, depending on the choice of a threshold or not. Fig. 2 shows a real time series from the dataset and two examples of recurrence plot considering those real time series, unthresholded and thresholded.

The choice of an generalizable threshold to perform matching between two RP is a non-trivial task, but it can be possible with few heuristics [36]. As in this work we aim to make use of color and texture information, we have adopted the unthresholded approach using the *Manhattan* norm and  $m = 1$ . This unthresholded approach is defined in Eq. (2). However, we can not rule out that

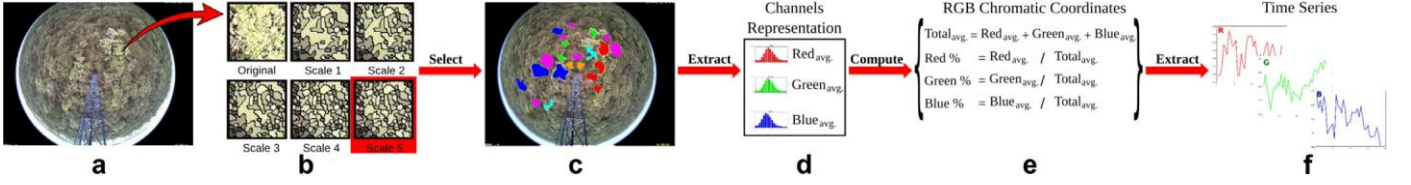


**Fig. 1.** The time series acquisition process pipeline. (a) Sample image of the cerrado savanna; (b) Different segmentation scales are computed and the coarse scale is selected; (c) Hemispherical image with the selected ROI's species; (d) Channel representation are extracted from ROI's; (e) RGB chromatic coordinates are computed; (f) Phenological time series extracted from digital images.

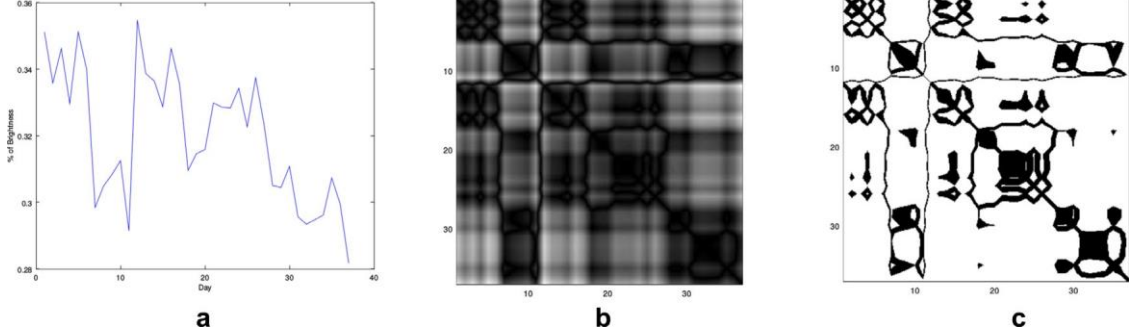


**Fig. 2.** In (a), example of time series, (b) is an example of unthresholded RP, and (c) is an example of thresholded RP with  $\Theta(\cdot) < 20$ ,  $N = 37$ , and  $m = 1$ .

the extraction of shape information [13] is a research line to be explored in future work.

$$R_{i,j} = |x_i - x_j|, x_i \in R^1, i, j = 1 \dots N \quad (2)$$

### 3.2. Recurrence plot for phenological time series representation

From phenology time series, it is possible to estimate changes on phenological events, such as leaf flushing when analyzing the green channel, or leaf color change and senescence using values from the red channel [3,33]. It requires the analysis of time series related to different color channels. The changing patterns along time are then validated with on-the-ground phenology observations.

However, color information in the RGB channels are highly correlated (i.e., changes in one channel may lead to variations in another), making harder to detect temporal changes in recurrent phenology events.

The novelty of this paper is to extend the notion of recurrence plots for the context of phenology. Here, we combine the time series into a single representation, making the phenological change analysis easier. The key contribution of our idea is the combination process we design to encode the time series into a single image.

**Fig. 3** (a)–(c) illustrates the process of computing RP-based representations. In (a), given the obtained time series in **Fig. 1**, the recurrence plot algorithm is applied on these time series to create their two-dimensional representation (distance matrix). Even at this step, a normalization technique is applied to convert real values to integer values in the typical range of grayscale images ([0, 255]). Then, in (b), a merging process is performed to join the three distance matrices into a single color image. Finally, in (c), many image descriptors may be used to encode visual properties (e.g., color, texture, and shape) from this color image into feature vectors. The feature vectors created through the use of image descriptors are later used as input to a machine learning method (e.g., support vector machine and  $k$ -Nearest Neighbors).

**Fig. 4** shows the recurrence plots computed using the defined ROIs. As RP provides a two-dimensional representation (distance square matrix), we can observe many different colors in the matrices, which are associated with the distance values between plots on the time series. The lowest distance values are closer to the

blue color and the highest distance values are closer to the red color. Notice that there are pattern differences among all of species used in this work.

## 4. Experimental setup

This section describes the baseline used, which is based on visual rhythms (**Section 4.1**); presents the classifier fusion framework adopted to combine VR-based and RP-based classifiers (**Section 4.2**), and, finally, introduces the experimental protocol (**Section 4.3**).

### 4.1. Baseline: visual rhythms (VR)

An effective way to analyze temporal properties from video data is by means of visual rhythms [28]. The objective is to create an abstraction of a video by coding the temporal change of pixel values along a specific sampling line [20].

In the context of phenology, a time series comprised of images taken by digital cameras at fixed time intervals can be viewed as a video of the vegetation, as proposed by [5]. However, instead of specific lines (e.g., diagonal, horizontal, and vertical), the interest here is to analyze unshapely regions related to plant species that are identified by phenology experts (see the initial step in **Fig. 3**).

Motivated by such limitations, [6] have generalized the notion of visual rhythms. From a generic point of view, a visual rhythm consists of temporal data samples grouped in an orderly manner. For that, they have designed a mapping function to convert a ROI into a vertical line. In the following, we briefly describe their strategy for extracting visual rhythms from phenology time series. For more details regarding their approach, refer to [9].

Let  $V = \{f_t\}, t \in [1, T]$  be a video, in domain  $2D + t$ , with  $T$  frames of dimensions  $W_V \times H_V$ ; and  $I$  be a binary image, with the same dimensions of  $V$ , in which white pixels indicate a ROI. Initially, the image  $I$  is converted into a list of Cartesian coordinates  $L_{xy} = \{(x, y) | I(x, y) = 1\}$ . Next, this list is used for computing the geometric center  $(x_c, y_c)$  of the ROI. Then, the Cartesian coordinate system of the elements in  $L_{xy}$  is translated to have its origin at the point  $(x_c, y_c)$ . After that, the Cartesian coordinates  $L_{xy}$  are converted to the polar coordinate system, creating a list of

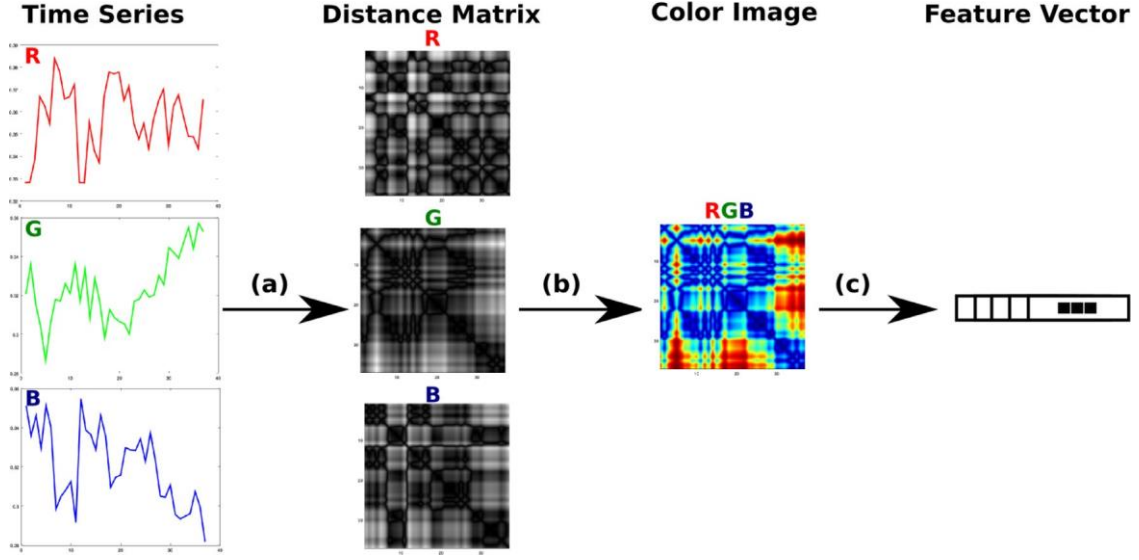


Fig. 3. The steps for feature extraction from the recurrence plot representation.

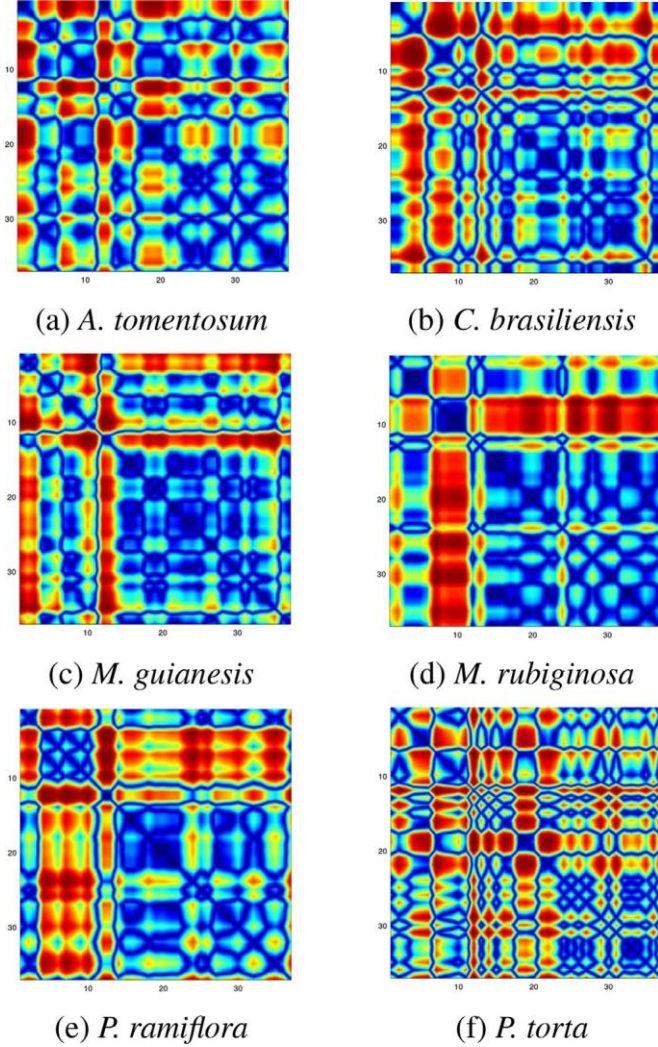


Fig. 4. Examples of recurrence plots for ROIs of each plant species. These images were created using the *Octave* software [14] with one-dimensional interpolation method.

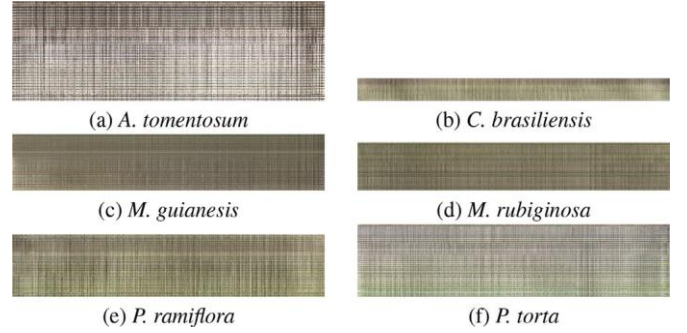


Fig. 5. Visual rhythms obtained for ROIs of some plant species. Text and figure have been extracted from [6].

polar coordinates  $Lr\theta$ . Thereafter, an index  $K = \{k \mid \forall (r, \theta) \in Lr\theta, k = 2\pi r + \theta\}$  is created to assign a unique value to each element in  $Lr\theta$ . Finally, the keys in the index  $K$  are sorted in an increasing order and then used to arrange the elements in  $Lxy$ .

In this way, they defined a visual rhythm as a mapping of each frame  $f_i$  into a vertical line on an image  $R^*$ , in domain  $1D + t$ , such that [6]:

$$R^*(t, z) = f_i(Lxy(z)), t \in [1, W_{R^*}], z \in [1, H_{R^*}],$$

where  $W_{R^*} = T$  and  $H_{R^*} = |Lxy|$  are its width and height, respectively. Figure 5 presents the visual rhythms produced by their approach using the ROIs from Fig. 3(b).

#### 42. The classifier fusion framework

This section presents a framework for classifier selection and fusion (FSVM), as devised in [16]. The objective of the fusion framework is to exploit the degree of agreement/disagreement among classifiers, concept known as diversity, with the objective of selecting the most suitable ones to be used in a combination scheme.

In the context of classifier fusion area and in this work, a classifier might be defined as a tuple containing a learning method (e.g., kNN) and a description technique (e.g., Color Histogram). Classifiers learn patterns from training instances and use learned models to assign unseen instances to appropriate classes. Once the training step is finished, a selection process is performed to define



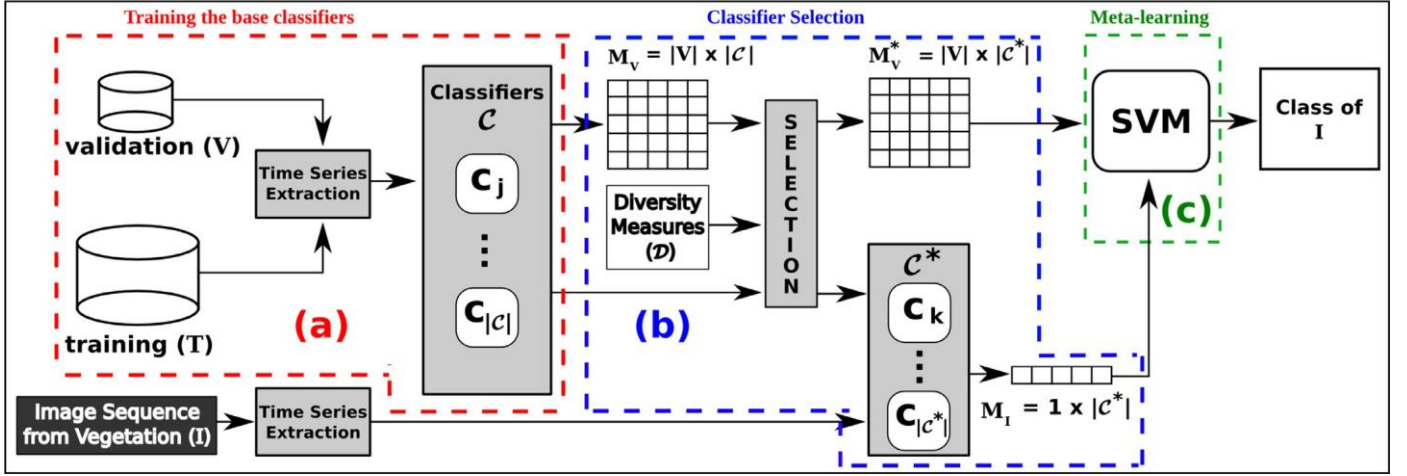


**Fig. 6.** Time series-based classifier selection and fusion framework adapted from [16]. In (a), given a classification problem with training examples, different classifiers are trained using data from training set  $T$ . In (b), the most discriminating classifiers are selected ( $C^*$ ) by taking into account diversity measures ( $D$ ). Finally, in (c), classifiers are combined in a meta-learning approach using a SVM technique.

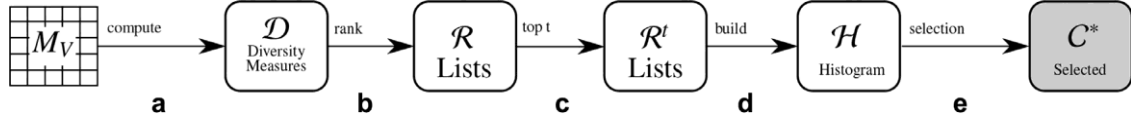


**Fig. 7.** The five steps for classifier selection are: (a) Compute diversity measures from the validation matrix  $M_V$ ; (b)  $R$  lists sorted by diversity measures scores; (c)  $R^t$  lists with top  $t$ ; (d) counts the number of occurrences of each classifier that satisfies a defined threshold; (e) Selected classifiers  $C^*$ . Text and figure have been extracted from [16].

classifiers whose combination, usually based on another learning method (meta-learning), is more promising. The objective is to determine the most discriminative methods, and, at the same time, boosting the classification performance at test time by selecting less, but more effective, classifiers.

Fig. 6 illustrates the framework FSVM for combining classifiers, while Fig. 7 illustrates the adopted five-step approach for selecting classifiers based on diversity measures, previously introduced by Faria et al. [16].

First, diversity measures (set  $D$  in Fig. 7) are used to assess the degree of agreement among available classifiers in  $C$  by taking into account the  $M_V$  matrix previously computed. That step is represented by arrow (a) in Fig. 7. Pairs of classifiers are then ranked according to their diversity score. Each diversity measure defines a different ranked list and, at the end of this step, a set  $R$  of ranked lists is produced (arrow (b)). In the following, a novel set of ranked lists  $R^t$  is computed by selecting the top  $t$  pairs of classifiers from each ranked list in  $R$  (arrow (c)), and a histogram  $H$  that counts the number of occurrences of a classifier in all ranked lists of  $R^t$  is computed (arrow (d)). Finally, the most frequent classifiers in  $H$ , whose accuracy is greater than a given threshold  $T$ , are combined by a fusion approach (arrow (e)).  $T$  is a threshold defined in terms of the average accuracy among all classifiers using the validation set  $V$ .

#### 4.3. Experimental protocol

In this work, we adopted the evaluation method used in [7]. It relies on the classification of time series extracted from pixels associated with individuals of a same species. For that, we used the algorithm introduced by [19] to segment the hemispheric image into small polygons, obtaining 8, 849 segmented regions (SR). Then, we associated each SR with a single ROI aiming to label it. A labeled region is created if there is at least 80% of overlapped area between an SR and a ROI. Finally, we extracted a time series from

each labeled region using the approach described in Section 2. In this way, we built a dataset of 892 time series separated into six classes, one for each plant species: *A. tomentosum* (96), *C. brasiliensis* (346), *M. guianensis* (36), *M. rubiginosa* (195), *P. ramiflora* (50), and *P. torta* (169).

In the following, we present four experiments performed to validate the use of the RP representation in plant recognition tasks.

First, in Section 5.1, we performed an effectiveness study concerning the performance of classifiers that exploit RP-based features associated with time series of different hours of day. In this experiment, we used the k-Nearest Neighbors (kNN) learning method. We set  $k = \{1\}$ , which achieved the best results in [12]. For describing time series encoded into a RP representation, we used seven traditional and recently proposed image descriptors: ACC [21], BIC [38], CCV [30], and GCH [39], for encoding color information; GFD [42], GIST [29], and HWD [22], for analyzing texture properties.

In the second experiment, in Section 5.2, we compared the proposed RP-based approach with another time series representation proposed by [6], called Visual Rhythm (VR). Two different effectiveness experiments have been done:

- (1) *Coarse-grained Analysis* (Section 5.2.1) that evaluates the effectiveness results of the recurrence plot-based and visual rhythms-based classifiers; and
- (2) *Fine-grained Analysis* (Section 5.2.2) that evaluates the best effectiveness results achieved by both representations (RP and VR) using different image descriptors (GFD and BIC).

In the third experiment, in Section 5.3, we performed a correlation analysis to find out agreement/disagreement between all classifiers involved in the previous experiment using RP and VR representations.

In the fourth experiment, in Section 5.4, we adopt a successful classifier fusion framework [16] to combine the most suitable classifiers using both approaches (RP and VR) representations.

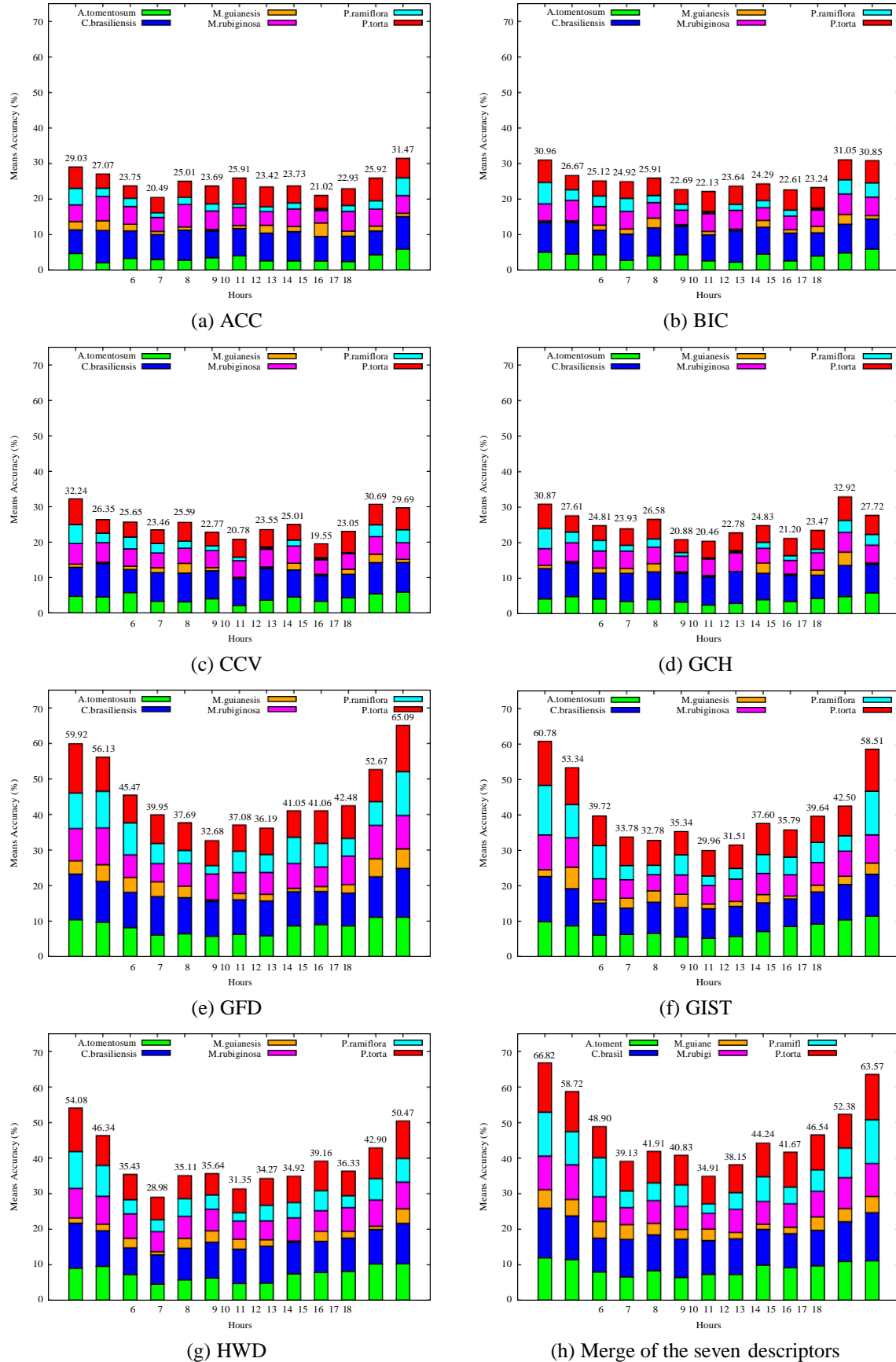


**Fig. 8.** In (a)–(g), effectiveness results of the kNN learning method using each of seven different image descriptors and in (f), results for all seven descriptors together..

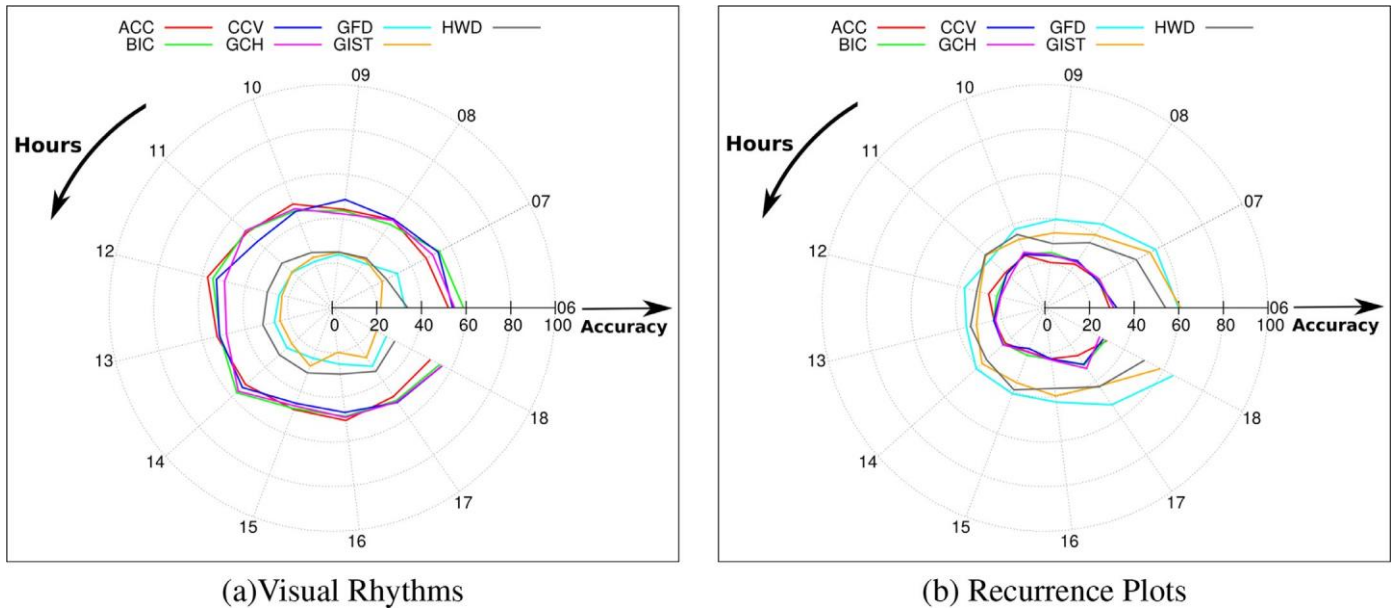


Fig. 9. Effectiveness results of the (a) visual rhythms-based and (b) recurrence plot-based kNN classifiers using seven image descriptors..

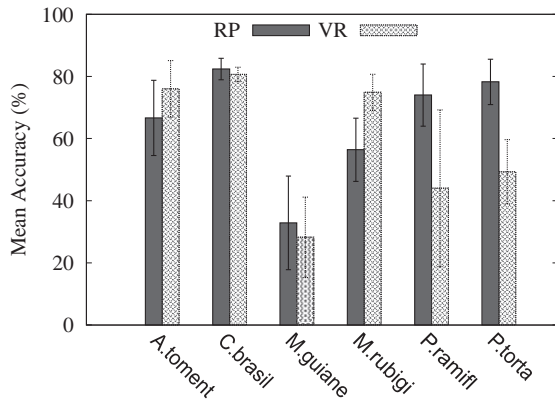


Fig. 10. The best effectiveness results for each representation approach. BIC color descriptor for Visual Rhythm approach and GFD texture descriptor for recurrence plots approach.

Finally, in Section 5.5, we conducted a behavioral study of the different approaches in small training scenarios.

## 5. Experimental results and discussion

### 5.1. Effectiveness results of RP-based classifiers

In these experiments, we analyze the behavior of the kNN learning method with each image descriptor (ACC, BIC, CCV, GCH, GFD, GIST, and HWD) for different hours of the day (from 6h to 18h).

We have adopted a 5-fold cross validation protocol, thus the evaluation measure used in this work is the arithmetic mean of the five accuracies (one accuracy per testing set). Furthermore, as the dataset is unbalanced (i.e., the number of samples in different classes is unequal), we computed each accuracy taking into account the size of classes in the testing set (weighted accuracy).

Fig. 8 (a)–(g) presents the effectiveness results for each of the image descriptors used in this work. Furthermore, in (h) we present the effectiveness results of all descriptors together. Notice that the x-axis refers to the hours of the day, while the y-axis refers to the used evaluation measure (Mean Accuracy).

As it can be observed, *C. brasiliensis* (in blue) and *P. torta* (in red) species may be considered the easiest species to be recognized among all the species, considering all hours of the day and all the image descriptors. However, *M. guianensis* (in orange) and *P. ramiflora* (in cyan) species are the hardest ones to be recognized considering all the six species. In almost all the experiments, the best results were achieved in the extreme hours of the day (6, 7, 17, and 18).

In relation to visual property (color and texture), the best effectiveness results achieved by the RP-based methods are those related to the use of texture descriptors (GFD, GIST, and HWD). Notice in Fig. 8(e) that our approach achieved the best result when consider a single descriptor (GFD) at 18h (65.09%). The worst result of a single descriptor was observed when the CCV color descriptor was used: 19.55% (Fig. 8(c) at 15h). However, the best effectiveness results for almost all hours of day have been achieved in (h), with the merge of all image descriptors.

### 5.2. Comparison of RP-based and VR-based classifiers

In this section, we compare the RP-based representations with the VR-based ones [6]. In the experiments with VR, we adopted the same experimental protocol (i.e., 5-fold cross validation and the same image descriptors and classifier) used with our RP-based approach.

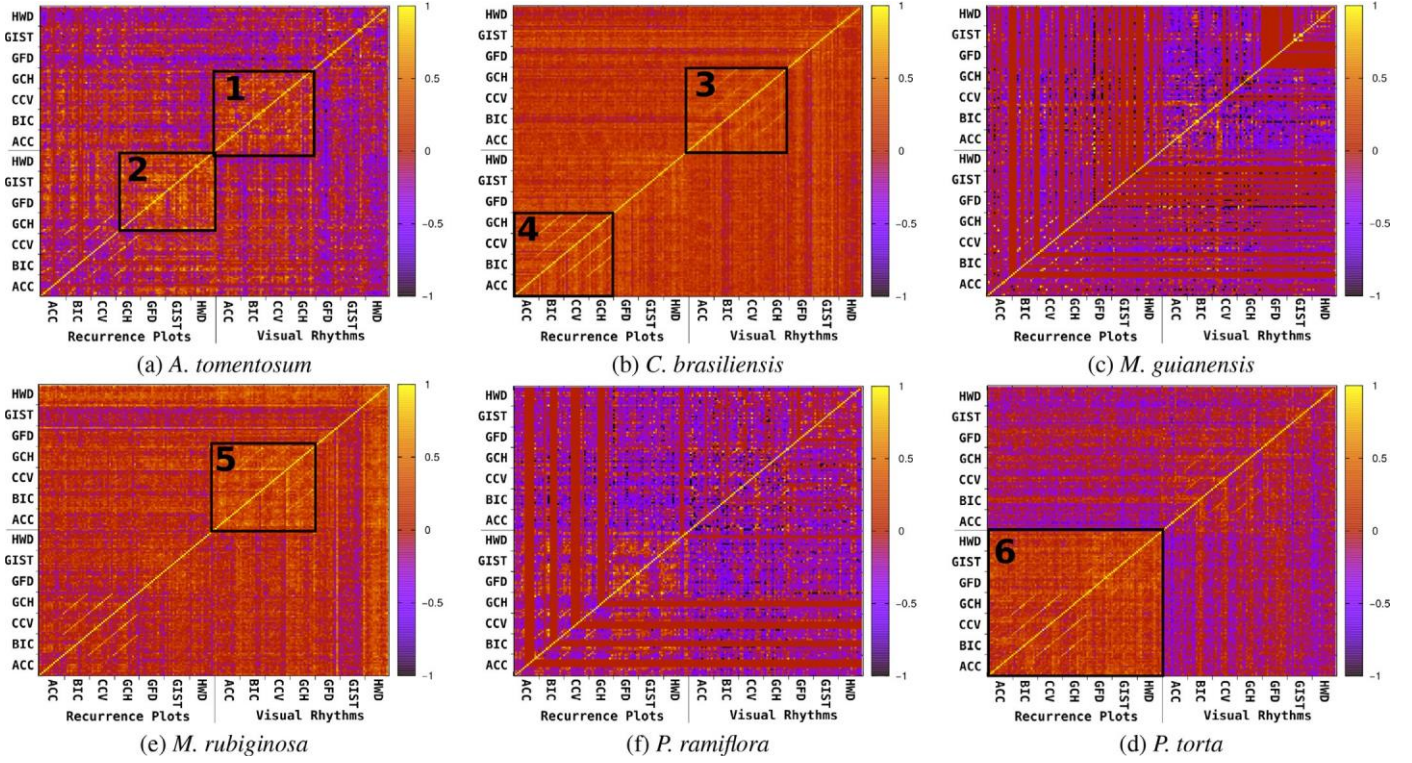
#### 5.2.1. Coarse-grained analysis

Fig. 9 shows two radar charts with effectiveness results of the recurrence plot-based and visual rhythms-based classifiers. These charts are composed of three parts, (1) radius, (2) slice of the perimeter, and (3) lines. The radius means the effectiveness measure values (mean balanced accuracy). The slices of the perimeter means each hours of day, from 6:00 to 18:00 h (UTC-3). Finally, the line means the performance of each kNN-1 learning method with one different image descriptor (ACC, BIC, CCV, GCH, GFD, GIST, and HWD).

Fig. 9 (a) are the seven image descriptors used in this work for visual rhythms-based classifiers and Fig. 9(b) are the same image descriptors for recurrence plots-based classifiers.

As it can be observed, in (a) the best results have been achieved by classifiers that use color image descriptors (ACC, BIC, CCV, and





**Fig. 11.** Correlation analysis considering all 182 available classifiers (2 representation approaches  $\times$  7 image descriptors  $\times$  13 hours = 182 classifiers). The lowest correlation coefficients are closer to the purple color ( $-1$ ) and the highest coefficients are closer to the yellow color ( $+1$ ). (For interpretation of the references to color in this figure legend, the reader is referred to the web version of this article)..

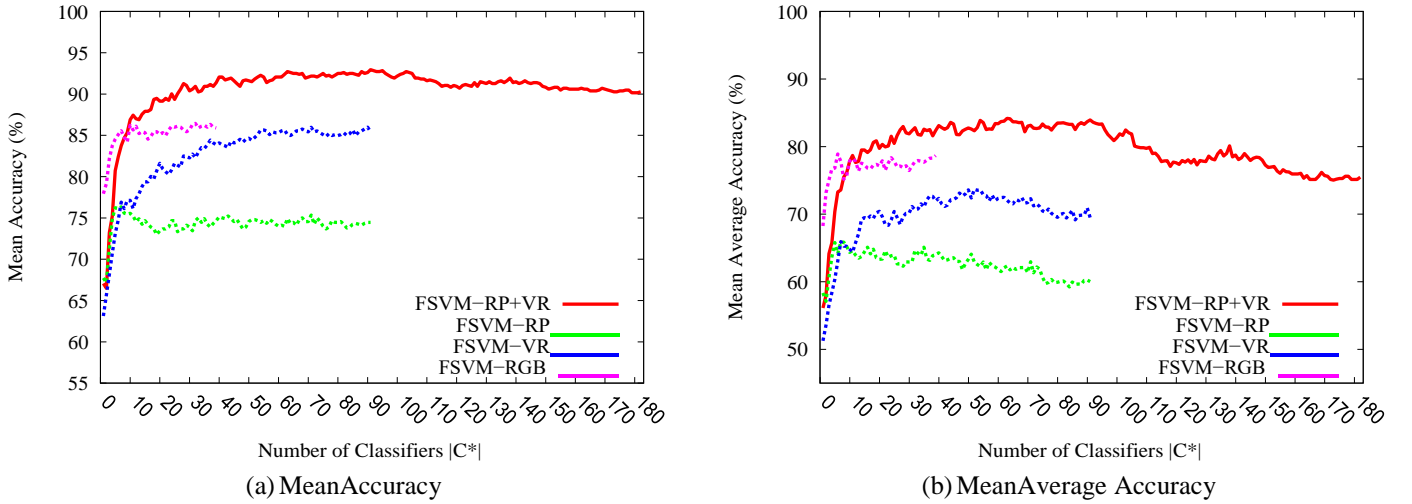


**Fig. 12.** Effectiveness performance considering (a) the mean accuracy and (b) the mean average accuracy when classifiers using RGB channels, RP, VR and both representations are combined.

GCH). However, in (b) the classifiers with texture image descriptors have achieved the best results (GFD, GIST, and HWD).

## 5.2.2. Fine-grained analysis

For a more detailed analysis, we performed a comparison between the RP and VR approaches considering their performance per class for the best achieved results. The best results of the RP and VR approaches were observed when used with GFD (texture) at 18h and BIC (color) at 6h, respectively. Fig. 10 shows this fine-grained analysis.

We can observe that the RP approach achieved better results in four (*C. brasiliensis*, *M. guianensis*, *P. ramiflora*, and *P. torta*) out

of the six species (see Fig. 10). The VR approach, in turn, yields better results for *A. tomentosum* and *M. rubiginosa*. Furthermore, in the experiments with *P. ramiflora*, and *P. torta* species, it is possible to notice a large difference between results achieved by the RP-based and VR-based approaches, around 30% of accuracy in both species.

## 5.3. Correlation analysis between RP-based and VR-based classifiers

This section presents the correlation analysis of each pair of classifiers for all 182 available classifiers aiming to identify

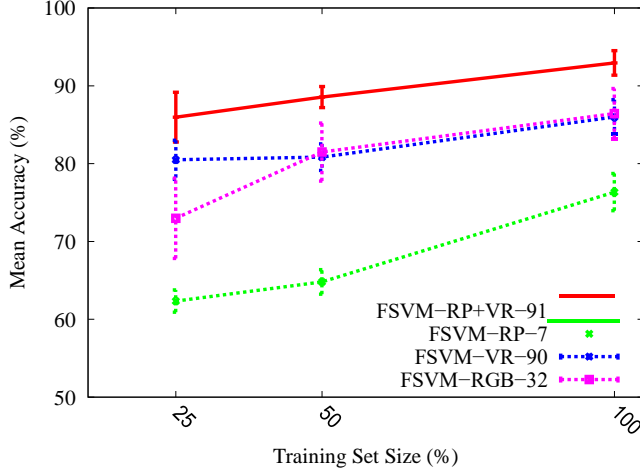


**Fig. 13.** Mean accuracy results of the best amount of classifiers for each approach using training sets with different sizes.

whether they might be combined by any fusion technique (e.g., Adaboost [18], Bagging [10], and meta-learning approach [16]).

The *Correlation Coefficient*  $\rho$  (COR) [25] has been used to assess the correlation of two classifiers  $c_i$  and  $c_j$ :

$$COR(c_i, c_j) = \frac{ad - bc}{(a+b)(c+d)(a+c)(b+d)}, \quad (3)$$

where  $a$  is the percentage of time series that both classifiers  $c_i$  and  $c_j$  classified correctly in a validation set. Value  $b$  is the percentage of time series that  $c_j$  hit and  $c_i$  missed,  $c$  is the opposite of  $b$ . The value  $d$  is the percentage of time series that both classifiers missed. The pairs of classifiers with lower COR values have greater degree of complementarity and are more likely to yield better results when combined. Range of COR is in  $[-1, +1]$ .

Fig. 11 presents the COR values for all possible combinations of pairs of classifiers considering the six classes. The lowest correlation coefficients are closer to the purple color ( $-1$ ) and the highest coefficients are closer to the yellow color ( $+1$ ). Furthermore, in this figure, there are six important regions that have been highlighted and they are explained below.

As we can observe in Fig. 11(a), in region (1), the RP-based classifiers with texture descriptors are more correlated among them. In region (2), the VR-based classifiers with color descriptors are more correlated among them. This fact means that different classifiers that use the same kind of visual properties (color or texture) in these approaches have predicted similar instances of the *A. tomentosum* species. However, outside these two regions, the same scenario can not be observed.

In general, although there are classifiers with high correlation (regions 3, 4, 5, and 6), the great majority of classifiers are non-correlated to each other (see purple color) for different species. Thus, there is a strong indication that the RP-based and VR-based classifiers used in this work might be combined to achieve better results for plant recognition task.

In this sense, we adopt a well successful classifier fusion framework [16] (Section 4.2) to address complementary information provided by RP-based and VR-based classifiers.

#### 5.4. Fusion of RP-based and VR-based classifiers

In this section, we adopt the framework reported in Section 4.2 (FSVM), with the objective of demonstrating that is possible to combine different RP-based and VR-based classifiers and to improve the effectiveness results in the plant recognition

task. In addition, we consider the fusion of RGB channels as a baseline approach [17].

Fig. 12 shows four curves, FSVM-RGB, FSVM-RP, FSVM-VR, and FSVM-RP+VR, which refer to the fusion of the RGB channels, recurrence plot, visual rhythms, and combination of RP and VR, respectively. The suffix FSVM refers to the selection and fusion framework, which was implemented using the SVM classifier in the fusion step (meta-learning).

Two evaluation measures, Accuracy and Average Accuracy, are considered. In these experiments, the framework combines each approach for different numbers of classifiers  $|C^*|$ . In pink, the framework combines  $|C^*| = \{1, \dots, 39\}$  RGB channels-based classifiers ( $39 = 3 \text{ channels} \times 13 \text{ h}$ ). In green, the framework combines RP-based classifiers  $|C^*| = \{2, \dots, 91\}$  ( $91 = 7 \text{ descriptors} \times 13 \text{ h}$ ). In blue, it uses the VR-based classifiers  $|C^*| = \{2, \dots, 91\}$ . Finally, in red, the framework combines all available classifiers (91 RP-based plus 91 VR-based classifiers, leading to a total of 182 classifiers). As we can observe, the fusion framework using both representation (RP+VR) achieved a huge improvement when compared to the use of the two representations in isolation.

As it can be observed, the FSVM-RGB approach has achieved the better results on the range  $1 \dots 8$  classifiers. However, FSVM-RP+VR achieved the best results when more than 8 classifiers are considered ( $9, \dots, 182$ ). Therefore, we could show that recurrence plot and visual rhythms representations address different and complementary information that might be combined to improve the effectiveness of plant identification systems.

#### 5.5. Training set size impact

In this section, we have conducted a study considering three different sizes for the training set (25%, 50%, and 100%), which represents 15%, 30% and 60% of the entire datasets, respectively. These subsets have been selected from original training set.

Fig. 13 shows comparative analysis of the four different approaches FSVM-RGB-32, FSVM-RP-90, FSVM-VR-7, and FSVM-RP+VR-91. Notice that FSVM approaches show up with a numerical suffix  $N$  (e.g.,  $N = \{7, 32, 90, 91\}$ ), which means the number of classifiers each approach has used achieving the best effectiveness results. Furthermore, we used again the 5-fold cross-validation protocol.

Notice that the FSVM-RP+VR-91 approach, which combines RP-based and VR-based classifiers, has achieved better results than other approaches for any training set size.

## 6. Conclusion

In this work, we proposed the use of a technique of nonlinear data analysis for time series representation in plant species recognition task. This technique, called recurrence plot, allows us to represent repeated events (the recurrence of states) on time series into two-dimensional representation. We have extracted feature vector from this new representation through use of different kinds of image descriptor (e.g., color and texture). The created feature vector is then used as input to a learning method, in our case, the  $k$ -Nearest Neighbor method.

The experiments performed in this work showed that there are differences in terms of classification performance depending on the plant species considered, as well as, the low correlation that exists between almost all used classifiers. In these experiments, we observed that texture descriptors describe better the image provided from recurrence plots representation. However, the visual rhythms achieved better results when used in color descriptors.

A correlation analysis between all of classifiers have been performed and we could observe that recurrence plot-based and visual rhythms-based classifiers have low correlation coefficients, i.e.,



both approaches describe complementary information that might be combined by fusion techniques with the objective of producing better effectiveness results in plant recognition tasks.

Furthermore, we have adopted a successful classifier fusion framework [16] to combine RP-based and VR-based classifiers and then improve the effectiveness results. We could show in practice the huge complementarity degree between those time-series representations.

Future work includes the use of other image descriptors to extract different visual features (e.g., shape description approaches based on contour and regions [13]). In addition, the proposed framework can be augmented to consider learning-to-rank methods (e.g., genetic programming [8]) for combining different descriptors. Another point to be explored is the use of RP for multispectral images or multisensor systems, which have more than three time series. In these scenarios, remote sensing approaches for channel selection and combination can be used. Finally, we also plan to perform an extensive study on different strategies for feature selection and classifier fusion.

## Acknowledgments

This research was supported by the [São Paulo Research Foundation FAPESP](#) and [Microsoft Research Virtual Institute](#) (grants [#2010/52113-5](#), [#2013/50169-1](#), and [#2013/50155-0](#)). BA received a master scholarship from CAPES and a doctoral fellowship from FAPESP (grant [#2014/00215-0](#)); LPCM and RST receive a Productivity Research Fellowship from [CNPq](#) (grants [310761/2014-0](#) and [306580/2012-8](#)). Also, we have been benefited from funds of CAPES, CNPq, and FAPESP (grants [#2009/18438-7](#) and [#2010/51307-0](#)).

## References

- [1] U.R. Acharya, S. Vinitha Sree, G. Swapna, R.J. Martis, J.S. Suri, Automated eeg analysis of epilepsy: a review, *Knowl. Based Syst.* 45 (2013) 147–165.
- [2] P.M. Addo, M. Billio, D. Guegan, Nonlinear dynamics and recurrence plots for detecting financial crisis. Documents de travail du Centre d'Economie de la Sorbonne 13024, Universit Pantho-Sorbonne (Paris 1), Centre d'Economie de la Sorbonne, 2013.
- [3] H. Ahrends, S. Etzold, W. Kutsch, R. Stoeckli, R. Bruegger, F. Jeanneret, H. Wanner, N. Buchmann, W. Eugster, Tree phenology and carbon dioxide fluxes: Use of digital photography for process-based interpretation at the ecosystem scale, *Clim. Res.* 39 (2009) 261–274.
- [4] B. Alberton, J. Almeida, R. Henneken, R. da S. Torres, A. Menzel, L.P.C. Morellato, Using phenological cameras to track the green up in a cerrado savanna and its on-the-ground validation, *Ecol. Inform.* 19 (2014) 62–70.
- [5] J. Almeida, J.A. dos Santos, B. Alberton, L.P.C. Morellato, R. da S. Torres, Plant species identification with phenological visual rhythms, in: *Proceedings of the IEEE International Conference on eScience (eScience'13)*, 2013a, pp. 148–154.
- [6] J. Almeida, J.A. dos Santos, B. Alberton, L.P.C. Morellato, R. da S. Torres, Visual rhythm-based time series analysis for phenology studies, in: *Proceedings of the IEEE International Conference on Image Processing (ICIP'13)*, 2013, pp. 4412–4416.
- [7] J. Almeida, J.A. dos Santos, B. Alberton, R. da S. Torres, L.P.C. Morellato, Applying machine learning based on multiscale classifiers to detect remote phenology patterns in cerrado savanna trees, *Ecol. Inform.* 23 (2014) 49–61.
- [8] J. Almeida, J.A. dos Santos, W.O. Miranda, B. Alberton, L.P.C. Morellato, R. da S. Torres, Deriving vegetation indices for phenology analysis using genetic programming, *Ecol. Inform.* 26 (2015) 61–69.
- [9] J. Almeida, J.A. dos Santos, B. Alberton, L.P.C. Morellato, R. da S. Torres, Phenological visual rhythms: compact representations for fine-grained plant species identification, *Pattern Recogn. Lett.* (2016), doi:10.1016/j.patrec.2015.11.028.
- [10] L. Breiman, Bagging predictors, *Mach. Learn.* 24 (2) (1996) 123–140.
- [11] H.-D. Cheng, X. Jiang, Y. Sun, J. Wang, Color image segmentation: advances and prospects, *Pattern Recogn.* 34 (12) (2001) 2259–2281.
- [12] J.C. Conti, F.A. Faria, J. Almeida, B. Alberton, L.P.C. Morellato, J.L. C., R. da S. Torres, Evaluation of time series distance functions in the task of detecting remote phenology patterns, in: *Proceedings of the IEEE International Conference on Pattern Recognition (ICPR'14)*, 2014, pp. 3126–3131.
- [13] R. da S. Torres, M. Hasegawa, S. Tabbone, J. Almeida, J.A. dos Santos, B. Alberton, L.P.C. Morellato, Shape-based time series analysis for remote phenology studies, in: *Proceedings of the IEEE International Geoscience and Remote Sensing Symposium (IGARSS'13)*, 2013, pp. 3598–3601.
- [14] J.W. Eaton, D. Bateman, S. Hauberg, GNU Octave Manual Version 3, Network Theory Ltd., 2008.
- [15] J.-P. Eckmann, S.O. Kamphorst, D. Ruelle, Recurrence plots of dynamical systems, *Europhys. Lett.* 4 (9) (1987) 973.
- [16] F.A. Faria, J.A. dos Santos, A. Rocha, R. da S. Torres, A framework for selection and fusion of pattern classifiers in multimedia recognition, *Pattern Recogn. Lett.* 39 (2014) 52–64.
- [17] F.A. Faria, J. Almeida, B. Alberton, L.P.C. Morellato, A. Rocha, R. da S. Torres, Time series-based classifier fusion for fine-grained plant species recognition, *Pattern Recogn. Lett.* (2016), doi:10.1016/j.patrec.2015.10.016.
- [18] Y. Freund, R.E. Schapire, Experiments with a new boosting algorithm, *Update* (1996) 148–156.
- [19] L. Guigues, J. Cocquerez, H. Le Men, Scale-sets image analysis, *Int. J. Comput. Vis.* 68 (2006) 289–317.
- [20] S.J.F. Guimarães, M. Couprie, A.A. Araújo, N.J. Leite, Video segmentation based on 2D image analysis, *Pattern Recogn. Lett.* 24 (7) (2003) 947–957.
- [21] J. Huang, R. Kumar, M. Mitra, W. Zhu, R. Zabih, Image indexing using color correlograms, in: *Proceedings of the IEEE International Conference on Computer Vision and Pattern Recognition (CVPR'97)*, 1997, pp. 762–768.
- [22] C.E. Jacobs, A. Finkelstein, D.H. Salesin, Fast multiresolution image querying, in: *Proceedings of the International Conference on Computer Graphics and Interactive Techniques (SIGGRAPH'95)*, 1995, pp. 277–286.
- [23] E.J. Keogh, K. Chakrabarti, S. Mehrotra, M.J. Pazzani, Locally adaptive dimensionality reduction for indexing large time series databases, in: *Proceedings of the ACM SIGMOD International Conference on Management of Data (ACM SIGMOD'01)*, 2001, pp. 151–162.
- [24] K. Kulkarni, P. Turaga, Recurrence textures for human activity recognition from compressive cameras, in: *Proceedings of the IEEE International Conference on Image Processing (ICIP'12)*, 2012, pp. 1417–1420.
- [25] L.I. Kuncheva, *Combining Pattern Classifiers: Methods and Algorithms*, Wiley-Interscience, 2004.
- [26] J. Lin, E.J. Keogh, L. Wei, S. Lonardi, Experiencing SAX: a novel symbolic representation of time series, *Data Min. Knowl. Discov.* 15 (2) (2007) 107–144.
- [27] L.P.C. Morellato, R.R. Rodrigues, H.F. Leitão Filho, C.A. Joly, Estudo comparativo da fenologia de espécies arbóreas de floresta de altitude e floresta mesófila semidecídua na serra do Iapi, Jundiá, São Paulo, Brazil. *J. Botany* 12 (1989) 85–98.
- [28] C.W. Ngo, T.C. Pong, R.T. Chin, Detection of gradual transitions through temporal slice analysis, in: *Proceedings of the IEEE International Conference on Computer Vision and Pattern Recognition (CVPR'99)*, 1999, pp. 1036–1041.
- [29] A. Oliva, A. Torralba, Modeling the shape of the scene: a holistic representation of the spatial envelope, *Int. J. Comput. Vis.* 42 (3) (2001) 145–175.
- [30] G. Pass, R. Zabih, J. Miller, Comparing images using color coherence vectors, in: *Proceedings of the ACM International Conference on Multimedia (ACM-MM'96)*, 1996, pp. 65–73.
- [31] I. Popivanov, R.J. Miller, Similarity search over time-series data using wavelets, in: *Proceedings of the IEEE International Conference on Data Engineering (ICDE'02)*, 2002, pp. 212–221.
- [32] P. Reys, M.G.G. Camargo, A.P. Teixeira, M.A. Assis, M.T. Grombone-Guaratini, L.P.C. Morellato, Estrutura e composição florística entre borda e interior de um cerrado sensu stricto e sua importância para propostas de recuperação, *Hoennea* 40 (3) (2013) 437–452.
- [33] A.D. Richardson, B.H. Braswell, D.Y. Hollinger, J.P. Jenkins, S.V. Ollinger, Near-surface remote sensing of spatial and temporal variation in canopy phenology, *Ecol. Appl.* 19 (2009) 1417–1428.
- [34] A.D. Richardson, J.P. Jenkins, B.H. Braswell, D.Y. Hollinger, S.V. Ollinger, M.L. Smith, Use of digital webcam images to track spring green-up in a deciduous broadleaf forest, *Oecologia* 152 (2007) 323–334.
- [35] M.D. Schwartz, *Phenology: An Integrative Environmental Science*, Springer, 2013.
- [36] D.F. Silva, V.M.A. de Souza, G.E.A.P.A. Batista, Time series classification using compression distance of recurrence plots, in: *Proceedings of the IEEE International Conference on Data Mining (ICDM'13)*, 2013, pp. 687–696.
- [37] V.M.A. Souza, D.F. Silva, G.E.A.P.A. Batista, Extracting texture features for time series classification, in: *Proceedings of the IEEE International Conference on Pattern Recognition (ICPR'14)*, 2014, pp. 1425–1430.
- [38] R. Stehling, M. Nascimento, A. Falcao, A compact and efficient image retrieval approach based on border/interior pixel classification, in: *Proceedings of the ACM International Conference on Information and Knowledge Management (CIKM'02)*, 2002, pp. 102–109.
- [39] M. Swain, D. Ballard, Color indexing, *Int. J. Comput. Vis.* 7 (1) (1991) 11–32.
- [40] X. Wang, A. Mueen, H. Ding, G. Trajcevski, P. Scheuermann, E.J. Keogh, Experimental comparison of representation methods and distance measures for time series data, *Data Min. Knowl. Discov.* 26 (2) (2013) 275–309.
- [41] D.M. Woebecke, G.E. Meyer, K. Von Bargen, D.A. Mortensen, Color indices for weed identification under various soil, residue, and lighting conditions, *Trans. ASAE* 38 (1995) 259–269.
- [42] D. Zhang, G. Lu, Shape-based image retrieval using generic fourier descriptor, *Signal Process.: Image Commun.* 17 (10) (2002) 825–848.

### Appendix E

Article published in the Journal Pattern Recognition Letters:

LEITE, R.A., SCHNORR, L, ALMEIDA JR, TORRES, R.S., ALBERTON, B., MORELLATO, LPC, COMBA, J. PhenoVis – Visual Phenological Analysis of Forest Ecosystems. **Information Sciences**, v. 372, p. 181-195, 2016.

Text formatting according to the Journal Information Sciences.

## PhenoVis – A tool for visual phenological analysis of digital camera images using chronological percentage maps

Roger A. Leite<sup>a</sup>, Lucas Mello Schnorr<sup>a</sup>, Jurandy Almeida<sup>b,d</sup>, Bruna Alberton<sup>c</sup>, Leonor Patricia C. Morellato<sup>c</sup>, Ricardo da S. Torres<sup>d</sup>, João L.D. Comba<sup>a,\*</sup>

<sup>a</sup> Institute of Informatics, Federal University of Rio Grande do Sul – UFRGS, Porto Alegre RS–91501-970 Brazil

<sup>b</sup> Institute of Science and Technology, Federal University of São Paulo – UNIFESP, São José dos Campos, SP–12247-014 Brazil

<sup>c</sup> Dept. of Botany, São Paulo State University – UNESP, Rio Claro, SP–13506-900 Brazil

<sup>d</sup> Institute of Computing, University of Campinas – UNICAMP Campinas, SP–13083-852 Brazil

**Keywords:** Phenology, Remote sensing, Vegetation index, Visual analytics, Similarity ranking

### 1. Introduction

Phenology studies the periodic phenomena of plants and their relationship to environmental conditions [39]. This analysis is crucial for accessing the impact on vegetation and ecosystem processes [29,32,39,42]. Examples of cyclic phenomena include flowering and fruiting in plants and the breeding season of birds and frogs, among others. The remote monitoring of vegetations using cameras has proved to be a promising approach to the study of plant phenology [30,38,40]. In this scenario, cameras capture daily pictures from a specific viewpoint at a specific time of the day. By comparing a sequence of images over time, it is possible to identify changes that are associated with phenological events [38]. For example, images that have a high number of pixels with dominant shades of green are often associated with areas mostly covered by leaves.

Due to the large number of images (at least 365 images per year), the visual analysis of large collections of images becomes too complex to be performed interactively. Instead, a single chromatic value is computed to represent the average color in each image. Among several chromatic coefficients described in the literature, the green chromatic coefficient ( $g_{cc}$ ) is widely used by the phenology community to understand periodic leafing patterns extracted from digital images [40]. The collection of values computed in the period of interest (usually one year) is displayed as a 2D line plot [3], and the analysis

\* Corresponding author. Fax: +55 (51) 3308-7308.

*E-mail addresses:* rogeraleite@gmail.com (R.A. Leite), schnorr@inf.ufrgs.br (L.M. Schnorr), jurandy.almeida@unifesp.br (J. Almeida), bru.alberton@gmail.com (B. Alberton), pmorella@rc.unesp.br (L.P.C. Morellato), rtorres@ic.unicamp.br (R.d.S. Torres), comba@inf.ufrgs.br, joao.comba@gmail.com (J.L.D. Comba).

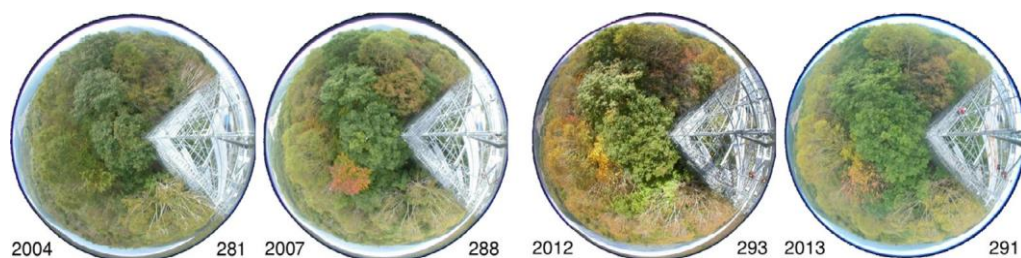


**Fig. 1.** Images of the Takayama forest from different years (2004, 2007, 2012, and 2013) and days (281, 288, 293, and 291), generated by the Phenological Eyes Network (PEN). Although the images look very different, they have the same average  $g_{cc} = 0.3905$ .



of this plot is used to identify interesting phenological events. It is well known that using the average as a comparison metric to analyze the images can potentially overlook important patterns and thus lead to wrong conclusions [14]. One motivation for this research is to address the shortcomings of using average scores in near-surface remote phenology.

Fig. 1 illustrates the problem with the average in four different images captured by the same device on different dates. Each image looks different when compared to the others, but all of them share the same  $g_{cc}$  average of 0.3905 (the pixels associated with the metallic structure are discarded). Therefore, by using the traditional average-based approach, phenologists will be led to conclude that these four images are the same even if they are completely different in reality. The similar distribution of the shades of green, yellow and brown in the images indicates that 2012 was a full fall season, whereas in 2004 the levels of green were much higher (Fig. 1).

In this work, we introduce PhenoVis, a visual analytics tool that aims at providing insightful ways to analyze phenological data. The main idea behind PhenoVis is the creation of more expressive visual encodings for phenological data visualization. We introduce the Chronological Percentage Maps (CPMs), a visual mapping technique that combines derived distributions from all images of a given year to create normalized stacked bar charts. Another problem we address is the lack of automation in the search for regular patterns in plant phenology. Current research in the field frequently uses the analyst's intuition to find patterns of plant phenology. This approach is potentially time-consuming, error-prone and unable to scale to larger datasets. PhenoVis uses the additional information encoded to support similarity searches, which is useful for comparing data from different years. It also provides a customizable multi-rank comparison of data from different years, with filters of specific periods within a year or sub-regions associated with given plant species.

In summary, we offer the following contributions: (a) PhenoVis, a visual analytics tool to perform a comparative analysis of phenological data for multiple years; (b) the design of CPMs, in which a more expressive representation of phenological data using percentage distributions is combined with a visual expression of this information using color-coded normalized stacked bar charts; (c) similarity algorithms that allow the search for similar phenological patterns across years, occurring in either a fixed or moving window of time; (d) customizable ranking comparison of years, with filters that allow selections of specific time periods or regions; and (e) case studies that validate PhenoVis in phenological analysis tasks such as pattern and outlier identification.

## 2. Related work

Below, we review visual analytics and information visualization techniques and approaches to analyse phenological data extracted from images.

### 2.1. Visualization and data Analysis

There is an extensive literature in the information visualization and visual analytics community on different ways to visually present information and to extract patterns from data [25]. Rectangular regions such as matrices are a common alternative for presenting aggregated data to allow identification of patterns. Pixel bar charts extend traditional bar charts by coloring pixels inside bars to represent information derived from data attributes [26]. The visual presentation of data follows a pixel-placement ordering, which was demonstrated to reveal patterns in data [24] as well as provide support for data mining queries. The underlying motivation behind pixel bars was an inspiration when designing PhenoVis, particularly the CPM representation and the ability to search for similar patterns in CPMs of different years.

There are several works that use matrix-encoded information to perform visual analysis. Stacked bar charts are used to display the temporal changes of traffic speed data in [8]. The normalized stacked bar charts used in CPMs resemble the images showed in their work, especially when using a categorical color mapping. The analysis of visual traffic also appears in [43], with trajectory information chronologically encoded into a

matrix. Matrices are used to compare genomic sequences in [2,34]. BallotMaps encode the votes received by politicians into matrices to identify voting patterns [46]. The Flowstrates approach encodes origin-destination data into a heatmap matrix, re-ordering rows to reveal interesting patterns [9]. In [36], a matrix encoding heart-rate information is used to identify unusual patterns during a running race. The exploration of dynamic graphs using matrix-encoded information is given in [12] and [18]. Climate change comparison using a global radial map is presented in [27]. Although it uses a radial representation, the compact representation resembles the CPM stacked bar charts. ThemeRiver [11,19,20] offers an alternative to stacked bar charts by displaying information in layers that are stacked in a symmetrical shape centered around the x-axis. This approach allows easy identification of predominant layers in time, particularly for datasets comprising a great number of layers. LineUp describes different ways to present multi-ranking attributes [17]. The multi-ranking visualization used in our work reveals the need for ranking visualization when performing comparative phenology analysis. We refer the reader to [1] for a comprehensive survey of other ways to perform visual analysis of time-oriented data.

## 22. *Phenological analysis*

Phenology analysis of satellite images often relies on average plots of computed vegetation indices. A web-based interface described in [10] displays time-series obtained from phenological and meteorological observations. TimeStats is a free software that offers tools for the visualization of long-term remote sensing data archives such as parametric and non-parametric methods for trend detection, linear regression, and frequency analysis [41]. EcoIP, a toolkit to estimate the onset and ending dates of phenological phases of plant species, relies on a Naïve Bayesian model created from a set of training images, which is used to provide temporal estimators [16]. A variety of color transformations is used to adjust the accuracy of the estimations. Another recent trend refers to the construction of toolboxes. Eerens, for example, developed SPIRITS, a stand-alone toolbox to produce evidence-based information for crop production analysts [13]. It includes a large number of features to analyze image time series and to create maps and graphs for vegetation status analysis. Different from those initiatives, our proposal relies on visual encodings designed to capture distribution aspects from vegetation data. A similar approach is taken in [5] and [6], which presented different strategies for encoding image time series as visual rhythms [33]. Such representations have proven to be a powerful tool for distinguishing the behavior of different plant species. The visual rhythm construction is similar to the CPM extraction process in the sense that they summarize image sequences in a single image representation. Despite the good results observed concerning the use of visual rhythm, no visual analytics tool has been proposed.

## 3. **PhenoVis**

PhenoVis is a visualization tool that includes a visual mapping representation called CPM, data analysis algorithms for identifying similar patterns in different years, and a ranking visualization module to present the similarity results. In this section, we describe each of these modules.

### 3.1. *Chronological percentage maps (CPMs)*

CPM is the main concept behind PhenoVis. Its construction consists of six steps that transform a sequence of images into a normalized stacked bar chart, as shown in Fig. 2. We detail these steps in the following sections.

#### *Step 1: Filtering by region of interest (ROI)*

The region of interest (ROI) (also called mask) is a portion of the input image that is the focus of the analysis, thus removing irrelevant areas that lack vegetation such as the observation tower. The ROI is user-configurable and implemented through a mask with the same dimensions as the input images. The mask is composed of black

and white pixels (a stencil image), where white represents selected regions. Two types of masks are used in PhenoVis: a community mask [21], which considers all plant species in the image; and a species mask [30], associated with a given plant species.

### Step 2: Data transformation using a vegetation index

The phenophases and length of the growing season (from start to end) are indicators of plant development across different years. The phenological analysis from images focuses on the following four checkpoints (or phenophases) of plant development [21,30]:

- Leaf expansion: plants start to turn green, and leaves are expanding;
- Peak or maturity: leaf growth reaches a plateau; i.e., leaves reach full size;
- Leaf fall or senescence: leaves change colors and start to fall;
- Post leaf fall: there are no leaves on the tree, representing the end of the growing season.

Among the several images taken at different times of the day, the image taken at noon is preferred for the analysis because it minimizes shadow effects. Therefore, only one image per day is used. The analysis considers the chromatic coefficients associated with each pixel in the image. Different vegetation indexes are described in [40]. The RGB chromatic coefficients ( $r_{cc}$ ,  $g_{cc}$  and  $b_{cc}$ ) are defined by respectively dividing each component (R, G, or B) by the sum of the other components ( $R + G + B$ ). The average plot of  $g_{cc}$  is a good indicator of phenophases due to the encoding of green pigments (e.g., chlorophyll) in leaves. Although most of our analysis used the  $g_{cc}$  chromatic coefficient, we also experimented with the *hue* index discussed in [15]. To use this index, it is necessary to convert colors from the RGB color space into the HSV (also called HSI) color space [44], which represents colors as hue (H), saturation (or lightness) (S), and value (or brightness) (V). HSV is associated with a single line of the CPM. In this example, all lines of the CPM are stacked in landscape mode.

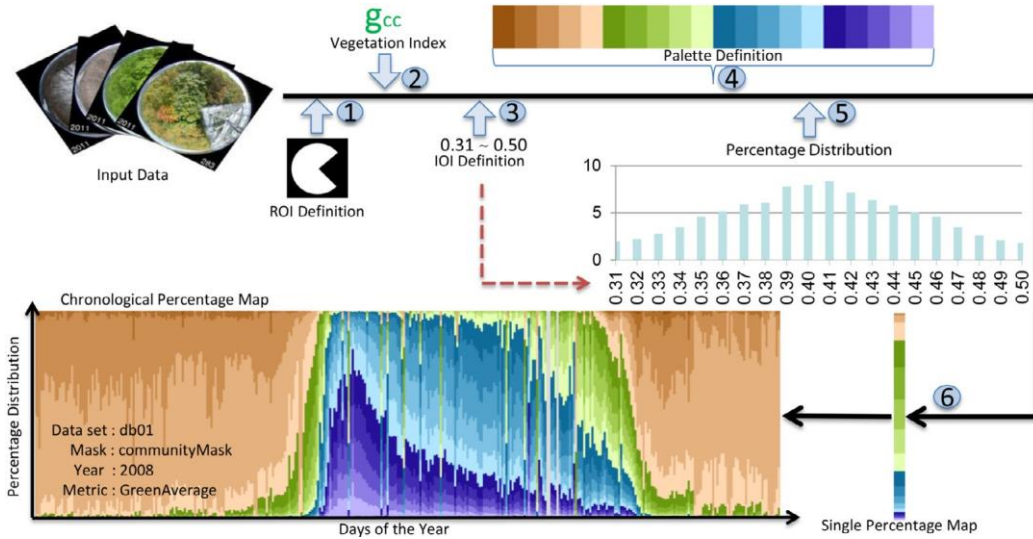


**Fig. 2.** The Chronological Percentage Map's six-step construction: (1) images are filtered by the community mask that defines the region of interest (ROI); (2) phenology metric ( $g_{cc}$ ) is computed; (3) interval of interest (IOI) filters the resulting values; (4) selection of the distribution granularity and associated color values; (5) percentage distribution is computed; (6) mapping color values to the percentage distribution. Each image generates a stacked bar chart defined in a cone using cylindrical coordinates, with shading variations defined by the angle around the central vertical axis of the cone (the hue component).

### Step 3: Filtering by interval of interest (IOI)

Each vegetation index has values in a particular range. For example,  $g_{cc}$  is normalized between 0 and 1. In practice, the range of  $g_{cc}$  found in vegetation images is much smaller, usually between 0.3 and 0.5 [47]. Since we compute a histogram of vegetation indexes, we narrow the limits of the histogram to a user-specified interval of interest (IOI), as shown in Fig. 2, step 3.

#### Step 4: Color palette and histogram granularity

Selecting a good color palette is essential in data analysis [28]. In PhenoVis we associate different colors with each bucket of the percentage histogram. The histogram granularity defines the size of a given bucket of the percentage distribution. The number of buckets is given by the number of colors available, and the range of the distribution is given by the IOI. There are trade-offs when selecting the size of the IOI, granularity, and the number of colors. For example, if the interval is small

and the number of colors is large, each dimension of the IOI will be semantically irrelevant because of the resultant tiny grain size. The same problem appears if the interval is too large and the number of colors is small. The best situation arises when there is a balance between the size of the IOI and the number of colors. The typical IOI for the  $g_{cc}$  varies from 0.3 to 0.5. Therefore, we chose 20 colors, with each bucket size being 0.01 wide.

For convenience, we have pre-defined a set of palettes. From this set, the categorical color table in Fig. 2, step 4 was the preferred choice when using  $g_{cc}$  indexes. The palette has four categories with different colors. Each of the five internal divisions of these four zones has distinct levels of saturation (from dark to light brown, for example). On the other hand, the standard hue color table is the choice when using *hue* indexes.

#### Step 5: Calculating the percentage data distribution

Each pixel in a given input image contributes one vegetation index value to the analysis, and when this value is multiplied by the number of images in a year (365), a huge amount of data is generated. Instead, the average of all indexes in an image is used, leading to only 365 indexes. Average plots of these indexes help identify phenophases; however, this analysis may be misleading since different images might have the same index (see Fig. 1). In PhenoVis, we store more information about each image than a single vegetation index. We use a histogram instead to encode the percentage distribution of vegetation indexes in an image. The range of the histogram is defined by the IOI, and the number of buckets by the size of color palette used. For indexes outside the IOI, we either discard the values or clamp them to the nearest extreme bucket. We repeat this process to compute one percentage distribution for each image.

In some situations two distinct RGB colors may have the same  $g_{cc}$  (Fig. 3), and would therefore be accumulated in the same histogram bin and mapped to the same color. In these situations, the *hue* index can be used alternatively. The corresponding hue values in Fig. 3 are different and can be mapped to distinct colors. Shades of green can be found around hue values of 120. In addition, the mapping of hues into colors can use the standard HSV palette at fixed *S* and *V* values. We did not replace  $g_{cc}$  by the *hue* index, but used it to gain additional insights when looking at the data.

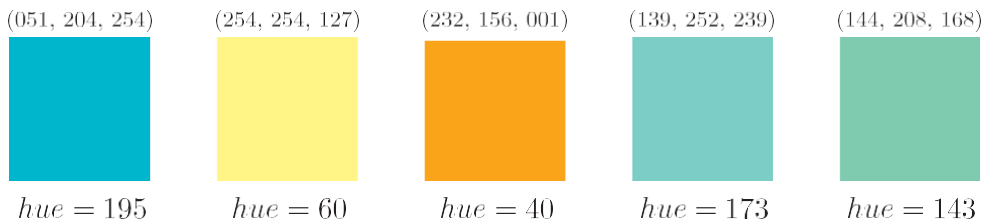


**Fig. 3.** Colors with the same  $g_{cc}$  of 0.4 (RGB codes are shown above each color). On the other hand, the corresponding *hue* values are distinct. By using the *hue* values to separate these colors, the histogram can better aggregate shades of green into closer bins.

### Step 6: Creating the normalized stacked bar chart

The percentage map of a single input image consists of a normalized stacked bar chart (vertical bar in Fig. 2, step 6). In this example, the height of the chart is proportional to the frequency count in the percentage distribution of the vegetation indexes. The width is associated with the number of pixels available for drawing the percentage map. Colors are defined by the palette being used and their corresponding histogram entries.

The chronological percentage map consists of a sequence of percentage maps stacked in chronological order, from top to bottom (portrait) or left to right (landscape). In our analysis, each CPM corresponds to all images from a single year. Fig. 4 and Fig. 5 demonstrate the percentage map and CPM chart for images captured in Japan (the TKY dataset [31,35]). Fig. 4 illustrates percentage maps for individual days of 2006; each map uses two vegetation indexes. The first one uses  $g_{cc}$

and a categorical color table where shades of green, blue, and purple respectively correspond to  $g_{cc}$  values between 35–40%, 40–45%, and 45–50%. The second one uses the *hue* index and the hue color mapping. The color mapping is applied over the input camera to illustrate the shading variations for each chromatic coefficient. Fig. 5 shows the complete CPM for all days in 2006. Higher  $g_{cc}$  values are associated with greener regions, and a clear pattern of growing season emerges in the middle of the year. In the hue mapping, the growing season is associated with shades of green. Fig. 5 illustrates CPM charts that use different vegetation indexes for the year 2006. This CPM allows us to investigate interesting patterns outside the growing season, which displays shades of red and blue.

## 32. Multi-year phenological analysis

The comparative analysis of data from different years is one question that drives plant phenological analysis. The comparison of the starting dates of a given phenophase (e.g. start of leaf growing season) allows us to identify how these values changed with the progression of the years. Automated similarity comparison of different phenophases is important in this process. PhenoVis provides an automatic similarity analysis, because more data is encoded in percentage distributions. The user can select a time interval directly over the CPM of one year, and PhenoVis will suggest a similarity rank of the other years based on this pattern. In this section, we describe how PhenoVis performs the similarity search and displays the visualization results.

### 32.1. Search period and ROIs

PhenoVis allows the user to define any period of a given year to serve as the basis of comparison against other years. This period of interest used for searches can be manually configured in the interface by specifying start and end dates. Since most queries are related to the analysis of pattern variations in specific phenophases, such as the leaf expansion or fall period, we allowed the user to select the period of interest from pre-defined phenophases. The search can be performed over the ROI of all plant species in the image (community mask), other pre-defined masks of any given species, or any region in general specified by the user.

### 32.2. Similarity metrics

PhenoVis offers four similarity techniques for automatic search: Mean Absolute Error (MAE), Mean Square Error (MSE), Mean Absolute Percentage Error (MAPE), and the Kullback-Leibler Divergence (KLD) as described in the supplementary material. The MAE is a usual estimator of the difference between two matrices. Used for the same reasons, MSE highlights significant gaps between values due to squared distance computations and is not recommended for noisy datasets. MAPE is a normalized solution based on the percentage of the similarity for two samples, while the KLD is a non-symmetric measure of the difference between probability distributions. The similarity is computed using two CPMs as input. The first parameter is the CPM query, defined by its start and end dates. The second parameter is the CPM candidate, which will necessarily have the same number of days as the target, but the start date may differ. The percentage distribution associated with each CPM subset is interpreted as a matrix of values in which the similarity metric is computed. Errors are computed for each matrix entry and accumulated in the resulting similarity error.



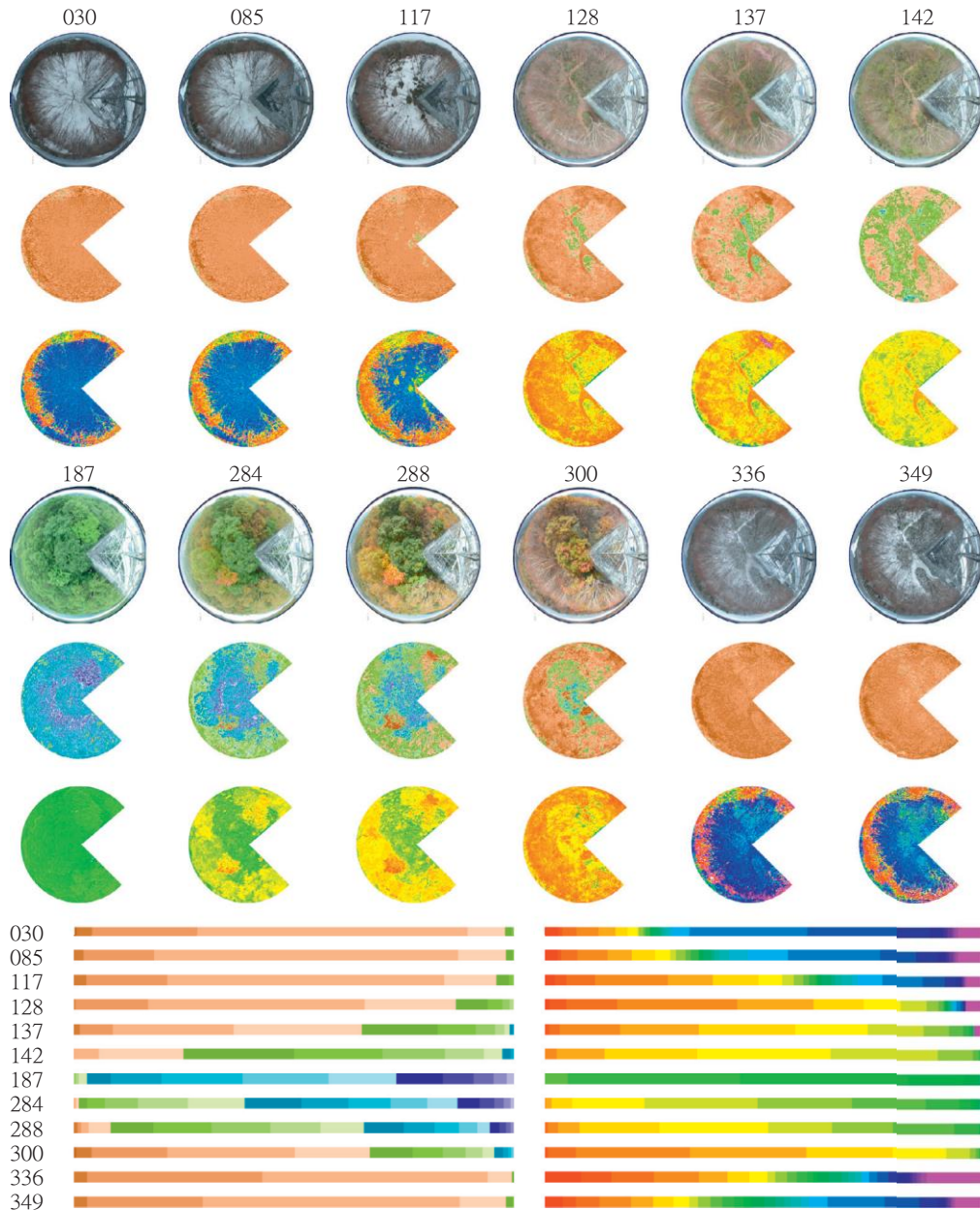


**Fig. 4.** Percentage maps for 12 days: original data for the respective days (row 1 and 4), recoloring of pixels using  $g_{cc}$  and a brown-green-blue-purple color mapping (rows 2 and 5), and recoloring using the hue index and hue mapping (rows 3 and 6). The percentage maps for the  $g_{cc}$  (left) and hue (right) indexes are shown.

### 323. Searching windows and filters

The query defines a time period in the CPM of a given year. The search for similar patterns looks for CPM subsets that have the same number of days as the query pattern. This search is implemented in two configurable ways. The first one, referred to as fixed window, looks for CPM subsets with matching start and end dates. The result of this comparison gives the years in which the same pattern occurred on the same days of the year. In the second way, referred to as moving window, the search looks for the same pattern but does not fix the starting day, allowing the window to move throughout the year. This search finds patterns that happened at a different time of the year (e.g., a late growing season) in other years. We also implemented a filter that allows a subset of the percentage distribution to be considered. If the analysis is interested only in  $g_{cc}$  values in the interval of 40% to 45%, the similarity search can be set to filter out values outside this interval. We also have an outlier filter that removes outliers (missing data or odd days) from the similarity search. An automatic outlier detection was implemented by taking into account the percentage distribution of a given day and the distribution of adjacent days.

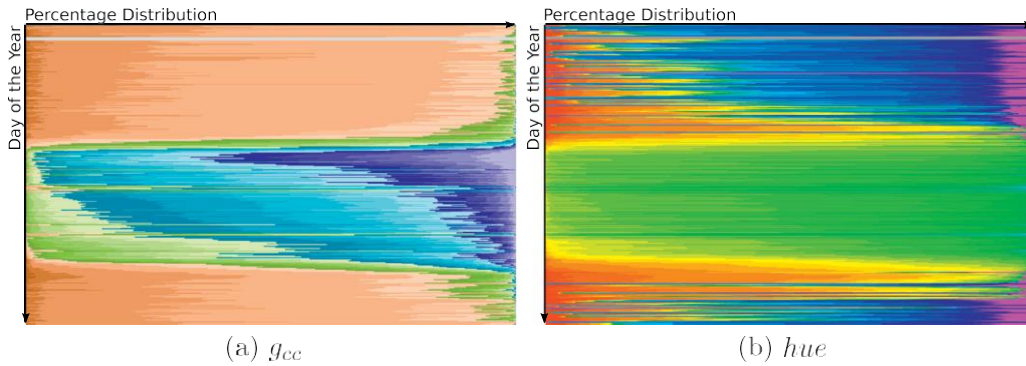


**Fig. 5.** CPM example for 365 days displayed in portrait mode. Each line corresponds to a normalized stacked bar chart mapped to the predefined color table: (a) categorical color table using the  $g_{cc}$  index, (b) HSV color table using the  $hue$  index.

### 3.3. Single and multi-year ranking

PhenoVis is also capable of creating a single or multi-year ranking according to the query and selected similarity technique. The ranking includes the distributions for different years in order of similarity and the similarity error, which allows the evaluation of how the years differ among them. The single-year ranking generates a histogram plot that allows the comparison of one specific year's distribution against all others. The goal of this ranking is to compare the phenophases of one year against the others. In the case of a moving window, the ranking also includes the distance (in days) of the closest pattern.

The multi-year ranking creates similarity searches between a pair of ROIs in a given period of time for every pair of years. This process first results several histogram plots, one for each year, that indicate how close or distant the other years are. These histograms can be normalized as needed; in PhenoVis we use three normalizations: single-year normalization, multi-year normalization, and global normalization (using the data for all years and all pairwise comparisons). The resulting histograms are drawn in red, green and blue, respectively. The second result is a histogram plot that summarizes the individual yearly histogram plots by associating a distance from one year to the others. In other words, this histogram displays the most common year and the most different years as distances between each other, which allows us to easily identify the average years. The resultant histogram is drawn in magenta. Fig. 6 illustrates the interface of PhenoVis, and samples of these histograms are shown in Fig. 6(b).

## 4. Visualization results and discussion

PhenoVis was implemented using the programming language *Processing* [37]. The input to the system is a collection of raw images grouped by year and a mask image that defines the region of interest. In off-line computation, the mask is applied for all input images, and the percentage distributions are computed and stored. PhenoVis was tested, under permission, with the Takayama Flux Site (TKY) dataset of the Phenological Eyes Network (PEN) [31,35]<sup>1</sup>. TKY is located in Japan, which has images from multiple years (from 2004 onward) of a deciduous broadleaf forest [30]. For the results below we used the  $600 \times 600$  image resolution database due to its reduced pre-processing time. Experiments conducted with the larger resolution dataset ( $2272 \times 1704$ ) showed similar results to the smaller dataset. We aim to extend our prototype for the larger resolution datasets, possibly using parallel computation to speed-up pre-processing time. We used the same regions of interest defined by [30] to identify three species: *Betula Ermanii*, *Quercus Crispula*, and *Acer Rufinerve*. Fig. 7 illustrates the location of the species in the image. A discussion of the results obtained using the TKY dataset can also be found in [22,23]. Our results use the following phenological phases described in [30] to evaluate the TKY dataset:

- Bud dormancy (BD): from January to early April (days 1 to 100);
- Leaf Expansion (LE): from late May to late June (days 140 to 180);
- Peak period (Peak): from early July to mid-September (days 181 to 258);
- Leaf Fall (LF): from late September to early November (days 263 to 315);
- Post Leaf Fall (PLF): from mid-November to late December (days 319 to 365);

<sup>1</sup> (<http://www.pheno-eye.org>).

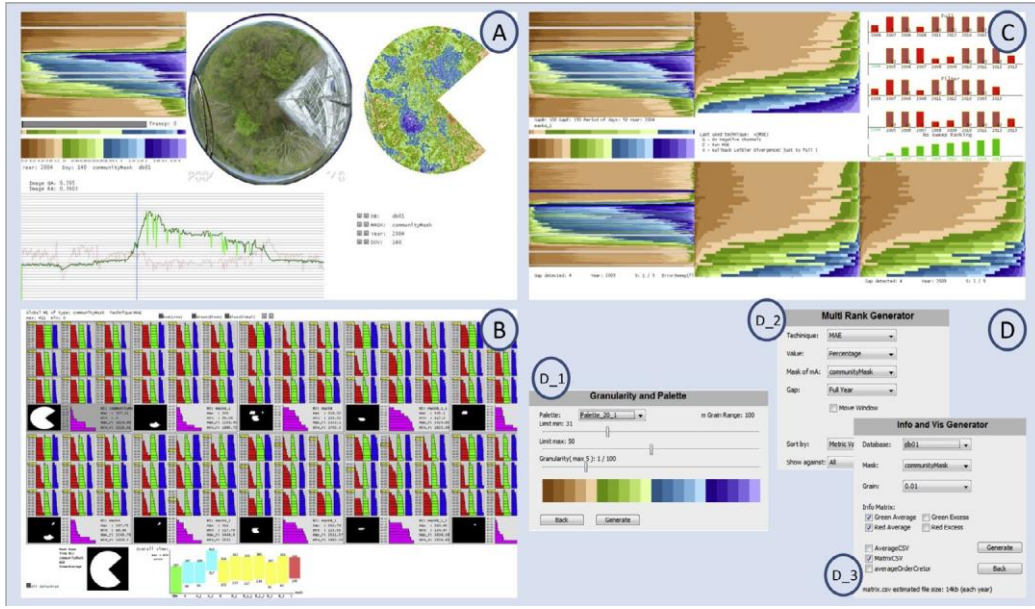


**Fig. 6.** Selected screenshots of the PhenoVis interface: (A) CPM analysis mode, with interaction to inspect individual images and specify query windows; (B) multi-rank results with pairwise comparison of all years; (C) single-rank results using fixed and moving windows. In (D), we display additional windows for configuring search parameters.

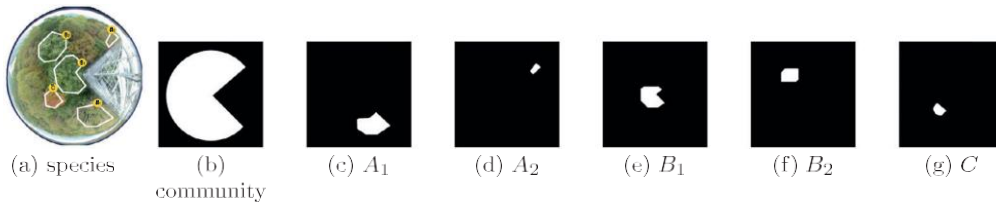


**Fig. 7.** Species location (a) and their masks: (b) community, (c) and (d) *Betula ermanii* (A1 and A2), (e) and (f) *Quercus crispula* (B1 and B2), and (g) *Acer rufinerve* (C)

The realization and evaluation of experiments received feedback from the phenology experts involved in this research. Selected screenshots of the interface are shown in Fig. 6. To increase the reproducibility of our work, we prepared a git repository with the core programs of PhenoVis<sup>2</sup>.

#### 4.1. CPM evaluation

In this section, we compare the CPM representation against average plots used in phenological studies, an evaluation of the CPM expressive power, and a novel outcome that consists of using the CPM as a species signature.

##### 4.1.1. Comparison against average-based plots

We use an example to illustrate how the CPM better displays changes in the data throughout the year than average plots. Fig. 8 shows the average plot based on the  $g_{cc}$  and  $r_{cc}$  (displayed as a green or red line) over the CPM for 2006. While the average has changed over time, it fails to illustrate the data's composition as CPM does. In the  $r_{cc}$  plot, we observe that the shading variations during the leaf-fall period can be easily spotted in the CPM. The red channel indicates the leaf senescence, which occurs in the fall; an expanded discussion on this can be found in [40].

Fig. 9 shows the difference between percentage maps and plots that have the same average. It shows four percentage maps of different days with the same  $g_{cc} = 0.3905$ . Although they have the same  $g_{cc}$  average, the percentage map is clearly different. Percentage maps and CPMs allow us to inspect differences in ways that average plots can not.



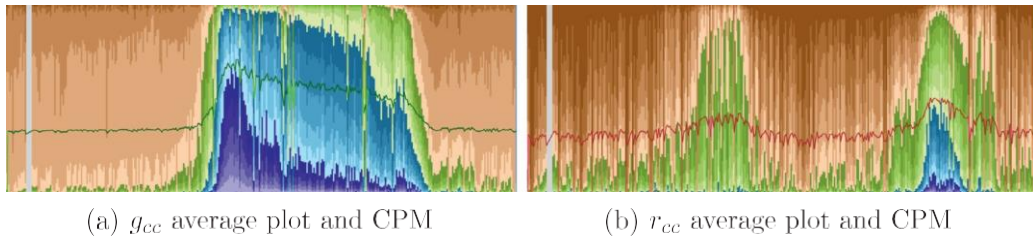


**Fig. 8.** CPM (landscape mode) and the corresponding  $g_{cc}$  and  $r_{cc}$  for the year (DOY) of 2006. The CPM better expresses the changes in the data than the average plots,



**Fig. 9.** Four percentage maps with the same  $g_{cc}$  average (0.3905). In the CPM representation, they show different aspects. The color palette is described in Step 4, Section 3.1.

#### 4.12. CPM expressive power

The side-by-side comparison of CPMs can reveal relevant patterns on the data. In Fig. 10, we give CPMs for the years 2004-2012. We observe that the years of 2004 and 2009 are different from the others. One possible explanation is that 2004 had the highest temperature and humidity indexes of all years. Another possible explanation is that the TKY site was attacked by typhoons. On the other hand, 2009 had the lowest humidity of all years and the lowest snow index, which reveals more of the terrain around trees during winter time.<sup>3</sup> Note that the *hue* index natural color associations have a direct relation to leaf exchange patterns.

#### 4.13. CPM as species visual signature

In this section, we evaluate how the expressive power of CPMs can be used as a species' visual signature. For this analysis, we used the manual species identification of [30] for the TKY dataset described before.

The placement of adjacent percentage maps in the CPM generates visual cues along the time axis. By exploiting this characteristic, we can see that different species create different CPM patterns. Fig. 11 shows the CPM for the *Betula*, *Quercus* and *Acer* species using the  $g_{cc}$  index for 2007 and 2008. In this analysis, we use  $g_{cc}$  and the categorical color table to identify different patterns. The three most relevant  $g_{cc}$  intervals in the categorical mapping are 35 – 40% (colored in green), 40 – 45% (colored in blue), and 45 – 50% (colored in purple). The patterns we observe for each species is consistent for the two years. However, they have distinct patterns when comparing one species against the other, especially during leaf growth and senescence phases. *Quercus* has a purple zone that shows a peak for the greening phase, which stabilizes in the rest of the growing season.

#### 4.2. Multi-year data analysis

We investigate in this section the ability of PhenoVis to perform data analysis and search for similar phenological patterns. The identification of inter-annual variability in phenological data series is of key importance to identify changes and trends that can be related to environmental drivers.

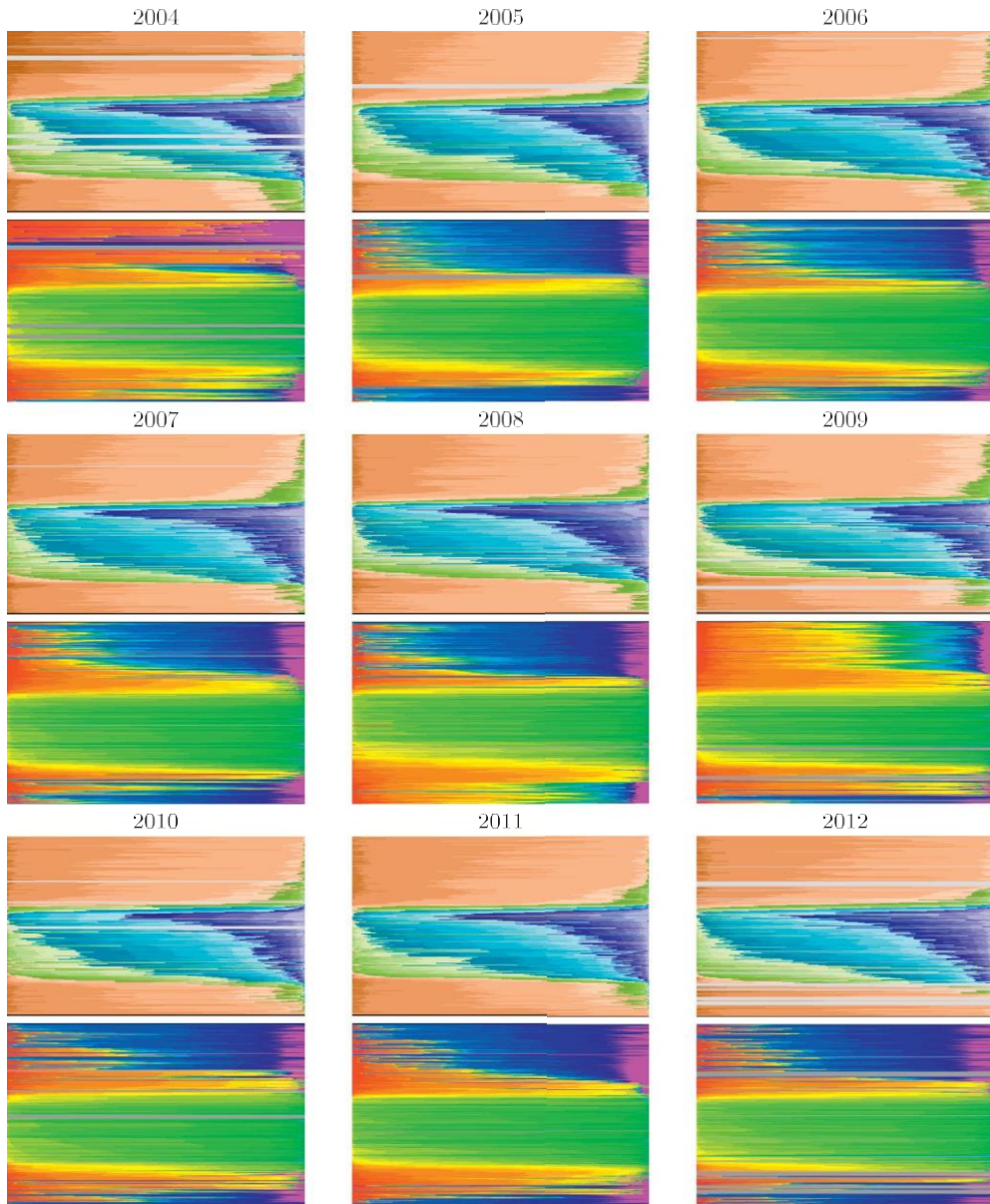
##### 4.2.1. Searching for similar phenological patterns

PhenoVis allows the user to specify a window of time over the CPM to define an interesting pattern to be searched. This pattern will be used as a query for similar patterns in other years. Fig. 12 shows the results of a search that uses as its query window the leaf expansion period of 2009 and the MSE similarity metric. The obtained results show that this pattern was most similar to the years 2008 and 2004 when using a fixed window. On the other hand, it was closer to 2007 and 2006 when using a moving window. As we can see, the ranking results can be different when the fixed and moving window searches are compared against each other. Moreover, as expected, the moving window approach presents a smaller error than the fixed window.

<sup>2</sup> <https://github.com/schnorr/phenology>.

<sup>3</sup> Both temperature and humidity information were obtained at <http://www.data.jma.go.jp>, using the station TAKAYAMA WMO Station ID:47617 (As of May

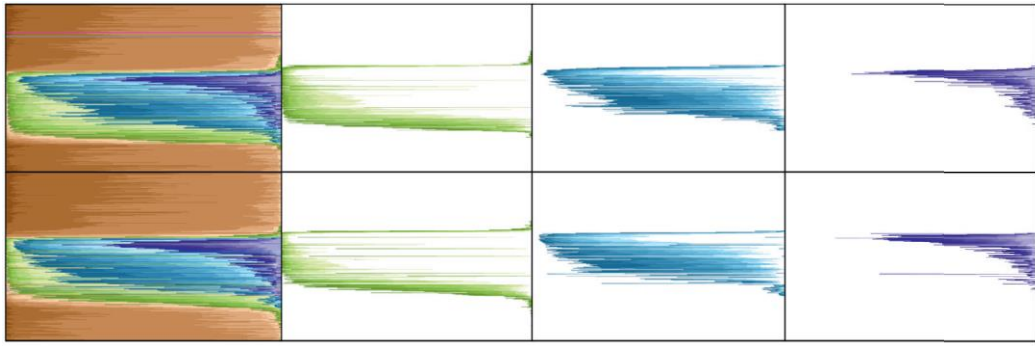
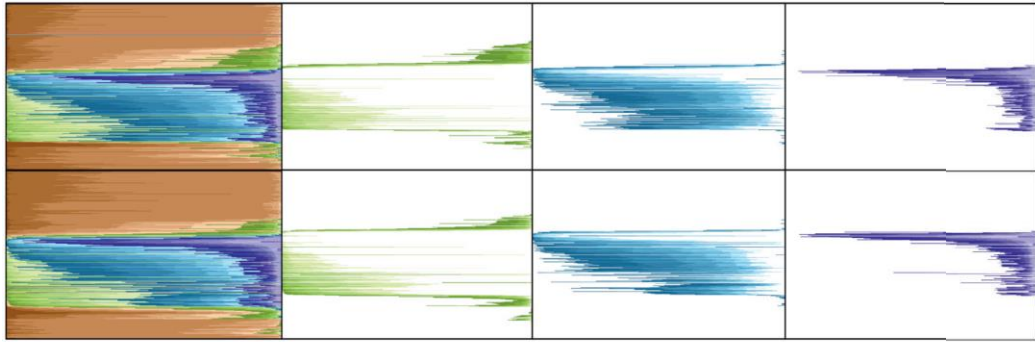
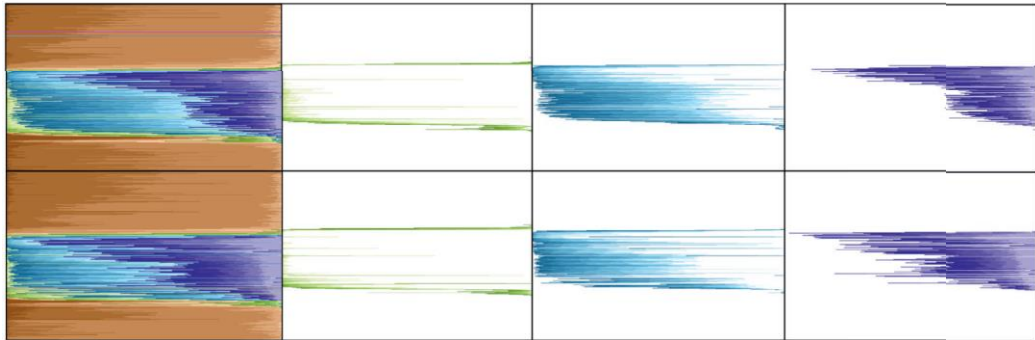
2015).



**Fig. 10.** CPMs for years 2004–2012 using the  $g_{cc}$  (rows 1, 3 and 5) and  $hue$  (rows 2, 4, and 6) indexes. We observe in the hue CPMs that years 2004 and 2009 were distinct from other years, while green colors consistently identify the leafing period.

#### 4.2.2. Multi-year ranking

In a single-rank analysis, the user selects a query pattern of a given year. Results are ordered by the distance computed using the similarity metric. The multi-rank performs pairwise comparisons of all years. Fig. 13 shows the results obtained with the multi-year ranking using the entire year as the time interval, and pairwise comparisons of the community and species ROIs. For each ROI (community, *Betula*, *Quercus* and *Acer*), the 9 histograms display in green the normalized distance of every year from 2004 to 2012 against the others. The histogram is sorted according to the error, with the most similar year on top and the most different year on the bottom. For example, in the community mask, the most different years were 2014 (for 5 other years), 2009 (for 3 years) and 2012 (for 1 year). For *Betula*, the most different years were 2012 (for 5 other years), 2009 (for 3 years) and 2004 (for 1 year); for *Quercus*, 2004 (for 8 other years) and 2009 (for 1 year); and for *Acer*, 2004 (for 6 other years) and 2009 (for 3 years). The purple histogram shows the combined information of all the histogram plots of a given ROI in a single summary plot. This summary plot confirms the information seen in the individual plots, which show that 2004, 2009 and 2012 were the most different years, while 2007 was the most similar year. For *Betula*, we observe that the most different year was 2012, as noted previously.

(a) *Betula ermanii*(b) *Quercus crispula*(c) *Acer rufrinerve*

**Fig. 11.** CPMs and zone highlights of different species for the years 2007 (top row), and 2008 (bottom). Observe the distinct patterns in the three zones (green, blue, and purple), which can serve as a visual signature to identify a given species.

In Fig. 14, we use the summary plots to refine our analysis to the pre-defined phenophases of the *Betula*, *Quercus*, and *Acer* species. For each phenophase described at the start of this section (BD, LE, Peak, LF and PLF), we display one summary plot. For *Betula*, the most different years in BD, LE, Peak, LF and PLF phenophases were 2004, 2008, 2004, 2012 and again 2012. For *Quercus*, the most different years in BD, LE, Peak, LF and PLF phenophases, were 2004, 2008, 2009, 2009 and 2012, while for *Acer*, they were 2004, 2004, 2009, 2012 and 2008. We also observe that, for BD, the year 2004 was the most different for the three species; for LE, it was 2008 (for two species); for Peak, it was 2009 (for two species); for LF, it was 2012 (for two species); and for PLF, it was also 2012 (for two species). Such analysis is easy to produce with the same encoding and reveals interesting aspects about the data that would be hard to extract from average plots.

In Fig. 15, we used the moving window to search for the specific pattern associated with the leaf expansion period of the years 2007 and 2008. The bar height indicates the number of days that the same pattern appears before or after the query pattern. For example, for 2007, the most similar pattern occurred five days earlier in 2004, two days later in 2005, one day later in 2006, and so forth. With respect to 2007, we observe that the leaf expansion happened earlier in 2004, 2008 and 2009, about the same day in 2010, and later in 2005, 2006, 2011 and 2012. For 2008, it happened one day earlier in 2009, about the same day in 2004, and later in the remaining years.



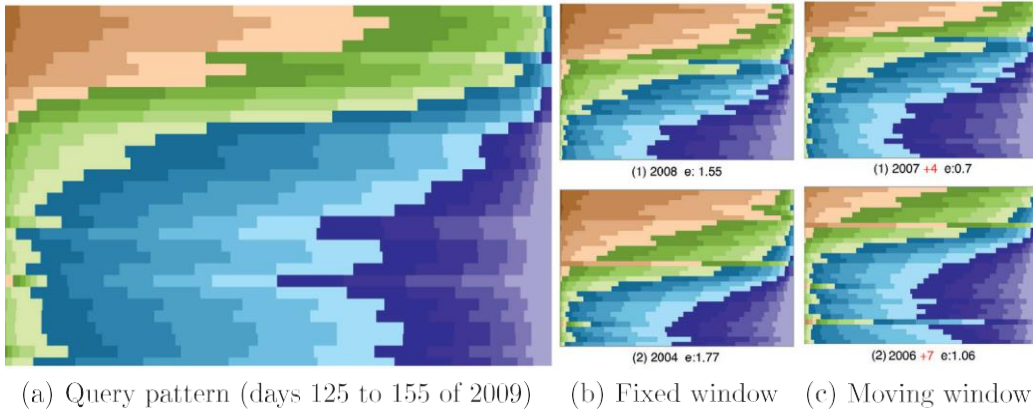


**Fig. 12.** Searching for similar phenological pattern using MSE: (a) query pattern; and top two results using (b) fixed and (c) moving window. Comparison errors are given after the letter 'e'; red numbers show the temporal shift in days from the matching pattern.

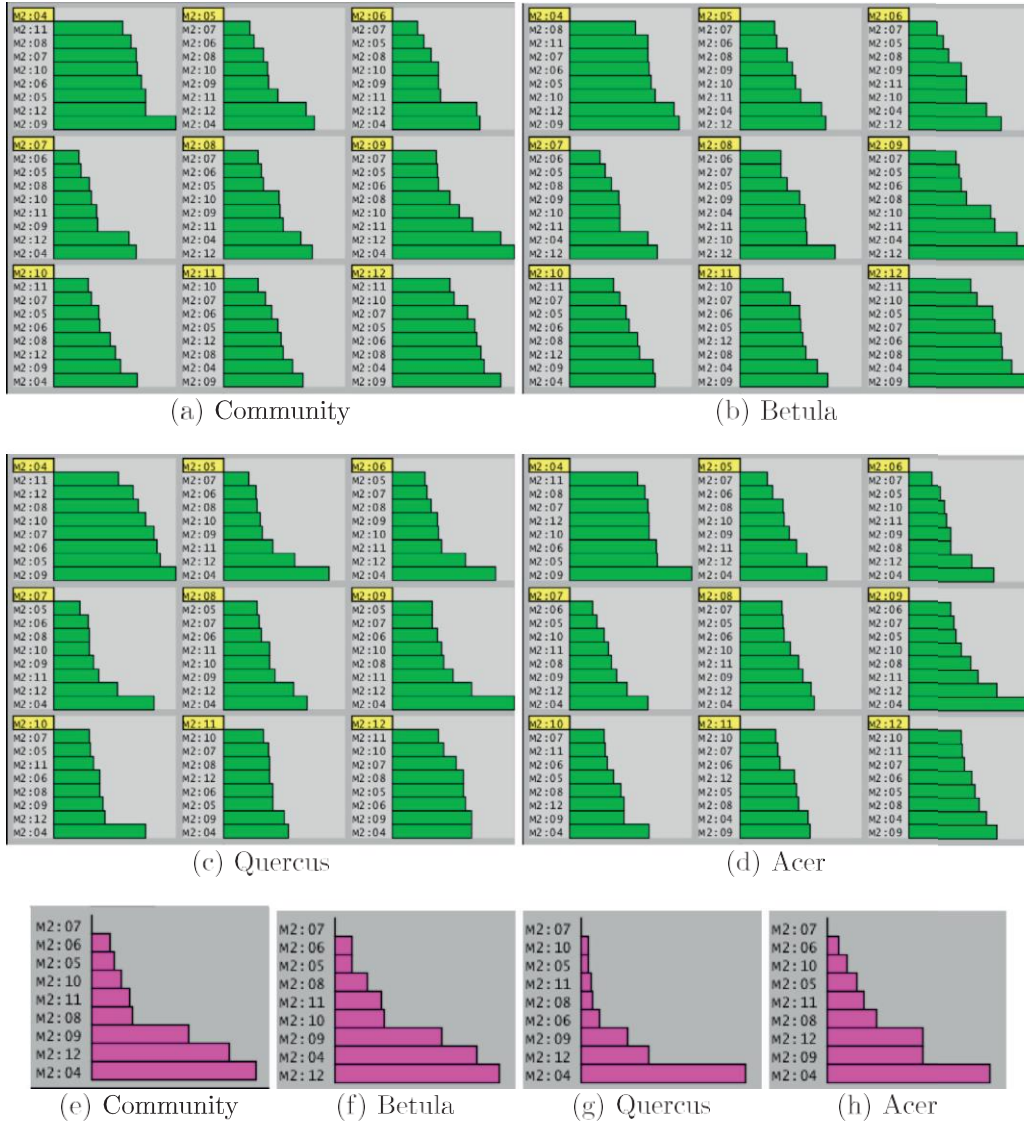


**Fig. 13.** Multi-rank comparisons of four ROIs (*Community*, *Betula*, *Quercus* and *Acer*) for the entire year: (a)-(d) normalized distance of every year from 2004 to 2012 against the others; (e)-(h) combined information of the green histogram plots of a given ROI into a single summary plot; the year 2007 was the year most similar to the others, while the years 2004, 2012, and 2009 were the most different ones.

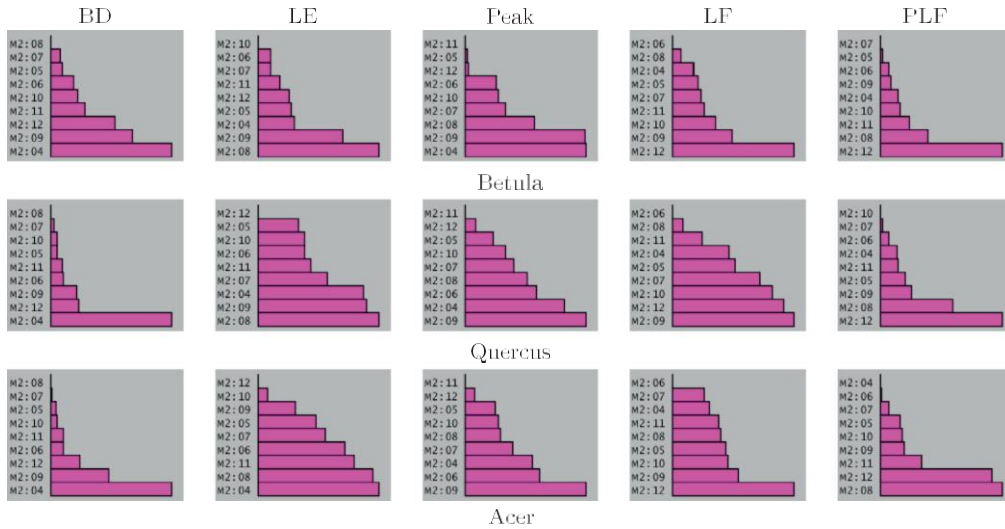


**Fig. 14.** Summary histograms of the community mask for specific phenological phases. The year 2004 was the most different for the three species; for LE, it was 2008 (for two species); for Peak, it was 2009 (for two species); for LF, it was 2012 (for two species); and for PLF, it was also 2012 (for two species).

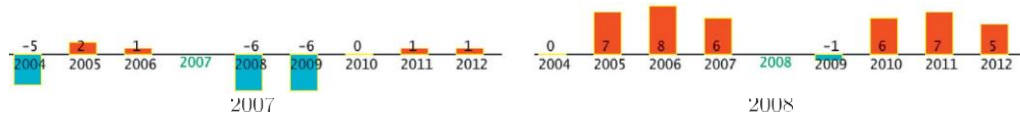


**Fig. 15.** The leaf-expansion period was used as input pattern in the moving window approach for the years 2007 and 2008: the bar heights represent the number of days that the result happened before (blue) or after (red) the query pattern.

## 5. Conclusions and future work

Plant phenology studies are based on the analysis of several years of data. Average yearly plots of vegetation indexes are the preferred approach to evaluate phenological changes. Despite good results, the analysis based on average values is limited and can constraint the knowledge discovery process.

In this paper, we present PhenoVis, a framework for the visual phenological analysis of forest ecosystems. It contains the chronological percentage maps (CPM), a novel representation that is capable of discovering additional patterns by encoding percentage distributions of the data. We demonstrated CPM in a number of analysis scenarios, showing the additional insights that CPMs can bring to the analysis and how it can be used to identify species. The evaluation showed how automatic pattern searches can facilitate the detection of phenological singularities related to weather variations.

As future work, we intend to automatically detect phenological patterns. Currently this process is manual: the user informs the start and end dates of the query pattern. Automatic suggestions can improve the analysis using, for example, a box-plot [45] of the distribution. Another possibility is to use more images per day, decreasing lighting variations and artifacts. We also plan to investigate the integration of the CPM representation with machine learning techniques [4,7] to perform automatic species identification.

## Acknowledgments

We thank the Phenological Eyes Network (PEN) for giving authorisation to use the TKY dataset (<http://www.pheno-eye.org>). We thank Shin Nagai and Kenlo Nishida Nasahara for the revision of this manuscript and suggestions to improve the final format. This research was supported by the São Paulo Research Foundation FAPESP and Microsoft Research Virtual Institute (grants #2010/52113-5, #2013/50169-1, and #2013/50155-0). BA received a master scholarship from CAPES and a doctoral fellowship from FAPESP (grant #2014/00215-0); LPCM and RST receive a Productivity Research Fellowship from CNPq. Also, we have benefited from funds given by CAPES, CNPq (grants 476685/2012-5, 309483/2011-5, 308851/2015-3), and FAPESP (grants #2007/52015-0, #2007/59779-6, #2009/18438-7, #2010/51307-0, and #2009/54208-6).

## Supplementary material

Supplementary material associated with this article can be found, in the online version, at [10.1016/j.ins.2016.08.052](https://doi.org/10.1016/j.ins.2016.08.052).

## References

- [1] W. Aigner, S. Miksch, H. Schumann, C. Tominski, Visualization of time-oriented data, Springer Science & Business Media, 2011.
- [2] D. Albers, C. Dewey, M. Gleicher, Sequence surveyor: Leveraging overview for scalable genomic alignment visualization, *Visual. Comput. Graphics, IEEE Trans.* 17 (12) (2011) 2392–2401.
- [3] B. Alberton, J. Almeida, R. Henneken, R.S. Torres, A. Menzel, L.P.C. Morellato, Using phenological cameras to track the green up in a cerrado savanna and its on-the-ground validation, *Ecol. Inf.* 19 (2014) 62–70.
- [4] J. Almeida, J.A. dos Santos, B. Alberton, R. da S. Torres, L.P.C. Morellato, Applying machine learning based on multiscale classifiers to detect remote phenology patterns in cerrado savanna trees, *Ecol. Inf.* 23 (0) (2014) 49–61. Special Issue on Multimedia in Ecology and Environment
- [5] J. Almeida, J.A. Santos, B. Alberton, L.P.C. Morellato, R.S. Torres, Plant species identification with phenological visual rhythms, in: IEEE International Conference on eScience (eScience'13), 2013, pp. 148–154.
- [6] J. Almeida, J.A. Santos, B. Alberton, L.P.C. Morellato, R.S. Torres, Visual rhythm-based time series analysis for phenology studies, in: IEEE International Conference on Image Processing (ICIP'13), 2013, pp. 4412–4416.
- [7] J. Almeida, J.A. Santos, W.O. Miranda, B. Alberton, L.P.C. Morellato, R.S. Torres, Deriving vegetation indices for phenology analysis using genetic programming, *Ecol. Inf.* 26 (2015) 61–69.
- [8] G. Andrienko, N. Andrienko, Spatio-temporal aggregation for visual analysis of movements, in: Visual Analytics Science and Technology, 2008. VAST '08. IEEE Symposium on, 2008, pp. 51–58.
- [9] I. Boyandin, E. Bertini, P. Bak, D. Lalanne, Flowstrates: An approach for visual exploration of temporal origin-destination data, *Comput. Graphics Forum* 30 (3) (2011) 971–980.
- [10] E. Bradley, D. Roberts, C. Still, Design of an image analysis website for phenological and meteorological monitoring, *Environ. Modell. Software* 25 (1) (2010) 107–116.
- [11] L. Byron, M. Wattenberg, Stacked graphs – geometry & aesthetics, *IEEE Trans. Visual. Comput. Graphics* 14 (6) (2008) 1245–1252, doi:10.1109/TVCG.2008.166.
- [12] W. Cui, X. Wang, S. Liu, N. Riche, T. Madhyastha, K.L. Ma, B. Guo, Let it flow: A static method for exploring dynamic graphs, in: Pacific Visualization Symposium (PacificVis), 2014 IEEE, 2014, pp. 121–128.
- [13] H. Eerens, D. Haesen, F. Rembold, F. Urbano, C. Tote, L. Bydekerke, Image time series processing for agriculture monitoring, *Environ. Modell. Software* 53 (2014) 154–162.
- [14] K. Fung, Numbers Rule Your World: The Hidden Influence of Probabilities and Statistics on Everything You Do, McGraw-Hill Education, 2010.
- [15] A.R. Gillespie, A.B. Kahle, R.E. Walker, Color enhancement of highly correlated images. I. Decorrelation and HSI contrast stretches, *Remote Sens. Environ.* 20 (3) (1986) 209–235.
- [16] J.A. Granados, E.A. Graham, P. Bonnet, E.M. Yuen, M.P. Hamilton, Ecoip: An open source image analysis toolkit to identify different stages of plant phenology for multiple species with pan-tilt-zoom cameras, *Ecol. Inf.* 15 (2013) 58–65.
- [17] S. Gratzl, A. Lex, N. Gehlenborg, H. Pfister, M. Streit, Lineup: Visual analysis of multi-attribute rankings, *Visual. Comput. Graphics, IEEE Trans.* 19 (12) (2013) 2277–2286.
- [18] S. Hadlak, H. Schumann, C. Cap, T. Wollenberg, Supporting the visual analysis of dynamic networks by clustering associated temporal attributes, *Visual. Comput. Graphics, IEEE Trans.* 19 (12) (2013) 2267–2276.
- [19] S. Havre, B. Hetzler, L. Nowell, Themeriver: visualizing theme changes over time, in: Information Visualization, 2000. InfoVis 2000. IEEE Symposium on, 2000, pp. 115–123, doi:10.1109/INFVIS.2000.885098.
- [20] S. Havre, E. Hetzler, P. Whitney, L. Nowell, Themeriver: visualizing thematic changes in large document collections, *IEEE Trans. Visual. Comput. Graphics* 8 (1) (2002) 9–20, doi:10.1109/2945.981848.
- [21] R. Ide, H. Oguma, Use of digital cameras for phenological observations., *Ecol. Inf.* 5 (5) (2010) 339–347.
- [22] T. Inoue, S. Nagai, T.M. Saitoh, H. Muraoka, K.N. Nasahara, H. Koizumi, Detection of the different characteristics of year-to-year variation in foliage phenology among deciduous broad-leaved tree species by using daily continuous canopy surface images, *Ecol. Inf.* 22 (2014) 58–68. <http://dx.doi.org/10.1016/j.ecoinf.2014.05.009>.
- [23] A. Ito, N. Saigusa, S. Murayama, S. Yamamoto, Modeling of gross and net carbon dioxide exchange over a cool-temperate deciduous broad-leaved forest in japan: Analysis of seasonal and interannual change, *Agric. For. Meteorol.* 134 (1–4) (2005) 122–134. <http://dx.doi.org/10.1016/j.agrformet.2005.11.002>.
- [24] D.A. Keim, Designing pixel-oriented visualization techniques: Theory and applications, *IEEE Trans. Visual. Comput. Graphics* 6 (1) (2000) 59–78.
- [25] D.A. Keim, Information visualization and visual data mining, *IEEE Trans. on Vis. and Comp. Graph.* 8 (1) (2002).
- [26] D.A. Keim, M.C. Hao, U. Dayal, M. Hsu, Pixel bar charts: A visualization technique for very large multi-attribute data sets, *Inf. Visual.* 1 (1) (2002) 20–34.
- [27] J. Li, K. Zhang, Z.-P. Meng, Vismate: Interactive visual analysis of station-based observation data on climate changes, in: Visual Analytics Science and Technology (VAST), 2014 IEEE Conference on, 2014, pp. 133–142.
- [28] S. Lin, J. Fortuna, C. Kulkarni, M. Stone, J. Heer, Selecting semantically-resonant colors for data visualization, *Comput. Graphics Forum* 32 (3pt4) (2013) 401–410.
- [29] J.T. Morissette, A.D. Richardson, A.K. Knapp, J.I. Fisher, E.A. Graham, J. Abatzoglou, B.E. Wilson, D.D. Breshears, G.M. Henebry, J.M. Hanes, L. Liang, Tracking the rhythm of the seasons in the face of global change: phenological research in the 21st century, *Front. Ecol. Environ.* 7 (5) (2009) 253–260.
- [30] S. Nagai, T. Maeda, M. Gamo, H. Muraoka, R. Suzuki, K.N. Nasahara, Using digital camera images to detect canopy condition of deciduous broad-leaved trees, *Plant Ecology & Diversity* 4 (1) (2011) 79–89.
- [31] K.N. Nasahara, S. Nagai, Review: Development of an in situ observation network for terrestrial ecological remote sensing: the phenological eyes network (PEN), *Ecol. Res.* 30 (2) (2015) 211–223.
- [32] G. Negi, Leaf and bud demography and shoot growth in evergreen and deciduous trees of central himalaya, india, *Trees* 20 (4) (2006) 416–429.
- [33] C.W. Ngo, T.C. Pong, R.T. Chin, Detection of gradual transitions through temporal slice analysis, in: IEEE International Conference on Computer Vision and Pattern Recognition (CVPR'99), 1999, pp. 1036–1041.
- [34] K.T. Nguyen, T. Ropinski, Large-scale multiple sequence alignment visualization through gradient vector flow analysis, in: Biological Data Visualization (BioVis), 2013 IEEE Symposium on, 2013, pp. 9–16.
- [35] K. Nishida, Phenological eyes network (PEN) - a validation network for remote sensing of the terrestrial ecosystems., *AsiaFlux Newslett.* 21 (2007) 9–13.
- [36] G. Oliveira, J. Comba, R. Torchelsen, M. Padilha, C. Silva, Visualizing running races through the multivariate time-series of multiple runners, 2012 25th SIBGRAPI Conf. Graphics, Patterns Images 0 (2013) 99–106.
- [37] C. Reas, B. Fry, Processing: A Programming Handbook for Visual Designers and Artists, MIT Press, 2014.
- [38] A.D. Richardson, B.H. Braswell, D.Y. Hollinger, J.P. Jenkins, S.V. Ollinger, Near-surface remote sensing of spatial and temporal variation in canopy phenology, *Ecol. Appl.* 19 (6) (2009) 1417–1428.
- [39] M.D. Schwartz, Phenology: an integrative environmental science, 2nd, Springer, 2013.
- [40] O. Sonnentag, K. Hufkens, C. Teshera-Sterne, A.M. Young, M. Friedl, B.H. Braswell, T. Milliman, J. O. Keefe, A.D. Richardson, Digital repeat photography for phenological research in forest ecosystems, *Agric. For. Meteorol.* 152 (2012).
- [41] T. Udelhoven, Timestats: A software tool for the retrieval of temporal patterns from global satellite archives, *IEEE J. Selected Topics Appl. Earth Observ. Remote Sens.* 4 (2) (2011) 310–317.

### **Appendix F**

Article published in the Journal Pattern Recognition Letters:

ALMEIDA, J., PEDRONETTE, D., ALBERTON, B., MORELLATO, L.P.C., TORRES, R.S. Unsupervised distance learning for plant species identification. JSTARS Journal of Selected Topics in Applied Earth Observations and Remote Sensing, v. 9 (12), p. 5325-5338, 2016.

## Unsupervised Distance Learning for Plant Species Identification

Jurandy Almeida<sup>1</sup>, Daniel C. G. Pedronette<sup>2</sup>, Bruna C. Alberton<sup>3</sup>, Leonor Patricia C. Morellato<sup>3</sup>, Ricardo da S. Torres<sup>4</sup>

<sup>1</sup> Institute of Science and Technology, Federal University of São Paulo (UNIFESP), São José dos Campos 12247-014, Brazil (e-mail: jurandy.almeida@unifesp.br).

<sup>2</sup> Department of Statistics, Applied Mathematics and Computation, São Paulo State University (UNESP), Rio Claro 13506-900, Brazil (e-mail: daniel@rc.unesp.br).

<sup>3</sup> Department of Botany, São Paulo State University (UNESP), Rio Claro 13506-900, Brazil (e-mail: bru.alberton@gmail.com; pmorella@rc.unesp.br).

<sup>4</sup> Institute of Computing, University of Campinas (UNICAMP), Campinas 13083-852, Brazil (e-mail: rtorres@ic.unicamp.br).

### Abstract:

Phenology is among the most trustworthy indicators of climate change effects on plants and animals. The recent application of repeated digital photographs to monitor vegetation phenology has provided accurate measures of plant life cycle changes over time. A fundamental requirement for phenology studies refers to the correct recognition of phenological patterns from plants by taking into account time series associated with their crowns. This paper presents a new similarity measure for identifying plants based on the use of an unsupervised distance learning scheme, instead of using traditional approaches based on pairwise similarities. We experimentally show that its use yields considerable improvements in time-series search tasks. In addition, we also demonstrate how the late fusion of different time series can improve the results on plant species identification. In some cases, significant gains were observed (up to +8.21% and +19.39% for mean average precision and precision at 10 scores, respectively) when compared with the use of time series in isolation.

*Index Terms*—Image analysis, plant identification, remote phenology, time series, unsupervised distance learning.

### I. INTRODUCTION

**P**LANT phenology studies recurrent plant life cycle events and is among the most trustworthy indicators of the impact of climate change on plants and animals [1]. Recently, digital repeated photographs have been applied to monitor vegetation phenology increasing the range of study sites and species and the accuracy of estimated changes on phenological events [1]–[3]. The proper identification of plant species based on their particular phenological patterns is a key issue for the phenological observation of tree crowns using phenocams [4], especially in tropical vegetations where one single image may encompass a large number of species [3]. Each crown in the image has to be match with the tree in the soil and then identified at species level, and further phenological patterns are identified to that species and analyzed [3], [5].

Existing approaches to cope with the task of plant identification based on phenological patterns rely on a feature extractor for encoding visual properties into feature vectors and on a similarity measure for comparing image data from their vectors, a pair known as descriptor [6]. In phenology studies, a common approach used for feature extraction is to compute for each image a chromatic or lighting coefficient associated with a visual property from all pixels of a given region of interest. Thus, a time series is obtained by computing this index for all days in an time period of interest [4], [7].

Besides the time-series modeling, the similarity measure adopted for comparing different times series also plays an

important role, directly affecting the quality of retrieval results. Given the broad application of time series, various similarity measures have been employed [8] for comparison and retrieval. In addition to the traditional Manhattan ( $L_1$ ) and Euclidean ( $L_2$ ) distances, other measures, such as the dynamic time warping distance and longest common subsequence, are commonly used [8]. In [9], shape descriptors are used to characterize time series. In [10], visual rhythms are used to simplify time series, enabling the use of image descriptors.

However, traditional solutions often perform only pairwise analysis, that is, the similarity measure considers only the information given by the pairs of time series being compared. In this scenario, the relationships among objects modeled by the time series are not considered. Therefore, the intrinsic structure of the collection is ignored. In this scenario, one suitable alternative relies on the use of methods that are capable of encoding information of the dataset structure. Relevance feedback approaches [11], for example, have been proposed for using the information obtained from user interactions for improving the quality of time-series retrieval tasks. Although effective, such supervised approaches require a lot of user intervention.

In this paper, we present a novel approach for redefining the similarity from time series and identifying plant species based on phenological patterns, without the use of any training data. We approach the plant identification task as a similarity-based time-series retrieval problem using unsupervised learning, in contrast to some supervised initiatives that have addressed this task in the context of image classification [5], [12]. For this, we



introduce the use of an unsupervised distance learning method called reciprocal  $k$ -nearest neighbor ( $k$ NN) distance [13] for plant species identification. The method exploits the relationships among time series, using a contextual rank-based approach for improving the effectiveness of retrieval tasks.

Unsupervised learning approaches have been used in time-series retrieval in order to learn a layer of feature representations from unlabeled data [14]. In opposite, the proposed approach does not require intermediary feature learning steps. A traditional distance measure is obtained based on the original features, giving rise to a set of ranked lists. Subsequently, a more effective distance is computed by analyzing the reciprocal references encoded in the rankings. Although common in image retrieval systems [15], [16], to the best of our knowledge, this is the first approach that exploits contextual rank-based measures [13] in time-series retrieval scenarios.

The proposed approach was validated on a dataset recorded during the main leaf flushing season [3], which is composed of about 2700 images. Several time series extracted from the digital image were evaluated and a large experimental evaluation was conducted. Various aspects are analyzed, considering individual features and fusion tasks. An approach for selecting the most discriminative features is also discussed. The experimental results show that our approach can improve the retrieval effectiveness considerably. While the best feature in isolation yields a precision of 73.12% at top-ten positions, the proposed approach achieves precision scores up to 87.30%.

This paper is organized as follows. Section II describes the time-series acquisition procedure. Section III describes the methodology adopted in this work. Section IV discusses the unsupervised distance learning approach. Section V discusses the experimental protocol, while Section VI presents achieved results. Finally, Section VII presents our conclusions and draws possible future work.

## II. TIME-SERIES ACQUISITION

We have been acquiring time series from digital images of a phenological monitoring, called near-surface remote phenology [17], in a cerrado savanna vegetation since August 2011. A digital camera was set up in the top of 18-m-high tower in an area of a cerrado sensu stricto, located at Itirapina, South-eastern Brazil. Camera was set up for taking a sequence of five JPEG images (at 1280×960 pixels of resolution) per hour, from 6:00 to 18:00 h (UTC-3). This study was based on a sample sequence of the time series, recorded between August 29th and October 3rd, 2011 (day of year 241 to 278), totalizing 2700 images, which corresponds to the main leaf flushing season of the cerrado community [3].

The image analysis was conducted by defining different regions of interest (ROIs), as described in [4] and defined in [3] for our target species (see Fig. 1). We analyzed 22 ROIs of six plant species randomly selected in the hemispheric image:

- 1) three regions for *Aspidosperma tomentosum* (red areas);
- 2) four regions for *Caryocar brasiliensis* (green areas);
- 3) two regions for *Myrcia guianensis* (blue areas);
- 4) seven regions for *Miconia rubiginosa* (orange areas);

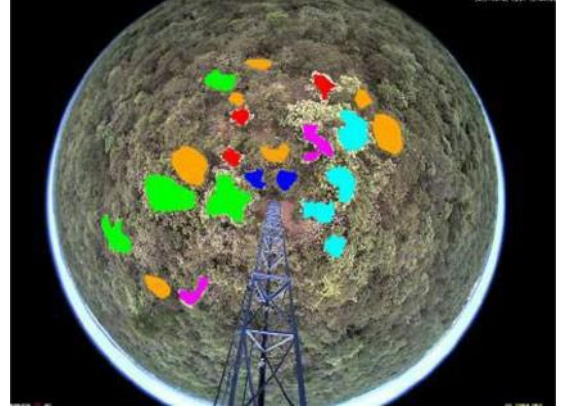


Fig. 1. ROIs defined for the analysis of cerrado-savanna digital images, following [3]. Each color represents a species: red = *Aspidosperma tomentosum*; green = *Caryocar brasiliensis*; blue = *Myrcia guianensis*; orange = *Miconia rubiginosa*; magenta = *Pouteria ramiflora*; cyan = *Pouteria torta*.

- 5) two regions for *Pouteria ramiflora* (magenta areas);
- 6) four regions for *Pouteria torta* (cyan areas).

According to the leaf exchange data from the on-the-ground field observations on leaf fall and leaf flush at our study site, those species were classified into three functional groups [3]:

- 1) deciduous, *A. tomentosum* and *C. brasiliensis*;
- 2) evergreen, *M. guianensis* and *M. rubiginosa*;
- 3) semideciduous, *P. ramiflora* and *P. torta*.

We analyzed each ROI by means of a normalized index developed by Gillespie *et al.* [18], called RGB chromatic coordinates (RGBcc). It is considered the most efficient index to distinguish leaves between monocots and dicots and to suppress light environment variation [19]. The normalized RGBcc indices undergo a nonlinear transform, as follows [18], [19]:

$$r_{cc} = \frac{R}{(R + tt + B)} \quad (1)$$

$$g_{cc} = \frac{tt}{(R + tt + B)} \quad (2)$$

$$b_{cc} = \frac{B}{(R + tt + B)} \quad (3)$$

where  $R$ ,  $tt$ , and  $B$  are the average pixel intensity of the red, green, and blue bands, respectively. By computing those values along the whole period, we obtained time series to use as input data for our proposed framework.

## III. TIME-SERIES RETRIEVAL

This section presents the methodology used to handle the plant identification task as a similarity-based time-series retrieval problem. First, Section III-A presents an overview of the time-series retrieval system. In the following, the main components of this system are formalized in Section III-B.

### A. Overview

In this work, the plant identification task is approached as a time-series retrieval problem, as proposed in [20]. In this

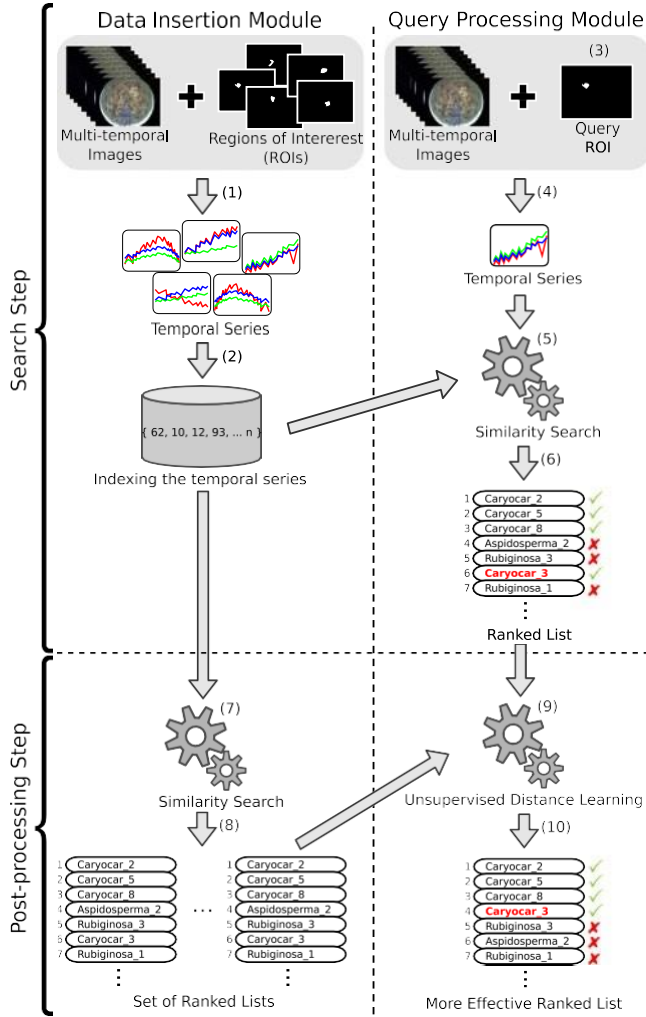


Fig. 2. Flowchart of the time-series retrieval system.

method, we provide a time series extracted from an image area associated with a given species, and we query for similar time series computed from other image areas that belong to the same species. The flowchart of the time-series retrieval system is illustrated in Fig. 2. Two main functionalities are supported by this system: data insertion and query processing. Each of those subsystems is composed of two basic steps: (i) search and (ii) post-processing.

In the search step, the data insertion module comprises: (1) the encoding of leaf change patterns from labeled image regions into time series by computing the normalized RGBcc indices along multitemporal data; and (2) the indexing of the extracted time series in a data repository. The query processing module consists of a query search, which are composed of the following steps: (3) the selection of a query pattern, which is an image area along the multitemporal images; (4) the extraction of the query's time series by computing the normalized RGBcc indices; (5) the search computation by similarity; (6) the final similarity ranking, including all patterns learned at the offline stages.

In the search step, the similarity computation considers only pairs of objects (regions and the respective times series). The post-processing step exploits more global relationships among time series with the aim of improving the effectiveness of retrieved results. In the data insertion module, the postprocessing step comprises: (7) a similarity search considering every region as a query; and (8) the computation of a ranked list for all queries. In the query processing module, the ranked lists are redefined by the following steps: (9) the unsupervised learning method compute more effective ranked lists; and (10) the final retrieval results are returned to the user.

### B. Formalization

Let  $\hat{I}$  be a digital image. Let  $\mathbf{R} = \{r_1, r_2, \dots, r_n\}$  be a collection of regions, such that for each region  $r_i \in \mathbf{R}$ , we have  $r_i \subset \hat{I}$  and each region contains a single species. Let  $n = |\mathbf{R}|$  denote the number of regions considered. Let  $X$  be a time series, defined as follows:

$$X = \{x_t, t \in T\} \quad (4)$$

where  $\mathcal{D}$  denotes a discrete index set. Let  $m$  be the number of days of observations; the index set is defined as  $\mathcal{D} = \bigcup_{i=1}^m \mathcal{D}_i$ , where  $\mathcal{D}_i = \{d_1, \dots, d_m\}$ .

Let  $\mathcal{C} = \{g, b\}$  be the set of chromatic indexes (defined by the normalized RGBcc indices). Let  $\mathcal{H} = \{0, 1, \dots, 23\}$  be a set defined by the hours of the day. Let  $\mathbf{X} = \{X_1, X_2, \dots, X_z\}$  denote a set of all time series obtained for every combination of chromatic index, hour of day and region.

We can define a function  $\psi : \mathcal{C} \times \mathcal{H} \times \mathbf{R} \rightarrow \mathbf{X}$ , which extracts a time series for a given chromatic index, hour of day, and region.<sup>1</sup> For example, the time series observed for the region “ $r_i$ ” by considering the  $g_{cc}$  index at “6 h” can be defined by  $X_{i,g,6} = \psi(r_i, g, 6)$ .

Let  $\rho$  be a time-series descriptor for a region, which can be defined as a tuple  $(\psi, \rho)$ , where  $\psi$  extracts a time series for a region  $r_i$  considering a chromatic index and a hour of day;  $\rho : \mathbf{X} \times \mathbf{X} \rightarrow \mathbf{R}$  is a distance function that computes the distance between two regions according to the distance between their respective time series. Formally, the distance between two regions  $r_i$  and  $r_j$  considering a chromatic index  $c$  and a hour  $h$  is defined by  $\rho(\psi(r_i, c, h), \psi(r_j, c, h))$ . For simplicity and readability purposes, we use the notation  $\rho(i, j)$  along the paper for denoting the distance between regions  $r_i$  and  $r_j$ , considering their respective times series.

The distance  $\rho(i, j)$  among all regions  $r_i, r_j \in \mathbf{R}$  can be computed to obtain a squared  $n \times n$  distance matrix  $A$ , such that  $A_{ij} = \rho(i, j)$ . Also based on the distance function  $\rho$ , a ranked list  $\tau_q$  can be computed in response to a query region  $r_q$ . The goal consists in retrieving the most similar regions  $r_i$  considering the respective time series.

The ranked list  $\tau_q = (r_1, r_2, \dots, r_n)$  can be defined as a permutation of the collection  $\mathbf{R}$ . A permutation  $\tau_q$  is a bijection from the set  $\mathbf{R}$  onto the set  $[N] = \{1, 2, \dots, n\}$ . For a permutation  $\tau_q$ , we interpret  $\tau_q(i)$  as the position (or rank) of region

<sup>1</sup>The extracted time series can be seen as feature vectors associated with an image area.

$r_i$  in the ranked list  $\tau_q$ . We can say that, if  $r_i$  is ranked before  $r_j$  in the ranked list of  $r_q$ , that is,  $\tau_q(i) < \tau_q(j)$ , then  $\rho(q, i) \leq \rho(q, j)$ . We also can take every region  $r_i \in R$  as a query  $r_q$ , in order to obtain a set  $L = \{\tau_1, \tau_2, \dots, \tau_n\}$  of ranked lists for each region.

The unsupervised distance learning problem consists in re-defining the distance  $\rho$  by computing a more effective distance function  $\rho_r$ . The objective of function  $\rho_r(i, j, )$  is to exploit the information encoded in the set of ranked lists. Formally,  $\rho_r : R \times R \times L \rightarrow L$  is a distance function between two regions  $r_i, r_j$  that considers the information encoded in the set of ranked lists.

We also consider the problem of distance fusion, in which we want to combine the information provided by two or more time series defined by different chromatic indexes and hours of day. In this case, we define a function  $\rho_{rf}$ , which takes as input various sets of ranked lists  $\{L_1, L_2, \dots, L_d\}$  computed using different pairs  $(c, h)$  where  $c \in C$  and  $h \in H$ .

#### IV. UNSUPERVISED DISTANCE LEARNING

In this paper, we exploit the contextual information available in relationships among time series by using a recently proposed unsupervised distance learning method based on ranking information [13]. Given a rank of most similar image regions considering their time series, the reciprocal  $k$ NN distance models the similarity between ranked lists in terms of the density of reciprocal neighborhoods.

##### A. Reciprocal Neighborhood

A neighborhood set  $N(q, k)$  contains the  $k$  most similar regions to a given query region  $r_q$  according to a distance function  $\rho$ . For the  $k$ -NN query, we have  $|N(q, k)| = k$ , which can be formally defined as

$$N(q, k) = \{S \subseteq R, |S| = k \wedge \forall r_i \in S, r_j \in R - S : \tau_q(i) < \tau_q(j)\}. \quad (5)$$

Since the nearest neighbor relationships are not symmetric [13], [21], [22], the set of  $k$ -reciprocal nearest neighbors of region  $r_q$  can be defined as [13], [22]

$$N_r(q, k) = \{r_i \in N(q, k) \wedge r_q \in N(i, k)\}. \quad (6)$$

Based on the reciprocal neighborhood set, a binary function  $f_r : R \times R \rightarrow \{0, 1\}$  can be defined, determining if two regions  $r_q, r_i \in R$  are reciprocal neighbors ( $f_r$  returns 1 if  $r_q$  and  $r_i$  are reciprocal neighbors, and 0 otherwise)

$$f_r(q, i) = |N_r(q, k) \cap \{r_i\}|. \quad (7)$$

##### B. Reciprocal $k$ NN Distance

The reciprocal  $k$ NN distance between two regions  $r_q, r_i$  is computed based on the number of reciprocal neighbors at top positions of their ranked lists [13]. For each pair of reciprocal neighbors, a weight is computed proportionally to their position in the ranked lists  $\tau_q$  and  $\tau_i$ . The function  $n_r(q, i)$  computes the score based on the number of reciprocal neighbors and their

respective weights

$$n(q, i) = \frac{\sum_{j \in N(q, k)} \sum_{l \in N(i, k)} f_r(j, l) \times w_r(q, j) \times w_r(i, l)}{k}$$

The weight is defined based on the position of these regions in ranked lists  $\tau_q$  and  $\tau_i$ , according to the function  $w_r$ :

$$w_r(q, j) = k + 1 - \tau_q(j). \quad (9)$$

The reciprocal  $k$ NN distance is defined as the inverse of the number of reciprocal neighbors  $n_r$ . Since the top positions of ranked lists are expected to contain the most relevant regions related to the query, the distance learning can be performed considering only the beginning of the ranked lists (until a parameter  $L$ ). From the  $L$  position to the end, the ranked lists remain the same. The reciprocal  $k$ NN distance  $\rho_r$  can be formally defined as follows:

$$\rho_r(q, i) = \begin{cases} \frac{1}{1 + n_r(q, i)}, & \text{if } \tau_q(i) \leq L \\ \tau_q(i), & \text{otherwise.} \end{cases} \quad (10)$$

##### C. Reciprocal $k$ NN Distance Fusion

The reciprocal  $k$ NN distance framework for distance fusion considers two main steps: 1) first, the sets of ranked lists are combined into a single set  $L_f$  through an intermediary distance  $\rho_f$ ; and 2) next, this set is used as input by the conventional reciprocal  $k$ NN distance discussed in the previous section for computing a final distance  $\rho_{rf}$ .

Given a time series and the respective set of ranked lists, the capability of this time series for determining the distance between  $r_q$  and  $r_i$  is estimated by the number of reciprocal neighbors score  $n_r$ . The quality estimation score  $e_j(q, i)$  is defined as

$$e_j(q, i) = (1 + n_r(q, q)) \times (1 + n_r(i, i)). \quad (11)$$

A multiplicative approach is used for computing the intermediary distance, considering, for each time series, the position from which on regions  $r_q$  and  $r_i$  become reciprocal neighbors ( $\max(\tau_{j_q}(i), \tau_{j_i}(q))$ ). The relevance of the position computed by each time series for the combined distance function is determined by the quality estimation score  $e_j(q, i)$ . The intermediary function  $\rho_f$  is defined as follows:

$$\rho_f(q, i) = \prod_{j=1}^d \max(\tau_{j_q}(i), \tau_{j_i}(q))^{e_j(q, i)}. \quad (12)$$

The intermediary function  $\rho_f$  is used to compute the set  $L_f$  with the combined ranked lists, which is submitted to the reciprocal  $k$ NN distance learning procedure as a single time series.

#### V. EXPERIMENTAL PROTOCOL

We carried out experiments to identify plant species (i.e., areas within the image) using time series extracted from pixels associated with individuals of a same species. For that, the Guigues algorithm [23] was used to segment the hemispheric image into small polygons, obtaining 8849 segmented regions (SR). Then, each SR was associated with a single ROI aiming to



label it. A labeled region is created if there is at least 80% of overlapped area between an SR and an ROI.<sup>2</sup> Thus, we built a dataset of 892 SRs separated into six classes, one for each species: *A. tomentosum* (96), *C. brasiliensis* (346), *M. guianensis* (36), *M. rubiginosa* (195), *P. ramiflora* (50), and *P. torta* (169).

For each SR, we extracted 39 different time series by considering the available periods during the day (13 hours: from 6:00 to 18:00 h) and the normalized RGBcc indices (three components:  $r_{cc}$ ,  $g_{cc}$ , and  $b_{cc}$ ). The similarity between two SRs is computed as a function of the distance between the time series extracted from their SRs. A time series is better than another if it ranks more SRs belonging to the same ROI of a query SR at the first positions. The distance function used for time-series comparison is the Manhattan ( $L_1$ ) distance, as suggested by Conti *et al.* [24]. In this way, we created 39 different time-series descriptors (features) to be used as input in our proposed framework.

The effectiveness of each approach was assessed using the metrics of precision and recall. Precision is the ratio of the relevant SRs in the retrieved set of SRs. Recall is the ratio of relevant SRs retrieved to the total number of relevant SRs in the database. A given SR is considered as relevant only if it belongs to the same ROI of a query SR. There is a tradeoff between precision and recall, i.e., increasing recall may decrease precision and vice versa. For this reason, we consider unique-value measurements in the validation: mean average precision (MAP), which is the mean of the precision scores obtained at the ranks of each relevant SR; and Precision at 10 (P10), which is the average precision after ten SRs are returned. MAP is a good indication of the effectiveness considering all positions of obtained ranked lists. P10, in turn, focuses on the effectiveness of the methods considering only the first positions of the ranked lists. Experiments were conducted using all the SRs from the dataset as queries. Reported results represent the average scores of all the SRs.

## VI. EXPERIMENTAL RESULTS

Various experiments were conducted, aiming at analyzing the proposed approach under different aspects. This section discusses the collected experimental results.

Our experiments are generally intended to:

- 1) compare the effectiveness achieved by individual time series before and after the unsupervised distance learning procedure;
- 2) evaluate the impact of distance fusion steps using the reciprocal  $k$ NN distance for combining time series;
- 3) analyze the improvements in the plant identification task obtained by the reciprocal  $k$ NN distance.

Section VI-A presents an evaluation of the input features. In Section VI-B, we perform a parameter space analysis of our approach. Section VI-C presents the experimental results regarding the use of reciprocal  $k$ NN distance for individual features, while Section VI-D addresses its use for distance fu-

sion. Section VI-E discusses the results obtained for most discriminative features. In Section VI-F, we compare our approach with other methods. Section VI-G presents a visual analysis of the results. Finally, Section VI-H describes performed experiments considering the use of a hyperspectral dataset targeting the classification of remote sensing pixels as belonging to two classes: savanna and forest. This is an important research problem as it may help on understanding vegetation-related land cover changes over time.

### A. Quantitative Feature Evaluation

As discussed in Section V, 39 different features are considered given by periods of the day (13 h: from 6:00 to 18:00 h) and the normalized RGBcc indices (three components:  $r_{cc}$ ,  $g_{cc}$ , and  $b_{cc}$ ). This sections aims at evaluating the effectiveness of each input feature for identification of plant species.

In Fig. 3, we report and compare the time series with respect to the MAP and P10 effectiveness measures, respectively. Note that the initial effectiveness values are low for both measures, which turns more challenging the use of unsupervised distance learning methods. The MAP scores varied from 28.95% to 42.16%, while P10 scores varied from 44.30% to 73.12%.

We can observe that the extreme hours (6 and 18 h) present the best effectiveness results, considering all the normalized RGBcc indices. This is probably due to sun illumination angle variations observed along the day. Slightly better effectiveness results can also be observed for the  $r_{cc}$  index.

### B. Impact of Parameters

The reciprocal  $k$ NN distance requires only two parameters:

- 1)  $k$ , which represents the size of the neighborhood set; and
- 2)  $L$ , which defines until which position the ranked lists are considered in the distance learning procedure. In general, the parameter  $L$  represents a tradeoff between effectiveness and efficiency, since higher values of  $L$  generally provide higher accuracy while requires higher computational efforts.

The size of the neighborhood set is the most important parameter of the method, defining the extension of the reciprocal neighborhood analysis. Therefore, we conducted an experiment aiming at determining the best value for the parameter  $k$ . We computed the MAP and P10 measures for each feature in isolation considering  $k = \{3, 10, 15, 20\}$ .

Fig. 4 presents two radar charts which show the impact of the parameter  $k$  on the MAP and P@10 measures obtained by each of the time series after using the reciprocal  $k$ NN distance. These charts are composed of three parts: radius, slice of the perimeter, and lines. The radius denotes the effectiveness score. The slices of the perimeter represent each of the time series. Finally, a line indicates the performance obtained by each time series when the parameter  $k$  is set to a given value.

As we can observe, the effectiveness scores were similar for different values of the parameter  $k$ , with a small advantage to  $k = 10$ . Therefore, the value of  $k = 10$  was used for all other experiments, demonstrating the robustness of our approach. For the parameter  $L$ , we used  $L = 400$ , as suggested in [13].

<sup>2</sup>In the remainder of this paper, when we refer to segmented regions obtained by the Guigues algorithm, we use the acronym SR, whereas when we refer to regions of interest related to tree crowns of plant species identified in the image, we use the acronym ROI.

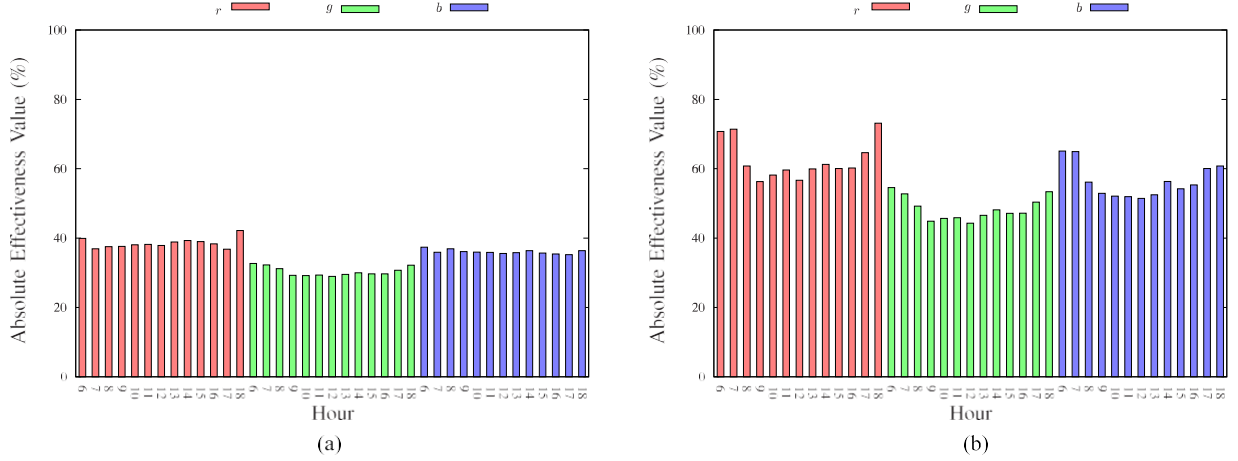


Fig. 3. Initial effectiveness scores obtained by each of the time series.

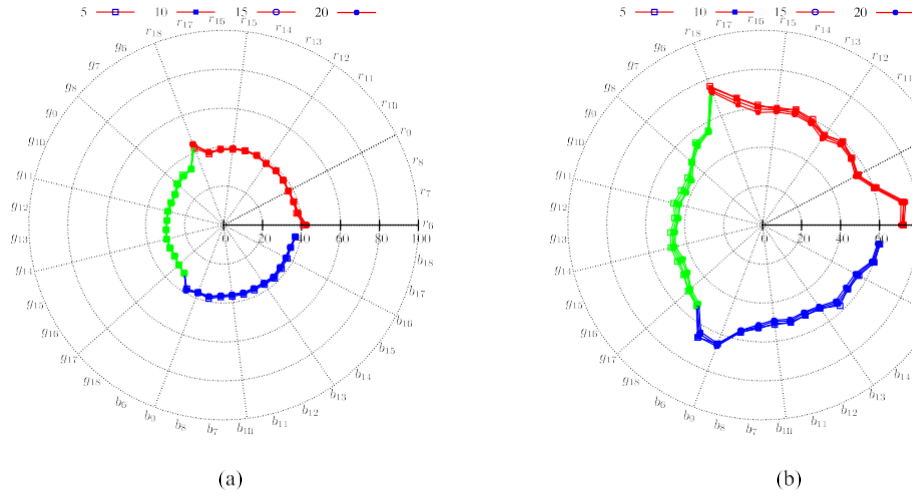


Fig. 4. Effectiveness results obtained for each of the time series after unsupervised distance learning by varying the parameter  $k$ . (a) MAP. (b) P10.

### C. Unsupervised Learning for Individual Features

Experiments were conducted for evaluating the use of the unsupervised distance learning for individual features. The main motivation consists in the conjecture that the reciprocal  $k$ NN distance can improve the effectiveness results, even considering information given by a single feature.

For evaluation purposes, we considered the MAP and P10 measures and report the relative gain, which is computed by the absolute gain divided by the initial score. Fig. 5 presents the individual relative gains obtained by each of the time series considering the MAP and P10 measures, respectively.

Despite of low effectiveness of the input individual features, positive gains were obtained in 35 and 22 out of 39 time series for MAP and P10, respectively. We can observe significant gains for MAP, reaching +6.72%. For P10, the gains are lower, but still significant, reaching +4.15%. Notice that the higher gains were obtained for features, which presented the higher initial effectiveness, e.g., features of the beginning and ending of the day and the  $r_{cc}$  index.

### D. Distance Fusion With Unsupervised Learning

Different features are expected to encode complementary information about the phenomenon modelled by the time series. Therefore, we conducted an experiment to evaluate the use of unsupervised distance learning for combining features. The considered combinations are:

- 1) all the normalized RGBcc indices for each hour of the day (13 combinations);
- 2) all the hours of the day for each of the normalized RGBcc indices (three combinations);
- 3) all hours of the day and all the normalized RGBcc indices (one combination).

Fig. 6 shows the MAP and P10 scores achieved by different time-series combinations. The results were sorted from higher to lower scores. The bars in gray indicate the combination of different chromatic indexes while bars in red, green, and blue indicate combination of different hours of the day. The percentage value at the top of each bar refers to the relative gain with respect to initial values for the best feature used for combination.

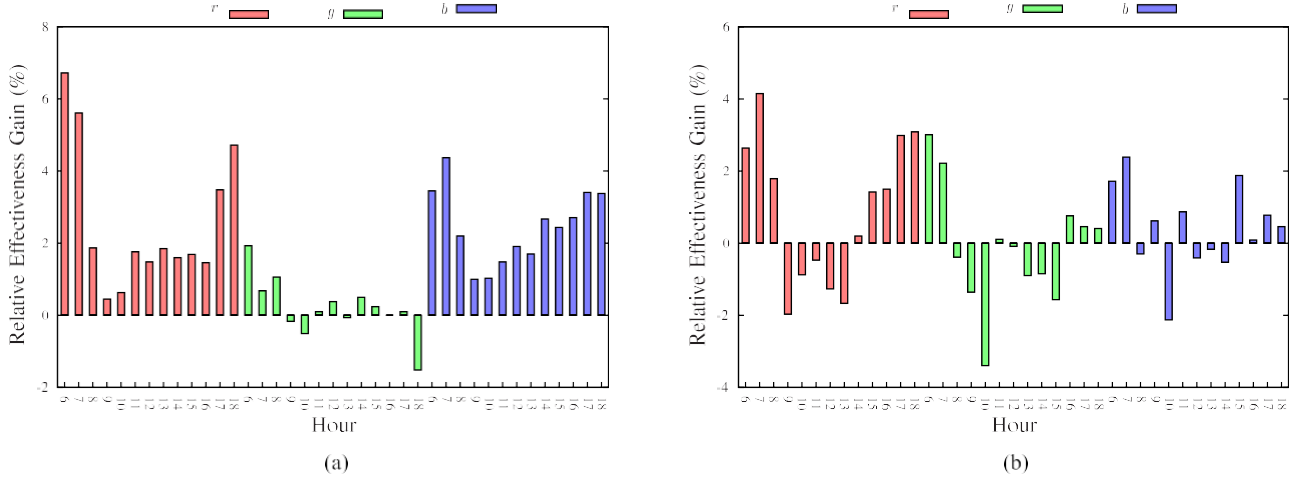


Fig. 5. Relative effectiveness gains obtained for each of the time series after unsupervised distance learning. (a) MAP. (b) P10.

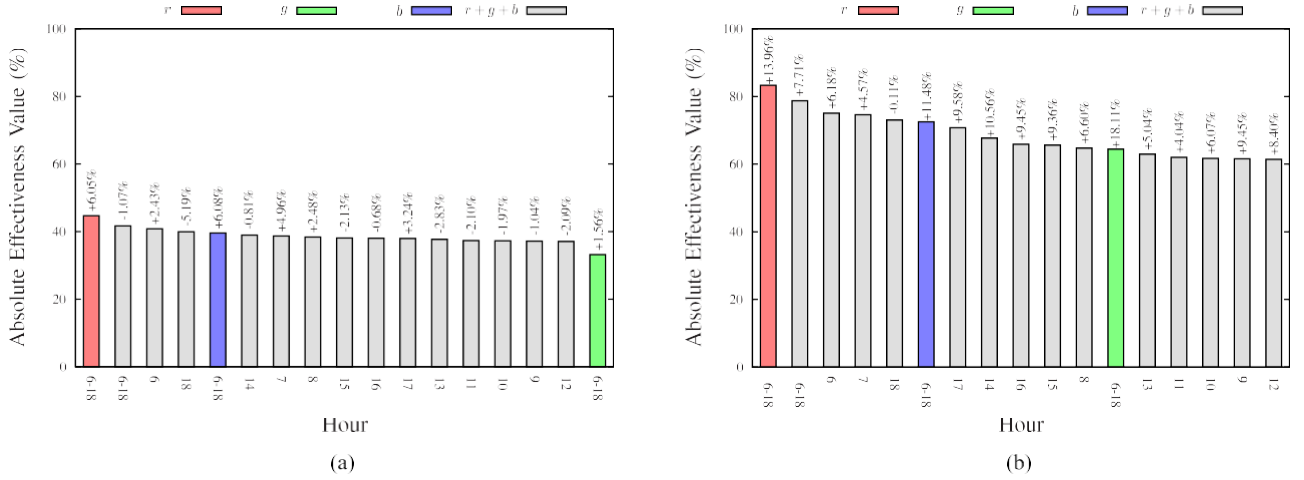


Fig. 6. Effectiveness results obtained by unsupervised distance learning for combining different time series. (a) MAP. (b) P10.

TABLE I  
SUMMARY RESULTS OF UNSUPERVISED DISTANCE LEARNING FOR PLANT  
SPECIES IDENTIFICATION BY CONSIDERING THE COMBINATION OF DIFFERENT  
TIME SERIES

Measure	Time Series	Initial Value	Reciprocal $k$ NN Distance	Relative Gain
MAP	Single ( $r_{18}$ )	42.16%	44.15%	+4.72%
	Fusion ( $r_{6-18}$ )	-	<b>44.71%</b>	+6.05%
P10	Single ( $r_{18}$ )	73.12%	75.38%	+3.09%
	Fusion ( $r_{6-18}$ )	-	<b>83.33%</b>	+13.96%

Notice the significant relative gains obtained for both measures, reaching +6.05% for MAP and +18.11% for P10.

In Table I, we compare the best results obtained for the combination and for each time series isolated with respect to the MAP and P10 measures, respectively. The relative gain of the combination was computed over initial values for the best feature in isolation. We can observe that the combination achieved

the best effectiveness scores, for both MAP and P10, reaching a relative gain of +13.96%.

#### E. Distance Fusion of Most Discriminative Features

The previous experiment has demonstrated the potential of the unsupervised learning to improve the results on plant identification tasks by combining different time series. In this section, we discuss more elaborate strategies to deal with distance fusion.

According to the results presented in previous sections, the extreme hours (early in the morning and late in the afternoon) outperformed the remaining ones. This finding is in accordance with results reported in previous works [5], [24]–[26]. It has motivated us to evaluate the use of unsupervised distance learning for combining only the most discriminative features.

Initially, we tested different combinations considering features of the beginning and ending of the day and the normalized RGBcc indices. The MAP and P10 scores achieved by the most promising combinations are presented in Fig. 7. We sorted the results from higher to lower scores, which makes the comparison

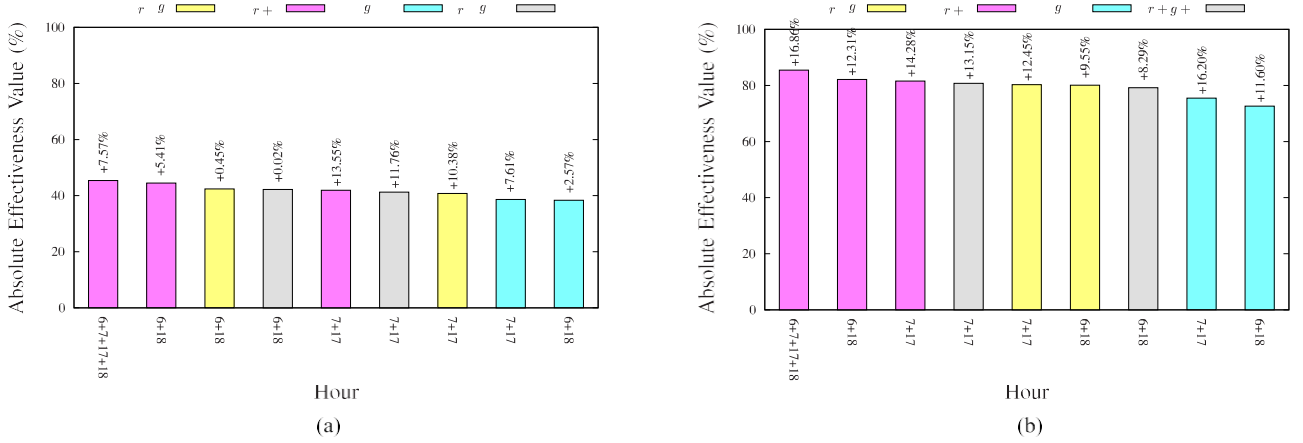


Fig. 7. Effectiveness results obtained by unsupervised distance learning for combining the most discriminative time series. (a) MAP. (b) P10.

easier. The colors of the bars indicate the combination of different chromatic indexes:

- 1) yellow refers to  $r_{cc}$  and  $g_{cc}$ ;
- 2) magenta refers to  $r_{cc}$  and  $b_{cc}$ ;
- 3) cyan refers to  $g_{cc}$  and  $b_{cc}$ ;
- 4) gray refers to all the normalized RGBcc indices.

The percentage value at the top of each bar refers to the relative gain with respect to initial values for the best feature used for combination. Significant relative gains can be observed for both measures, reaching +13.55% for MAP and +16.86% for P10.

Based on those positive results, we performed a behavior analysis of the unsupervised distance learning method using different numbers of features. In this experiment, we selected time series based on initial effectiveness values, as discussed in Section VI-A. At first, we sorted the 39 evaluated features in a decreasing order of their absolute effectiveness scores. Then, each feature was selected according to its rank, i.e., the best was the first, the second best was the second, and so on. At each step, the next feature was combined with all the previous ones.

A 5-fold cross validation was used for checking the consistency (i.e., the nonrandomness) of those rankings across different query sets. This procedure was performed as follows. Initially, we randomly partitioned the input dataset into five equal-sized subsets, called folds. Then, we performed similarity search on four folds using the fold left out as query set. This process was repeated five times, each time leaving a different fold aside as query set.

The nonparametric Friedman test was performed to verify the consistency of the rankings obtained using different folds as query set. It checks whether the measured average ranks are significantly different from the mean rank. The analysis of the experiment confirms the consistency of those rankings, rejecting the null hypothesis that there is no agreement among the query sets ( $p$ -value  $< 0.001$ ). According to the Kendall's coefficient of concordance ( $W$ ), there is a high level of agreement between the query sets ( $W = 0.975$ ).

Fig. 8 shows the behavior of the unsupervised distance learning in combining the most discriminative features. We show the

MAP and P10 scores as the most effective features are used for distance fusion. The horizontal lines indicate the effectiveness scores for the best feature in isolation and form a baseline for our proposed framework. The vertical lines indicate sets of features, which achieved the highest effectiveness scores when combined with the unsupervised distance learning method. We can see that, as more features are considered for distance fusion, more effective results are obtained, until reach a peak. This is an expected behavior, because different features may complement each other, which aggregates more information. From a certain point, however, nonrelevant results from the less effective features exceed relevant results from the most effective ones and the gain decreases. Also note that the optimal sets of features are different depending on the measure (MAP or P10). As MAP considers all the positions from the ranked lists, a smaller set is enough. On the other hand, as P10 refers to the first positions of the ranked lists, it benefits from the combination of more features.

Table II presents the best results obtained for different combination strategies and for each time series isolated with respect to the MAP and P10 measures, respectively. The relative gain of the combination was computed over initial values for the best feature in isolation. Notice that, for both MAP and P10, the best effectiveness scores were obtained by combining the most discriminative features, reaching a relative gain of +19.36%.

#### F. Comparison With State-of-the-Art

While the pairwise distance measures are broadly studied in several areas, with comparative studies, the context-based distances based on unsupervised learning schemes are relatively new, especially regarding rank-based methods.

Aiming at providing a comparison of our approach with the state of the art, we conducted an experiment employing an unsupervised fusion approach for combining the most discriminative times series selected in the previous section. The graph fusion [27], [28] method is a recent approach that has been broadly used in image retrieval last years. A similar parameter setting was considered, with  $k = 10$  for this method.

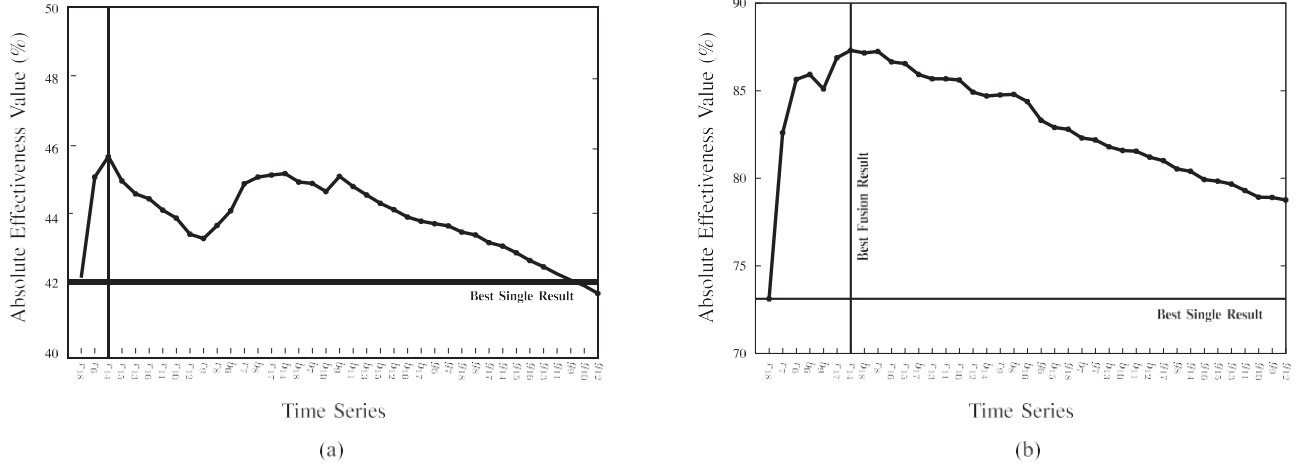


Fig. 8. Effectiveness results obtained by unsupervised distance learning for combining the most discriminative time series. (a) MAP. (b) P10.

TABLE II  
SUMMARY RESULTS OF UNSUPERVISED DISTANCE LEARNING FOR PLANT SPECIES IDENTIFICATION BY CONSIDERING THE COMBINATION OF THE MOST DISCRIMINATIVE TIME SERIES

Measure	Time Series	Initial Value	Reciprocal $k$ NN Distance	Relative Gain
MAP	Single ( $r_{18}$ )	42.16%	44.15%	+4.72%
	Fusion ( $r_6 - r_{18}$ )	-	44.71%	+6.05%
	Fusion ( $r_{18} + r_6 + r_{14}$ )	-	<b>45.62%</b>	+8.21%
P10	Single ( $r_{18}$ )	73.12%	75.38%	+3.09%
	Fusion ( $r_6 - r_{18}$ )	-	83.33%	+13.96%
	Fusion ( $r_{18} + r_7 + r_6 + b_6 + b_9 + r_{17} + r_{14}$ )	-	<b>87.30%</b>	+19.39%

TABLE III  
COMPARISON WITH STATE-OF-THE-ART BASED ON GRAPH FUSION

Measure	Time Series	Reciprocal $k$ NN Distance	Graph Fusion
MAP	Fusion ( $r_{18} + r_6 + r_{14}$ )	45.62%	37.36%
P10	Fusion ( $r_{18} + r_7 + r_6 + b_6 + b_9 + r_{17} + r_{14}$ )	87.30%	70.22%

The results of conducted comparison are presented in Table III. As we can observe, the effectiveness results achieved by our approach are higher considering both P10 and MAP measures. It is worth mentioning that, if effectiveness results are higher than those obtained for the best individual features, it is commonly considered positive for unsupervised fusion approaches, once there is no training data available. Notice that the proposed approach yielded effectiveness results significantly higher than the best feature in isolation.

### G. Qualitative and Visual Analysis

Once the quantitative results demonstrated significant gains for effectiveness measures, this section conduct a qualitative analysis using visual representations for evaluating the impact of the use of unsupervised distance learning. First, we analyze the neighborhood relationships among regions and species. In the following, we present the visualization of identified species in the original images used for extraction the time series.

For the neighborhood relationships analysis, a binary image representation is employed. In the binary image, each pixel  $p(i, j)$  has its color defined as black if the region  $r_j$  is among the  $k$ -NN of region  $r_i$ . In addition, the axis of the image is defined with regions sorted according to the plant species, such that an effective retrieval is expected to produce blocks of black pixels.

In order to explicitly highlight the potential of the unsupervised distance learning, we chose the  $g_{12}$  feature to conduct those analyses. Such a feature was chosen due to the following reasons: first, it is in agreement with the general standard of analyzing the green color change at midday hours adopted in ecological studies [4], [29], [30], and moreover, the worst result in the plant identification task was obtained by this feature in isolation, as reported in Section VI-A.

Fig. 9 shows the binary image representation of the neighborhood relationships for the  $g_{cc}$  index at 12 h. Different neighborhood sizes are considered, with  $k = 10, 20$ , and  $50$  in Fig. 9(a)–(c), respectively. Small and very diffuse blocks can be observed, mainly for 50-NN.



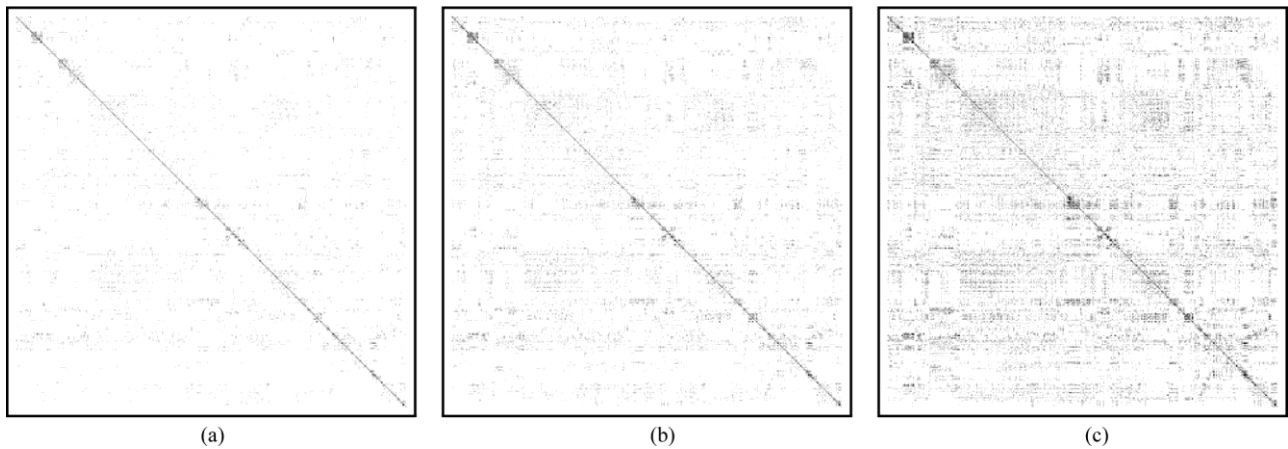


Fig. 9. Neighborhood relationship among the regions for the  $g_{12}$  feature and various sizes. (a) 10-NN. (b) 20-NN. (c) 50-NN.

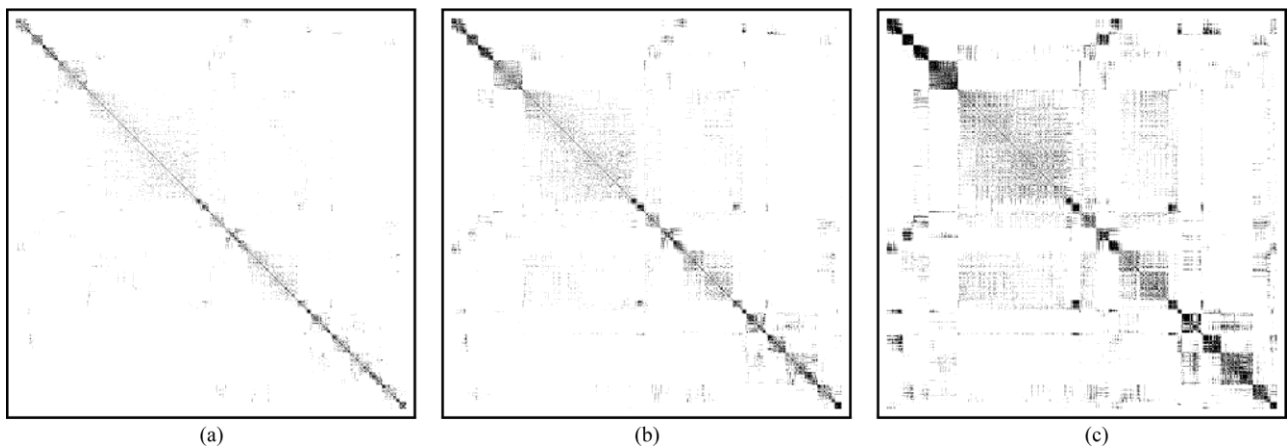


Fig. 10. Neighborhood relationship: Reciprocal  $k$ NN distance fusion and various sizes. (a) 10-NN. (b) 20-NN. (c) 50-NN.

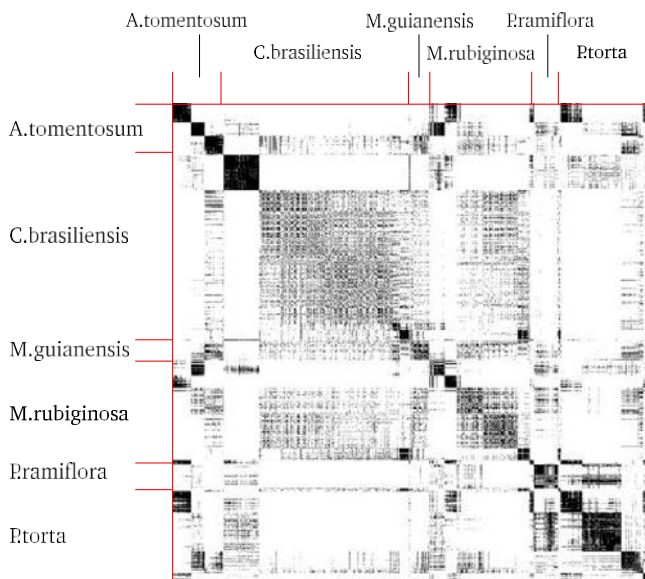


Fig. 11. Impact of the reciprocal  $k$ NN distance fusion on plant identification tasks, considering 50-NN neighborhood.

Fig. 10 illustrates an analogous representation considering the reciprocal  $k$ NN distance fusion and the best combination of features identified in previous section. We can clearly observe very distinct blocks for 50-NN and even for 20-NN.

Fig. 11 presents the 50-NN representation with a legend indicating the plant species in the axis of the image. As expected, the majority of the blocks are localized in the main diagonal, which demonstrates that regions of the same species are among the nearest neighbors of each other. Blocks out of the main diagonal may indicate functional groups and constitute a future line of investigation.

Figs. 12 and 13 present a different view of the results, showing the performance without and with the unsupervised distance learning for the individual queries (i.e., specific lines of the previous images) that achieved the best and the worst result, respectively. In those figures, each region is colored according to its distance to the query using a colormap from blue to red, where the red colors denote nearest regions (i.e., associate with similar species) and the blue ones represent furthest regions (i.e., relate to different species). The yellow circles indicate the relevant regions to the query (i.e., are from a same species).

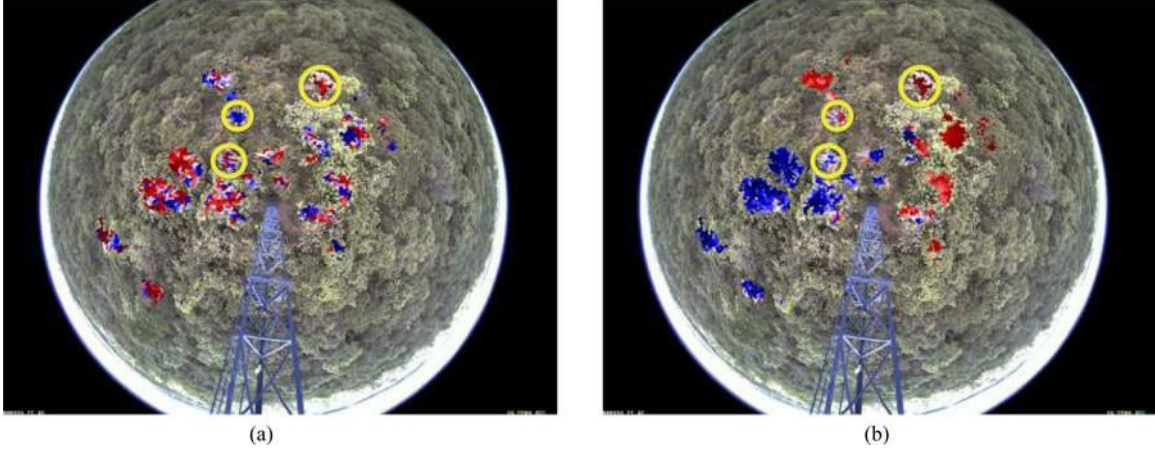


Fig. 12. Results obtained for the query that achieved the highest score, showing the performance without and with the unsupervised distance learning. Each region is colored according to its distance to the query using a colormap from blue to red. The red colors denote nearest regions whereas the blue ones represent furthest regions. The yellow circles indicate the relevant regions to the query. (a)  $g_{12}$  feature in isolation. (b) Reciprocal  $kNN$  distance fusion.

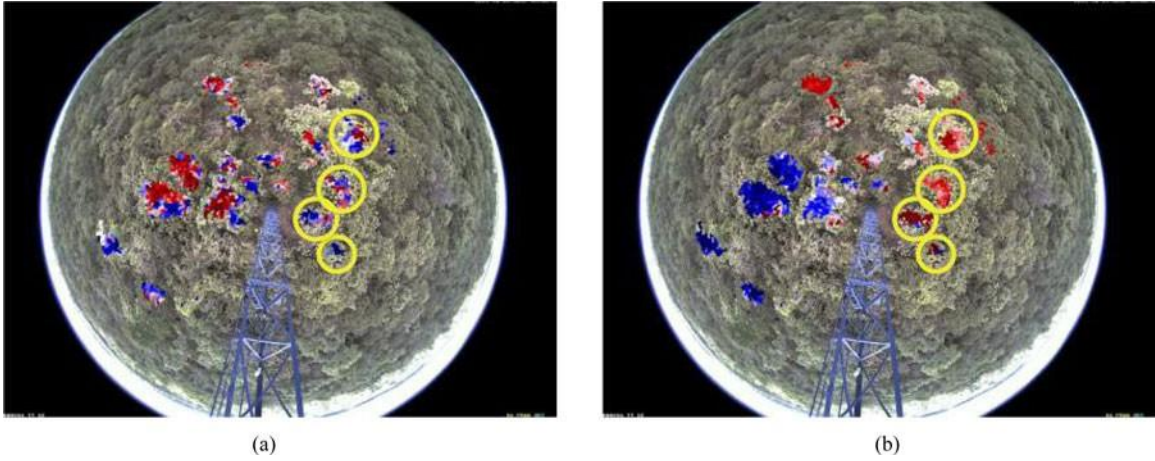


Fig. 13. Results obtained for the query that achieved the lowest score, showing the performance without and with the unsupervised distance learning. Each region is colored according to its distance to the query using a colormap from blue to red. The red colors denote nearest regions whereas the blue ones represent furthest regions. The yellow circles indicate the relevant regions to the query. (a)  $g_{12}$  feature in isolation. (b) Reciprocal  $kNN$  distance fusion.

Ideally, the regions inside the yellow circles should be colored in red and all the remaining ones should be colored in blue, indicating a perfect prediction of individuals from a same species. Observe that it is hard to distinguish whether species are similar or not by considering only the  $g_{12}$  feature, since the areas in red and blue colors are diffuse [see Figs. 12(a) and 13(a)]. Regardless of the initial performance, we can notice the significant improvements yielded by the reciprocal  $kNN$  distance fusion, which clearly separates the plant species, thus producing large same-colored areas [see Figs. 12(b) and 13(b)].

#### H. Experiments With Hyperspectral Data

Also, we evaluated the proposed method on a hyperspectral dataset, i.e., with more than three bands. For that, experiments were conducted on data collected by the sensor USGS Landsat 5 TM Raw Scenes (Orthorectified) in various regions from South America, between January 2000 and December 2011. The

sensor offers images composed of seven spectral bands at 30-m spatial resolution with a temporal frequency of 16 days.<sup>3</sup>

The geographical coordinates used as ground truth in this study are a modified subset of the inventory data used by [31]. These data correspond to centroid coordinates of field sampled quadrants of tropical vegetation labeled either as forest or savanna. We selected the subset of these quadrants corresponding to tropical South America and visualized each of the quadrants using Google Earth images from 2016 superimposed with the MODIS pixel grid of 250×250 m using Series Views [32]. For each of those quadrants, we visually assessed whether a MODIS pixel was or not completely filled with a labeled vegetation type (i.e., savannas or forests). Pixels that were not entirely filled with the corresponding vegetation type were either replaced by a neighboring pixel fulfilling these criteria or discarded (when a suitable pixel could not be found nearby). In addition, locations

<sup>3</sup><http://landsat.usgs.gov> (As of July 2016)

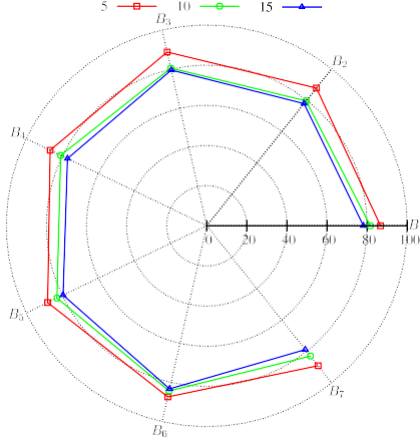


Fig. 14. Classification accuracy obtained for each of the bands after unsupervised distance learning by using a  $k$ -NN classifier with different values of  $k$ .

at which the label assigned to that vegetation type could not be visually confirmed were also discarded. The centroid coordinate of each remaining pixel was then obtained and used to extract the satellite data used for classification purposes. Therefore, subsequent analyses were performed using 183 savannas and 110 forest locations.

For each location, we extracted seven different time series by considering the available bands (seven components:  $B_1$  to  $B_7$ ). The distance function used for time-series comparison is the Manhattan (L1) distance. In the experiments, we adopted the evaluation protocol used in [33] and [34]. It relies on the classification of time series extracted from locations associated with a given vegetation type. For that, we used a  $k$ -NN classification model: a given location is classified by a majority vote of its neighbors, being assigned to the class most common among its  $k$ -NN.

Our experiments intend to evaluate the accuracy of a  $k$ -NN classifier before and after the use of the unsupervised distance learning procedure. For that, we adopted the same value of the parameter  $k$  used both for the  $k$ -NN classifier and the reciprocal  $k$ NN distance algorithm. Similar to the retrieval-based protocol, the size of the neighborhood set plays an important role, defining the extension of the reciprocal neighborhood analysis. Therefore, the first experiment was conducted aiming at determining the best value for the parameter  $k$ . We computed the classification accuracy for each band in isolation considering  $k = \{5, 10, 15\}$ .

Fig. 14 presents the classification accuracy obtained by different bands and different values of  $k$ . We can clearly observe that the accuracy of  $k = 5$  achieved the higher scores for all the bands. Therefore, we choose the value of  $k = 5$  for next experiments.

Fig. 15 shows the accuracy scores of a 5-NN classifier obtained for each band based on the initial distance. Observe that the best result in isolation was achieved by the band  $B_7$ , reaching a classification accuracy of 89.08%.

The next experiment was conducted to evaluate the use of the unsupervised distance learning for each individual band. Fig. 16 presents the relative gains obtained by the use of the reciprocal

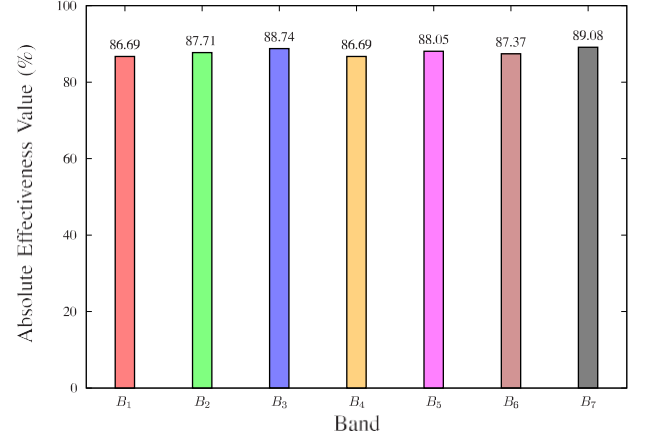


Fig. 15. Initial accuracy scores obtained for each band using a 5-NN classifier.

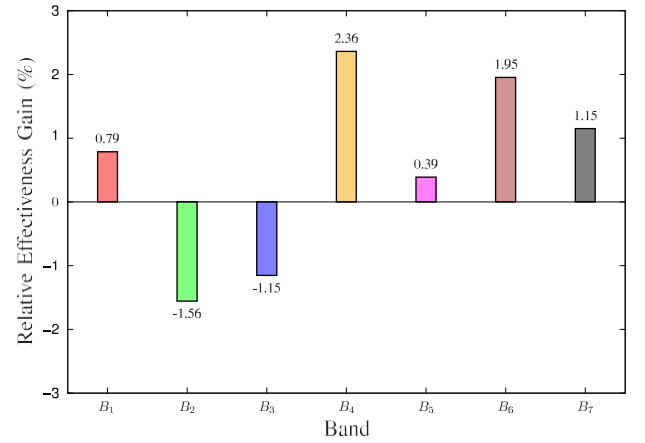


Fig. 16. Relative effectiveness gains obtained for each of the bands after unsupervised distance learning.

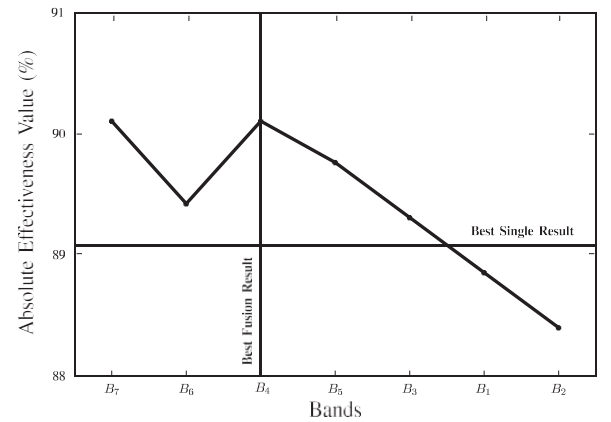


Fig. 17. Classification accuracy obtained by unsupervised distance learning for combining the most discriminative bands.

$k$ NN distance algorithm for each band. The best gains can be observed for the band  $B_4$ , which obtained a relative gain of +2.36%, reaching a final accuracy of 88.74%. On other hand, the band  $B_7$  obtained a relative gain of +1.15%, reaching a final accuracy score of 90.10%. This score is higher than any accuracy score obtained by the initial distance, considering all the bands.



Finally, we also evaluated the combination of different bands. For that, an experimental protocol similar to the previous fusion experiments (see Section VI-E) was considered. Thus, we selected the most discriminative bands by ordering their classification accuracy after the unsupervised distance learning. Fig. 17 shows the classification accuracy obtained by our proposed framework. The horizontal line indicates the accuracy score for the best band in isolation and the vertical line indicates the best fusion result (obtained for the bands  $B_7 + B_6 + B_4$ ). We can observe that the curve presents a very similar behavior to the previous fusion experiments (see Fig. 8), achieving a higher accuracy result than the best band in isolation.

## VII. CONCLUSION

This paper presented a new similarity measure for plant identification tasks involved in remote monitoring of phenology with digital cameras. In order to obtain global measures that encode information of the dataset structure, we proposed the use of an unsupervised distance learning method called reciprocal  $k$ NN distance [13].

A comparative analysis of different features, as well as their possible combinations created by our approach, has been conducted in our experiments. Results obtained with our proposed framework applied to about 2700 images taken from a tropical cerrado savanna vegetation demonstrate that it can largely improve the plant identification results, reaching gains of more than 19%.

One possible limitation of the work refers to the problems caused by distortions within the generated images. For example, the visual properties associated with regions close to the borders probably contain a lot of noise, which may impact the effectiveness of the method. This is reason that we have avoided using them in our evaluation protocol (see the selected regions in Fig. 1). Another issue refers to parameter settings of the proposed method. An in-depth evaluation of suitable values for them is left for future work. Another issue refers to the time span of images used. We expect to check the consistence of the results with longer time series in future work.

Future work includes the evaluation of other features for identifying plants based on phenological time series and a rigorous analysis of the influence of parameters employed in our approach in order to determine which configuration produces the best results, as well as perform an extensive study on different strategies for feature selection and distance fusion.

## ACKNOWLEDGMENT

The authors are grateful to J. F. H. Albarac'in and V. de Lima Dantas for their assistance with the hyperspectral dataset.

## REFERENCES

- [1] M. D. Schwartz, *Phenology: An Integrative Environmental Science*, 2nd ed. New York, NY, USA: Springer, 2013.
- [2] L. P. C. Morellato, M. G. G. Camargo, and E. Gressler, "A review of plant phenology in South and Central America," in *Phenology: An Integrative Environmental Science*, M. D. Schwartz, Ed. New York, NY, USA: Springer, 2013, ch. 6, pp. 91–113.
- [3] B. Alberton, J. Almeida, R. Henneken, R. S. Torres, A. Menzel, and L. P. C. Morellato, "Using phenological cameras to track the green up in a cerrado savanna and its on-the-ground validation," *Ecol. Informat.*, vol. 19, pp. 62–70, 2014.
- [4] A. D. Richardson, B. H. Braswell, D. Y. Hollinger, J. P. Jenkins, and S. V. Ollinger, "Near-surface remote sensing of spatial and temporal variation in canopy phenology," *Ecol. Appl.*, vol. 19, pp. 1417–1428, 2009.
- [5] J. Almeida, J. A. dos Santos, B. Alberton, R. da S. Torres, and L. P. C. Morellato, "Applying machine learning based on multiscale classifiers to detect remote phenology patterns in Cerrado savanna trees," *Ecol. Informat.*, vol. 23, pp. 49–61, 2014.
- [6] R. da S. Torres and A. X. Falcão, "Content-based image retrieval: Theory and applications," *J. Theor. Appl. Informat.*, vol. 13, no. 2, pp. 161–185, 2006.
- [7] O. Sonnentag, "Digital repeat photography for phenological research in forest ecosystems," *Agricultural Forest Meteorol.*, vol. 152, pp. 159–177, 2012.
- [8] T. Skopal and B. Bustos, "On nonmetric similarity search problems in complex domains," *ACM Comput. Surveys*, vol. 43, no. 4, pp. 34:1–34:50, 2011.
- [9] R. da S. Torres, "Shape-based time series analysis for remote phenology studies," in *Proc. IEEE Int. Geosci. Remote Sens. Symp.*, 2013, pp. 3598–3601.
- [10] J. Almeida, J. A. Santos, B. Alberton, L. P. C. Morellato, and R. S. Torres, "Phenological visual rhythms: Compact representations for fine-grained plant species identification," *Pattern Recognit. Lett.*, vol. 81, pp. 90–100, 2015, [Online]. Available: <http://doi:10.1016/j.patrec.2015.11.028>.
- [11] B. Eravci and H. Ferhatosmanoglu, "Diversity based relevance feedback for time series search," *Proc. VLDB Endowment*, vol. 7, no. 2, pp. 109–120, Oct. 2013.
- [12] J. Almeida, J. A. dos Santos, B. Alberton, R. da S. Torres, and L. P. C. Morellato, "Remote phenology: Applying machine learning to detect phenological patterns in a Cerrado savanna," in *Proc. IEEE Int. Conf. eSci.*, 2012, pp. 1–8.
- [13] D. C. G. Pedronette, O. A. B. Penatti, R. T. Calumby, and R. da S. Torres, "Unsupervised distance learning by reciprocal  $k$ NN distance for image retrieval," in *Proc. Int. Conf. Multimedia Retrieval*, 2014, p. 345.
- [14] M. Lngkvist, L. Karlsson, and A. Loutfi, "A review of unsupervised feature learning and deep learning for time-series modeling," *Pattern Recognit. Lett.*, vol. 42, pp. 11–24, 2014.
- [15] M. Donoser and H. Bischof, "Diffusion processes for retrieval revisited," in *Proc. IEEE Conf. Comput. Vis. Pattern Recog.*, 2013, pp. 1320–1327.
- [16] D. C. G. Pedronette, O. A. B. Penatti, and R. da S. Torres, "Unsupervised manifold learning using reciprocal knn graphs in image re-ranking and rank aggregation tasks," *Image Vis. Comput.*, vol. 32, no. 2, pp. 120–130, 2014.
- [17] A. D. Richardson, J. P. Jenkins, B. H. Braswell, D. Y. Hollinger, S. V. Ollinger, and M. L. Smith, "Use of digital webcam images to track spring greening in a deciduous broadleaf forest," *Oecologia*, vol. 152, pp. 323–334, 2007.
- [18] A. R. Gillespie, A. B. Kahle, and R. E. Walker, "Color enhancement of correlated images. ii. channel ratio and "chromaticity" transformation techniques," *Remote Sens. Environ.*, vol. 22, no. 3, pp. 343–365, 1987.
- [19] D. M. Wobbecke, G. E. Meyer, K. Von-Bargen, and A. D. Mortensen, "Color indices for weed identification under various soil, residue, and lighting conditions," *Trans. ASAE*, vol. 38, pp. 259–269, 1995.
- [20] J. Almeida, J. A. Santos, W. O. Miranda, B. Alberton, L. P. C. Morellato, and R. S. Torres, "Deriving vegetation indices for phenology analysis using genetic programming," *Ecol. Informat.*, vol. 26, pp. 61–69, 2015.
- [21] H. Jegou, C. Schmid, H. Harzallah, and J. Verbeek, "Accurate image search using the contextual dissimilarity measure," *IEEE Trans. Pattern Anal. Mach. Intell.*, vol. 32, no. 1, pp. 2–11, Jan. 2010.
- [22] D. Qin, S. Gammeter, L. Bossard, T. Quack, and L. van Gool, "Hello neighbor: Accurate object retrieval with  $k$ -reciprocal nearest neighbors," in *Proc. IEEE Conf. Comput. Vision Pattern Recognit.*, Jun. 2011, pp. 777–784.
- [23] L. Guigues, J. Cocquerez, and H. Le Men, "Scale-sets image analysis," *Int. J. Comput. Vis.*, vol. 68, pp. 289–317, 2006.
- [24] J. C. Conti, "Evaluation of time series distance functions in the task of detecting remote phenology patterns," in *Proc. IEEE Int. Conf. Pattern Recog.*, 2014, pp. 3126–3131.
- [25] J. Almeida, J. A. dos Santos, B. Alberton, L. P. C. Morellato, and R. da S. Torres, "Visual rhythm-based time series analysis for phenology studies," in *Proc. IEEE Int. Conf. Image Process.*, 2013, pp. 4412–4416.

- [26] J. Almeida, J. A. dos Santos, B. Alberton, L. P. C. Morellato, and R. da S. Torres, "Plant species identification with phenological visual rhythms," in *Proc. IEEE Int. Conf. eSci.*, 2013, pp. 148–154.
- [27] S. Zhang, M. Yang, T. Cour, K. Yu, and D. N. Metaxas, "Query specific fusion for image retrieval," in *Proc. 12th Eur. Conf. Comput. Vision*, 2012, pp. 660–673.
- [28] S. Zhang, M. Yang, T. Cour, K. Yu, and D. Metaxas, "Query specific rank fusion for image retrieval," *IEEE Trans. Pattern Anal. Mach. Intell.*, vol. 37, no. 4, pp. 803–815, Apr. 2015.
- [29] H. Ahrends, "Tree phenology and carbon dioxide fluxes: Use of digital photography for process-based interpretation at the ecosystem scale," *Climate Res.*, vol. 39, pp. 261–274, 2009.
- [30] R. Ide and H. Oguma, "A cost-effective monitoring method using digital time-lapse cameras for detecting temporal and spatial variations of snowmelt and vegetation phenology in alpine ecosystems," *Ecol. Inform.*, vol. 16, pp. 25–34, 2013.
- [31] V. L. Dantas, M. Hirota, R. S. Oliveira, and J. G. Pausas, "Disturbance maintains alternative biome states," *Ecol. Lett.*, vol. 19, pp. 12–19, 2016.
- [32] R. M. Freitas, "Virtual laboratory of remote sensing series: Visualization of MODIS EVI2 data set over south america," *J. Comput. Interdisciplinary Sci.*, vol. 2, pp. 57–64, 2011.
- [33] F. A. Faria, J. Almeida, B. Alberton, L. P. C. Morellato, A. Rocha, and R. S. Torres, "Time series-based classifier fusion for fine-grained plant species recognition," *Pattern Recognit. Lett.*, vol. 81, pp. 101–109, 2015, [Online]. Available: [http://doi: 10.1016/j.patrec.2015.10.016](http://doi:10.1016/j.patrec.2015.10.016).
- [34] F. A. Faria, J. Almeida, B. Alberton, L. P. C. Morellato, and R. S. Torres, "Fusion of time series representations for plant recognition in phenology studies," *Pattern Recognit. Lett.*, 2016, [Online]. Available: [http://doi: 10.1016/j.patrec.2016.03.005](http://doi:10.1016/j.patrec.2016.03.005), to be published.